Rijks*universiteit* Groningen

Time-Dependent Current-Density-Functional Theory for Molecules

PROEFSCHRIFT

ter verkrijging van het doctoraat in de
Wiskunde en Natuurwetenschappen
aan de Rijksuniversiteit Groningen
op gezag van de
Rector Magnificus, dr. F. Zwarts,
in het openbaar te verdedigen op
vrijdag 18 maart 2005
om 14:45 uur

door

Meta van Faassen
geboren op 20 maart 1978
te Groningen

Promotor:	prof. dr. R. Broer
Copromotores:	dr. ir. P. L. de Boeij dr. R. van Leeuwen
Beoordelingscommissie:	prof. dr. J. Knoester prof. dr. E. J. Baerends prof. dr. G. Vignale

Time-Dependent Current-Density-Functional Theory for Molecules

Meta van Faassen

Meta van Faassen
Time-dependent current-density-functional theory for molecules
Proefschrift Rijks*universiteit* Groningen

Het promotieonderzoek beschreven in dit proefschrift werd uitgevoerd in de theoretische chemie groep van het Materials Science Centre (MSC) aan de Rijks*universiteit* Groningen, Nijenborgh 4, 9747 AG, Groningen. Het onderzoek werd grotendeels financieel mogelijk gemaakt door de Nederlandse organisatie voor wetenschappelijk onderzoek (NWO), afdeling chemische wetenschappen (CW).

Dit proefschrift maakt onderdeel uit van de MSC Ph.D.-thesis series 2005 (nummer 02)
ISSN 1570-1530

© Meta van Faassen, 2005

Nederlandse Organisatie voor Wetenschappelijk Onderzoek

Contents

Introduction

In the late 1990s there was a commercial in the Netherlands for a herbal energy drink with the slogan: “It works because of herbs!” As a scientist one immediately wonders when hearing this slogan: What are these “magic herbs” and why are these herbs supposed to work? Even though we will explore a completely different matter in this thesis, we will see at the end of this introduction that the question that we will try to answer in this thesis is very similar.

In this thesis we will explore the response of molecules to an external perturbation (an electric field). One of the reasons to study these properties is that they have a direct relation with the design of new compounds for optics and photonics applications. To calculate these response properties we solve the time-dependent Schrödinger equation using time-dependent current-density-functional theory. Here we will introduce this method and its approximations. We will start with explaining the basics behind ground state density functional theory and then move to the time-dependent case.

The starting point for any (nonrelativistic) quantum chemical calculation on a stationary isolated N-electron system is the time-independent Schrödinger equation given by

$$\hat{H}\Psi\left(\mathbf{x}_1,\mathbf{x}_2,\ldots,\mathbf{x}_N\right)=E\Psi\left(\mathbf{x}_1,\mathbf{x}_2,\ldots,\mathbf{x}_N\right), \tag{0.1}$$

where E is the electronic energy, $\Psi\left(\mathbf{x}_1,\mathbf{x}_2,\ldots,\mathbf{x}_N\right)$ is the many-electron wave function, and $\hat{H}$ is the Hamilton operator. The wave function is a function of the space and spin coordinates of the N electrons and describes the correlated motion of these N interacting particles. In 1964 Hohenberg and Kohn [1] discovered that alternatively one can fully describe a stationary state by its ground state density. Even the many-body wave function itself can be obtained from this quantity. The advantages of using the density instead of the wave function are clear, the density is an intuitive and physically observable quantity and it only depends on three spatial coordinates instead of $3N$ spatial coordinates. They also showed that the total energy can be written as a density functional and that the exact ground state energy can be found by minimization of this functional. It were Kohn and Sham [2] who showed that it is possible to obtain the interacting density from a system of noninteracting particles, the Kohn-Sham system. The electrons then obey a simple one-particle Schrödinger equation but with an *effective* potential,

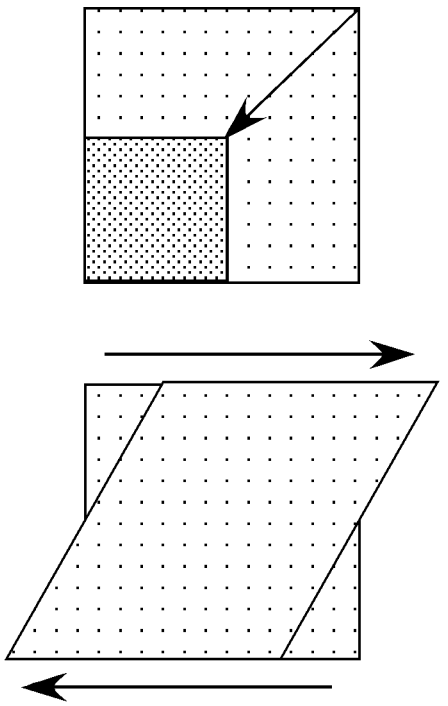

Longitudinal response:

$$\nabla \cdot \mathbf{j}(\mathbf{r},t) = -\frac{\partial \rho(\mathbf{r},t)}{\partial t} \neq 0$$

$$\nabla \times \mathbf{j}(\mathbf{r},t) = 0$$

Transverse response:

$$\nabla \cdot \mathbf{j}(\mathbf{r},t) = -\frac{\partial \rho(\mathbf{r},t)}{\partial t} = 0$$

$$\nabla \times \mathbf{j}(\mathbf{r},t) \neq 0$$

Figure 0-1. The top figure depicts a block of density that is compressed. In this case the density changes, but the rotation of the current density does not; the response is purely longitudinal. The second picture shows what happens if shear stresses work on our block, the density remains the same, but the rotation of the current density is nonzero. In this case the response is purely transverse.

$$v_{\text{eff}}(\mathbf{r}) = v_{\text{ext}}(\mathbf{r}) + v_H(\mathbf{r}) + v_{\text{xc}}(\mathbf{r}) \tag{0.2}$$

where the first term is the external potential, the second term includes the classical part of the electron-electron interaction, and the final term contains everything else. This exchange-correlation (xc) potential is unknown and needs to be approximated. Finding a good functional is one of the greatest challenges of density functional theory. The simplest functional is the local density approximation (LDA) [2], which is based upon the theory of the homogeneous electron gas.

Density functional theory (DFT) as described above can be extended to describe time-dependent systems (TDDFT) [3] and it can be used to describe response properties of a system in an external electric field. It is of course also possible that one wants to include the coupling to a time-dependent magnetic field. In this case a time-dependent vector potential enters the theory and the current density appears in the theory. This led to the development of time-dependent

current DFT (TDCDFT) [4-6]. The coupling to magnetic fields is not the only reason to use TDCDFT. Consider, for example, a solid in an electric field using periodic boundary conditions. The basic argument is that a *uniform* macroscopic current cannot be described by TDDFT for this system, as in that case the density does not change anywhere in the bulk but only at the surface [7]. Another reason to use TDCDFT comes from the fact that we know that any field can be split in a longitudinal and transverse part,

$$\mathbf{A} = \mathbf{A}_{\mathrm{L}} + \mathbf{A}_{\mathrm{T}} \tag{0.3}$$

where

$$\begin{aligned} \nabla \cdot \mathbf{A}_{\mathrm{T}} &= 0 \\ \nabla \times \mathbf{A}_{\mathrm{L}} &= 0 \end{aligned} \tag{0.4}$$

For example in isotropic systems the response for these fields will result in longitudinal and transverse current densities. In Figure 0-1 we show that in case of the transverse response the density does not change in the bulk of the system, it only changes at the surface. It turns out that these surface effects influence the response of the bulk region. If the system is very large, we can only describe this effect with a very nonlocal functional or by taking the current density into account. There is another very important reason to use TDCDFT and that is that Vignale and Kohn [8,9] showed that there is no local *density* approximation for the scalar xc-potential at finite frequency, but there is a consistent local approximation for a vector xc-potential in terms of the *current density*. Besides making this observation they also derived an expression for this vector xc-potential, the Vignale-Kohn (VK) functional. In this thesis we will look at the *static* response of *finite* systems. So why should we use current DFT?

The simplest xc-potential within TDDFT is the adiabatic local density approximation (ALDA), which is a direct extension of the ground state LDA functional. Even though this functional is very simple, it turns out to give very good results in general. However, there are also failures. A very clear failure is the large overestimation of the static polarizability of long molecular chains [10,11] compared with other, wave function based methods. We give the results for polyacetylene in Figure 0-2. The ALDA, but also more advanced generalized gradient approximations (GGA), is unable to describe the highly nonlocal exchange and correlation effects found in these systems [10,11].

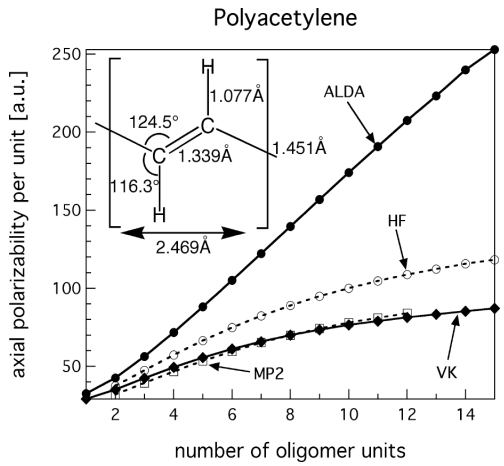

Figure 0-2. ALDA and VK static axial polarizability of polyacetylene compared with restricted Hartree-Fock [12] and MP2 [13] results.

A lot of research has been done to improve the ALDA because for these large systems it is often not possible to do an accurate wave function based calculation. The only correlated calculations that have been done on the larger oligomers of some systems are MP2 calculations [13-15]. One way to overcome the shortcomings of the ALDA within DFT is to employ optimized effective potentials (OEP) [16-19] or approximations to this potential [20,21]. Basis of the success of these exchange-only potentials is their explicit dependence on the orbitals, which allows for a nonlocal dependence on the density. However, these approaches are currently restricted to the exchange-only approximation.

We see from Figure 0-1 that for large systems, such as these polymeric systems, the influence of the surface on the response can only be described by such nonlocal functionals or by taking the current density into account. As mentioned above Vignale and Kohn showed that it is indeed possible to describe nonlocal effects by using a vector xc-potential that depends on the current density. It turns out that this VK-functional does have a contribution in the static limit and gives a large correction to the ALDA for the static polarizability of polyacetylene (see Figure 0-2) and we obtain values close to available MP2 results. As we shall show in this thesis we find similar results for other π-conjugated systems.

We see for polyacetylene that the VK-functional works well. But does it work for all systems? And does it work for all response properties? Another major question is: *Why* does it work? Is it because of some “magic herbs”, or can we find a better explanation?

These are the questions we will explore in this thesis.

Outline of this thesis

In Chapter 1 ground state density functional theory (DFT) is introduced. We first give the theorems that were proven by Hohenberg and Kohn in the 1960s and are the foundation of DFT [1]. The important result that follows from these theorems is that if one wants to fully describe a

stationary electronic system, it is sufficient to know the ground state density. We also give the practical scheme that Kohn and Sham [2] devised on the basis of a noninteracting many particle system (the "Kohn-Sham" system) and that allows us to actually do DFT calculations.

In Chapter 2 we show how the ground state DFT formalism can be extended to the time-dependent regime (TDDFT). In the 1980s Runge and Gross showed that there is a time-dependent version of the Hohenberg-Kohn theorems [3] that allows us to write down time-dependent versions of the Kohn-Sham equations. Ghosh and Dhara [4,5] later showed that it is also possible to prove the Hohenberg-Kohn theorems in the case of time-dependent *current-density-functional* theory (TDCDFT). In this thesis we do not give this proof by Ghosh and Dhara, but instead we give a more elegant proof by Vignale [6].

In Chapter 3 we show how to obtain response properties like static and frequency dependent polarizabilities and excitation energies within the framework of linear response theory. We closely follow the method of Casida (Ref. [22]) for TDDFT and extend this method to the case of TDCDFT.

The fact that we are using TDCDFT allows us to use a functional that is dependent on the current density. In Chapter 4 we thoroughly describe such a functional, namely the VK-functional [8,9,23,24]. Since this functional can be cast in the form of a hydrodynamic equation, we also give some background on hydrodynamics and elasticity. We then give some of the historic motivation behind the derivation of the VK-functional, followed by a short overview of how this functional was derived. We also give the functional in its spin-dependent form. We use the functional only in the static limit ($\omega \to 0$) and we show what the consequences are of taking this limit on the VK-functional. We shortly comment on the validity of using this functional for finite and inhomogeneous systems like atoms and molecules.

In Chapter 5 we show how we implemented the linear response equations of TDCDFT and the VK-functional in the Amsterdam Density Functional program package (ADF) [25]. Since the implementation of the linear response equations TDDFT is explained in depth by Stan van Gisbergen [26] we concentrate on the changes that need to be made to include the current-dependent formalism.

In Chapter 6 we give our results for the static polarizabilities of a large number of oligomers, including the model hydrogen chain. These are the results that we published in *Phys. Rev. Lett.* ***88****, 186401 (2002)* and *J. Chem. Phys.* ***118****, 1044 (2003)*. We show that by treating the exchange-correlation effects using the VK-functional we are able to obtain polarizabilities in good agreement with accurate wave function methods. The VK-functional achieves large corrections

to the adiabatic local-density approximation (ALDA) that is known to overestimate the polarizability considerably for conjugated oligomers. Moreover the large N behavior of VK as described by a power law is found to be in good agreement with reference data. The only molecular chain that we studied for which the VK-functional does not give a large correction is the model hydrogen chain.

From the good results for the conjugated oligomers we expect that also the polarizability of the much larger tubular fullerenes will improve. In Chapter 7 we give our results for the tubular fullerenes $C_{60+i\times10}$, where i = 0–5, and the closely related [5,5] carbon nanotube that we published in *Chem. Phys. Lett.* ***395****, 274 (2004)*. Comparing the results obtained within the conventional ALDA with those obtained using the VK-functional it is found that the extra long-range exchange-correlation effects described by the current-density functional are important to consider, especially for the longest fullerenes. For the systems studied the TDCDFT results are in good agreement with available experimental results, and the agreement with available *ab initio* self-consistent-field results and results from a point–dipole interaction model is much better than when using the ALDA.

Apart from the polarizability we also studied excitation energies of several systems. In Chapter 8 we study a variety of singlet excitations for a benchmark set of molecules. The $\pi\rightarrow\pi^*$ excitation energies obtained with the VK-functional are in good agreement with experiment and other theoretical results and they are in general an improvement upon the adiabatic local density approximation. In case of the $n\rightarrow\pi^*$ transitions the VK-functional fails, giving results that are strongly overestimated compared to experimental results and theoretical reference data. The benchmark set also contains some other types of excitations for which neither clear failures nor improvements are observed. We published this data in *J. Chem. Phys.* ***120****, 8353 (2004)*.

In Chapter 9 we study the $\pi\rightarrow\pi^*$ singlet excitations of several π-conjugated oligomers and the lowest singlet excitations of the hydrogen chain. From our results for the polarizability of these systems we expect a large effect when using the VK-functional. By studying the dependence of the excitation spectrum on the chain length we conclude that the reduction of the static polarizability when using the VK-functional has two origins. First, the excitation energies of transitions with a large transition dipole are shifted upward. Second, the HOMO-LUMO character and oscillator strength of the lowest transition within the ALDA are transferred to higher transitions. The lowest transitions that have considerable oscillator strength obtained with the VK-functional have excitation energies that are in most cases in better agreement with

available reference data then the ALDA. We published this data in *J. Chem. Phys.* ***121****, 10707 (2004).*

The VK failures observed in the molecular systems are reproduced in the much simpler case of atoms. In Chapter 10 we perform a thorough analysis of the VK-functional for atoms. For these systems the VK-functional can be rewritten in spherical coordinates, simplifying the analysis. We show a graph of the VK exchange-correlation electric field of a $2s \rightarrow 3s$ transition in B^+ and we show the effect of the VK-functional on transitions in several other atoms. We find that for the $s \rightarrow p$ transitions the excitation energy is strongly overestimated with VK. This is also what follows from an independent study by Ullrich and Burke [27]. A slight modification of the transverse exchange-correlation kernel in the high-density region strongly reduces the error for the $s \rightarrow p$ transitions, while keeping the $s \rightarrow s$ transitions in agreement with experiment. Using this simple modified kernel for transitions in molecules shows that the excitation energies for the $n \rightarrow \pi^*$ transitions are strongly reduced, sometime leading to a large underestimation, while the $\pi \rightarrow \pi^*$ transitions obtained with the VK-functional remain in agreement with experiment and other theoretical results. For the polyacetylene oligomers we still find a large correction for the axial static polarizability with the modified kernel compared to the ALDA. Surprisingly, modifying the transverse kernel leads to a larger correction of the axial static polarizability of the model hydrogen chain, giving results closer to other theoretical values.

Chapter 1

Introduction to density functional theory

Prior to describing time-dependent density functional theory, we give a short overview of the ground state density functional theory (DFT) formalism. A recent fundamental overview of ground state DFT can be found in Ref. [28]. Books on this topic include Refs. [29] and [30].

1.1 Solving the Schrödinger equation

We would like to solve the time-independent Schrödinger equation for an isolated *N*-electron system in the Born-Oppenheimer nonrelativistic approximation, given by

$$\hat{H}\Psi\left(\mathbf{x}_1,\mathbf{x}_2,\ldots,\mathbf{x}_N\right)=E\Psi\left(\mathbf{x}_1,\mathbf{x}_2,\ldots,\mathbf{x}_N\right), \tag{1.1}$$

where E is the electronic energy, $\Psi\left(\mathbf{x}_1,\mathbf{x}_2,\ldots,\mathbf{x}_N\right)$ is the *N*-electron wave function, and $\hat{H}$ is the Hamilton operator given by

$$\hat{H}=\hat{T}+\hat{V}+\hat{W}\,. \tag{1.2}$$

In this equation $\hat{T}$ is the kinetic energy operator, $\hat{V}$ the external potential, and $\hat{W}$ the two-particle interaction. The coordinates $\mathbf{x}_i$ of electron i consist of space coordinates $\mathbf{r}_i$ and spin coordinate σ_i. Atomic units $\left(\hbar=m_e=e=4\pi\varepsilon_0=1\right)$ will be used throughout this thesis. The separate terms of Eq. (1.2) are explicitly given by:

$$\hat{T}=\sum_{i=1}^{N}\left(-\tfrac{1}{2}\nabla_i^2\right) \tag{1.3}$$

$$\hat{V}=\sum_{i=1}^{N}\upsilon\left(\mathbf{r}_i\right) \tag{1.4}$$

$$\hat{W} = \sum_{i<j}^{N} \frac{1}{\left|\mathbf{r}_i - \mathbf{r}_j\right|}, \tag{1.5}$$

where the two-particle interaction $\hat{W}$ is the Coulomb potential. We define the density operator by,

$$\hat{\rho}(\mathbf{r}) = \sum_{i=1}^{N} \delta(\mathbf{r} - \mathbf{r}_i). \tag{1.6}$$

Eq. (1.4) can be written in terms of this density operator as:

$$\hat{V} = \int \upsilon(\mathbf{r})\hat{\rho}(\mathbf{r})d\mathbf{r}, \tag{1.7}$$

its expectation value being:

$$\begin{aligned} \langle \Psi | \hat{V} | \Psi \rangle &= \int \Psi^*(\mathbf{x}_1, \mathbf{x}_2, \ldots, \mathbf{x}_N) \hat{V} \Psi(\mathbf{x}_1, \mathbf{x}_2, \ldots, \mathbf{x}_N) d\mathbf{x}_1 d\mathbf{x}_2 \ldots d\mathbf{x}_N \\ &= \int \rho(\mathbf{r})\upsilon(\mathbf{r})d\mathbf{r} \end{aligned}, \tag{1.8}$$

where we have introduced the Dirac bracket notation. The last equation contains the electron density, which is the expectation value of the density operator

$$\begin{aligned} \rho(\mathbf{r}) &= \langle \Psi | \hat{\rho}(\mathbf{r}) | \Psi \rangle \\ &= N \int \left|\Psi(\mathbf{r}\sigma_1, \ldots, \mathbf{r}_N\sigma_N)\right|^2 d\mathbf{r}_2 \ldots d\mathbf{r}_N d\sigma_1 \ldots d\sigma_N \end{aligned}. \tag{1.9}$$

When a system is in a state Ψ, which does not necessarily satisfies Eq. (1.1), the expectation value for the energy (i.e. the average of many measurements of the energy) is given by

$$E[\Psi] = \frac{\langle \Psi | \hat{H} | \Psi \rangle}{\langle \Psi | \Psi \rangle}. \tag{1.10}$$

Since each measurement gives one of the eigenvalues of the Hamiltonian operator $\hat{H}$ it follows that

$$E[\Psi] \geq E_0 \tag{1.11}$$

where E_0 is the energy of the ground state. Minimization of the *functional* $E[\Psi]$ will give a true ground state wave function Ψ_0 and energy $E[\Psi] = E_0$ (more information about functionals can be found in Appendix A). To ensure that the final Ψ will be normalized we use the method

of Lagrange multipliers in our minimization. Minimizing the quantity $\left[\langle\Psi|\hat{H}|\Psi\rangle - E\langle\Psi|\Psi\rangle\right]$ instead of just $\langle\Psi|\hat{H}|\Psi\rangle$, where E is the Lagrange multiplier, satisfies the constraint $\langle\Psi|\Psi\rangle = 1$. The Euler-Lagrange equations can be restated in a form that is equivalent to the Schrödinger equation where the Lagrange multipliers can be identified as the energy eigenvalues ,

$$\delta E = \delta\langle\Psi|\hat{H}|\Psi\rangle - E\delta\langle\Psi|\Psi\rangle = 0 . \tag{1.12}$$

Note that the energy is now a functional of *N* and $v(\mathbf{r})$. Equation (1.12) must be solved for Ψ as a function of *E*, then *E* needs to be adjusted until normalization is achieved. This variational procedure is the starting point of many *ab initio* quantum chemical methods. These methods expand the wave function Ψ in a finite set of basis functions and use the variational procedure to find the coefficients of this expansion. Since it is usually not possible to work with a complete set of basis functions approximations need to be made. The simplest *ab initio* quantum chemical method is the Hartree-Fock approximation where one tries to find the best single Slater determinant that minimizes Eq. (1.10). Going beyond the ansatz of a single-determinant wave function can reduce the limitations of the Hartree-Fock method. Such approaches include many-body perturbation techniques and the linear mixing of many determinants (called configuration interaction) [31]. In the next section we discuss another quantum chemical method that has the electron density as the basic variable instead of the wave function, this method is density functional theory (DFT).

1.2 The Hohenberg-Kohn theorems

The advantage of DFT is that it is not necessary to calculate the complicated *N*-electron wave function $\Psi(\mathbf{x}_1, \mathbf{x}_2, \ldots, \mathbf{x}_N)$. Instead one can restrict oneself to calculating the much simpler electron density $\rho(\mathbf{r})$, a fact that was first proven by Hohenberg and Kohn [1]. Their first Hohenberg-Kohn theorem states that the density $\rho(\mathbf{r})$ of a nondegenerate ground state uniquely determines the external potential $v(\mathbf{r})$ up to an arbitrary constant. From this theorem it follows that $\rho(\mathbf{r})$ determines the ground state wave function Ψ and through it all electronic properties. We proof this theorem in Appendix B.1. The consequence of the one-to-one mapping between the wave function Ψ and the density $\rho(\mathbf{r})$ is that the ground state density uniquely determines the expectation value of any operator $\hat{O}$

$$\langle \Psi[\rho] | \hat{O} | \Psi[\rho] \rangle = O[\rho]. \tag{1.13}$$

With this result we can define a universal Hohenberg-Kohn functional F_{HK} ,which is independent of the potential $\hat{V}$, as

$$F_{\mathrm{HK}}[\rho] = \langle \Psi[\rho] | \hat{T} + \hat{W} | \Psi[\rho] \rangle \tag{1.14}$$

and we find for the ground state energy functional $E_{\upsilon}[\rho]$

$$E_{\upsilon}[\rho] = \int \rho(\mathbf{r}) \upsilon(\mathbf{r}) d\mathbf{r} + F_{\mathrm{HK}}[\rho]. \tag{1.15}$$

The second Hohenberg-Kohn theorem states that for a trial density $\tilde{\rho}(\mathbf{r})$ such that $\tilde{\rho}(\mathbf{r}) \geq 0$ and $\int \tilde{\rho}(\mathbf{r}) d\mathbf{r} = N$,

$$E_0 = E_{\upsilon_0}[\rho_0] \leq E_{\upsilon_0}[\tilde{\rho}]. \tag{1.16}$$

This is the analogue of the variational principle for wave functions. This means that the exact ground state energy can be found by minimization of the energy functional

$$E_0 = \min_{\tilde{\rho}} E_{\upsilon_0}[\tilde{\rho}]. \tag{1.17}$$

An important point within DFT that we have not addressed up to now is the so-called υ-representability problem. A density is defined to be υ-representable if it is the density associated with the anti-symmetric ground-state wave function of a Hamiltonian of the form (1.2) with some external potential υ. The functional F_{HK} , for example, is only defined on the set of υ-representable densities. The υ-representability problem deals with the question of what constraints one has to put on the density to make sure it is υ-representable. This problem is discussed in more detail in Refs. [30] and [32]. In the following we will assume our densities to be υ-representable.

1.3 The Kohn-Sham equations

While the Hohenberg-Kohn theorem shows it is possible to use the ground state density to calculate properties of the system, it does not provide a way of finding the ground state density. Kohn and Sham provided a route to this [2]. The practical scheme that Kohn and Sham devised is based on a hypothetical system of noninteracting electrons, chosen in such a way that the density of this system is identical to the exact density of the physical system under

consideration. It also reintroduces the concept of orbitals into the theory as we shall later see. An elegant way to derive these so-called Kohn-Sham equations is by means of Legendre transforms as derived by Van Leeuwen [28], which we give here. A more traditional way of deriving these equations is by means of the Euler-Lagrange equation as can be found in many textbooks on this subject (for example Refs. [29] and [30]).

We start our derivation with the Schrödinger equation,

$$\left(\hat{T}+\hat{V}+\hat{W}\right)\left|\Psi[v]\right\rangle = E[v]\left|\Psi[v]\right\rangle, \tag{1.18}$$

where the ground state energy $E[v]$ and the wave function $\Psi[v]$ are considered to be functionals of the external potential and the two-particle interaction $\hat{W}$ is kept fixed. Instead of this equation we can also write,

$$E[v] = \left\langle \Psi[v]\middle|\hat{H}\middle|\Psi[v]\right\rangle. \tag{1.19}$$

The goal is to go from the potential as the basic variable to the electron density. The reason why this is possible is that the density and the potential are conjugate variables, which means that the contribution of the external potential to the total energy occurs only via an integral of the potential times the density. We can now take the *functional derivative* (see appendix A for the definition) of the energy functional $E[v]$ with respect to the potential v,

$$\begin{aligned}\frac{\delta E}{\delta v(\mathbf{r})} &= \left\langle \frac{\delta\Psi}{\delta v(\mathbf{r})}\middle|\hat{H}\middle|\Psi\right\rangle + \left\langle\Psi\middle|\hat{H}\middle|\frac{\delta\Psi}{\delta v(\mathbf{r})}\right\rangle + \left\langle\Psi\middle|\frac{\delta\hat{H}}{\delta v(\mathbf{r})}\middle|\Psi\right\rangle \\ &= E[v]\frac{\delta}{\delta v(\mathbf{r})}\langle\Psi|\Psi\rangle + \langle\Psi|\hat{\rho}(\mathbf{r})|\Psi\rangle \\ &= \langle\Psi|\hat{\rho}(\mathbf{r})|\Psi\rangle = \rho(\mathbf{r})\end{aligned}, \tag{1.20}$$

where we made explicit use of the fact that $\Psi[v]$ satisfies the Schrödinger equation with $\hat{H} = \hat{H}[v]$ as well as the normalization condition $\langle\Psi|\Psi\rangle = 1$, and that the external potential is defined as in Eq. (1.7). To go to the density as the basic variable we can use the technique of Legendre transforms. We can define the following Legendre transforms,

$$F[\rho] = E[v] - \int \rho(\mathbf{r})\, v(\mathbf{r})\, d\mathbf{r} = \left\langle \Psi[v]\middle|\hat{T}+\hat{W}\middle|\Psi[v]\right\rangle, \tag{1.21}$$

where v should now be regarded as a functional of ρ. We have already shown that the uniqueness of the mapping between v and ρ is guaranteed by the first Hohenberg-Kohn theorem.

Again $F[\rho]$ is only defined for the set of v-representable densities, but as mentioned before we assume all our densities are v-representable. Using the relation derived in Eq. (1.20) it follows that,

$$\begin{aligned}\frac{\delta F}{\delta\rho(\mathbf{r})} &= \int \frac{\delta E}{\delta v(\mathbf{r}')}\frac{\delta v(\mathbf{r}')}{\delta\rho(\mathbf{r})}d\mathbf{r}' - \frac{\delta}{\delta\rho(\mathbf{r})}\int \rho(\mathbf{r}')v(\mathbf{r}')d\mathbf{r}' \\ &= \int \rho(\mathbf{r}')\frac{\delta v(\mathbf{r}')}{\delta\rho(\mathbf{r})}d\mathbf{r}' - \int \rho(\mathbf{r}')\frac{\delta v(\mathbf{r}')}{\delta\rho(\mathbf{r})}d\mathbf{r} - \int \frac{\delta\rho(\mathbf{r}')}{\delta\rho(\mathbf{r})}v(\mathbf{r}')d\mathbf{r}. \\ &= -\int \delta(\mathbf{r}'-\mathbf{r})v(\mathbf{r}')d\mathbf{r}' = -v(\mathbf{r})\end{aligned} \tag{1.22}$$

As mentioned above we consider a system of noninteracting particles in order to derive the Kohn-Sham equations. Analogous to the hypothetical system described above, we can write the following energy functional for this system with effective external potential v_s and noninteracting wave function $|\Phi[v_s]\rangle$,

$$E_s[v_s] = \langle \Phi[v_s] | \hat{T} + \hat{V}_s | \Phi[v_s] \rangle, \tag{1.23}$$

with Legendre transform,

$$F_s[\rho] = E_s[v_s] - \int \rho(\mathbf{r})v_s(\mathbf{r})d\mathbf{r} = \langle \Phi[v_s] | \hat{T} | \Phi[v_s] \rangle \tag{1.24}$$

and derivatives

$$\frac{\delta E_s}{\delta v_s(\mathbf{r})} = \rho(\mathbf{r}) \tag{1.25}$$

$$\frac{\delta F_s}{\delta\rho(\mathbf{r})} = -v_s(\mathbf{r}). \tag{1.26}$$

The $F_s[\rho]$ in equation (1.24) is nothing more than the kinetic energy of the noninteracting system. Therefore we will from now on denote this quantity by $T_s[\rho]$. We can now define the so-called exchange-correlation functional $E_{\mathrm{xc}}[\rho]$ by,

$$F[\rho] = T_s[\rho] + \tfrac{1}{2}\iint \frac{\rho(\mathbf{r})\rho(\mathbf{r}')}{|\mathbf{r}-\mathbf{r}'|}d\mathbf{r}d\mathbf{r}' + E_{\mathrm{xc}}[\rho]. \tag{1.27}$$

Here we assume that the noninteracting system is chosen such that its density corresponds with the ground state density of the interacting system. Functional differentiating Eq. (1.27) with respect to the density $\rho(\mathbf{r})$ gives,

$$\upsilon_s(\mathbf{r}) = \upsilon(\mathbf{r}) + \int \frac{\rho(\mathbf{r}')}{|\mathbf{r}-\mathbf{r}'|} d\mathbf{r}' + \upsilon_{\mathrm{xc}}(\mathbf{r}), \tag{1.28}$$

where,

$$\upsilon_{\mathrm{xc}}(\mathbf{r}) = \frac{\delta E_{\mathrm{xc}}}{\delta \rho(\mathbf{r})} \tag{1.29}$$

defines the exchange-correlation potential. We can write the ground state wave function of a nondegenerate noninteracting system $|\Phi[\upsilon_s]\rangle$ as the antisymmetrized product of single particle orbitals $\phi_i(\mathbf{r})$ (i.e. a Slater determinant). Combining Eqs. (1.21) and (1.27) we obtain,

$$\begin{aligned} E[\upsilon] = &-\frac{1}{2}\sum_{i=1}^{N} \phi_i^*(\mathbf{r}) \nabla^2 \phi_i(\mathbf{r}) d\mathbf{r} + \int \rho(\mathbf{r}) \upsilon(\mathbf{r}) d\mathbf{r} \\ &+ \frac{1}{2} \iint \frac{\rho(\mathbf{r}) \rho(\mathbf{r}')}{|\mathbf{r}-\mathbf{r}'|} d\mathbf{r} d\mathbf{r}' + E_{\mathrm{xc}}[\rho] \end{aligned} . \tag{1.30}$$

We also obtain a one-particle Schrödinger equation,

$$\left(-\frac{1}{2}\nabla^2 + \upsilon(\mathbf{r}) + \int \frac{\rho(\mathbf{r}')}{|\mathbf{r}-\mathbf{r}'|} d\mathbf{r}' + \upsilon_{\mathrm{xc}}(\mathbf{r}) \right) \phi_i(\mathbf{r}) = \varepsilon_i \phi_i(\mathbf{r}) \tag{1.31}$$

and

$$\rho(\mathbf{r}) = \sum_{i=1}^{N} |\phi_i(\mathbf{r})|^2 . \tag{1.32}$$

Equations (1.30), (1.31), and (1.32) constitute the ground state Kohn-Sham equations [2]. These equations reduce the problem of finding the ground state density to finding a good approximation for the exchange-correlation energy. Since $\upsilon_s(\mathbf{r})$ depends on $\rho(\mathbf{r})$ the equations need to be solved self-consistently. From a guessed density one can obtain $\upsilon_s(\mathbf{r})$ and then find a new $\rho(\mathbf{r})$ from (1.31) and (1.32). One can then continue the cycle by finding a new $\upsilon_s(\mathbf{r})$ from this density and continue until self-consistency is reached.

1.4 Approximate exchange-correlation functionals

The simplest approximation one can make for the exchange-correlation energy is the local density approximation (LDA). In this approximation the exchange-correlation energy functional is given by

$$E_{\mathrm{xc}}^{\mathrm{LDA}}[\rho]=\int \rho(\mathbf{r})\varepsilon_{\mathrm{xc}}^{\mathrm{hom.}}\left(\rho(\mathbf{r})\right)d\mathbf{r}\,, \tag{1.33}$$

where $\varepsilon_{\mathrm{xc}}^{\mathrm{hom.}}(\rho)$ is the exchange-correlation energy per particle for a homogeneous electron gas evaluated at the local density $\rho(\mathbf{r})$. In this way the system is treated locally as a homogeneous electron gas. It would be expected that this approximation would only be successful for systems with a slowly varying density, but is turns out that the LDA is very successful even for very inhomogeneous systems such as atoms and molecules. The functional $\varepsilon_{\mathrm{xc}}^{\mathrm{hom.}}(\rho)$ can be split into an exchange and a correlation part. The exchange part is given by the Dirac exchange-energy functional [33],

$$\varepsilon_{\mathrm{x}}(\rho)=-\frac{3}{4}\left(\frac{3}{\pi}\rho\right)^{1/3}. \tag{1.34}$$

Accurate values for the correlation part $\varepsilon_{\mathrm{c}}(\rho)$ have been obtained by quantum Monte-Carlo calculations and have been fitted to analytical functions. The parameterization of Vosko, Wilk, and Nusair (VWN) [34] is implemented in many quantum chemical codes. Even though the LDA is successful, it has many shortcomings. For example, it neglects all nonlocal effects. It is therefore not to be expected that the LDA works in cases where the density varies strongly. Also the exchange part of the functional does not exactly cancel the self-energy part of the Hartree term, which leads to incorrect asymptotic behavior for finite systems.

Including gradients of the density in the functional can make a considerable improvement upon the LDA. A successful way to construct these gradient expanded functionals is by use of the generalized gradient approximation (GGA) [35-37]. These GGA functionals can be written as,

$$E_{\mathrm{xc}}^{\mathrm{GGA}}[\rho]=\int \rho(\mathbf{r})\varepsilon_{\mathrm{xc}}^{\mathrm{GGA}}\left(\rho(\mathbf{r}),\nabla\rho(\mathbf{r})\right)d\mathbf{r}\,. \tag{1.35}$$

The function $\varepsilon_{\mathrm{xc}}^{\mathrm{GGA}}$ is usually an analytic function with parameters that are fitted to experiment or determined by exact sum rules. The GGAs already give accurate results for many properties and systems. A newer class of GGAs are the meta-GGAs [38] that depend explicitly on the

kinetic energy density of the Kohn-Sham system. These more flexible functionals are not only dependent on the density but also on the Kohn-Sham orbitals. The GGAs and meta-GGAs improve upon the LDA but they still do not have the correct asymptotic behavior. Van Leeuwen and Baerends proposed a density functional that does have the correct asymptotic behavior [39]. Another density functional that has a correct asymptotic behavior is developed with the method of statistical averaging of (model) orbital potentials (SAOP) [40]. This potential is especially constructed for the calculation of molecular response properties and its shape reflects the atomic shell structure.

Many more functionals have been developed, and the development of more accurate functionals is an ongoing process.

Chapter 2

Time-dependent (current-)density-functional theory

In this chapter we describe the time-dependent (current-)density-functional theory (TDCDFT). We also describe how to obtain response properties such as polarizabilities and excitation energies from this theory. Gross, Dobson, and Petersilka give a thorough description of time-dependent density-functional theory (TDDFT) in their review paper [41]. Van Leeuwen gives a more fundamental description of the theory [42]. Other reviews are given by Casida Refs. [22] and [43].

2.1 The Runge-Gross theorem

The first Hohenberg-Kohn theorem states that the density $\rho(\mathbf{r})$ of a nondegenerate ground state uniquely determines the external potential $v(\mathbf{r})$ up to an arbitrary constant. Within time-dependent density functional theory we need to prove the existence of an exact mapping between the external potential and the time-dependent density $\rho(\mathbf{r},t)$. Runge and Gross proved this relation [3]. The proof is based directly on the time-dependent Schrödinger equation,

$$i\frac{\partial}{\partial t}\Psi(t) = \hat{H}(t)\Psi(t). \tag{2.1}$$

We give the full proof of Runge and Gross in Appendix B.2. Here we give a short outline of this proof. We will always work in the Schrödinger picture unless stated otherwise. The time-dependent Hamilton operator accounts for the possibility of a time dependent potential $\hat{V}(t)$.

An important constraint on the proof is that we consider only densities $\rho(\mathbf{r},t)$ that evolve from a fixed initial state $|\Psi_0\rangle$ due to some potential $v(\mathbf{r},t)$. The initial time t_0 is assumed to be finite and the potentials $v(\mathbf{r},t)$ are assumed to have a Taylor expansion around t_0. This condition of Taylor expandability excludes potentials that are switched-on adiabatically from $t_0 = -\infty$. In order to establish the time-dependent equivalent of the first Hohenberg-Kohn theorem we need to show that two densities $\rho(\mathbf{r},t)$ and $\rho'(\mathbf{r},t)$ evolving from a common

initial state $|\Psi_0\rangle$ under influence of two potentials $v(\mathbf{r},t)$ and $v'(\mathbf{r},t)$ always differ provided that the potentials differ by more than a purely time-dependent function,

$$v(\mathbf{r},t) \neq v'(\mathbf{r},t) + c(t). \tag{2.2}$$

If this is true, there is a one-to-one mapping between time-dependent densities and potentials and a time-dependent density functional theory can be constructed. The first step in the proof is to show that the corresponding current densities $\mathbf{j}(\mathbf{r},t)$ and $\mathbf{j}'(\mathbf{r},t)$ differ for $t > t_0$. Using the quantum mechanical equation of motion for the expectation value of an operator $\hat{A}(t)$,

$$\frac{\partial}{\partial t}\langle\Psi(t)|\hat{A}(t)|\Psi(t)\rangle = \langle\Psi(t)|\frac{\partial\hat{A}}{\partial t} - i\left[\hat{A}(t),\hat{H}(t)\right]|\Psi(t)\rangle. \tag{2.3}$$

and the fact that the wave functions $|\Psi\rangle$ and $|\Psi'\rangle$ evolve from a common initial state, one obtains [3],

$$\begin{aligned}\frac{\partial}{\partial t}\left(\mathbf{j}(\mathbf{r},t) - \mathbf{j}'(\mathbf{r},t)\right)\Big|_{t=t_0} &= -i\langle\Psi_0|\left[\hat{\mathbf{j}}_p(\mathbf{r}),\hat{H}(t_0) - \hat{H}'(t_0)\right]|\Psi_0\rangle \\ &= -\rho_0(\mathbf{r})\nabla\left(v(\mathbf{r},t_0) - v'(\mathbf{r},t_0)\right)\end{aligned}, \tag{2.4}$$

with initial density $\rho_0(\mathbf{r}) = \rho(\mathbf{r},t_0)$. The paramagnetic current density operator is given by

$$\hat{\mathbf{j}}_p(\mathbf{r}) = \frac{1}{2i}\sum_{i=1}^{N}\left(\nabla_{\mathbf{r}_i}\delta(\mathbf{r}-\mathbf{r}_i) + \delta(\mathbf{r}-\mathbf{r}_i)\nabla_{\mathbf{r}_i}\right). \tag{2.5}$$

After repeated use of the equation of motion one finds,

$$\frac{\partial^{k+1}}{\partial t^{k+1}}\left(\mathbf{j}(\mathbf{r},t) - \mathbf{j}'(\mathbf{r},t)\right)\Big|_{t=t_0} = -\rho_0(\mathbf{r})\nabla w_k(\mathbf{r}) \tag{2.6}$$

where

$$w_k(\mathbf{r}) = \frac{\partial^k}{\partial t^k}\left(v(\mathbf{r},t) - v'(\mathbf{r},t)\right)\Big|_{t=t_0}. \tag{2.7}$$

If Eq. (2.2) holds there must be some lowest *k* for which

$$\frac{\partial^{k+1}}{\partial t^{k+1}}\left(\mathbf{j}(\mathbf{r},t) - \mathbf{j}'(\mathbf{r},t)\right)\Big|_{t=t_0} \neq 0, \tag{2.8}$$

and hence the current densities start to differ for $t > t_0$.

This first part of the proof establishes a one-to-one correspondence between the (v-representable) current density and the potential. To show that there is also a one-to-one correspondence between the density and the potential we can make use of the continuity equation,

$$\frac{\partial}{\partial t}\left(\rho(\mathbf{r},t)-\rho'(\mathbf{r},t)\right)=-\nabla\cdot\left(\mathbf{j}(\mathbf{r},t)-\mathbf{j}'(\mathbf{r},t)\right) \tag{2.9}$$

and obtain

$$\left.\frac{\partial^{k+2}}{\partial t^{k+2}}\left(\rho(\mathbf{r},t)-\rho'(\mathbf{r},t)\right)\right|_{t=t_0}=\nabla\cdot\left(\rho_0(\mathbf{r})\nabla w_k(\mathbf{r})\right). \tag{2.10}$$

To prove that $\rho(\mathbf{r},t)$ and $\rho'(\mathbf{r},t)$ become different infinitesimally later than t_0 we need to show that the right hand side of Eq. (2.10) cannot vanish identically. This proof is done by *reductio ad absurdum*: Assume that $\nabla\cdot\left(\rho_0(\mathbf{r})\nabla w_k(\mathbf{r})\right)\equiv 0$ and evaluate the integral

$$\begin{aligned}\int\rho_0(\mathbf{r})\left|\nabla w_k(\mathbf{r})\right|^2 d\mathbf{r} &= -\int w_k(\mathbf{r})\nabla\cdot\left(\rho_0(\mathbf{r})\nabla w_k(\mathbf{r})\right)d\mathbf{r} \\ &\quad +\oint\left(\rho_0(\mathbf{r})w_k(\mathbf{r})\nabla w_k(\mathbf{r})\right)\cdot d\mathbf{S} \\ &\geq 0\end{aligned}, \tag{2.11}$$

where Gauss' theorem has been used. The surface integral vanishes for physically realistic potentials because for such potentials the $w_k(\mathbf{r})$ fall off at least as $1/r$ and the density decays exponentially. Together with our assumption that the first integral on the right hand side is zero this means that the integral on the left hand side must vanish. Since the integrand is semi definite positive,

$$\rho_0(\mathbf{r})\left|\nabla w_k(\mathbf{r})\right|^2\equiv 0 \tag{2.12}$$

and $\rho_0(\mathbf{r})>0$ everywhere, which means that $\left|\nabla w_k(\mathbf{r})\right|^2=0$ in contradiction to $w_k(\mathbf{r})\neq$ const.. This completes the proof.

Another important point that follows from Eq. (2.10) is that the difference of $\rho(\mathbf{r},t)$ and $\rho'(\mathbf{r},t)$ is linear in $w_k(\mathbf{r})$. This means that the density difference is already nonvanishing to first order in $\left(v(\mathbf{r},t)-v'(\mathbf{r},t)\right)$. A consequence of this is that it ensures the invertibility of linear response operators [42].

2.2 The time-dependent Kohn-Sham equations

Just like in case of the ground state we can consider a system of noninteracting particles with the same density as the fully interacting system and we assume noninteracting v-representability. The one-to-one correspondence of time-dependent densities and time-dependent potentials then allows us to write down the time-dependent analog of the Kohn-Sham equations,

$$\left(-\frac{1}{2}\nabla^2 + v_s(\mathbf{r},t)\right)\phi_i(\mathbf{r},t) = i\frac{\partial}{\partial t}\phi_i(\mathbf{r},t) \tag{2.13}$$

where the density,

$$\rho(\mathbf{r},t) = \sum_{i=1}^{N}\left|\phi_i(\mathbf{r},t)\right|^2 \tag{2.14}$$

is that of the interacting system. The Kohn-Sham potential can be written as,

$$v_s(\mathbf{r},t) = v(\mathbf{r},t) + v_H(\mathbf{r},t) + v_{\mathrm{xc}}(\mathbf{r},t) \tag{2.15}$$

where $v(\mathbf{r},t)$ is the external time-dependent field and the Hartree potential is defined as,

$$v_H(\mathbf{r},t) = \int \frac{\rho(\mathbf{r}',t)}{|\mathbf{r}-\mathbf{r}'|}d\mathbf{r}' . \tag{2.16}$$

Equation (2.15) defines the time-dependent xc-potential $v_{\mathrm{xc}}(\mathbf{r},t)$. Since $v_s(\mathbf{r},t)$ depends on $\rho(\mathbf{r},t)$ a self-consistent procedure needs to be used to solve the equations.

In Chapter 1 we showed that approximate solutions to the Schrödinger equation can be found by using the variational principle. For the time-dependent case one could correspondingly use the stationary action principle. But as is shown in Ref. [42] this action principle cannot be used in TDDFT. In this reference it is also shown that one can define an extended type of action functional and to define this action functional one has to use the time contour method due to Keldysh [44].

2.3 Time-dependent exchange-correlation functionals

The simplest approximation one can make for the exchange-correlation functional in the time-dependent case is the adiabatic local density approximation (ALDA), which is a straightforward extension of the local density approximation (LDA). In this approximation the static LDA functional is used for the dynamical properties, but evaluated at the time-dependent density

$$v_{\mathrm{xc}}^{\mathrm{ALDA}}(\mathbf{r},t) = v_{\mathrm{xc}}^{\mathrm{hom.}}(\rho(\mathbf{r},t)) = \frac{d}{d\rho}\left(\rho\varepsilon_{\mathrm{xc}}^{\mathrm{hom.}}(\rho)\right)\Big|_{\rho=\rho(\mathbf{r},t)} \tag{2.17}$$

where $\varepsilon_{\mathrm{xc}}^{\mathrm{hom.}}(\rho)$ is again the exchange-correlation energy per particle for a homogeneous electron gas. From this definition one would expect that the ALDA is only a good approximation for nearly homogeneous densities. But it turns out that the ALDA gives rather accurate results even in atoms and molecules where the density varies rapidly (many references are given in Ref. [41]). A quantity that will be important when we study linear response properties (Chapter 3) is the exchange-correlation kernel. It is defined as the functional derivative

$$f_{\mathrm{xc}}(\mathbf{r},\mathbf{r}',t,t') = \frac{\delta v_{\mathrm{xc}}(\mathbf{r},t)}{\delta\rho(\mathbf{r}',t')}\,. \tag{2.18}$$

For the ALDA one obtains,

$$f_{\mathrm{xc}}^{\mathrm{ALDA}}(\mathbf{r},\mathbf{r}',t,t') = \delta(t-t')\delta(\mathbf{r}-\mathbf{r}')\frac{d^2}{d\rho^2}\left(\rho\varepsilon_{\mathrm{xc}}^{\mathrm{hom.}}(\rho)\right)\Big|_{\rho=\rho_0(\mathbf{r})}\,. \tag{2.19}$$

It should be noted that the Fourier-transformed quantity

$$f_{\mathrm{xc}}^{\mathrm{ALDA}}(\mathbf{r},\mathbf{r}';\omega) = \delta(\mathbf{r}-\mathbf{r}')\frac{d^2}{d\rho^2}\left(\rho\varepsilon_{\mathrm{xc}}^{\mathrm{hom.}}(\rho)\right)\Big|_{\rho=\rho_0(\mathbf{r})} \tag{2.20}$$

has no frequency dependence.

Even though the ALDA gives good results in general, in some cases this simple approximation does not suffice. An important example is the static axial polarizability of conjugated oligomers, which is greatly overestimated within the ALDA. The local approximation and also more advanced generalized gradient approximations are unable to describe the highly nonlocal exchange and correlation effects found in these quasi-one-dimensional systems [10,11]. A solution to this problem is to employ optimized effective potentials [17] derived from the energy functional that includes exact exchange (see Refs. [18] and [19] and references therein), or approximations to this potential such as the Krieger-Li-Iafrate [20] and common-energy-denominator approximations [21,45].

We will show in this thesis that another way to improve the results of the ALDA is to use a current dependent functional in conjunction with time-dependent current-density-functional theory. One of such functionals is the VK-functional, which is an important subject of this thesis

and will be discussed in Chapter 4. In the next section we describe the foundations of time-dependent current-density-functional theory.

2.4 Time-dependent current-density-functional theory

Dhara and Ghosh [4,5] adapted the time-dependent density-functional formalism to many-electron systems subjected to external electromagnetic fields with arbitrary time-dependence. This theory was originally developed to include magnetic fields [46] but as we shall show later in this thesis it can also be important to include the current in case of an electric field. Recently Vignale [6] derived this theorem in a different way, this is the proof we give here.

The derivation is again based on the time-dependent Schrödinger equation (2.1) but with a modified Hamiltonian,

$$\hat{H}(t)=\sum_{i=1}^{N}\left[\frac{1}{2}\left(-i\nabla_i+\mathbf{A}(\mathbf{r}_i,t)\right)^2+v(\mathbf{r}_i,t)\right]+\sum_{i<j}U(\mathbf{r}_i,\mathbf{r}_j) \tag{2.21}$$

where $v(\mathbf{r},t)$ and $\mathbf{A}(\mathbf{r},t)$ are external scalar and vector potentials which are Taylor expandable in a neighborhood of $t = 0$, and $U(\mathbf{r}_i,\mathbf{r}_j)$ is a two-particle interaction. Let $\rho(\mathbf{r},t)$ and $\mathbf{j}(\mathbf{r},t)$ be the density and current density that evolve under $\hat{H}$ from a given initial state $|\Psi_0\rangle$. One can proof that the same density and current density can be obtained from another many-particle system with Hamiltonian,

$$\hat{H}'(t)=\sum_{i=1}^{N}\left[\frac{1}{2}\left(-i\nabla_i+\mathbf{A}'(\mathbf{r}_i,t)\right)^2+v'(\mathbf{r}_i,t)\right]+\sum_{i<j}U'(\mathbf{r}_i,\mathbf{r}_j) \tag{2.22}$$

starting from an initial state $|\Psi_0'\rangle$ that gives the same $\rho(\mathbf{r},0)$ and $\mathbf{j}(\mathbf{r},0)$ as $|\Psi_0\rangle$. Note that this Hamiltonian does not only have different potentials, but we also allow the two-particle interaction U to be different. The potentials $v'(\mathbf{r},t)$ and $\mathbf{A}'(\mathbf{r},t)$ are uniquely determined by $v(\mathbf{r},t)$, $\mathbf{A}(\mathbf{r},t)$, $|\Psi_0\rangle$, and $|\Psi_0'\rangle$ up to a gauge transformation

$$v'(\mathbf{r},t)\to v'(\mathbf{r},t)-\frac{\partial}{\partial t}\Lambda \tag{2.23}$$

$$\mathbf{A}'(\mathbf{r},t)\to \mathbf{A}'(\mathbf{r},t)+\nabla\Lambda(\mathbf{r},t), \tag{2.24}$$

where Λ is an arbitrary function of $\mathbf{r}$ and t that satisfies the initial condition $\Lambda(\mathbf{r},0)=0$.

The first step in the proof is that a gauge transformation will be made that eliminates the scalar potential at all times. This can be done by choosing,

$$\frac{\partial}{\partial t}\Lambda(\mathbf{r},t)=v(\mathbf{r},t),\quad \Lambda(\mathbf{r},0)=0 \tag{2.25}$$

and we assume that such a transformation has also been done in the primed system. The current density operator of the unprimed system is given by

$$\hat{\mathbf{j}}(\mathbf{r},t)=\frac{1}{2}\sum_i\left\{\mathbf{v}_i(t),\delta(\mathbf{r}-\mathbf{r}_i)\right\} \tag{2.26}$$

where the anti-commutator is denoted as $\left\{\hat{A},\hat{B}\right\}\equiv\hat{A}\hat{B}+\hat{B}\hat{A}$. The velocity operator is given by,

$$\mathbf{v}_i(t)=-i\nabla_i+\mathbf{A}(\mathbf{r}_i,t). \tag{2.27}$$

When calculating the expectation value of Eq. (2.26) and performing a partial integration, the delta function disappears and one recovers a more common expression for the current density. Analogous expressions to Eqs. (2.26) and (2.27) can be written down for the primed system.

The current density obeys the following equation of motion [6]

$$\begin{aligned}\frac{d\mathbf{j}(\mathbf{r},t)}{dt}&=\frac{\partial\mathbf{j}(\mathbf{r},t)}{\partial t}+i\left\langle\left[H(t),\hat{\mathbf{j}}(\mathbf{r},t)\right]\right\rangle\\&=\rho(\mathbf{r},t)\frac{\partial\mathbf{A}(\mathbf{r},t)}{\partial t}-\mathbf{j}(\mathbf{r},t)\times\left(\nabla\times\mathbf{A}(\mathbf{r},t)\right)+\mathbf{F}(\mathbf{r},t)+\nabla\cdot\sigma(\mathbf{r},t)\end{aligned}, \tag{2.28}$$

where we recognize that $-\partial\mathbf{A}/\partial t$ is the electric field and $\nabla\times\mathbf{A}$ the magnetic field. In this equation $\langle\ldots\rangle$ denotes the expectation value of the unprimed system at time *t*, and the stress tensor $\sigma(\mathbf{r},t)$ and the internal force density $\mathbf{F}(\mathbf{r},t)$ are defined as,

$$\sigma_{\alpha\beta}(\mathbf{r},t)=-\left\langle\tfrac{1}{4}\sum_i\left\{\hat{v}_\alpha,\left\{\hat{v}_\beta,\delta(\mathbf{r}-\mathbf{r}_i)\right\}\right\}\right\rangle \tag{2.29}$$

$$\mathbf{F}(\mathbf{r},t)=-\left\langle\sum_i\delta(\mathbf{r}-\mathbf{r}_i)\sum_{j\neq i}\nabla_{\mathbf{r}_i}U(\mathbf{r}_i-\mathbf{r}_j)\right\rangle \tag{2.30}$$

and the divergence of the stress tensor is a vector with components $[\nabla\cdot\sigma(\mathbf{r},t)]_\alpha=\Sigma_\beta\,\partial\sigma(\mathbf{r},t)/\partial\mathbf{r}_\beta$. If the same density and current density are indeed obtained from the primed system, one has,

$$\frac{d\mathbf{j}(\mathbf{r},t)}{dt}=\rho(\mathbf{r},t)\frac{\partial\mathbf{A}'(\mathbf{r},t)}{\partial t}-\mathbf{j}(\mathbf{r},t)\times\left(\nabla\times\mathbf{A}'(\mathbf{r},t)\right)+\mathbf{F}'(\mathbf{r},t)+\nabla\cdot\sigma'(\mathbf{r},t) \tag{2.31}$$

where $\langle\ldots\rangle'$ denotes the average in the quantum state of the primed system at time t. Subtracting Eqs. (2.28) and (2.31) one obtains,

$$\rho(\mathbf{r},t)\frac{\partial\Delta\mathbf{A}(\mathbf{r},t)}{\partial t}=\mathbf{j}(\mathbf{r},t)\times\left(\nabla\times\Delta\mathbf{A}(\mathbf{r},t)\right)+\mathbf{Q}(\mathbf{r},t)-\mathbf{Q}'(\mathbf{r},t) \tag{2.32}$$

where $\Delta\mathbf{A}(\mathbf{r},t)\equiv\mathbf{A}'(\mathbf{r},t)-\mathbf{A}(\mathbf{r},t)$ and

$$\mathbf{Q}(\mathbf{r},t)\equiv\mathbf{F}(\mathbf{r},t)+\nabla\cdot\sigma(\mathbf{r},t) \tag{2.33}$$

while $\mathbf{Q}'(\mathbf{r},t)$ is the primed counterpart of $\mathbf{Q}(\mathbf{r},t)$. Equation (2.32) determines the vector potential $\mathbf{A}'(\mathbf{r},t)$ that produces the same current density as $\mathbf{A}(\mathbf{r},t)$. The only question that remains to be answered is whether a solution to this equation exists and whether it is unique. It is not straightforward to prove the existence and uniqueness of the solution because $\mathbf{A}'(\mathbf{r},t)$ also enters the equation in an implicit way through $\mathbf{Q}'(\mathbf{r},t)$. Since we assume that $\mathbf{A}(\mathbf{r},t)$ and $\mathbf{A}'(\mathbf{r},t)$ are Taylor expandable around $t = 0$, the difference is Taylor expandable too. One can therefore write,

$$\Delta\mathbf{A}(\mathbf{r},t)=\sum_{k=0}^{\infty}\frac{1}{k!}\left.\frac{\partial^k\Delta\mathbf{A}(\mathbf{r})}{\partial t^k}\right|_{t=0}t^k=\sum_{k=0}^{\infty}\Delta\mathbf{A}_k(\mathbf{r})t^k\,. \tag{2.34}$$

Substituting this into Eq. (2.32) and keeping only terms of order t^l one obtains,

$$\begin{aligned}\sum_{k=0}^{l}\rho_{l-k}(\mathbf{r})\left[\frac{\partial\Delta\mathbf{A}(\mathbf{r},t)}{\partial t}\right]_k&=\sum_{k=0}^{l}\left\{\mathbf{j}_{l-k}(\mathbf{r})\times\left(\nabla\times\Delta\mathbf{A}_k(\mathbf{r})\right)\right\}\\&\quad+\left[\mathbf{Q}(\mathbf{r},t)\right]_l-\left[\mathbf{Q}'(\mathbf{r},t)\right]_l\end{aligned} \tag{2.35}$$

where $\rho_k(\mathbf{r})$ and $\mathbf{j}_k(\mathbf{r})$ denote the k^{th} coefficients in the Taylor expansions of the density and current density around $t = 0$. In general we denote $[f(t)]_l$ as the l^{th} coefficient in the Taylor expansion of a function $f(t)$ around $t = 0$. Since the vector potential and the time-dependent Schrödinger equation (Eq. (2.1)) are analytic one is allowed to do these Taylor expansions. Eq. (2.34) can be rewritten using,

$$\left[\frac{\partial\Delta\mathbf{A}(\mathbf{r},t)}{\partial t}\right]_k=(k+1)\Delta\mathbf{A}_{k+1}(\mathbf{r}) \tag{2.36}$$

yielding

$$\begin{aligned}\rho_0(\mathbf{r})(l+1)\Delta\mathbf{A}_{l+1}(\mathbf{r}) = &-\sum_{k=0}^{l-1}\rho_{l-k}(\mathbf{r})(k+1)\Delta\mathbf{A}_{k+1}(\mathbf{r}) \\ &+\sum_{k=0}^{l}\left\{\mathbf{j}_{l-k}(\mathbf{r})\times\left(\nabla\times\Delta\mathbf{A}_k(\mathbf{r})\right)\right\} \\ &+\left[\mathbf{Q}(\mathbf{r},t)\right]_l-\left[\mathbf{Q}'(\mathbf{r},t)\right]_l\end{aligned} \tag{2.37}$$

This equation is a recursion relation for the coefficients of the Taylor expansion of $\Delta\mathbf{A}(\mathbf{r},t)$ if $\Delta\mathbf{A}_{l+1}(\mathbf{r})$ is expressed in terms of $\Delta\mathbf{A}_k(\mathbf{r})$ with $k \le l$. That this is the case is immediately clear for the terms in which $\Delta\mathbf{A}_k(\mathbf{r})$ appears explicitly. But there are also implicit $\Delta\mathbf{A}_k$ s that are contained in the coefficients of the expansion of the expectation value of the stress tensor. From the time-dependent Schrödinger equation (2.1) it can be seen that the l^{th} coefficient in the Taylor expansion of $|\Psi(t)\rangle$ and $|\Psi'(t)\rangle$ is entirely determined by coefficients of order $k < l$ in the Taylor expansion of $\mathbf{A}$ and $\mathbf{A}'$. From this it follows that all the quantities on the right hand side of Eq. (2.37) are completely determined by the coefficients $\Delta\mathbf{A}_k(\mathbf{r})$ with $k \le l$. In order to make this recursion relation work the initial value of $\Delta\mathbf{A}$, $\Delta\mathbf{A}_0(\mathbf{r}) = \mathbf{A}'(\mathbf{r},0) - \mathbf{A}(\mathbf{r},0)$, still needs to be determined. Since the densities and current densities of the primed and unprimed systems are equal it immediately follows that,

$$\rho(\mathbf{r},0)\Delta\mathbf{A}_0(\mathbf{r}) = \langle\Psi'(0)|\hat{\mathbf{j}}_p(\mathbf{r})|\Psi'(0)\rangle - \langle\Psi(0)|\hat{\mathbf{j}}_p(\mathbf{r})|\Psi(0)\rangle \tag{2.38}$$

where $\hat{\mathbf{j}}_p$ is the paramagnetic current density as defined in Eq. (2.5) and has the same form for the primed and unprimed system. The recursion relation (2.37) together with the initial condition (2.38) completely determines the Taylor expansion of the vector potential $\mathbf{A}'(\mathbf{r},t)$ that yields, in the primed system, the same current density that $\mathbf{A}(\mathbf{r},t)$ yields in the unprimed one. It was assumed that knowledge of the coefficients of the Taylor expansion of $\mathbf{A}'(\mathbf{r},t)$ is equivalent to a knowledge of the function $\mathbf{A}'(\mathbf{r},t)$ itself, provided that this series converges within a non-vanishing convergence radius $t_c > 0$. If this is the case $\mathbf{A}'(\mathbf{r},t)$ is uniquely determined, since under this assumption the solution for $\mathbf{A}'(\mathbf{r},t)$ can be computed up to t_c and then the process can be iterated taking t_c as the initial time. Since under reasonable assumptions the convergence radius will not be zero for physical systems [6] this guarantees that the solution for $\mathbf{A}'(\mathbf{r},t)$ is indeed unique.

In the case that the primed system coincides with the unprimed system, i.e. $U = U'$ and $|\Psi(0)\rangle = |\Psi'(0)\rangle$, Eq. (2.38) implies that $\Delta\mathbf{A}_0(\mathbf{r}) = 0$. It then follows from Eq. (2.37) that $\Delta\mathbf{A}_k(\mathbf{r}) = 0$ for all k, so $\mathbf{A}'(\mathbf{r}) = \mathbf{A}(\mathbf{r})$ at all times. This is a statement of the Runge-Gross theorem for TDCDFT: it states that two vector potentials that produce the same current density

starting from the same initial state of a many-particle system must necessarily coincide, up to a gauge transformation. It follows that the map from vector potentials to current densities is invertible.

If the primed system is noninteracting, i.e. $U' = 0$, this theorem shows that the current density produced by a vector potential $\mathbf{A}$ in an interacting many-particle system can also be obtained in a noninteracting system, under the action of a suitable vector potential $\mathbf{A}'$. The theorem therefore provides a solid basis for the use of the time-dependent Kohn-Sham equations. These Kohn-Sham equations are given by,

$$\left(\frac{1}{2}\left[-i\nabla + \mathbf{A}_s(\mathbf{r},t)\right]^2 + v_s(\mathbf{r},t)\right)\phi_i(\mathbf{r},t) = i\frac{\partial}{\partial t}\phi_i(\mathbf{r},t) \tag{2.39}$$

$$\begin{aligned}\mathbf{j}(\mathbf{r},t) = &\frac{1}{2i}\sum_{i=1}^{N}\left(\phi_i^*(\mathbf{r},t)\nabla\phi_i(\mathbf{r},t) - \phi_i(\mathbf{r},t)\nabla\phi_i^*(\mathbf{r},t)\right) \\ &+\sum_{i=1}^{N}\left|\phi_i(\mathbf{r},t)\right|^2\mathbf{A}_s(\mathbf{r},t)\end{aligned}. \tag{2.40}$$

where $\mathbf{j}(\mathbf{r},t)$ is the current of the interacting system. These equations again need to be solved in a self-consistent fashion.

It remains to find a good approximation for the effective vector potential, which is uniquely determined by the initial state of the Kohn-Sham system as well as by the external potentials. As mentioned before we will go into more detail on such a functional in Chapter 4. In the next chapter we first describe how to obtain linear response properties such as polarizabilities, excitation energies, and oscillator strengths within the framework of time-dependent current-density-functional theory.

Chapter 3

Linear response within time-dependent current-density-functional theory

In the previous chapter we introduced the basic equations of time-dependent (current) density functional theory. In this chapter we show how to obtain properties like static and frequency dependent polarizabilities and excitation energies within the framework of linear response theory. From now on we only consider current-density-functional theory. Extensive discussions on linear response theory within ordinary TDDFT can be found in Refs. [22,42,43].

3.1 Linear response theory

We wish to describe the response of our system to a small external perturbation. This perturbation can for example be an external field. Consider a time-independent Hamiltonian $\hat{H}_0$ with an *arbitrary* time-dependent perturbation $\hat{H}(t) = \hat{H}_0 + \hat{H}_1(t)$. The change of the expectation value of a time-independent operator $\hat{A}$ as a result of this perturbation is

$$\delta A \equiv \delta\left\langle \hat{A} \right\rangle(t) = \langle \Psi(t) | \hat{A} | \Psi(t) \rangle - \langle \Psi_0 | \hat{A} | \Psi_0 \rangle \tag{3.1}$$

where Ψ_0 is the ground state wave function corresponding to $\hat{H}_0$ and $\Psi(t)$ is the solution of the time-dependent Schrödinger equation with the full Hamiltonian $\hat{H}(t)$. It is convenient to move to the Heisenberg picture with respect to $\hat{H}_0$, giving for $\Psi(t)$,

$$\left|\Psi(t)\right\rangle_H = e^{i\hat{H}_0 t} \left|\Psi(t)\right\rangle . \tag{3.2}$$

The time-evolution of this wave function can then be obtained through the following equation of motion,

$$i\frac{\partial}{\partial t}\left|\Psi(t)\right\rangle_H = \hat{H}_1(t)_H \left|\Psi(t)\right\rangle_H , \tag{3.3}$$

where

$$\hat{H}_1(t)_H = e^{i\hat{H}_0 t}\hat{H}_1(t)e^{-i\hat{H}_0 t}\,. \tag{3.4}$$

Equation (3.3) is identical to

$$\left|\Psi(t)\right\rangle_H = \left|\Psi_0\right\rangle - i\int_0^t \hat{H}_1(t')_H \left|\Psi(t')\right\rangle_H dt'\,. \tag{3.5}$$

We can now insert Eq. (3.5) in the right hand side of this same equation and generate a series in orders of $\hat{H}_1$. Since we want to do linear response we drop all terms of higher order and obtain

$$\left|\Psi(t)\right\rangle_H = \left|\Psi_0\right\rangle - i\int_0^t \hat{H}_1(t')_H \left|\Psi_0\right\rangle dt' + O\left(\hat{H}_1^2\right). \tag{3.6}$$

The expectation value of the operator $\hat{A}$ as a function of time is given by

$$\begin{aligned}\left\langle\Psi_H(t)\right|\hat{A}\left|\Psi_H(t)\right\rangle &= \left\langle\Psi_0\right|\hat{A}\left|\Psi_0\right\rangle \\ &\quad -i\int_0^t\left\langle\Psi_0\right|\left[\hat{A}(t)_H,\hat{H}_1(t')_H\right]\left|\Psi_0\right\rangle dt' + O\left(\hat{H}_1^2\right)\end{aligned} \tag{3.7}$$

where $\left[\hat{a},\hat{b}\right]$ is the commutator of operators $\hat{a}$ and $\hat{b}$. The idea of linear response theory is that $\hat{H}_1$ represents a small perturbation on the system and that terms quadratic (or higher order) in $\hat{H}_1$ are negligible. For the change of the expectation value of the operator $\hat{A}$ we then have

$$\delta A(t) \approx A_1(t) = -i\int_0^t\left\langle\Psi_0\right|\left[\hat{A}(t)_H,\hat{H}_1(t')_H\right]\left|\Psi_0\right\rangle dt' \tag{3.8}$$

Now consider the following perturbation,

$$\hat{H}_1(t)_H = \sum_i \hat{Q}_i(t)_H\,\varphi_i(t) \tag{3.9}$$

where the $\hat{Q}_i(t)$ are arbitrary time-dependent operators and the $\varphi_i(t)$ arbitrary time-dependent functions. Then the change of the expectation value of the operator $\hat{Q}_i(t)$ is given by

$$\begin{aligned}\delta Q_i(t) &= -i\int_0^t\left\langle\Psi_0\right|\left[\hat{Q}_i(t)_H,\sum_j\hat{Q}_j(t)_H\,\varphi_j(t)\right]\left|\Psi_0\right\rangle dt' \\ &= \sum_j\int_0^\infty \chi_{ij}(t,t')\varphi_j(t')dt'\end{aligned}\,. \tag{3.10}$$

Here $\chi_{ij}(t,t')$ is the response function given by

$$\chi_{ij}(t,t') = -i\Theta(t-t')\langle\Psi_0|\left[\hat{Q}_i(t)_H, \hat{Q}_j(t')_H\right]|\Psi_0\rangle \tag{3.11}$$

where $\Theta(t-t')$ is the Heaviside step function that allows us to extend the integration range to infinity and therefore ensures causality (i.e. $\chi_{ij}(t-t') = 0$ for $t < t'$). Now we can insert the resolution of the identity and go back to the Schrödinger picture to obtain

$$\begin{aligned}
&\langle\Psi_0|\hat{Q}_i(t)_H\,\hat{Q}_j(t')_H|\Psi_0\rangle = \sum_m \langle\Psi_0|\hat{Q}_i(t)_H|\Psi_m\rangle\langle\Psi_m|\hat{Q}_j(t')_H|\Psi_0\rangle \\
&= \sum_m \langle\Psi_0|e^{i\hat{H}_0 t}\hat{Q}_i e^{-i\hat{H}_0 t}|\Psi_m\rangle\langle\Psi_m|e^{i\hat{H}_0 t'}\hat{Q}_j e^{-i\hat{H}_0 t'}|\Psi_0\rangle \\
&= \sum_m e^{i(E_0-E_m)(t-t')}\langle\Psi_0|\hat{Q}_i|\Psi_m\rangle\langle\Psi_m|\hat{Q}_j|\Psi_0\rangle
\end{aligned}, \tag{3.12}$$

where Ψ_m is the exact eigenstate and E_m the exact eigenvalue of the operator $\hat{H}_0$. A similar expression is obtained for the other part of the commutator. From this it follows that the response function only depends on the time difference $(t-t')$. We obtain for the response function

$$\begin{aligned}
\chi_{ij}(t-t') = -i\Theta(t-t')\sum_m \Big\{ &e^{i(E_0-E_m)(t-t')}\langle\Psi_0|\hat{Q}_i|\Psi_m\rangle\langle\Psi_m|\hat{Q}_j|\Psi_0\rangle \\
&- e^{i(E_m-E_0)(t-t')}\langle\Psi_0|\hat{Q}_j|\Psi_m\rangle\langle\Psi_m|\hat{Q}_i|\Psi_0\rangle\Big\}
\end{aligned}. \tag{3.13}$$

A Fourier transform with respect to $(t-t')$ gives the response function in the frequency domain,

$$\chi(\omega) = \lim_{\eta\to 0^+}\sum_m\left(\frac{\langle\Psi_0|\hat{Q}_i|\Psi_m\rangle\langle\Psi_m|\hat{Q}_j|\Psi_0\rangle}{\omega-(E_m-E_0)+i\eta} - \frac{\langle\Psi_0|\hat{Q}_j|\Psi_m\rangle\langle\Psi_m|\hat{Q}_i|\Psi_0\rangle}{\omega+(E_m-E_0)+i\eta}\right), \tag{3.14}$$

where use has been made of the integral representation of the Heaviside function,

$$\Theta(\tau) = -\frac{1}{2\pi i}\lim_{\eta\to 0^+}\int_{-\infty}^{\infty}\frac{e^{-i\omega\tau}}{\omega+i\eta}d\omega\,. \tag{3.15}$$

Eq. (3.14) is the spectral or Lehmann [47] representation of the response function. We see from the Lehmann representation that the poles of the response function correspond to the excitation energies of the system.

3.2 Linear response within TDCDFT

In many works on TDDFT only the density response is considered. One of the reasons to keep our description so general is because we want to describe the response of both the density and

the current density. We use the general description of the previous section, but for the Kohn-Sham system of noninteracting particles.

To keep the description as general as possible we include the spin-dependence. We are only allowed to use a spin-dependent description if the Runge-Gross theorem can be proven for the spin-dependent case. It turns out that this is indeed so in the case of collinear spins [48]. The time- and spin-dependent Kohn-Sham equations within TDCDFT are

$$\left(\frac{1}{2}\left[-i\nabla+\mathbf{A}_{s,\sigma}(\mathbf{r},t)\right]^2+\upsilon_{s,\sigma}(\mathbf{r},t)\right)\phi_{n\sigma}(\mathbf{r},t)=i\frac{\partial}{\partial t}\phi_{n\sigma}(\mathbf{r},t), \tag{3.16}$$

where σ indicates the spin component. The full Hamiltonian is given by,

$$\hat{H}(t)=\sum_{\sigma}\sum_{i=1}^{N_\sigma}\hat{h}_\sigma(\mathbf{r}_i,t) \tag{3.17}$$

and

$$\hat{h}_\sigma(\mathbf{r},t)=\frac{1}{2}\left[-i\nabla+\mathbf{A}_{s,\sigma}(\mathbf{r},t)\right]^2+\upsilon_{s,\sigma}(\mathbf{r},t). \tag{3.18}$$

We now consider the following perturbation,

$$\hat{H}_1(t)=\sum_{\sigma}\int\left[\hat{\mathbf{j}}_{p,\sigma}(\mathbf{r})\cdot\delta\mathbf{A}_{s,\sigma}(\mathbf{r},t)+\frac{1}{2}\hat{\rho}_\sigma(\mathbf{r})\delta\mathbf{A}^2_{s,\sigma}(\mathbf{r},t)-\hat{\rho}_\sigma(\mathbf{r})\delta\upsilon_{s,\sigma}(\mathbf{r},t)\right]d\mathbf{r}, \tag{3.19}$$

where the density operator is defined in Eq. (1.6) and the (physical) current density operator in Eq. (2.5). Comparing this perturbation with Eq. (3.9) and using the theory of the previous section we obtain for the induced density and the induced current density of the noninteracting system (in the frequency domain),

$$\begin{aligned}\delta\rho_{s,\sigma}(\mathbf{r},\omega)=\sum_{\sigma'}\Big\{&\int\chi^{\sigma\sigma'}_{\rho\mathbf{j}}(\mathbf{r},\mathbf{r}',\omega)\cdot\delta\mathbf{A}_{s,\sigma'}(\mathbf{r}',\omega)d\mathbf{r}'\\&+\int\chi^{\sigma\sigma'}_{\rho\rho}(\mathbf{r},\mathbf{r}',\omega)\delta\upsilon_{s,\sigma'}(\mathbf{r}',\omega)d\mathbf{r}'\Big\}\end{aligned} \tag{3.20}$$

$$\begin{aligned}\delta\mathbf{j}_{s,\sigma}(\mathbf{r},\omega)=\sum_{\sigma'}\Big\{&\int\left(\chi^{\sigma\sigma'}_{\mathbf{jj}}(\mathbf{r},\mathbf{r}',\omega)+\rho_{0,\sigma'}(\mathbf{r})\delta(\mathbf{r}-\mathbf{r}')\right)\cdot\delta\mathbf{A}_{s,\sigma'}(\mathbf{r}',\omega)d\mathbf{r}'\\&+\int\chi^{\sigma\sigma'}_{\mathbf{j}\rho}(\mathbf{r},\mathbf{r}',\omega)\delta\upsilon_{s,\sigma'}(\mathbf{r}',\omega)d\mathbf{r}'\Big\}\end{aligned}. \tag{3.21}$$

In Eq. (3.21) an extra diamagnetic term enters as a consequence of the fact that we now consider a time-dependent vector potential, while in the previous section we assumed that our vector potential was time-independent. The response functions are given by

$$\chi_{AB}^{\sigma\sigma'}(\mathbf{r},\mathbf{r}',\omega)=\delta_{\sigma\sigma'}\sum_{n,n'}\left(n_{n\sigma}-n_{n'\sigma'}\right)\frac{\phi_{n\sigma}^{*}(\mathbf{r})\hat{A}\phi_{n'\sigma'}(\mathbf{r})\phi_{n'\sigma'}^{*}(\mathbf{r}')\hat{B}\phi_{n\sigma}(\mathbf{r}')}{\left(\varepsilon_{n\sigma}-\varepsilon_{n'\sigma'}\right)+\omega+i\eta} \tag{3.22}$$

where n and n' run over all orbitals. In this equation the density operator $\hat{\rho}=1$ and the paramagnetic current operator $\hat{\mathbf{j}}_p=-i\left(\nabla-\nabla^{\dagger}\right)/2$ can be substituted for the operators $\hat{A}$ and $\hat{B}$, and the $n_{n\sigma}$ are the occupation numbers of the Kohn-Sham orbitals. The diamagnetic term in Eq. (3.21) can also be included by making use of the conductivity sum rule,

$$\left[\chi_{\mathbf{jj}}^{s,\sigma\sigma'}(\mathbf{r},\mathbf{r}',0)\right]_{ij}+\rho_{0,\sigma}(\mathbf{r})\delta_{\sigma\sigma'}\delta_{ij}\delta(\mathbf{r}-\mathbf{r}')=0 \tag{3.23}$$

where $\rho_{0,\sigma}(\mathbf{r})$ is the spin-restricted ground state density for which $\rho_{0,\uparrow}(\mathbf{r})=\rho_{0,\downarrow}(\mathbf{r})=\rho_0(\mathbf{r})/2$. This sum rule is exact for the longitudinal component, but neglects the very small Landau diamagnetic contribution for the transverse component [49]. Using this sum rule we obtain,

$$\begin{aligned}\delta\mathbf{j}_{s,\sigma}(\mathbf{r},\omega)=\sum_{\sigma'}\Big\{&\int\left(\chi_{\mathbf{jj}}^{\sigma\sigma'}(\mathbf{r},\mathbf{r}',\omega)-\chi_{\mathbf{jj}}^{\sigma\sigma'}(\mathbf{r},\mathbf{r}',0)\right)\cdot\delta\mathbf{A}_{s,\sigma'}(\mathbf{r}',\omega)\,d\mathbf{r}'\\&+\int\chi_{\mathbf{j}\rho}^{\sigma\sigma'}(\mathbf{r},\mathbf{r}',\omega)\delta v_{s,\sigma'}(\mathbf{r}',\omega)\,d\mathbf{r}'\Big\}\end{aligned}. \tag{3.24}$$

The induced density and current density of Eqs. (3.20) and (3.21) (or (3.24)) are derived for the noninteracting Kohn-Sham system. From the extended Runge-Gross theorem we know that there exists a δv_s and a $\delta\mathbf{A}_s$ such that the change in the density and current density of the interacting and noninteracting systems will be identical:

$$\delta\rho_{\sigma}(\mathbf{r},\omega)=\delta\rho_{s,\sigma}(\mathbf{r},\omega) \tag{3.25}$$

$$\delta\mathbf{j}_{\sigma}(\mathbf{r},\omega)=\delta\mathbf{j}_{s,\sigma}(\mathbf{r},\omega). \tag{3.26}$$

We now have a way to obtain the exact induced density and current density using TDCDFT.

Until now we still have a general formalism. At this point we introduce some assumptions and a gauge, which we will use in all of the following. Our first assumption is that we work in the spin-restricted case and that there are no fractional occupation numbers. So $n_{n\uparrow}=n_{n\downarrow}=1$ for the occupied states and $n_{n\uparrow}=n_{n\downarrow}=0$ for the unoccupied states. Since, for atoms and molecules, the spectrum is discrete below the ionization level we can set the infinitesimal η in Eq. (3.22) to

zero. Another choice we make is that we choose Kohn-Sham orbitals that are real valued. This can always be done if the ground state of the system is time reversal invariant (i.e. in the absence of a magnetic field). We can now rewrite the response function as,

$$\chi_{AB}^{\sigma\tau}(\mathbf{r},\mathbf{r}',\omega)=\delta_{\sigma\tau}\sum_{i,a}\frac{\phi_{i\sigma}^{*}(\mathbf{r})\hat{A}\phi_{a\tau}(\mathbf{r})\phi_{a\tau}^{*}(\mathbf{r}')\hat{B}\phi_{i\sigma}(\mathbf{r}')}{(\varepsilon_{i\sigma}-\varepsilon_{a\tau})+\omega} + \left(\frac{\phi_{i\sigma}^{*}(\mathbf{r})\hat{A}\phi_{a\tau}(\mathbf{r})\phi_{a\tau}^{*}(\mathbf{r}')\hat{B}\phi_{i\sigma}(\mathbf{r}')}{(\varepsilon_{i\sigma}-\varepsilon_{a\tau})-\omega}\right)^{*} \tag{3.27}$$

where i runs over the occupied orbitals and a over the unoccupied orbitals, σ and τ are the corresponding spin variables. We also need to make a choice for the gauge of the potentials δv_s and $\delta\mathbf{A}_s$. We can write the first order changes in the scalar and vector potential as,

$$\delta v_{s,\sigma}(\mathbf{r},\omega)=\delta v_H(\mathbf{r},\omega)+\delta v_{\mathrm{xc},\sigma}(\mathbf{r},\omega) \tag{3.28}$$

and

$$\delta\mathbf{A}_{s,\sigma}(\mathbf{r},\omega)=\delta\mathbf{A}_{\mathrm{ext}}(\mathbf{r},\omega)+\delta\mathbf{A}_{\mathrm{xc},\sigma}(\mathbf{r},\omega), \tag{3.29}$$

where $\delta v_H(\mathbf{r},\omega)$ represents the first order change in the Hartree potential, $\delta\mathbf{A}_{\mathrm{ext}}(\mathbf{r},\omega)$ is the external field, and $\delta v_{\mathrm{xc},\sigma}(\mathbf{r},\omega)$ and $\delta\mathbf{A}_{\mathrm{xc},\sigma}(\mathbf{r},\omega)$ are the first order changes in the spin dependent scalar and vector exchange-correlation (xc) potentials. We have chosen the gauge in such a way that the external field is completely represented by the vector potential and that the induced Hartree potential is described by the scalar potential δv_H. For this gauge choice $\delta v_{\mathrm{ext}}(\mathbf{r},\omega)=0$ and $\delta\mathbf{A}_{\mathrm{ind}}(\mathbf{r},\omega)=0$ if we neglect retardations [50] and microscopic magnetic effects. This is consistent with the neglect of the Breit [51,52] corrections in the ground-state calculation. We choose our gauge such that only terms linear in $\delta\rho_{\uparrow}(\mathbf{r},\omega)$ and $\delta\rho_{\downarrow}(\mathbf{r},\omega)$ are retained in $\delta v_{\mathrm{xc},\sigma}(\mathbf{r},\omega)$, while all terms linear in $\delta\mathbf{j}_{\uparrow}(\mathbf{r},\omega)$ and $\delta\mathbf{j}_{\downarrow}(\mathbf{r},\omega)$ are gauge transformed to $\delta\mathbf{A}_{\mathrm{xc},\sigma}(\mathbf{r},\omega)$. In this way we keep contact with the ordinary TDDFT formulation. Since we work in the spin-restricted case and none of the operators operate on the spin, the continuity equation $\nabla\cdot\delta\mathbf{j}_{\sigma}(\mathbf{r},\omega)-i\omega\delta\rho_{\sigma}(\mathbf{r},\omega)=0$ holds for each spin component separately. Therefore we can consider $\delta\rho_{\sigma}(\mathbf{r},\omega)$ as a functional of $\delta\mathbf{j}_{\sigma}(\mathbf{r},\omega)$ and $\delta\mathbf{A}_{\mathrm{xc},\sigma}[\delta\mathbf{j}_{\uparrow},\delta\mathbf{j}_{\downarrow}]$ is a functional of $\delta\mathbf{j}_{\uparrow}(\mathbf{r},\omega)$ and $\delta\mathbf{j}_{\downarrow}(\mathbf{r},\omega)$ only. The first order changes in the xc-contribution can be given in the form

$$\delta v_{\mathrm{xc},\sigma}(\mathbf{r},\omega)=\sum_{\sigma'}\int f_{\mathrm{xc}}^{\sigma\sigma'}(\mathbf{r},\mathbf{r}',\omega)\delta\rho_{\sigma'}(\mathbf{r}',\omega)d\mathbf{r}' \tag{3.30}$$

and

$$\delta \mathbf{A}_{\mathrm{xc},\sigma}(\mathbf{r},\omega) = \sum_{\sigma'} \int \mathbf{f}_{\mathrm{xc}}^{\sigma\sigma'}(\mathbf{r},\mathbf{r}',\omega)\delta \mathbf{j}_{\sigma'}(\mathbf{r}',\omega)d\mathbf{r}' . \tag{3.31}$$

where we defined $f_{\mathrm{xc}}^{\sigma\sigma'}$ and $\mathbf{f}_{\mathrm{xc}}^{\sigma\sigma'}$, the spin-dependent scalar and tensor xc-kernels.

We see that our expressions for the induced density and current density (Eqs. (3.20) and (3.24)) are dependent on the scalar and vector potentials. These scalar and vector potentials are themselves dependent on the induced density and current density. Therefore we need to solve the response equations in a self-consistent way.

3.3 The polarizability

The reason to develop linear response theory within TDCDFT is that we want to use it to calculate (first order) properties as the polarizability and the excitation spectrum. We first show how to obtain the polarizability.

When a molecule is placed in an electric field it acquires an induced dipole moment given by the following relationship

$$\delta\mu(\omega) = -\int \mathbf{r}\delta\rho(\mathbf{r},\omega)d\mathbf{r} . \tag{3.32}$$

Since we work in the spin-restricted case we dropped the spin index here. Using the continuity equation $\nabla\cdot\delta\mathbf{j}(\mathbf{r},\omega) - i\omega\delta\rho(\mathbf{r},\omega) = 0$ we can write the induced dipole moment in terms of the induced current density,

$$\delta\mu(\omega) = \frac{i}{\omega}\int \delta\mathbf{j}(\mathbf{r},\omega)d\mathbf{r} . \tag{3.33}$$

In linear response the dipole moment and the polarizability are related by

$$\mu_i(\omega) = \mu_i^{(0)} + \sum_j \alpha_{ij}(\omega)E_{\mathrm{ext},j}(\omega), \tag{3.34}$$

where $\mu^{(0)}$ is the static dipole moment, and $\alpha_{ij}(\omega)$ are the elements of the polarizability tensor. From Eq. (3.33) we see that the polarizability tensor can be calculated once we have obtained $\delta\mathbf{j}(\mathbf{r},\omega)$ for a given external field $\mathbf{E}_{\mathrm{ext}}(\omega)$. If we consider an external field with only a component in the *j* direction, only one term contributes in Eq. (3.34), and we obtain

$$\alpha_{ij}(\omega) = \frac{i}{\omega}\frac{1}{E_{\mathrm{ext},j}(\omega)}\int \delta j_i(\mathbf{r},\omega)d\mathbf{r} . \tag{3.35}$$

3.4 The excitation spectrum

3.4.1 Splitting of the problem in a singlet and triplet part

Before we show how to obtain the excitation energies and oscillator strengths, we show that it is possible to split our problem in a singlet and triplet part. We start from the fact that we can show (Appendix E) that for a spin restricted ground state with $S^2|\Psi_0\rangle = S_z|\Psi_0\rangle = 0$, the following equalities hold for the response functions $\chi^{\uparrow\uparrow} = \chi^{\downarrow\downarrow}$ and $\chi^{\uparrow\downarrow} = \chi^{\downarrow\uparrow}$. We also know that

$$f_{Hxc}(1,2) = \chi_s^{-1}(1,2) - \chi^{-1}(1,2) \tag{3.36}$$

where $(1,2)$ stands for the space and time coordinates of particles 1 and 2 (so we went back to the time domain) and f_{Hxc} is the response kernel including the Hartree term. From this it follows that $f_{xc}^{\uparrow\uparrow} = f_{xc}^{\downarrow\downarrow}$ and $f_{xc}^{\uparrow\downarrow} = f_{xc}^{\downarrow\uparrow}$ and similarly for the tensor kernels $\mathbf{f}_{xc}^{\uparrow\uparrow} = \mathbf{f}_{xc}^{\downarrow\downarrow}$ and $\mathbf{f}_{xc}^{\uparrow\downarrow} = \mathbf{f}_{xc}^{\downarrow\uparrow}$.

From these observations we can show that we can split our problem in a singlet and triplet part. In order to do this we first recognize that the Hartree-xc response kernel has the same structure as the response function. We can write the response function in the form

$$\chi^{\sigma\sigma'}(1,2) = \chi_s^{\sigma\sigma'}(1,3) + \sum_{\tau\eta}\int \chi_s^{\sigma\tau}(1,2) f_{Hxc}^{\tau\eta}(3,4) \chi^{\eta\sigma'}(4,2) d3d4\,. \tag{3.37}$$

We can write out the sum in the following way

$$\chi^{\uparrow\uparrow} = \chi_s^{\uparrow\uparrow} + \chi_s^{\uparrow\uparrow} f_{Hxc}^{\uparrow\uparrow} \chi^{\uparrow\uparrow} + \chi_s^{\uparrow\uparrow} f_{Hxc}^{\uparrow\downarrow} \chi^{\downarrow\uparrow} + \chi_s^{\uparrow\downarrow} f_{Hxc}^{\downarrow\uparrow} \chi^{\uparrow\uparrow} + \chi_s^{\uparrow\downarrow} f_{Hxc}^{\downarrow\downarrow} \chi^{\downarrow\uparrow} \tag{3.38}$$

$$\chi^{\uparrow\downarrow} = \chi_s^{\uparrow\downarrow} + \chi_s^{\uparrow\uparrow} f_{Hxc}^{\uparrow\uparrow} \chi^{\uparrow\downarrow} + \chi_s^{\uparrow\uparrow} f_{Hxc}^{\uparrow\downarrow} \chi^{\downarrow\downarrow} + \chi_s^{\uparrow\downarrow} f_{Hxc}^{\downarrow\uparrow} \chi^{\uparrow\downarrow} + \chi_s^{\uparrow\downarrow} f_{Hxc}^{\downarrow\downarrow} \chi^{\downarrow\downarrow} \tag{3.39}$$

where we used a short notation leaving out the integral sign. Adding and subtracting the above equations and using the symmetry relations defined above we can rewrite these equations as

$$\chi^{\uparrow\uparrow} + \chi^{\uparrow\downarrow} = \chi_s^{\uparrow\uparrow} + \chi_s^{\uparrow\downarrow} + \left(\chi_s^{\uparrow\uparrow} + \chi_s^{\uparrow\downarrow}\right)\left(f_{Hxc}^{\uparrow\uparrow} + f_{Hxc}^{\uparrow\downarrow}\right)\left(\chi^{\uparrow\uparrow} + \chi^{\uparrow\downarrow}\right) \tag{3.40}$$

$$\chi^{\uparrow\uparrow} - \chi^{\uparrow\downarrow} = \chi_s^{\uparrow\uparrow} - \chi_s^{\uparrow\downarrow} + \left(\chi_s^{\uparrow\uparrow} - \chi_s^{\uparrow\downarrow}\right)\left(f_{Hxc}^{\uparrow\uparrow} - f_{Hxc}^{\uparrow\downarrow}\right)\left(\chi^{\uparrow\uparrow} - \chi^{\uparrow\downarrow}\right). \tag{3.41}$$

Now

$$\chi^{\uparrow\uparrow} + \chi^{\uparrow\downarrow} = \frac{1}{2}\left(\chi^{\uparrow\uparrow} + \chi^{\uparrow\downarrow} + \chi^{\downarrow\uparrow} + \chi^{\downarrow\downarrow}\right) = \frac{1}{2}\chi_{\rho\rho}(1,2) \tag{3.42}$$

where

$$\chi_{\rho\rho}(1,2) = -i\Theta(t_1 - t_2)\langle\Psi_0|\left[\hat{\rho}(\mathbf{r}_1,t_1),\hat{\rho}(\mathbf{r}_2,t_2)\right]|\Psi_0\rangle \tag{3.43}$$

and $\hat{\rho}(\mathbf{r}) = \hat{\rho}_\uparrow(\mathbf{r}) + \hat{\rho}_\downarrow(\mathbf{r})$ is the total density operator. Similarly we find for the minus combination,

$$\chi^{\uparrow\uparrow} - \chi^{\uparrow\downarrow} = \frac{1}{2}\left(\chi^{\uparrow\uparrow} - \chi^{\uparrow\downarrow} - \chi^{\downarrow\uparrow} + \chi^{\downarrow\downarrow}\right) = \frac{1}{2}\chi_{mm}(1,2) \tag{3.44}$$

where

$$\chi_{mm}(1,2) = -i\Theta(t_1 - t_2)\langle\Psi_0|\left[\hat{m}_z(\mathbf{r}_1,t_1),\hat{m}_z(\mathbf{r}_2,t_2)\right]|\Psi_0\rangle \tag{3.45}$$

and $\hat{m}_z(\mathbf{r}) = \hat{\rho}_\uparrow(\mathbf{r}) - \hat{\rho}_\downarrow(\mathbf{r})$ is the spin polarization density operator. The original response function therefore splits into two equations,

$$\chi_{\rho\rho}(1,2) = \chi_s(1,2) + \frac{1}{2}\int \chi_s(1,3)\left(f_{Hxc}^{\uparrow\uparrow}(3,4) + f_{Hxc}^{\uparrow\downarrow}(3,4)\right)\chi(4,2)\,d3d4 \tag{3.46}$$

$$\chi_{mm}(1,2) = \chi_{s,mm}(1,2) + \frac{1}{2}\int \chi_{s,mm}(1,3)\left(f_{Hxc}^{\uparrow\uparrow}(3,4) - f_{Hxc}^{\uparrow\downarrow}(3,4)\right)\chi_{mm}(4,2)\,d3d4\,. \tag{3.47}$$

So we have the usual density-density response function $\chi_{\rho\rho}(1,2) = \delta\rho(1)/\delta\upsilon(2)$; the poles of which correspond to what in Casida's work are denoted as singlet excitations. This can be understood from the fact that the matrix elements of $\hat{\rho}$ are only nonzero for states with $\Delta S = 0$ (as we showed in Appendix E). The other response function describes the change in spin-density due to an applied magnetic field in the z-direction, i.e. $\chi_{mm}(1,2) = \delta m_z(1)/\delta B_z(2)$. Its poles correspond to what in Casida's work are denoted as triplet excitations. This can be understood from the fact that the matrix elements of $\hat{m}_z$ only couple to states with $\Delta S = 1$ (as we showed in Appendix E). In the next section we use this possibility to split our equations in a singlet and triplet part.

3.4.2 The excitation energies

For obtaining the excitation spectrum we closely follow the method of Casida (Ref. [22]) for TDDFT. We extend this method to the case of TDCDFT within the approximations we stated at the end of section 3.2. In this section we first show how to obtain the excitation energies.

We can rewrite the total spin integrated induced density and induced current density (Eqs. (3.20) and (3.24)) in the following form

$$\delta\rho(\mathbf{r},\omega)=\sum_{\sigma}\sum_{i,a}\left[\phi_{i\sigma}(\mathbf{r})\phi_{a\sigma}(\mathbf{r})\mathrm{P}_{ai\sigma}(\omega)+\phi_{a\sigma}(\mathbf{r})\phi_{i\sigma}(\mathbf{r})\mathrm{P}_{ia\sigma}(\omega)\right], \tag{3.48}$$

$$\begin{aligned}\delta\mathbf{j}(\mathbf{r},\omega)=\sum_{\sigma}\sum_{i,a}\Bigg[&\frac{-\omega}{(\varepsilon_{i\sigma}-\varepsilon_{a\sigma})}\phi_{i\sigma}(\mathbf{r})\hat{\mathbf{j}}_p\phi_{a\sigma}(\mathbf{r})\mathrm{P}_{ai\sigma}(\omega)\\&+\frac{\omega}{(\varepsilon_{i\sigma}-\varepsilon_{a\sigma})}\phi_{a\sigma}(\mathbf{r})\hat{\mathbf{j}}_p\phi_{i\sigma}(\mathbf{r})\mathrm{P}_{ia\sigma}(\omega)\Bigg].\end{aligned} \tag{3.49}$$

We have defined a so-called " P -matrix"

$$\begin{aligned}\mathrm{P}_{ai\sigma}(\omega)=\frac{1}{(\varepsilon_{i\sigma}-\varepsilon_{a\sigma})+\omega}\Bigg[&\frac{-\omega}{(\varepsilon_{i\sigma}-\varepsilon_{a\sigma})}\int\phi_{a\sigma}(\mathbf{r})\hat{\mathbf{j}}_p\phi_{i\sigma}(\mathbf{r})\delta\mathbf{A}_{s,\sigma}(\mathbf{r},\omega)d\mathbf{r}\\&+\int\phi_{a\sigma}(\mathbf{r})\delta\upsilon_{s,\sigma}(\mathbf{r},\omega)\phi_{i\sigma}(\mathbf{r})d\mathbf{r}\Bigg]\end{aligned} \tag{3.50}$$

and we define $\mathrm{P}_{ia\sigma}(\omega)=\mathrm{P}^{*}_{ai\sigma}(-\omega)$. In Appendix C we show in more detail how we come to this form of the P -matrix. Inserting the definitions for $\delta\mathbf{A}_{\mathrm{s}}$ and $\delta\upsilon_{\mathrm{s}}$ (Eqs. (3.28) and (3.29)) in Eq. (3.50) and substituting $\delta\rho$ and $\delta\mathbf{j}$ with Eqs. (3.48) and (3.49) we obtain

$$\begin{aligned}\mathrm{P}_{ai\sigma}(\omega)=\frac{1}{(\varepsilon_{i\sigma}-\varepsilon_{a\sigma})+\omega}\Bigg[&\frac{-\omega}{(\varepsilon_{i\sigma}-\varepsilon_{a\sigma})}\int\phi_{a\sigma}(\mathbf{r})\hat{\mathbf{j}}_p\phi_{i\sigma}(\mathbf{r})\delta\mathbf{A}_{\mathrm{ext},\sigma}(\mathbf{r},\omega)d\mathbf{r}\\&+\sum_{jb\tau}\left(K^{\sigma\tau}_{ai,bj}(\omega)\mathrm{P}_{bj\tau}(\omega)+K^{\sigma\tau}_{ai,jb}(\omega)\mathrm{P}_{jb\tau}(\omega)\right)\Bigg]\end{aligned} \tag{3.51}$$

where we have defined an in general frequency dependent coupling matrix,

$$\begin{aligned}K^{\sigma\tau}_{ia,jb}(\omega)=&\iint\phi_{i\sigma}(\mathbf{r})\phi_{a\sigma}(\mathbf{r})\left[\frac{1}{|\mathbf{r}-\mathbf{r}'|}+f^{\sigma\tau}_{\mathrm{xc}}(\mathbf{r},\mathbf{r}',\omega)\right]\phi_{b\tau}(\mathbf{r}')\phi_{j\tau}(\mathbf{r}')d\mathbf{r}d\mathbf{r}'\\&+\frac{-\omega^2}{(\varepsilon_{i\sigma}-\varepsilon_{a\sigma})(\varepsilon_{j\sigma}-\varepsilon_{b\sigma})}\iint\phi_{i\sigma}(\mathbf{r})\hat{\mathbf{j}}_p\phi_{a\sigma}(\mathbf{r})\mathbf{f}^{\sigma\tau}_{\mathrm{xc}}(\mathbf{r},\mathbf{r}',\omega)\phi_{b\tau}(\mathbf{r}')\hat{\mathbf{j}}_p\phi_{j\tau}(\mathbf{r}')d\mathbf{r}d\mathbf{r}'\end{aligned}. \tag{3.52}$$

If the ALDA is used for the scalar exchange-correlation kernel $f^{\sigma\tau}_{\mathrm{xc}}$ and if for the tensor exchange-correlation kernel $\mathbf{f}^{\sigma\tau}_{\mathrm{xc}}$ one approximates $\mathbf{f}_{\mathrm{xc}}(\mathbf{r},\mathbf{r}',\omega)=c(\mathbf{r},\mathbf{r}')/\omega^2$, where $c(\mathbf{r},\mathbf{r}')=\lim_{\omega\to 0}\omega^2\mathbf{f}_{\mathrm{xc}}(\mathbf{r},\mathbf{r}',\omega)$, then the coupling matrix becomes frequency independent. We shall see in Chapter 4 that this approximation is the leading term in the current-dependent VK-

functional in the limit $\omega \to 0$. Therefore we will use this approximation in the following. In general, however, the tensor xc-kernel will have a more complicated frequency dependence. In order to preserve the causal structure of the response equations the Kramers-Kronig relation requires that the kernel will have both real and imaginary components. In our approximation we assume that the imaginary component is small and can be neglected for the calculation of excitation energies. This approximation is in keeping with a weak frequency dependence of the real part of $\omega^2 \mathbf{f}_{\mathrm{xc}}(\mathbf{r},\mathbf{r}',\omega)$ and is reasonable for frequencies much smaller than the local plasma frequency $\omega_p = \sqrt{4\pi\rho_0}$ of the relevant density region. For molecules, this relevant region is the often valence region with $r_s \approx 1$ ($r_s = \sqrt[3]{3/4\pi\rho_0}$) that corresponds to $\omega_p \approx 47$ eV, which is much larger than typical excitation energies we will study.

Using the definition $\mathrm{P}_{ai\sigma}(\omega) = \mathrm{P}^*_{ia\sigma}(-\omega)$ we can write an equation for $\mathrm{P}_{ia\sigma}(\omega)$ similar to Eq. (3.51) and rewrite the equations for $\mathrm{P}_{ai\sigma}(\omega)$ and $\mathrm{P}_{ia\sigma}(\omega)$ to obtain the following set of linear equations:

$$\begin{aligned}&\sum_{jb\tau}\left[\delta_{\sigma\tau}\delta_{ij}\delta_{ab}\left(\left(\varepsilon_{a\sigma}-\varepsilon_{i\sigma}\right)+\omega\right)+K^{\sigma\tau}_{ia,jb}\right]\mathrm{P}_{jb\tau}(\omega)+\sum_{jb\tau}K^{\sigma\tau}_{ia,bj}\mathrm{P}_{bj\tau}(\omega)\\&=\frac{-\omega}{\left(\varepsilon_{i\sigma}-\varepsilon_{a\sigma}\right)}\int\phi_{i\sigma}(\mathbf{r})\hat{\mathbf{j}}_p\phi_{a\sigma}(\mathbf{r})\delta\mathbf{A}_{\mathrm{ext},\sigma}(\mathbf{r},\omega)d\mathbf{r}\end{aligned}, \tag{3.53}$$

and

$$\begin{aligned}&\sum_{jb\tau}\left[\delta_{\sigma\tau}\delta_{ij}\delta_{ab}\left(\left(\varepsilon_{a\sigma}-\varepsilon_{i\sigma}\right)-\omega\right)+K^{\sigma\tau}_{ai,bj}\right]\mathrm{P}_{bj\tau}(\omega)+\sum_{jb\tau}K^{\sigma\tau}_{ai,jb}\mathrm{P}_{jb\tau}(\omega)\\&=\frac{\omega}{\left(\varepsilon_{i\sigma}-\varepsilon_{a\sigma}\right)}\int\phi_{a\sigma}(\mathbf{r})\hat{\mathbf{j}}_p\phi_{i\sigma}(\mathbf{r})\delta\mathbf{A}^*_{\mathrm{ext},\sigma}(\mathbf{r},\omega)d\mathbf{r}\end{aligned}. \tag{3.54}$$

In analogy with Ref. [22] we can put these equations in a form that originates from time-dependent Hartree-Fock theory,

$$\left\{\begin{bmatrix}\mathbf{A} & \mathbf{B}\\ \mathbf{B} & \mathbf{A}\end{bmatrix}-\omega\begin{bmatrix}-\mathbf{1} & 0\\ 0 & \mathbf{1}\end{bmatrix}\right\}\begin{pmatrix}\mathbf{X}\\ \mathbf{Y}\end{pmatrix}=\begin{pmatrix}\delta\tilde{\mathbf{A}}_{\mathrm{ext}}\\ \delta\tilde{\mathbf{A}}'_{\mathrm{ext}}\end{pmatrix}. \tag{3.55}$$

The matrices are given by

$$X_{jb\tau} = \mathrm{P}_{jb\tau}(\omega) \tag{3.56}$$

$$Y_{jb\tau} = \mathrm{P}_{bj\tau}(\omega) \tag{3.57}$$

$$A_{ia\sigma,jb\tau} = \delta_{\sigma\tau}\delta_{ab}\delta_{ij}\left(\varepsilon_{a\sigma} - \varepsilon_{i\sigma}\right) + K_{ia\sigma,jb\tau} \tag{3.58}$$

$$B_{ia\sigma,jb\tau} = K_{ia\sigma,bj\tau} \tag{3.59}$$

$$\left[\delta\tilde{\mathbf{A}}_{\text{ext}}\right]_{ia\sigma} = \frac{-\omega}{\left(\varepsilon_{i\sigma} - \varepsilon_{a\sigma}\right)}\int \phi_{i\sigma}\left(\mathbf{r}\right)\hat{\mathbf{j}}_p\phi_{a\sigma}\left(\mathbf{r}\right)\delta\mathbf{A}_{\text{ext},\sigma}\left(\mathbf{r},\omega\right)d\mathbf{r} \tag{3.60}$$

$$\left[\delta\tilde{\mathbf{A}}'_{\text{ext}}\right]_{ia\sigma} = \frac{\omega}{\left(\varepsilon_{i\sigma} - \varepsilon_{a\sigma}\right)}\int \phi_{a\sigma}\left(\mathbf{r}\right)\hat{\mathbf{j}}_p\phi_{i\sigma}\left(\mathbf{r}\right)\delta\mathbf{A}^{*}_{\text{ext},\sigma}\left(\mathbf{r},\omega\right)d\mathbf{r}\,. \tag{3.61}$$

We already showed that the poles of the response function correspond to the excitation energies. At these resonances an infinitely small perturbation can cause an infinitely large density change. In the above description this can only occur if the matrix on the left of Eq. (3.55) has a zero eigenvalue at the excitation energy. This leads to,

$$\begin{bmatrix}\mathbf{A} & \mathbf{B}\\ \mathbf{B} & \mathbf{A}\end{bmatrix}\begin{pmatrix}\mathbf{X}\\ \mathbf{Y}\end{pmatrix} = \omega\begin{bmatrix}-\mathbf{1} & 0\\ 0 & \mathbf{1}\end{bmatrix}\begin{pmatrix}\mathbf{X}\\ \mathbf{Y}\end{pmatrix}. \tag{3.62}$$

If we assume a closed-shell system for which $\phi_{i\uparrow} = \phi_{i\downarrow}$ for all i, we can split this matrix equation in a singlet and triplet part by the unitary transformation,

$$\begin{pmatrix}\mathbf{X}^S\\ \mathbf{X}^T\end{pmatrix} = \frac{1}{\sqrt{2}}\begin{pmatrix}1 & 1\\ 1 & -1\end{pmatrix}\begin{pmatrix}\mathbf{X}^{\uparrow}\\ \mathbf{X}^{\downarrow}\end{pmatrix} \tag{3.63}$$

$$\begin{pmatrix}\mathbf{Y}^S\\ \mathbf{Y}^T\end{pmatrix} = \frac{1}{\sqrt{2}}\begin{pmatrix}1 & 1\\ 1 & -1\end{pmatrix}\begin{pmatrix}\mathbf{Y}^{\uparrow}\\ \mathbf{Y}^{\downarrow}\end{pmatrix}. \tag{3.64}$$

After some algebra (see Appendix D) we obtain,

$$\begin{aligned}&\left(\mathbf{C}^{S/T} - \mathbf{D}^{S/T}\right)^{1/2}\left(\mathbf{C}^{S/T} + \mathbf{D}^{S/T}\right)\left(\mathbf{C}^{S/T} - \mathbf{D}^{S/T}\right)^{1/2}\left(\mathbf{X}^{S/T} + \mathbf{Y}^{S/T}\right)'\\ &= \omega^2\left(\mathbf{X}^{S/T} + \mathbf{Y}^{S/T}\right)'\end{aligned} \tag{3.65}$$

where $\left(\mathbf{X}^{S/T} + \mathbf{Y}^{S/T}\right)' = \left(\mathbf{C}^{S/T} - \mathbf{D}^{S/T}\right)^{-1/2}\left(\mathbf{X}^{S/T} + \mathbf{Y}^{S/T}\right)$ and

$$\left(C^{S/T}_{ia,jb} - D^{S/T}_{ia,jb}\right) = \delta_{ab}\delta_{ij}\left(\varepsilon_a - \varepsilon_i\right) \tag{3.66}$$

$$\left(C^{S}_{ia,jb} + D^{S}_{ia,jb}\right) = 2\left(K^{\uparrow\uparrow}_{ia,jb} + K^{\uparrow\downarrow}_{ia,jb}\right) \tag{3.67}$$

$$\left(C^{T}_{ia,jb} + D^{T}_{ia,jb}\right) = 2\left(K^{\uparrow\uparrow}_{ia,jb} - K^{\uparrow\downarrow}_{ia,jb}\right). \tag{3.68}$$

We used $K^{\uparrow\uparrow} = K^{\downarrow\downarrow}$ and $K^{\uparrow\downarrow} = K^{\downarrow\uparrow}$. Eq. (3.65) is a Hermitian eigenvalue equation of the following form:

$$\mathbf{\Omega}^{S/T}\mathbf{F}^{S/T}_{n} = \omega_{n}{}^{2}\mathbf{F}^{S/T}_{n} \tag{3.69}$$

where the ω_n are the excitation energies. The $\mathbf{\Omega}$ matrices are given by,

$$\Omega^{S}_{ia,jb} = \delta_{ab}\delta_{ij}\left(\varepsilon_{a} - \varepsilon_{i}\right)^{2} + 2\sqrt{\varepsilon_{a} - \varepsilon_{i}}\left(K^{\uparrow\uparrow}_{ia,jb} + K^{\uparrow\downarrow}_{ia,jb}\right)\sqrt{\varepsilon_{b} - \varepsilon_{j}} \tag{3.70}$$

$$\Omega^{T}_{ia,jb} = \delta_{ab}\delta_{ij}\left(\varepsilon_{a} - \varepsilon_{i}\right)^{2} + 2\sqrt{\varepsilon_{a} - \varepsilon_{i}}\left(K^{\uparrow\uparrow}_{ia,jb} - K^{\uparrow\downarrow}_{ia,jb}\right)\sqrt{\varepsilon_{b} - \varepsilon_{j}}\,. \tag{3.71}$$

The elements of **F** are given by

$$F^{S}_{ia\sigma} = \frac{1}{\sqrt{2}}\frac{1}{\sqrt{\varepsilon_{a\sigma} - \varepsilon_{i\sigma}}}\left(\mathrm{P}_{ia\sigma} + \mathrm{P}_{ai\sigma}\right) \tag{3.72}$$

$$F^{T}_{ia\sigma} = \frac{1}{\sqrt{2}}\frac{1}{\sqrt{\varepsilon_{a\sigma} - \varepsilon_{i\sigma}}}\left(\mathrm{P}_{ia\sigma} - \mathrm{P}_{ai\sigma}\right). \tag{3.73}$$

If the **F**'s are renormalized, which we assume from this point onward, they form a complete orthonormal set,

$$\sum_{n}\mathbf{F}_{n}\mathbf{F}^{\dagger}_{n} = 1\,. \tag{3.74}$$

So, once we have obtained the coupling matrix we can form the $\mathbf{\Omega}$ matrices for the singlet and triplet case and find the excitation energies from Eq. (3.69).

3.4.3 The oscillator strengths

We would also like to determine the oscillator strengths corresponding to the excitations. If we know the Kohn-Sham response function and the xc-kernel (vector or scalar) we know the true response function from Eq. (3.37). From the response function we can in principle obtain the excitation energies and oscillator strengths directly.

In the following we will derive equations to obtain the oscillator strengths that are convenient to implement and closely follow the derivation by Casida [22]. For this we go back to Eq. (3.55) for which we can write the separate equations as

$$\begin{aligned} \mathbf{AX} + \mathbf{BY} + \omega\mathbf{X} &= \delta\tilde{\mathbf{A}}_{\text{ext}} \\ \mathbf{BX} + \mathbf{AY} - \omega\mathbf{X} &= \delta\tilde{\mathbf{A}}'_{\text{ext}} \end{aligned} . \tag{3.75}$$

If we add and subtract the above equations, we obtain,

$$\begin{aligned} (\mathbf{A}+\mathbf{B})(\mathbf{X}+\mathbf{Y}) + \omega(\mathbf{X}-\mathbf{Y}) &= \delta\tilde{\mathbf{A}}_{\text{ext}} + \delta\tilde{\mathbf{A}}'_{\text{ext}} \\ (\mathbf{A}-\mathbf{B})(\mathbf{X}-\mathbf{Y}) + \omega(\mathbf{X}+\mathbf{Y}) &= \delta\tilde{\mathbf{A}}_{\text{ext}} - \delta\tilde{\mathbf{A}}'_{\text{ext}} \end{aligned} . \tag{3.76}$$

If we assume a real perturbation (like an electric field) we obtain

$$\begin{aligned} (\mathbf{A}+\mathbf{B})(\mathbf{X}+\mathbf{Y}) + \omega(\mathbf{X}-\mathbf{Y}) &= 2\delta\tilde{\mathbf{A}}_{\text{ext}} \\ (\mathbf{A}-\mathbf{B})(\mathbf{X}-\mathbf{Y}) + \omega(\mathbf{X}+\mathbf{Y}) &= 0 \end{aligned} \tag{3.77}$$

which we can combine into

$$\left[(\mathbf{A}+\mathbf{B}) - \omega^2 (\mathbf{A}-\mathbf{B})^{-1}\right](\mathbf{X}+\mathbf{Y}) = 2\delta\tilde{\mathbf{A}}_{\text{ext}} . \tag{3.78}$$

We note at this point that

$$\frac{1}{2}\left(X_{jb\tau} + Y_{jb\tau}\right) = \frac{1}{2}\left(\mathrm{P}_{jb\tau}(\omega) + \mathrm{P}_{bj\tau}(\omega)\right) = \frac{1}{2}\left(\mathrm{P}_{jb\tau}(\omega) + \mathrm{P}^{*}_{jb\tau}(-\omega)\right), \tag{3.79}$$

which is the Fourier transform of the real part of $\delta\mathrm{P}_{jb\tau}(t)$. We can now substitute $(\mathbf{X}+\mathbf{Y}) = 2(\mathrm{Re}\,\delta\mathrm{P})(\omega)$ in Eq. (3.78) and obtain

$$\left[(\mathbf{A}+\mathbf{B}) - \omega^2 (\mathbf{A}-\mathbf{B})^{-1}\right](\mathrm{Re}\,\delta\mathrm{P})(\omega) = \delta\tilde{\mathbf{A}}_{\text{ext}} . \tag{3.80}$$

Defining the diagonal matrix $\mathbf{S} = (\mathbf{A}-\mathbf{B})^{-1}$ and multiplying from the left with $\mathbf{S}^{-1/2}$,

$$\mathbf{S}^{-1/2}\left[(\mathbf{A}+\mathbf{B}) - \omega^2\mathbf{S}\right]\mathbf{S}^{-1/2}\mathbf{S}^{1/2}(\mathrm{Re}\,\delta\mathrm{P})(\omega) = \mathbf{S}^{-1/2}\delta\tilde{\mathbf{A}}_{\text{ext}} \tag{3.81}$$

so

$$\left[\mathbf{S}^{-1/2}(\mathbf{A}+\mathbf{B})\mathbf{S}^{-1/2} - \omega^2\right]\mathbf{S}^{1/2}(\mathrm{Re}\,\delta\mathrm{P})(\omega) = \mathbf{S}^{-1/2}\delta\tilde{\mathbf{A}}_{\text{ext}} \tag{3.82}$$

and hence

$$(\mathrm{Re}\,\delta\mathrm{P})(\omega) = \mathbf{S}^{-1/2}\left[\mathbf{S}^{-1/2}(\mathbf{A}+\mathbf{B})\mathbf{S}^{-1/2} - \omega^2\right]^{-1}\mathbf{S}^{-1/2}\delta\tilde{\mathbf{A}}_{\text{ext}} . \tag{3.83}$$

We finally obtain,

$$\left(\mathrm{Re}\,\delta\mathrm{P}\right)(\omega) = -\mathbf{S}^{-1/2}\left[\omega^2\mathbf{1} - \boldsymbol{\Omega}\right]^{-1}\mathbf{S}^{-1/2}\delta\tilde{\mathbf{A}}_{\mathrm{ext}}\,. \tag{3.84}$$

We have now written the Fourier transform of the real part of $\delta\mathrm{P}_{jb\tau}(t)$ in terms of the $\boldsymbol{\Omega}$ matrix (note that in this case the matrix is not split in its singlet and triplet parts). The polarizability can be written in terms of $\left(\mathrm{Re}\,\delta\mathrm{P}\right)(\omega)$ by substituting Eq. (3.49) for $\delta\mathbf{j}$ in Eq. (3.35) and making use of the relations $\mathbf{E}_{\mathrm{ext}} = i\omega\mathbf{A}_{\mathrm{ext}}$ and

$$\int \phi^*_{i\sigma}(\mathbf{r})\hat{\mathbf{r}}\phi_{a\sigma}(\mathbf{r})\,d\mathbf{r} = \frac{i}{\left(\varepsilon_{a\sigma} - \varepsilon_{i\sigma}\right)}\int \phi^*_{i\sigma}(\mathbf{r})\hat{\mathbf{j}}_p\phi_{a\sigma}(\mathbf{r})\,d\mathbf{r}\,. \tag{3.85}$$

We then find [22]

$$\alpha_{xz}(\omega) = 2\mathbf{x}^{\dagger}\mathbf{S}^{-1/2}\left[\boldsymbol{\Omega} - \omega^2\mathbf{1}\right]^{-1}\mathbf{S}^{-1/2}\mathbf{z} \tag{3.86}$$

where

$$x_{ia\sigma} = \int \phi^*_{i\sigma}(\mathbf{r})\hat{x}\phi_{a\sigma}(\mathbf{r})\,d\mathbf{r} \tag{3.87}$$

and similar expressions are obtained for the other Cartesian coordinates. In our case $\boldsymbol{\Omega}$ is frequency independent and we can use the following spectral expansion,

$$\left[\boldsymbol{\Omega} - \omega^2\mathbf{1}\right]^{-1} = \sum_n \frac{\mathbf{F}_n\mathbf{F}_n^{\dagger}}{\omega_n^2 - \omega^2}\,. \tag{3.88}$$

The sum over states (SOS) expression for the polarizability is given by

$$\alpha_{xz}(\omega) = 2\sum_n \frac{\left(E_n - E_0\right)\langle\Psi_0|\hat{x}|\Psi_n\rangle\langle\Psi_n|\hat{z}|\Psi_0\rangle}{\left(E_n - E_0\right)^2 - \omega^2}\,, \tag{3.89}$$

where E_0 and E_n are the (true) energies of the ground and excited states respectively, and Ψ_0 and Ψ_n are the wave functions of the respective states. The SOS expression for the average polarizability is

$$\bar{\alpha}(\omega) = \sum_n \frac{f_n}{\omega_n^2 - \omega^2}\,, \tag{3.90}$$

where $\omega_n = E_n - E_0$. If we now use the spectral expansion in Eq. (3.86) and compare the result with Eqs. (3.89) and (3.90) we find for the transition dipole moment in the *x*-direction

$$\langle\Psi_0|\hat{x}|\Psi_n\rangle = \mathbf{x}^{\dagger}\mathbf{S}^{-1/2}\mathbf{F}_n\omega_n^{-1/2}\,. \tag{3.91}$$

The oscillator strengths are then given by

$$f_n = \frac{2}{3}\left(\left|\mathbf{x}^\dagger \mathbf{S}^{-1/2}\mathbf{F}_n\right|^2 + \left|\mathbf{y}^\dagger \mathbf{S}^{-1/2}\mathbf{F}_n\right|^2 + \left|\mathbf{z}^\dagger \mathbf{S}^{-1/2}\mathbf{F}_n\right|^2\right). \tag{3.92}$$

According to the Thomas-Reiche-Kuhn (TRK) sum rule the sum of the oscillator strengths equals the number of electrons (see for example Ref. [53]). This sum rule can be used as an indication of the quality of the basis set.

Until now we made no reference to any wave function, but we would like to be able to calculate which orbitals contribute to a particular excitation. We need to make some assumptions on the ground state wave function in order to assign the states Ψ_n . Casida [22] proposes to assume that Ψ_0 is a single determinant, Φ , of Kohn-Sham orbitals and that the matrix elements of the dipole operator are linearly independent. Eq. (3.91) then becomes (in the notation of second quantization),

$$\begin{aligned}\left(\mathbf{S}^{-1/2}\mathbf{F}_n\right)_{ia\sigma} &= \sqrt{\varepsilon_{a\sigma} - \varepsilon_{i\sigma}}\,\mathbf{F}_n \\ &= \omega_n^{1/2}\left\langle \Phi \middle| \hat{a}_{i\sigma}^\dagger \hat{a}_{a\sigma} \middle| \Psi_n \right\rangle\end{aligned} \tag{3.93}$$

where $\hat{a}_{i\sigma}^\dagger$ and $\hat{a}_{a\sigma}$ are Fermi operators. This determines the coefficients of the singly excited configurations in the following expansion of the excited state:

$$\Psi_n = \sum_{ia\sigma}^{n_{i\sigma}-n_{a\sigma}>0} \sqrt{\frac{\varepsilon_{a\sigma} - \varepsilon_{i\sigma}}{\omega_n}}\, F_{ia\sigma}^n \hat{a}_{a\sigma}^\dagger \hat{a}_{i\sigma} \Phi + \ldots . \tag{3.94}$$

Within the RESPONSE code of the Amsterdam Density Functional program package (see Chapter 5)), which we use for our calculations, a further assumption is made. Namely that the excitation energies are close to the Kohn-Sham orbital energy differences, thus that the $F_{ia\sigma}^n$ can be interpreted as the expansion coefficients in Eq. (3.94). This assumption is not expected to have a large effect on the qualitative trends of the assignments.

We have now derived everything we need to obtain the excitation spectrum within TDCDFT. In the next chapter we concentrate on a particular choice for the vector xc-potential, namely the VK-functional.

Chapter 4

The Vignale-Kohn functional

In this chapter we go into more detail on one particular current-dependent functional, namely the VK-functional [8,9,23,24]. Since the exchange-correlation field in the VK theory is similar in form to the viscoelastic force that appears in the Navier-Stokes equation, we first give a short overview of the theory of viscoelastic fluids. We then give an overview of the origins of the VK-functional and we give the functional in its spin-independent and spin-dependent forms.

4.1 Introduction

Vignale and Kohn [8,9] derived their functional completely on the basis of the properties of the inhomogeneous electron gas. Later Vignale, Ullrich and Conti [23] showed that this vector exchange-correlation potential can be recast in the form that can be recognized from the theory of viscoelasticity. In view of this we first give a short review of the theory of fluid mechanics and elasticity in Sections 4.2 and 4.3, and the combined theory of viscoelasticity in Section 4.4.

In Section 4.5 we give the historic motivation of the development of the VK-functional. The rest of this chapter contains an overview of the original derivation of the functional, the spin dependent form of the VK-functional, and the functional in the static limit.

4.2 Fluid mechanics

In this section we establish the equations of motion that govern the state of a moving fluid. A detailed description of the theory of fluid mechanics can for example be found in Ref. [54]. The phenomena considered in fluid mechanics are macroscopic; this means that the fluid is regarded as a continuous medium. This means that if we speak of a small volume element we mean an element that is small compared to the volume of the body under consideration, but large compared to the distances between the molecules. We can mathematically describe the state of a moving fluid by functions that give the distribution of the fluid velocity $\mathbf{v}(\mathbf{r},t)$ and of any two thermodynamic quantities relevant to the fluid (for example the pressure $p(\mathbf{r},t)$ and the density $\rho(\mathbf{r},t)$). It is important to note that $\mathbf{v}(\mathbf{r},t)$ is the velocity of the fluid at a given point $\mathbf{r}$ in space

and at a given time *t*. So it refers to fixed points in space and not to specific particles of the fluid. These remarks also apply to other quantities like the pressure and density.

The equation that expresses the conservation of matter is the continuity equation,

$$\nabla \cdot \mathbf{j} = -\frac{\partial \rho}{\partial t}, \tag{4.1}$$

where $\mathbf{j} = \rho \mathbf{v}$ is the mass flux density. The equation of continuity is valid for *any* fluid. The equation of motion of the fluid is Euler's equation

$$\rho \frac{\partial \mathbf{v}}{\partial t} + \rho(\mathbf{v} \cdot \nabla)\mathbf{v} = -\nabla p + \mathbf{F}^{\text{ext}}, \tag{4.2}$$

where p is the pressure and the external forces per unit volume are contained in $\mathbf{F}^{\text{ext}}$, the body force. Euler's equation is only valid for an ideal fluid, in which thermal conductivity and viscosity are unimportant. Euler's equation can alternatively be written in the following form,

$$\frac{\partial}{\partial t}(\rho v_i) = -\sum_k \frac{\partial \Pi_{ik}}{\partial x_k}, \tag{4.3}$$

where we have ignored the body force. Π_{ik} is the momentum flux density tensor given by

$$\Pi_{ik} = p\delta_{ik} + \rho v_i v_k . \tag{4.4}$$

In order to obtain equations describing the motion of a viscous fluid, we have to include additional terms in the equation of motion of an ideal fluid. The momentum flux for the ideal fluid represents a completely reversible transfer of momentum, due to the mechanical transport of the different particles of fluid from place to place and to the pressure forces acting in the fluid. The viscosity causes another, irreversible, transfer of momentum from points where the velocity is large to points where it is small. The equation of motion of a viscous fluid may be obtained by adding a term $-\sigma'_{ik}$ to the momentum flux, which gives the irreversible transfer of momentum in the fluid. We thus obtain

$$\Pi_{ik} = p\delta_{ik} + \rho v_i v_k - \sigma'_{ik} = \rho v_i v_k - \sigma_{ik} . \tag{4.5}$$

Where

$$\sigma_{ik} = -p\delta_{ik} + \sigma'_{ik} \tag{4.6}$$

is called the stress tensor, and σ'_{ik} the viscous stress tensor. Since friction can only occur if different fluid particles move with different velocities, σ'_{ik} must depend on the space derivatives

of the velocity. If the velocity gradients are small, we may suppose that the momentum transfer due to viscosity depends only on the first derivatives of the velocity and is a linear function of these derivatives. We know that σ'_{ik} must vanish for **v** = constant since in that case there is no internal friction in the fluid. For the same reason $\mathbf{v} = \boldsymbol{\Omega} \times \mathbf{r}$ must vanish (where $\boldsymbol{\Omega}$ is the angular velocity) when the fluid is in uniform rotation. The latter condition is true for the following sums:

$$\frac{\partial v_i}{\partial x_k} + \frac{\partial v_k}{\partial x_i}. \tag{4.7}$$

So σ'_{ik} must contain these symmetrical combinations of the velocity derivatives. The most general tensor of rank two that satisfies the above conditions is

$$\sigma'_{ik} = \eta\left(\frac{\partial v_i}{\partial x_k} + \frac{\partial v_k}{\partial x_i} - \frac{2}{3}\sum_l \delta_{ik}\frac{\partial v_l}{\partial x_l}\right) + \zeta\sum_l \delta_{ik}\frac{\partial v_l}{\partial x_l}, \tag{4.8}$$

where η and ζ are the coefficients of viscosity. If the fluid is isotropic these coefficients are independent of velocity. The coefficients are both positive.

The equations of motion can now be obtained by adding $\partial\sigma'_{ik}/\partial x_k$ to the right hand side of Euler's equation. We then obtain

$$\begin{aligned}\rho\left(\frac{\partial v_i}{\partial t} + \sum_k v_k\frac{\partial v_i}{\partial x_k}\right) = &-\frac{\partial p}{\partial t} + F_i^{\text{ext}} \\ &+\sum_k \frac{\partial}{\partial x_k}\left\{\eta\left(\frac{\partial v_i}{\partial x_k} + \frac{\partial v_k}{\partial x_i} - \frac{2}{3}\sum_l \delta_{ik}\frac{\partial v_l}{\partial x_l}\right)\right\} + \frac{\partial}{\partial x_i}\left(\zeta\sum_l \frac{\partial v_l}{\partial x_l}\right).\end{aligned} \tag{4.9}$$

The quantities η and ζ are functions of pressure and temperature and are in general not constant throughout the fluid. If we assume that they do not change noticeably in the fluid and can be regarded as constants, we can write the equations of motion in vector form as

$$\rho\frac{D\mathbf{v}}{Dt} = \rho\left(\frac{\partial \mathbf{v}}{\partial t} + (\mathbf{v}\cdot\nabla)\mathbf{v}\right) = -\nabla p + \mathbf{F}^{\text{ext}} + \eta\nabla^2\mathbf{v} + \left(\zeta + \frac{1}{3}\eta\right)\nabla(\nabla\cdot\mathbf{v}), \tag{4.10}$$

where D/Dt is the convective derivative. This is the Navier-Stokes equation.

4.3 Elasticity

In the previous section we established the equations of motion of a fluid. We can also regard a solid body as a continuous media. It is the theory of elasticity that deals with the mechanics of solid bodies. A detailed description of the theory of elasticity can for example be found in Ref. [55].

When dealing with an elastic material instead of a liquid, we need consider the displacement vector **u** instead of the velocity **v**. The displacement vector describes the deformation of a body and is given by

$$u_i = x_i' - x_i$$

where the x_i refers to the original coordinates and x_i' to the coordinates of the displaced points. When the body is deformed the change in an element of length is given by the symmetrical strain tensor u_{ik},

$$u_{ik} = \frac{1}{2}\left(\frac{\partial u_i}{\partial x_k} + \frac{\partial u_k}{\partial x_i} + \sum_l \frac{\partial u_l}{\partial x_i}\frac{\partial u_l}{\partial x_k} \right). \tag{4.11}$$

Except for some special cases, a small deformation will also mean that u_i and its derivatives are small. If the first derivative is already small, than the last term of Eq. (4.11) will be even smaller. So for small deformations we only need to keep the linear terms,

$$u_{ik} = \frac{1}{2}\left(\frac{\partial u_i}{\partial x_k} + \frac{\partial u_k}{\partial x_i} \right). \tag{4.12}$$

After a deformation, the body will try to go back to its equilibrium state. The internal forces that arise when the body returns to equilibrium are called internal stresses. The external volume force density and these internal stresses give the total volume force density,

$$F_i = F_i^{\text{ext}} + \sum_k \frac{\partial \sigma_{ik}}{\partial x_k}. \tag{4.13}$$

The tensor σ_{ik} is, just like in the previous section, called the stress tensor. The form of the stress tensor for an elastic body is of course different from that of a liquid.

The change in volume in a deformation is given by the sum u_{ii}, if this sum is zero; the volume of the body is unchanged by the deformation. If only the shape of the body changes and its volume stays constant the deformation is called a pure shear. The opposite of this is a deformation that changes the volume of the body, but not its shape. The tensor of such a

deformation is $u_{ik} = \text{constant} \times \delta_{ik}$, this deformation is called a hydrostatic compression. We can describe any deformation by the sum of a pure shear and a hydrostatic compression. For this we can use the identity

$$u_{ik} = \left(u_{ik} - \frac{1}{3}\sum_l \delta_{ik} u_{ll} \right) + \frac{1}{3}\sum_l \delta_{ik} u_{ll} \,, \tag{4.14}$$

where the first part clearly is a pure shear and the second part is the hydrostatic compression. Using this decomposition and assuming we are dealing with a homogeneous isotropic body, we can find that the stress tensor is given in terms of the strain tensor by [55]

$$\begin{aligned} \sigma_{ik} &= 2\mu\left(u_{ik} - \frac{1}{3}\sum_l \delta_{ik} u_{ll} \right) + K\delta_{ik} u_{ll} \\ &= \mu\left(\frac{\partial u_i}{\partial x_k} + \frac{\partial u_k}{\partial x_i} \right) - \frac{2}{3}\mu \sum_l \delta_{ik} \frac{\partial u_l}{\partial x_l} + K\sum_l \delta_{ik} \frac{\partial u_l}{\partial x_l} \,, \\ &= \mu\left(\frac{\partial u_i}{\partial x_k} + \frac{\partial u_k}{\partial x_i} - \frac{2}{3}\sum_l \delta_{ik} \frac{\partial u_l}{\partial x_l} \right) + K\sum_l \delta_{ik} \frac{\partial u_l}{\partial x_l} \end{aligned} \tag{4.15}$$

where K is the *bulk modulus* or modulus of hydrostatic compression and μ is the *shear modulus* or modulus of rigidity. Substituting this stress tensor in Eq. (4.13) we obtain (in vector notation)

$$\rho \frac{D^2\mathbf{u}}{Dt^2} = \mathbf{F}^{\text{ext}} + \mu\nabla^2\mathbf{u} + \left(K + \frac{1}{3}\mu \right) \nabla\left(\nabla \cdot \mathbf{u} \right). \tag{4.16}$$

The similarity between this equation and Eq. (4.10) is obvious.

4.4 A unified viscoelastic description

In the previous two sections we described two seemingly very different systems, a fluid and a solid body. The first being described by the coefficients of viscosity η and ζ, the latter being described by the bulk modulus K and the shear modulus μ. In highly viscous fluids the sharp distinction between a fluid and a solid vanishes. Let us regard such a fluid that is elastically deformed during short intervals of time. When the deformation ceases, shear stresses remain in the fluid, although these are damped in the course of time. We indicate the time during which stresses are damped by τ. Let the fluid be subjected to external forces that vary periodically in time with frequency ω. If the period $1/\omega$ is large compared with the relaxation time, i.e. $\omega\tau \ll 1$, the fluid will behave as a viscous fluid. In this regime $\mu(\omega)$ is negligible and $\eta(\omega)$ and $\zeta(\omega)$ are finite. If the frequency is sufficiently large, i.e. $\omega\tau \gg 1$, the fluid will behave as

an amorphous solid. In this regime the viscosities are small and $\mu(\omega)$ has a finite value. The bulk modulus does not show a significant dependence on frequency in both cases.

In the previous section we obtained the equation of motion for a solid, Eq. (4.16). On the left hand side of this equation, we have the convective derivative,

$$\frac{D^2\mathbf{u}}{Dt^2} = \frac{D\mathbf{v}}{Dt} = \frac{\partial \mathbf{v}}{\partial t} + (\mathbf{v}\cdot\nabla)\mathbf{v}\,. \tag{4.17}$$

The quantity $\rho(\mathbf{v}\cdot\nabla)\mathbf{v}$ is of second order in the velocity, since we look at the linear response of our system we obtain for Eq. (4.16),

$$\rho\frac{\partial^2\mathbf{u}}{\partial t^2} = \mathbf{F}^{\text{ext}} + \mu\nabla^2\mathbf{u} + \left(K + \frac{1}{3}\mu\right)\nabla(\nabla\cdot\mathbf{u})\,. \tag{4.18}$$

Let us consider time-dependent forces of the form

$$\mathbf{F}(\mathbf{r},t) = \frac{1}{(2\pi)^4}\int\int \mathbf{F}(\mathbf{q},\omega)e^{i(\mathbf{q}\cdot\mathbf{r}-\omega t)}d\mathbf{q}d\omega\,, \tag{4.19}$$

which induce time-dependent displacements

$$\mathbf{u}(\mathbf{r},t) = \frac{1}{(2\pi)^4}\int\int \mathbf{u}(\mathbf{q},\omega)e^{i(\mathbf{q}\cdot\mathbf{r}-\omega t)}d\mathbf{q}d\omega\,. \tag{4.20}$$

We can write the force as the time derivative of a vector potential **A**,

$$\mathbf{F}(\mathbf{r},t) = \rho\frac{\partial\mathbf{A}(\mathbf{r},t)}{\partial t} \tag{4.21}$$

and introduce the current density

$$\mathbf{j}(\mathbf{r},t) = \rho\frac{\partial\mathbf{u}(\mathbf{r},t)}{\partial t}\,. \tag{4.22}$$

Fourier transforming Eq. (4.18) we obtain,

$$\begin{aligned} -i\omega\mathbf{j}(\mathbf{q},\omega) = -i\omega\rho\mathbf{A}(\mathbf{q},\omega) + \mu\frac{1}{\rho}\frac{q^2}{i\omega}\mathbf{j}(\mathbf{q},\omega) \\ +\left(K+\frac{1}{3}\mu\right)\frac{1}{\rho}\frac{\mathbf{q}(\mathbf{q}\cdot\mathbf{j}(\mathbf{q},\omega))}{i\omega} \end{aligned}\,. \tag{4.23}$$

In the same way we can rewrite the Navier-Stokes equation, Eq. (4.10). Eventually we want to obtain a uniform expression for a viscoelastic body, therefore we would like to rewrite the pressure term in Eq. (4.10) in terms of the bulk modulus $K = \rho \partial p / \partial \rho$. We can rewrite the pressure term using the continuity equation

$$\rho(\mathbf{q},\omega) = \frac{\mathbf{q}}{\omega} \cdot \mathbf{j}(\mathbf{q},\omega) \tag{4.24}$$

to obtain

$$-\nabla p(\mathbf{q},\omega) = -\frac{K}{\rho}\nabla\rho(\mathbf{q},\omega) = \frac{K}{\rho}\mathbf{q}\left(\frac{\mathbf{q}\cdot\mathbf{j}(\mathbf{q},\omega)}{i\omega}\right). \tag{4.25}$$

The Navier-Stokes equation can than be rewritten as,

$$\begin{aligned} -i\omega\mathbf{j}(\mathbf{q},\omega) = -i\omega\rho\mathbf{A}(\mathbf{q},\omega) - i\omega\eta\frac{1}{\rho}\frac{q^2}{i\omega}\mathbf{j}(\mathbf{q},\omega) \\ +\left(K - i\omega\zeta - \frac{1}{3}\eta\right)\frac{1}{\rho}\frac{\mathbf{q}(\mathbf{q}\cdot\mathbf{j}(\mathbf{q},\omega))}{i\omega} \end{aligned}. \tag{4.26}$$

Equation (4.26) only differs from Eq. (4.23) in the following: (i) The shear modulus μ is replaced by the imaginary quantity $-i\omega\eta$, which vanishes at $\omega = 0$. (ii) The bulk modulus K acquires an imaginary part $-i\omega\zeta$.

We can now combine Eqs. (4.23) and (4.26) to obtain the expression for the viscoelastic case,

$$\begin{aligned} -i\omega\mathbf{j}(\mathbf{q},\omega) = -i\omega\rho\mathbf{A}(\mathbf{q},\omega) + \tilde{\mu}(\omega)\frac{1}{\rho}\frac{q^2}{i\omega}\mathbf{j}(\mathbf{q},\omega) \\ +\left(\tilde{K}(\omega) + \frac{1}{3}\tilde{\mu}(\omega)\right)\frac{1}{\rho}\frac{\mathbf{q}(\mathbf{q}\cdot\mathbf{j}(\mathbf{q},\omega))}{i\omega} \end{aligned} \tag{4.27}$$

where we defined the complex frequency-dependent viscoelastic coefficients,

$$\tilde{K}(\omega) = K(\omega) - i\omega\zeta(\omega) \tag{4.28}$$

$$\tilde{\mu}(\omega) = \mu(\omega) - i\omega\eta(\omega). \tag{4.29}$$

An important difference between a solid and a fluid is that a solid has an essentially real $\tilde{\mu}$ and the fluid has an essentially imaginary $\tilde{\mu}$.

4.5 Historic motivation for the development of the VK-functional

In Chapter 3 we saw that in the case of linear response the scalar xc-potential is given by

$$\delta v_{\mathrm{xc}}(\mathbf{r},\omega) = \int f_{\mathrm{xc}}(\mathbf{r},\mathbf{r}',\omega)\,\delta\rho(\mathbf{r}',\omega)\,d\mathbf{r}' \tag{4.30}$$

where the xc-kernel f_{xc} is a functional of the ground state density $\rho_0(\mathbf{r})$. The simplest approximation for this xc-kernel is the frequency independent adiabatic local density approximation (ALDA) of Eq. (2.19). The ALDA is only valid when the external potential is slowly varying in time as well as in space. In a first step towards overcoming the restriction to slow variation in time, Gross and Kohn (GK) [56] considered the case where both $\rho_0(\mathbf{r})$ and $\delta\rho(\mathbf{r})$ are sufficiently slowly varying functions of $\mathbf{r}$. Their approximation was designed to preserve the local relationship between δv_{xc} and the density, while including retardation in time. They proposed the following form of the xc-kernel,

$$\delta v_{\mathrm{xc}}^{\mathrm{GK}}(\mathbf{r},\omega) = f_{\mathrm{xc}}^{\mathrm{hom.}}\left(\omega;\rho_0(\mathbf{r})\right)\delta\rho(\mathbf{r},\omega) \tag{4.31}$$

where $f_{\mathrm{xc}}^{\mathrm{hom.}}$ is the xc-kernel of the homogeneous electron gas and $f_{\mathrm{xc}}^{\mathrm{hom.}}\left(\omega;\rho_0(\mathbf{r})\right) = \int f_{\mathrm{xc}}^{\mathrm{hom.}}\left(|\mathbf{r}-\mathbf{r}'|;\omega;\rho_0(\mathbf{r})\right)d\mathbf{r}'$. This is a frequency dependent function that for $\omega = 0$ reduces to the ALDA. Later Dobson [57] found that this approximation violates the so-called harmonic potential theorem (HPT) according to which the density follows rigidly the classical motion of the center of mass when subjected to a static harmonic potential $Kr^2/2$. Dobson observed that the HPT could be satisfied by requiring that the GK approximation be applied in a frame of reference that is moving with the local velocity of the electron fluid. This led to the following approximation [57]

$$\begin{aligned}\delta v_{\mathrm{xc}}^{\mathrm{Dobson}}(\mathbf{r},\omega) = f_{\mathrm{xc}}^{\mathrm{hom.}}\left(\omega;\rho_0(\mathbf{r})\right)\left[\delta\rho(\mathbf{r},\omega) - \frac{\nabla\rho_0(\mathbf{r})\cdot\delta\mathbf{j}(\mathbf{r},\omega)}{i\omega\rho_0(\mathbf{r})}\right] \\ + f_{\mathrm{xc}}^{\mathrm{hom.}}\left(\omega=0;\rho_0(\mathbf{r})\right)\frac{\nabla\rho_0(\mathbf{r})\cdot\delta\mathbf{j}(\mathbf{r},\omega)}{i\omega\rho_0(\mathbf{r})}\end{aligned}. \tag{4.32}$$

So this xc-potential is a functional of the density and the *current* density. The fact that the current density enters in the Dobson functional is especially interesting since the current density on a point in the system can probe a rigid translation of the system itself. It is a local indicator of a nonlocal effect.

In order to gain more insight in the problem with the GK potential the theory was studied under transformation to an accelerated frame of reference. Vignale [58] observed for such

transformations that, if $\rho'(\mathbf{r},t)=\rho(\mathbf{r}+\mathbf{x}(t),t)$, where $\rho(\mathbf{r},t)$ is an arbitrary time-dependent density and $\mathbf{x}(t)$ is an arbitrary time-dependent vector, the xc-potentials associated with the densities $\rho(\mathbf{r},t)$ and $\rho'(\mathbf{r},t)$ must satisfy the symmetry relation

$$v_{\mathrm{xc}}[\rho';\mathbf{r},t]=v_{\mathrm{xc}}[\rho;\mathbf{r}+\mathbf{x}(t),t]. \tag{4.33}$$

This symmetry relation is violated by Eq. (4.31). From this relation it can also be deduced that f_{xc} for a non-uniform system is of long range in space and does not admit a gradient expansion [59]. Therefore a local-density approximation for the time-dependent xc-potential in general does not exist. Vignale and Kohn showed [8] that this result is a consequence of the choice to represent the xc-potential as a functional of the density.

4.6 The VK-functional

The arguments in the previous section suggest the development of a functional that is dependent on the current density. This implies moving to time-dependent current-density functional theory (Chapter 2 and Chapter 3). In Chapter 3 we saw that in the case of linear response the vector xc-potential is given by

$$\delta\mathbf{A}_{\mathrm{xc}}(\mathbf{r},\omega)=\int\mathbf{f}_{\mathrm{xc}}(\mathbf{r},\mathbf{r}',\omega)\delta\mathbf{j}(\mathbf{r}',\omega)d\mathbf{r}'. \tag{4.34}$$

where we choose to work in the same gauge as Vignale and Kohn [8,9], in which everything is contained in the vector potential. The tensor xc-kernel $\mathbf{f}_{\mathrm{xc}}(\mathbf{r},\mathbf{r}',\omega)$ is defined as

$$f_{\mathrm{xc},ij}(\mathbf{r},\mathbf{r}',\omega)=\chi_{s,ij}^{-1}(\mathbf{r},\mathbf{r}',\omega)-\chi_{ij}^{-1}(\mathbf{r},\mathbf{r}',\omega)+\frac{1}{\omega^2}\nabla_i\frac{1}{|\mathbf{r}-\mathbf{r}'|}\nabla_j \tag{4.35}$$

where χ_s and χ are the response functions for the noninteracting Kohn-Sham system and the interacting system respectively. It is clear that this tensor xc-kernel is the central unknown quantity. Vignale and Kohn [8,9] derived some exact properties for this kernel and from these found an expression for the exchange-correlation vector potential. It goes beyond the scope of this thesis to show the complete derivation of their functional. Therefore we only show some important steps and considerations in this section.

Vignale and Kohn first derived some properties of $\mathbf{f}_{\mathrm{xc}}$ for the case of the homogeneous electron gas. For this system it is convenient to work with the Fourier transform with respect to $|\mathbf{r}-\mathbf{r}'|$ and *t*. Using the fact that any field can be split up in a longitudinal and transverse part and the properties of the homogeneous electron gas, one can show that the xc-kernel has the following structure,

$$f_{\mathrm{xc},ij}^{\mathrm{hom.}}(\mathbf{k},\omega)=\frac{1}{\omega^2}\Big[f_{\mathrm{xcL}}(\mathbf{k},\omega)k_ik_j+f_{\mathrm{xcT}}(\mathbf{k},\omega)\Big(|\mathbf{k}|^2\,\delta_{ij}-k_ik_j\Big)\Big] \tag{4.36}$$

where f_{xcL} and f_{xcT} are the longitudinal and transverse response kernels and are properties of the *homogeneous* electron gas. Their Fourier transform is given by

$$f(\mathbf{k},\omega)=\int\int f(\mathbf{r},t)\,e^{-i(\mathbf{k}\cdot\mathbf{r}-\omega t)}d\mathbf{r}dt\ . \tag{4.37}$$

One can show that in the limit $k\to 0$ the functions $f_{\mathrm{xcL(T)}}$ are finite functions of the frequency

$$\lim_{k\to 0} f_{\mathrm{xcL(T)}}(\mathbf{k},\omega)=f_{\mathrm{xcL(T)}}(\omega)\,. \tag{4.38}$$

With this relation one obtains that

$$f_{\mathrm{xc},ij}^{\mathrm{hom.}}(\mathbf{k},\omega)=\frac{1}{\omega^2}\Big[f_{\mathrm{xcL}}(\omega)k_ik_j+f_{\mathrm{xcT}}(\omega)\Big(|\mathbf{k}|^2\,\delta_{ij}-k_ik_j\Big)\Big] \tag{4.39}$$

is a good approximation in the limit of small wave vector *k*, which for fixed frequency means that $k\ll k_F$ and $k\ll\omega/\upsilon_F$ where k_F and υ_F are the Fermi momentum and velocity.

In the second part of the derivation Vignale and Kohn consider a weakly modulated electron gas that has the following ground state density,

$$\rho_0(\mathbf{r})=\bar{\rho}\big(1+2\gamma\cos(\mathbf{q}\cdot\mathbf{r})\big) \tag{4.40}$$

The parameter γ measures the amplitude of the density oscillation and $\mathbf{q}$ measures the wavelength of the oscillation, so together they determine the inhomogeneity of the system. In their derivation Vignale and Kohn assume that this system is slowly varying ($q\ll k_F,\omega/\upsilon_F$) and almost uniform ($\gamma\ll 1$). The objective is to find the exact $\mathbf{f}_{\mathrm{xc}}$ for this system to first order in γ.

The density is periodic in the direction $\mathbf{a}$; $\rho_0(\mathbf{r}+\mathbf{a})=\rho_0(\mathbf{r})$ for $\mathbf{q}\cdot\mathbf{a}=2\pi m$ where *m* is an integer. The xc-kernel has the same periodicity,

$$f_{\mathrm{xc},ij}(\mathbf{r}+\mathbf{a},\mathbf{r}'+\mathbf{a},\omega)=f_{\mathrm{xc},ij}(\mathbf{r},\mathbf{r}',\omega) \tag{4.41}$$

One can then show that $\mathbf{f}_{\mathrm{xc}}$ has the expansion

$$f_{\mathrm{xc},ij}(\mathbf{r},\mathbf{r}',\omega)=\frac{1}{(2\pi)^3}\sum_{m=-\infty}^{\infty}\int f_{\mathrm{xc},ij}(\mathbf{k}+m\mathbf{q},\mathbf{k},\omega)\,e^{i(\mathbf{k}+m\mathbf{q})\cdot\mathbf{r}}e^{-i\mathbf{k}\cdot\mathbf{r}'}d\mathbf{k} \tag{4.42}$$

where the coefficients are defined as

$$f_{\mathrm{xc},ij}\left(\mathbf{k}+m\mathbf{q},\mathbf{k},\omega\right)=\frac{1}{V}\int\int f_{\mathrm{xc},ij}\left(\mathbf{r},\mathbf{r}',\omega\right)e^{-i(\mathbf{k}+m\mathbf{q})\cdot\mathbf{r}}e^{i\mathbf{k}\cdot\mathbf{r}'}d\mathbf{r}d\mathbf{r}' \tag{4.43}$$

where V is the volume of the system. To first order in γ only the coefficients with $m=0,\pm1$ contribute to the expansion of Eq. (4.42). For $m=0$ one obtains

$$f_{\mathrm{xc},ij}\left(\mathbf{k},\mathbf{k},\omega\right)=f_{\mathrm{xc}}^{\mathrm{hom.}}\left(\mathbf{k},\omega\right) \tag{4.44}$$

to first order in γ. The only task that remains is to find an expression for $\mathbf{f}_{\mathrm{xc}}\left(\mathbf{k}\pm\mathbf{q},\mathbf{k},\omega\right)$. The form of this function is completely determined by Eq. (4.39) and a set of exact relations for the xc-kernel. The first of these relations is the Onsager symmetry relation,

$$f_{\mathrm{xc},ij}\left(\mathbf{k}+m\mathbf{q},\mathbf{k},\omega\right)=f_{\mathrm{xc},ji}\left(-\mathbf{k},-\mathbf{k}-m\mathbf{q},\omega\right) \tag{4.45}$$

that is valid if the unperturbed system has time-reversal symmetry (i.e. in the absence of magnetic fields). The second relation is referred to by Vignale and Kohn as the Ward identity,

$$\lim_{\mathbf{q}\to0}f_{\mathrm{xc},ij}\left(\mathbf{k}+\mathbf{q},\mathbf{k},\omega\right)=\gamma\bar{\rho}\frac{\partial f_{\mathrm{xc},ij}^{\mathrm{hom.}}\left(\mathbf{k},\omega\right)}{\partial\bar{\rho}}. \tag{4.46}$$

There are two more relations that arise from the fact that the xc-field does not apply forces or torques to the system. From these zero-force and zero-torque theorems it follows that

$$\lim_{\mathbf{k}\to0}f_{\mathrm{xc},ij}\left(\mathbf{k}+\mathbf{q},\mathbf{k},\omega\right)=\frac{-\gamma}{\omega}\left[\delta f_{\mathrm{xcL}}\left(\omega\right)q_iq_j+f_{\mathrm{xcT}}\left(\omega\right)\left(q^2\delta_{ij}-q_iq_j\right)\right] \tag{4.47}$$

$$\lim_{\mathbf{k}\to0}\sum_{j,k}\varepsilon_{ljk}\frac{\partial f_{\mathrm{xc},ij}\left(\mathbf{k}+\mathbf{q},\mathbf{k},\omega\right)}{\partial k_k}=\frac{-\gamma}{\omega}\left[\delta f_{\mathrm{xcL}}\left(\omega\right)-3f_{\mathrm{xcT}}\left(\omega\right)\right]\sum_k\varepsilon_{lki}q_k\,. \tag{4.48}$$

From these relations the following expression for $\mathbf{f}_{\mathrm{xc}}\left(\mathbf{k}+\mathbf{q},\mathbf{k},\omega\right)$ is obtained;

$$\begin{aligned}f_{\mathrm{xc},ij}\left(\mathbf{k}+\mathbf{q},\mathbf{k},\omega\right)=\frac{-\gamma}{\omega^2}\Big[&\left(\delta f_{\mathrm{xcL}}\left(\omega\right)-f_{\mathrm{xcT}}\left(\omega\right)\right)q_iq_j\\&+f_{\mathrm{xcT}}\left(\omega\right)\delta_{ij}q^2-\bar{\rho}\frac{\partial f_{\mathrm{xcT}}\left(\omega\right)}{\partial\bar{\rho}}\delta_{ij}\mathbf{k}\cdot\left(\mathbf{k}+\mathbf{q}\right)\\&+A\left(\bar{\rho},\omega\right)\left(k_i+q_i\right)k_j-B\left(\bar{\rho},\omega\right)k_i\left(k_j+q_j\right)\Big]\end{aligned} \tag{4.49}$$

where

$$A\left(\bar{\rho},\omega\right)=\bar{\rho}\left(2\frac{\partial f_{\mathrm{xcT}}\left(\omega\right)}{\partial\bar{\rho}}-\frac{\partial f_{\mathrm{xcL}}\left(\omega\right)}{\partial\bar{\rho}}\right)+3f_{\mathrm{xcT}}\left(\omega\right)-\delta f_{\mathrm{xcL}}\left(\omega\right) \tag{4.50}$$

$$B(\bar{\rho},\omega)=\bar{\rho}\frac{\partial f_{\mathrm{xcT}}(\omega)}{\partial\bar{\rho}}+3f_{\mathrm{xcT}}(\omega)-\delta f_{\mathrm{xcL}}(\omega). \tag{4.51}$$

The vector xc-potential is then given as,

$$\begin{aligned}\delta A_{\mathrm{xc},i}(\mathbf{r},\omega)&=\sum_j\int f_{\mathrm{xc},ij}(\mathbf{r},\mathbf{r}',\omega)\,j_j(\mathbf{r}',\omega)\,d\mathbf{r}'\\&=\frac{1}{(2\pi)^3}\sum_j\int f^{\mathrm{hom.}}_{\mathrm{xc},ij}(\mathbf{k},\omega)\,j_j(\mathbf{k},\omega)\,e^{i\mathbf{k}\cdot\mathbf{r}}d\mathbf{k}\\&+\frac{1}{(2\pi)^3}\sum_{\sigma=\pm1}e^{i\sigma\mathbf{q}\cdot\mathbf{r}}\sum_j\int f_{\mathrm{xc},ij}(\mathbf{k}+\sigma\mathbf{q},\mathbf{k},\omega)\,j_j(\mathbf{k},\omega)\,e^{i\mathbf{k}\cdot\mathbf{r}}d\mathbf{k}\end{aligned} \tag{4.52}$$

where the expansion of Eq. (4.42) has been used and the Fourier transform of the current density is defined as

$$j_j(\mathbf{k},\omega)=\int j_j(\mathbf{r}',\omega)\,e^{-i\mathbf{k}\cdot\mathbf{r}'}d\mathbf{r}'. \tag{4.53}$$

The vector xc-potential of Eq. (4.52) satisfies the HPT and is a local functional of the current density.

Inserting the explicit forms of Eq. (4.39) and Eq. (4.49) into Eq. (4.52) and using the explicit for of the density modulation of Eq. (4.40) the expression for the VK-functional in the form derived by Vignale, Ullrich and Conti is obtained[23]

$$i\omega\delta A_{\mathrm{xc},i}(\mathbf{r},\omega)=\partial_i\delta v^{\mathrm{ALDA}}_{\mathrm{xc}}-\frac{1}{\rho_0(\mathbf{r})}\sum_j\partial_j\sigma_{\mathrm{xc},ij}(\mathbf{r},\omega) \tag{4.54}$$

where the tensor σ_{xc} is given by

$$\begin{aligned}\sigma_{\mathrm{xc},ij}(\mathbf{r},\omega)&=\tilde{\eta}_{\mathrm{xc}}(\omega;\rho_0)\left[\partial_i u_j(\mathbf{r},\omega)+\partial_j u_i(\mathbf{r},\omega)-\frac{2}{3}\delta_{ij}\nabla\cdot\mathbf{u}(\mathbf{r},\omega)\right]\\&+\tilde{\zeta}_{\mathrm{xc}}(\omega;\rho_0)\delta_{ij}\nabla\cdot\mathbf{u}(\mathbf{r},\omega)\end{aligned} \tag{4.55}$$

$\mathbf{u}=\mathbf{j}/\rho_0$ is the velocity field and the coefficients are given by

$$\tilde{\eta}_{\mathrm{xc}}(\omega;\rho_0)=-\frac{\rho_0^2}{i\omega}f_{\mathrm{xcT}}(\omega;\rho_0) \tag{4.56}$$

$$\tilde{\zeta}_{\mathrm{xc}}(\omega;\rho_0)=-\frac{\rho_0^2}{i\omega}\left(f_{\mathrm{xcL}}(\omega;\rho_0)-\frac{4}{3}f_{\mathrm{xcT}}(\omega;\rho_0)-f_{\mathrm{xcL}}(\omega=0;\rho_0)\right). \tag{4.57}$$

In the first sections of this chapter we outlined the theory of viscoelasticity. We can now immediately see that Eq. (4.55) is of the form of a viscoelastic stress tensor with viscosity coefficients $\tilde{\eta}_{\mathrm{xc}}(\omega;\rho_0)$ and $\tilde{\zeta}_{\mathrm{xc}}(\omega;\rho_0)$.

4.7 The spin-dependent VK-functional

We also want to use the VK-functional for the calculation of singlet and triplet excitation energies. For this it is necessary to consider the spin dependent VK-functional [60,61].

Before we consider the spin dependent VK-functional for an inhomogeneous system, we consider first the case of the homogeneous electron gas. We denote the spin variable by σ. In the case of the homogeneous electron gas the scalar and vector xc-kernels, $f_{\mathrm{xc}}^{\sigma\sigma'}(\mathbf{r},\mathbf{r}',\omega)$ and $\mathbf{f}_{\mathrm{xc}}^{\sigma\sigma'}(\mathbf{r},\mathbf{r}',\omega)$, merely depend on the separation $|\mathbf{r}-\mathbf{r}'|$. If we Fourier transform $\mathbf{f}_{\mathrm{xc}}^{\sigma\sigma'}(\mathbf{r},\mathbf{r}',\omega)$ with respect to $|\mathbf{r}-\mathbf{r}'|$ one arrives at the following form (compare with Eq. (4.36)):

$$f_{\mathrm{xc},ij}^{\mathrm{hom.},\sigma\sigma'}(\mathbf{k},\omega)=\frac{1}{\omega^2}\left[f_{\mathrm{xcL}}^{\sigma\sigma'}(\mathbf{k},\omega)k_ik_j+f_{\mathrm{xcT}}^{\sigma\sigma'}(\mathbf{k},\omega)\left(k^2\delta_{ij}-k_ik_j\right)\right]. \tag{4.58}$$

This defines the longitudinal and transverse spin-dependent xc-kernels $f_{\mathrm{xcL}}^{\sigma\sigma'}(\mathbf{k},\omega)$ and $f_{\mathrm{xcT}}^{\sigma\sigma'}(\mathbf{k},\omega)$. Qian and Vignale showed that for the homogeneous electron gas the small k expansion of these kernels is given by [60,61],

$$f_{\mathrm{xcL(T)}}^{\sigma\sigma'}(k,\omega)\simeq\frac{A(\omega)}{k^2}\frac{\sigma\sigma'\rho^2}{4\rho_\sigma\rho_{\sigma'}}+B_{\mathrm{L(T)}}^{\sigma\sigma'}(\omega)+O\left(k^2\right), \tag{4.59}$$

where $A(\omega)$ and $B_{\mathrm{L(T)}}^{\sigma\sigma'}(\omega)$ are complex functions of the frequency, $\rho_0(\mathbf{r})=\rho_{0,\uparrow}(\mathbf{r})+\rho_{0,\downarrow}(\mathbf{r})$, and $\sigma=+1$ for spin-up and $\sigma=-1$ for spin-down. The first term is divergent for $k\to 0$, therefore we shall denote $A(\omega)$ the singular component and $B_{\mathrm{L(T)}}^{\sigma\sigma'}(\omega)$ the regular component. Note that for spin restricted singlet excitations we need to sum over all spin variables, in that case the contribution of $A(\omega)$ vanishes.

One can now try to develop a spin-dependent VK-functional. The spin-dependent vector xc-potential is related to the induced current density by

$$\delta\mathbf{A}_{\mathrm{xc},\sigma}(\mathbf{r},\omega)=\sum_{\sigma'}\int\mathbf{f}_{\mathrm{xc}}^{\sigma\sigma'}(\mathbf{r},\mathbf{r}',\omega)\delta\mathbf{j}_{\sigma'}(\mathbf{r}',\omega)d\mathbf{r}'. \tag{4.60}$$

In an isotropic electron gas one can split the transverse and longitudinal components and obtain, after a Fourier transformation,

$$\delta A_{\mathrm{xc},\sigma}^{L(T)}(\mathbf{k},\omega)=\frac{k^2}{\omega^2}\sum_{\sigma'}\int f_{\mathrm{xc,L(T)}}^{\sigma\sigma'}(\mathbf{k},\omega)\,\delta j_{\sigma'}^{L(T)}(\mathbf{k},\omega)\,d\mathbf{r}' \tag{4.61}$$

where the factor k^2/ω^2 exactly cancels the small k singularity in Eq. (4.59). One can now substitute Eq. (4.59) in Eq. (4.61) and go through similar calculations as were done to derive the spin-independent VK equation [62,63]. One then obtains the following spin dependent version of the VK-functional [60,61]

$$\begin{aligned} i\omega\delta\mathbf{A}_{\mathrm{xc},\sigma}(\mathbf{r},\omega)&=\nabla\delta v_{\mathrm{xc},\sigma}^{\mathrm{ALDA}}(\mathbf{r},\omega)+i\omega\delta\mathbf{A}_{\mathrm{xc},\sigma}^{\mathrm{viscoel.}}(\mathbf{r},\omega)\\ &\quad-\frac{i\rho^2A(\omega)}{4\omega}\sum_{\sigma'}\frac{\sigma\sigma'}{\rho_\sigma\rho_{\sigma'}}\delta\mathbf{j}_{\sigma'}(\mathbf{r},\omega) \end{aligned}\quad . \tag{4.62}$$

For an inhomogeneous electron gas (with $k\ll k_F,\omega/v_F$ and $\gamma\ll 1$) one can replace $\rho\to\rho_0(\mathbf{r})$ in Eq. (4.62) (and Eq. (4.59)). This is allowed because the zero-force, zero-torque, Onsager, and Ward identities are still valid so one can do the same analysis as in the previous section and obtain [62],

$$\begin{aligned} \delta\mathbf{E}_{\mathrm{xc},\sigma}(\mathbf{r},\omega)&=\nabla\delta v_{\mathrm{xc},\sigma}^{\mathrm{ALDA}}(\mathbf{r},\omega)+i\omega\delta\mathbf{A}_{\mathrm{xc},\sigma}^{\mathrm{viscoel.}}(\mathbf{r},\omega)\\ &\quad-\frac{i\rho_0(\mathbf{r})^2A(\omega)}{4\omega}\sum_{\sigma'}\frac{\sigma\sigma'}{\rho_{0,\sigma}(\mathbf{r})\rho_{0,\sigma'}(\mathbf{r})}\delta\mathbf{j}_{\sigma'}(\mathbf{r},\omega) \end{aligned} \tag{4.63}$$

where we used the relation between the electric field and the vector potential; $\mathbf{E}=i\omega\mathbf{A}$. For the spin-restricted singlet case this expression reduces to the spin-independent VK-functional of Eq. (4.54). The first term in Eq. (4.63) is the ALDA contribution and the second term is related to the *spin-dependent* viscoelastic stress tensor $\sigma_{\mathrm{xc},\sigma}(\mathbf{r},\omega)$ by,

$$\delta A_{\mathrm{xc},\sigma,i}^{\mathrm{viscoel.}}(\mathbf{r},\omega)=\frac{i}{\omega\rho_0(\mathbf{r})}\sum_j\partial_j\sigma_{\mathrm{xc},\sigma,ij}(\mathbf{r},\omega)\,, \tag{4.64}$$

$$\begin{aligned} \sigma_{\mathrm{xc},\sigma,\mathrm{ij}}(\mathbf{r},\omega)=\sum_{\sigma'}\Big\{&\tilde{\eta}_{\mathrm{xc}}^{\sigma\sigma'}(\mathbf{r},\omega)\Big[\partial_j u_{\sigma',i}(\mathbf{r},\omega)+\partial_i u_{\sigma',j}(\mathbf{r},\omega)-\frac{2}{3}\delta_{ij}\nabla\cdot\mathbf{u}_{\sigma'}(\mathbf{r},\omega)\Big]\\ &+\tilde{\zeta}_{\mathrm{xc}}^{\sigma\sigma'}(\mathbf{r},\omega)\delta_{ij}\nabla\cdot\mathbf{u}_{\sigma'}(\mathbf{r},\omega)\Big\} \end{aligned}. \tag{4.65}$$

where $\mathbf{u}_\sigma(\mathbf{r},\omega)=\delta\mathbf{j}_\sigma(\mathbf{r},\omega)/\rho_{0,\sigma}(\mathbf{r})$. The coefficients $\tilde{\eta}_{\mathrm{xc}}^{\sigma\sigma'}(\omega)$ and $\tilde{\zeta}_{\mathrm{xc}}^{\sigma\sigma'}(\omega)$ are related to the regular component of the xc-kernel of the homogeneous electron gas by the following relations [60],

$$\tilde{\eta}_{\mathrm{xc}}^{\sigma\sigma'}(\omega) = -\frac{\rho_{0,\sigma}\rho_{0,\sigma'}}{i\omega} B_{\mathrm{T}}^{\sigma\sigma'}(\omega), \tag{4.66}$$

$$\tilde{\zeta}_{\mathrm{xc}}^{\sigma\sigma'}(\omega) = -\frac{\rho_{0,\sigma}\rho_{0,\sigma'}}{i\omega}\left(B_{\mathrm{L}}^{\sigma\sigma'}(\omega) - \frac{4}{3} B_{\mathrm{T}}^{\sigma\sigma'}(\omega) - \frac{\partial^2 \varepsilon_{\mathrm{xc}}}{\partial\rho_{0,\sigma}\partial\rho_{0,\sigma'}} \right), \tag{4.67}$$

where $\varepsilon_{\mathrm{xc}}(\rho_0)$ is the xc-energy per unit volume of the homogeneous electron gas of density ρ_0. The third term in Eq. (4.63) is new in the spin dependent formulation and comes directly from the $1/k^2$ singularity in Eq. (4.59). The essential feature of this new term is that it produces damping of the spin-current proportional to the relative velocity between up- and down-spin electrons [60]. Whenever the up- and down-spin currents travel with different average velocities they exert friction on each other, this is known as "spin drag"[64]. However we will see that in the limit of $\omega \to 0$ (which is the limit we will work in) this term disappears.

4.8 The coefficients η and ζ and the static limit

In this section we further specify the coefficients $\tilde{\eta}_{\mathrm{xc}}(\omega)$ and $\tilde{\zeta}_{\mathrm{xc}}(\omega)$ (spin-dependent and spin-independent) and the singular part of the spin-dependent VK-functional and we show their forms in the static limit ($\omega \to 0$). From now we work only in this limit.

The static limit can only be used if indeed the frequency dependence of the longitudinal and transverse xc-kernels of the electron gas is weak. For frequencies much smaller than the local plasma frequency $\omega_p = \sqrt{4\pi\rho_0}$ of the relevant density region, this approximation is reasonable [65,66]. For molecules, this relevant region is often the valence region with $r_s \approx 1$ that corresponds to $\omega_p \approx 47$ eV , which is much larger than typical excitation energies. There is also a technical reason for taking the static limit: we can presently only include real valued xc-kernels (Chapter 5). Furthermore including only the frequency dependence of the real part of the electron gas kernel without the imaginary part will destroy the causal structure of the response equations. It should be kept in mind that the VK-functional is derived in order to obtain a local approximation for the scalar xc-kernel at *finite* frequency. We do not expect large changes to our results if we would include frequency dependence. This is also supported by recent work on infinite polyacetylene chains and crystals by Berger, De Boeij and Van Leeuwen [67], where the dielectric function changes only slightly when introducing frequency dependence. It is not immediately clear that the VK-functional can have a considerable contribution in the limit $\omega \to 0$.

Let us first consider the spin-independent case. The viscosity coefficients are given by

$$\tilde{\eta}_{\mathrm{xc}}(\omega) = -\frac{\rho_0^2}{i\omega} f_{\mathrm{xcT}}(\omega), \tag{4.68}$$

$$\tilde{\zeta}_{\mathrm{xc}}(\omega) = -\frac{\rho_0^2}{i\omega}\left(f_{\mathrm{xcL}}(\omega) - \frac{4}{3} f_{\mathrm{xcT}}(\omega) - \frac{d^2\varepsilon_{\mathrm{xc}}(\rho_0)}{d\rho_0^2} \right), \tag{4.69}$$

where $\varepsilon_{\mathrm{xc}}(\rho_0)$ is the xc-energy per unit volume of the homogeneous electron gas of density ρ_0. We need expressions for the longitudinal and transverse response kernels $f_{\mathrm{xcL(T)}}(\omega)$, which are smooth functions for small frequencies [66]. It turns out that when taking the limit to zero frequency it is very important to keep track of the order of the limits $\omega \to 0$ and $k \to 0$. If one takes the limit $\omega \to 0$ first for the longitudinal xc-kernel this leads to

$$\lim_{k\to 0} f_{\mathrm{xcL}}(k, \omega = 0) = \frac{d^2\varepsilon_{\mathrm{xc}}}{d\rho_0^2}, \tag{4.70}$$

but the $f_{\mathrm{xcL(T)}}(\omega)$ are defined by taking the limit $k \to 0$ first. Conti and Vignale showed that the following rigorous low frequency limits can be obtained from an analysis of the transport equation in the Landau theory of Fermi liquids [49],

$$\lim_{\omega\to 0}\left(f_{\mathrm{xcL}}(\omega) - \frac{4}{3} f_{\mathrm{xcT}}(\omega) - \frac{d^2\varepsilon_{\mathrm{xc}}(\rho_0)}{d\rho_0^2} \right) = 0 \tag{4.71}$$

$$\lim_{\omega\to 0} f_{\mathrm{xcT}}(\omega) = \frac{2E_F}{5\rho_0} \frac{F_2^s/5 - F_1^s/3}{1 + F_1^s/3}. \tag{4.72}$$

where $E_F = k_F^2/2$ is the Fermi energy and the $F_l^{s/a}$ are the Landau parameters. From these relations we see that $\lim_{\omega\to 0} f_{\mathrm{xcL}}(\omega) \neq d^2\varepsilon_{\mathrm{xc}}/d\rho_0^2$. We also see from these equations that $\omega\tilde{\zeta}_{\mathrm{xc}}(\omega)$ vanishes for $\omega \to 0$ but the shear modulus $\omega\tilde{\eta}_{\mathrm{xc}}(\omega)$ remains finite. The strange fact that the shear modulus does not vanish in the limit of $\omega \to 0$ (unlike in ordinary liquids) is a result of taking this order of limits. The VK-functional has a contribution even in the static limit.

It remains to find values for $f_{\mathrm{xcT}}(0;\rho_0)$. Nifosì, Conti and Tosi [68] did a mode-coupling calculation for the electron gas and obtained values for the shear modulus μ_{xc} for a number of r_s values. We can then use that $f_{\mathrm{xcT}}(0) = \mu_{\mathrm{xc}}/\rho_0^2$ and obtain values for $f_{\mathrm{xcT}}(0;\rho_0)$ at these r_s values. To obtain values for any r_s we do a cubic spline interpolation taking into account the exact exchange-only quadratic behavior for small r_s ($f_{\mathrm{xcT}}(\omega) = 3\pi/10k_F^2$ [9]). More details on this procedure and the values for $f_{\mathrm{xcT}}(0;\rho_0)$ can be found in section 5.5. More recently Qian

and Vignale [66] used the explicit values of the Landau parameters obtained in Ref. [69] to obtain values for $\mu_{\rm xc}$, we also use these values in some of our calculations.

In the spin-dependent case we do not only need to find expressions for $\tilde{\eta}_{\rm xc}^{\sigma\sigma'}(\omega)$ and $\tilde{\zeta}_{\rm xc}^{\sigma\sigma'}(\omega)$ in the limit $\omega \to 0$, but also for the singular component $A(\omega)$. For $\omega \to 0$ $\mathrm{Im}\, A(\omega) \propto \omega^3$ and $\mathrm{Re}\, A(\omega) \propto \omega^2$ so $\lim_{\omega\to 0} A(\omega) = 0$. For the regular component $B_{\rm L(T)}^{\sigma\sigma'}(\omega)$ we have the exact relation [60] $\lim_{\omega\to 0}\{(B_{\rm L}^{\sigma\sigma'}(\omega) - 4B_{\rm T}^{\sigma\sigma'}(\omega)/3 - \partial^2\varepsilon_{\rm xc}/\partial\rho_{0,\sigma}\partial\rho_{0,\sigma'})/\omega\} = 0$, hence the coefficient $\omega\tilde{\zeta}_{\rm xc}^{\sigma\sigma'}(\omega)$ also vanishes in this limit. Therefore we only need to consider $\tilde{\eta}_{\rm xc}^{\sigma\sigma'}(\omega)$ for which we have the following singlet and triplet combinations [60]:

$$\begin{aligned}\tilde{\eta}_{\rm xc}^{S}(\omega) &= -\sum_{\sigma\sigma'} \frac{\rho_{0,\sigma}\rho_{0,\sigma'}}{i\omega} B_{\rm T}^{\sigma\sigma'}(\omega) \\ &= \frac{-\rho_0^2}{i\omega} f_{\rm xc}^{\rm T}(\omega) = \tilde{\eta}_{\rm xc}(\omega)\end{aligned} \tag{4.73}$$

$$\begin{aligned}\tilde{\eta}_{\rm xc}^{T}(\omega) &= -\sum_{\sigma\sigma'} \sigma\sigma' \frac{\rho_{0,\sigma}\rho_{0,\sigma'}}{i\omega} B_{\rm T}^{\sigma\sigma'}(\omega) \\ &= \frac{-\rho_0^2}{i\omega} B^{\rm T}(\omega)\end{aligned} \tag{4.74}$$

respectively called the density-density and spin-spin channels by Qian, Constantinescu and Vignale [61]. Eq. (4.74) defines $B^{\rm T}(\omega)$. The coefficient $\tilde{\eta}_{\rm xc}^{S}(\omega)$ is identical to the $\tilde{\eta}_{\rm xc}(\omega)$ of the spin-independent case, the only new thing that we need is $\lim_{\omega\to 0} B^{\rm T}(\omega)$. This quantity is also related to the Landau parameters,

$$B^{\rm T}(0) = \frac{2E_F}{\rho_0}\frac{F_2^a/25 - F_1^s/15}{1 + F_1^s/3}. \tag{4.75}$$

We can now use the explicit values of the Landau parameters F_2^a and F_1^s [69] and again do a cubic spline interpolation taking into account the exact quadratic behavior for small r_s. We give the values for $B^{\rm T}(0)$ at the values for r_s for which the Landau parameters are known in Chapter 5.

4.9 Application to molecules

In this thesis we apply the VK-functional in order to calculate the excitation energies and polarizability of molecules. It is not immediately clear that the VK-functional is valid for these finite systems. In any case the VK-functional satisfies some important constraints with arbitrary

time-dependence and inhomogeneity, as occur for molecules in external fields. These are the zero-force and zero-torque theorems and the HPT [9].

We showed in this chapter that the VK-functional is valid under the constraint that $k, q << k_F, \omega/\upsilon_F$, which is the region above the particle hole continuum. For the wave vector of the applied optical field the constraints $k << k_F, \omega/\upsilon_F$ are trivially met for molecular systems as $k = \omega/c << k_F$ and the speed of light $c >> \upsilon_F$. For the inhomogeneity wave vector $q = |\nabla n_0|/n_0$ the situation is less clear. In the valence region we have $q \approx k_F$ and $q\upsilon_F \approx 1$, whereas in the asymptotic outer region $q >> k_F$ and $q\upsilon_F << 1$. We should point out, however, that for finite systems, like molecules, the essential response features do not change much with frequency below the excitation gap ω_{gap} . If we take this ω_{gap} as the characteristic frequency, then both constraints are not strongly violated in the outer valence region. Moreover, it should be noted that the particle-hole regime (the regime in the $(\mathbf{q}\text{-}\omega)$ plane where the noninteracting response function $\chi_0(\mathbf{q}, \omega)$ has poles), for which the VK derivation is not justified, is to a large extent taken into account by the explicit evaluation of the Kohn-Sham response functions.

In view of these arguments we consider it worthwhile to explore the merits of the VK-functional for molecular systems. As we will show in this thesis the VK-functional can yield excellent results for these systems, but we will also see cases for which the VK-functional fails.

Chapter 5
Implementation

In this chapter we describe how we implemented the linear response equations of Chapter 3 and the VK-functional (Chapter 4) in the Amsterdam Density Functional program package (ADF) [25]. Since the implementation of the linear response equations for time-dependent density functional theory is thoroughly explained by Stan van Gisbergen [26] we concentrate on the changes that need to be made to include the current-dependent formalism.

5.1 The ADF RESPONSE code

Here we give a short outline of the implementation of the linear density response equations in the Amsterdam Density Functional program package (ADF) [25] RESPONSE code. A more extended discussion can be found in the Ph.D. thesis of Stan van Gisbergen [26] and in Ref. [70].

ADF is a quantum chemical program that makes use of the fact that one can expand the molecular orbitals as a linear combination of atomic orbitals (LCAO). In contrast to most quantum chemical programs ADF uses Slater-type orbitals (STOs) instead of Gaussian orbitals (GTOs) for these atomic orbitals (AOs). The STOs resemble the atomic orbitals more closely, since they have a cusp at the nucleus and decay more slowly in the outer region of the atom. Because the STOs better resemble the atomic orbitals, less are needed to obtain a good accuracy for the calculations. Using STOs does yield awkward multi-center integrals in the evaluation of the Coulomb potential. This is remedied in ADF by employing an auxiliary set of fit functions. Like the basis functions, the fit functions are Slater-type exponential functions centered on the atoms. The true density, a sum of products of basis functions, is then approximated by a linear combination of the fit functions. Within this approximation the Coulomb potential belonging to the fitted density can be obtained analytically [71].

The ground state DFT calculation will provide one-particle eigenfunctions, the Kohn-Sham (KS) orbitals. In the time-dependent code we will evaluate matrix elements between these KS orbitals. Since they can be expanded in AOs we can also choose to evaluate the matrix elements between the AOs. The use of KS orbitals has the advantage that the full molecular symmetry can

be exploited, saving memory and CPU time for highly symmetric systems. When one uses AOs distance effects can be used, neglecting the overlap between AOs centered on nuclei that are far apart. This approach is better suited for large systems of low symmetry. In our implementation of the TDCDFT equations and the VK-functional, we choose to use the KS orbitals. Therefore we concentrate on this approach. The RESPONSE code provides both options. More information on the implementation of the AO approach can be found in the references mentioned above. We note that all orbitals in ADF are real valued.

We will first explain the implementation of the ordinary (current density independent) TDDFT equations. The equations that are solved in TDDFT are basically the same as we derived for TDCDFT in Chapter 3, only with a different P-matrix and coupling matrix, and no reference is made to the current density. The P-matrix and coupling matrix of TDDFT are given by

$$\mathrm{P}_{ai\sigma}(\omega) = \frac{1}{(\varepsilon_{i\sigma} - \varepsilon_{a\sigma}) + \omega} \int \phi_{a\sigma}(\mathbf{r}) \delta v_{s,\sigma}(\mathbf{r},\omega) \phi_{i\sigma}(\mathbf{r}) d\mathbf{r} \tag{5.1}$$

$$K^{\sigma\tau}_{ia,jb}(\omega) = \iint \phi_{i\sigma}(\mathbf{r}) \phi_{a\sigma}(\mathbf{r}) \left[\frac{1}{|\mathbf{r}-\mathbf{r}'|} + f_{\mathrm{xc}}^{\sigma\tau}(\mathbf{r},\mathbf{r}',\omega) \right] \phi_{b\tau}(\mathbf{r}') \phi_{j\tau}(\mathbf{r}') d\mathbf{r} d\mathbf{r}' . \tag{5.2}$$

This P-matrix and coupling matrix can then be used in the linear response theory of Chapter 3.

The equations for the excitation energies and polarizability can be solved using a ‘direct’ method. This requires storing all matrix elements of the coupling matrix K, which implies storing and calculating all $N_{\mathrm{occ}}^2 \times N_{\mathrm{virt}}^2$ matrix elements. For large molecules and basis sets this quickly becomes unfeasible. Also solving the set of linear equations (for the polarizability) and the eigenvalue problem (for the excitation energies) requires $N_{\mathrm{occ}}^3 \times N_{\mathrm{virt}}^3$ floating point operations, which is again unfeasible for large systems. Therefore the equations are solved in an iterative manner. The linear equations from which we obtain the polarizability are solved using the Direct Inversion in the Iterative Subspace (DIIS) method originating from Pulay [72,73]. We need to find an accurate trial vector for this method. A reliable starting point is setting the coupling matrix to zero, leading to the so-called uncoupled polarizability, which is usually a good estimate of the polarizability. The eigenvalue problem from which we obtain the excitation energies, is solved using the Davidson algorithm [74]. With this method one only obtains a selected number of (usually the lowest) eigenvalues. Again accurate trial vectors need to be found and setting the coupling matrix to zero turns out to be a reliable starting point also in this

case. The excitation energies in the first cycle of the iteration are in that case equal to the KS orbital energy differences.

Both iterative procedures merely require repeated matrix-vector multiplications. Due to the special structure of the response kernel, we do not need to construct the full coupling matrix at any time. Several methods have been implemented in order to make these multiplications more efficient. One of these is expanding the KS orbitals in the basis functions (the AOs). As mentioned, even though this method is implemented, we will not use it for our extension to TDCDFT. We refer to Ref. [70] for a thorough review of this procedure. In order to further reduce computational cost use can be made of full molecular symmetry. The big advantages of using the full molecular symmetry are the reduction of the number of integration points and the number of integrals to be calculated. Only the integration points that belong to a symmetry-unique wedge need to be used. This reduces the number of integration points by the number of group operators. The number of integrals is also considerably reduced using the knowledge of the irreducible representations of the orbitals and operators. Only the matrix elements that belong to the completely symmetrical representation (e.g. the A_1 representation) will be nonzero. A third advantage of using the molecular symmetry is that only equivalent symmetry blocks (for excitation energy calculations) and equivalent external fields (for polarizability calculations) need to be treated at the same time. A detailed account on how the molecular symmetry is implemented can again be found in Ref. [70].

Another method that is used to increase computational efficiency is parallelization. The major part of this parallelization is achieved by domain decomposition, i.e. subdivision of number of integration points in blocks and distributing these blocks over the different processors. Each processor performs his part of the numerical integration and in the end all the results are combined.

In the latest versions of ADF several linear scaling techniques have been implemented, we will not use these in our implementation of the TDCDFT equations and will therefore not go into further detail on this.

5.2 Implementation of the TDCDFT equations

In order to include the current density in the RESPONSE code, we only need to change the $\mathbf{P}$-matrix and the coupling matrix. The extra terms that we need to calculate are the matrix elements of the paramagnetic current density (Eq. (2.5)) and a current dependent functional. In

the next sections we go into detail on how we included the current dependent VK-functional. Here we give some details about the implementation of the TDCDFT equations.

There is a simple relation between the matrix elements of the current density and the dipole matrix elements,

$$\frac{i}{\left(\varepsilon_{a\sigma}-\varepsilon_{i\sigma}\right)}\int \phi_{i\sigma}^{*}\left(\mathbf{r}\right)\hat{\mathbf{j}}_{p}\phi_{a\sigma}\left(\mathbf{r}\right)d\mathbf{r}=\int \phi_{i\sigma}^{*}\left(\mathbf{r}\right)\hat{\mathbf{r}}\phi_{a\sigma}\left(\mathbf{r}\right)d\mathbf{r}\,, \tag{5.3}$$

which means that we can use similar routines to calculate the paramagnetic current matrix elements as are already included to calculate the dipole matrix elements.

Another point that we need to take care of in our implementation is that in ADF all functions that are calculated are real valued. Within TDCDFT we automatically have to deal with imaginary functions. For example, since the orbitals are chosen to be real valued, the matrix elements of the paramagnetic current density will be purely imaginary. But there is a "trick" that we can use, such that we can use real valued functions throughout. We can write the induced density as,

$$\begin{aligned}\delta\rho_{\sigma}\left(\mathbf{r},\omega\right)=\sum_{\sigma'}\Big\{&\int \chi_{\rho\mathbf{j}}^{\sigma\sigma'}\left(\mathbf{r},\mathbf{r}',\omega\right)\cdot\frac{i}{\omega}\delta\mathbf{E}_{s,\sigma'}\left(\mathbf{r}',\omega\right)d\mathbf{r}'\\&+\int \chi_{\rho\rho}^{\sigma\sigma'}\left(\mathbf{r},\mathbf{r}',\omega\right)\delta\upsilon_{s,\sigma'}\left(\mathbf{r}',\omega\right)d\mathbf{r}'\Big\}\end{aligned} \tag{5.4}$$

where we used that $\delta\mathbf{E}_{\mathrm{s},\sigma}\left(\mathbf{r},\omega\right)=i\omega\delta\mathbf{A}_{\mathrm{s},\sigma}\left(\mathbf{r},\omega\right)$. We will use in the following $\mathbf{E}_{\mathrm{ext}}\left(\omega\right)=-i\omega\hat{\mathbf{e}}$, where $\hat{\mathbf{e}}$ is a unit vector. The scalar potential is given by

$$\delta\upsilon_{\mathrm{s},\sigma}\left(\mathbf{r},\omega\right)=\sum_{\sigma'}\int\left\{\frac{1}{\left|\mathbf{r}-\mathbf{r}'\right|}+f_{\mathrm{xc}}^{\sigma\sigma'}\left(\mathbf{r},\mathbf{r}',\omega\right)\right\}\delta\rho_{\sigma'}\left(\mathbf{r}',\omega\right)d\mathbf{r}'\,. \tag{5.5}$$

We now use the fact that we can write any function as a combination of a real valued and a pure imaginary part,

$$\delta\rho_{\sigma}\left(\mathbf{r},\omega\right)=\delta\rho'_{\sigma}\left(\mathbf{r},\omega\right)+i\delta\rho''_{\sigma}\left(\mathbf{r},\omega\right) \tag{5.6}$$

$$\delta\upsilon_{s,\sigma}\left(\mathbf{r},\omega\right)=\delta\upsilon'_{s,\sigma}\left(\mathbf{r},\omega\right)+i\delta\upsilon''_{s,\sigma}\left(\mathbf{r},\omega\right) \tag{5.7}$$

Substituting Eqs. (5.6) and (5.7) in Eqs. (5.4) and (5.5), and separating the real and imaginary parts, we obtain

$$\delta\rho'_{\sigma}\left(\mathbf{r},\omega\right)=\sum_{\sigma'}\int \chi_{\rho\rho}^{\sigma\sigma'}\left(\mathbf{r},\mathbf{r}',\omega\right)\delta\upsilon'_{s,\sigma'}\left(\mathbf{r}',\omega\right)d\mathbf{r}' \tag{5.8}$$

$$i\delta\rho''_\sigma(\mathbf{r},\omega)=\sum_{\sigma'}\left\{i\int\chi^{\sigma\sigma'}_{\rho\mathbf{j}}(\mathbf{r},\mathbf{r}',\omega)\cdot\frac{1}{\omega}\delta\mathbf{E}_{s,\sigma'}(\mathbf{r}',\omega)\,d\mathbf{r}'+i\int\chi^{\sigma\sigma'}_{\rho\rho}(\mathbf{r},\mathbf{r}',\omega)\delta\upsilon''_{s,\sigma'}(\mathbf{r}',\omega)\,d\mathbf{r}'\right\} \tag{5.9}$$

$$\delta\upsilon'_{s,\sigma}(\mathbf{r},\omega)=\sum_{\sigma'}\int\left[\frac{1}{|\mathbf{r}-\mathbf{r}'|}+f_{\mathrm{xc}}^{\sigma\sigma'}(\mathbf{r},\mathbf{r}',\omega)\right]\delta\rho'_\sigma(\mathbf{r}',\omega)\,d\mathbf{r}' \tag{5.10}$$

$$i\delta\upsilon''_{s,\sigma}(\mathbf{r},\omega)=\sum_{\sigma'}i\int\left[\frac{1}{|\mathbf{r}-\mathbf{r}'|}+f_{\mathrm{xc}}^{\sigma\sigma'}(\mathbf{r},\mathbf{r}',\omega)\right]\delta\rho''_{\sigma'}(\mathbf{r}',\omega)\,d\mathbf{r}'\,. \tag{5.11}$$

Equations (5.8) and (5.10) have the trivial solution $\delta\rho'_\sigma(\mathbf{r},\omega)=\delta\upsilon'_{s,\sigma}(\mathbf{r},\omega)=0$, we are then left with Eqs. (5.9) and (5.11),

$$\delta\rho''_\sigma(\mathbf{r},\omega)=\sum_{\sigma'}\left\{\int\chi^{\sigma\sigma'}_{\rho\mathbf{j}}(\mathbf{r},\mathbf{r}',\omega)\cdot\frac{1}{\omega}\delta\mathbf{E}_{s,\sigma'}(\mathbf{r}',\omega)\,d\mathbf{r}'+\int\chi^{\sigma\sigma'}_{\rho\rho}(\mathbf{r},\mathbf{r}',\omega)\delta\upsilon''_{s,\sigma'}(\mathbf{r}',\omega)\,d\mathbf{r}'\right\} \tag{5.12}$$

$$\delta\upsilon''_{s,\sigma}(\mathbf{r},\omega)=\sum_{\sigma'}\int\left[\frac{1}{|\mathbf{r}-\mathbf{r}'|}+f_{\mathrm{xc}}^{\sigma\sigma'}(\mathbf{r},\mathbf{r}',\omega)\right]\delta\rho''_{\sigma'}(\mathbf{r}',\omega)\,d\mathbf{r}'\,. \tag{5.13}$$

From this it follows that if we use $\delta\rho_\sigma(\mathbf{r},\omega)=i\delta\rho''_\sigma(\mathbf{r},\omega)$ we can rewrite all our equations in terms of real functions only. With this definition of the induced density, the induced current density will also be real valued. The procedure described above is still valid when we include the VK-functional. The physical reason that $\delta\rho_\sigma(\mathbf{r},\omega)$ is purely imaginary is that we do not include dissipation in our theory, so the current must be 90 degrees out of phase with the electric field. This implies that the density must be in phase with the electric field.

5.3 Implementation of the spin-independent VK-functional

The most extensive part of our implementation is the inclusion of the VK-functional,

$$\delta\mathbf{E}_{\mathrm{xc}}(\mathbf{r},\omega)=\nabla\delta\upsilon_{\mathrm{xc}}^{\mathrm{ALDA}}(\mathbf{r},\omega)+i\omega\delta\mathbf{A}_{\mathrm{xc}}^{\mathrm{viscoel.}}(\mathbf{r},\omega)\,, \tag{5.14}$$

$$\delta A_{\mathrm{xc},i}^{\mathrm{viscoel.}}(\mathbf{r},\omega)=\frac{i}{\omega\rho_0(\mathbf{r})}\sum_j\partial_j\sigma_{\mathrm{xc},ij}(\mathbf{r},\omega)\,. \tag{5.15}$$

In this section we consider the implementation of the spin-independent VK-functional, in the next section we show what changes need to be made to include the spin-dependence. From Eq. (3.50) we see that we only need to calculate the matrix elements between the Kohn-Sham orbitals and the perturbation to obtain the induced density and the induced current density. We do not need to calculate the VK vector potential explicitly. We choose a gauge in which the ALDA contribution of the VK-functional is part of the scalar potential (we are always allowed to choose such a gauge). The matrix elements of the remaining contribution can then be expressed as

$$H_{ia}(\omega) = -\langle \phi_a | \frac{1}{2}\left(\hat{\mathbf{j}}_p \cdot \delta \mathbf{A}_{\mathrm{xc}}^{\mathrm{viscoel.}}(\mathbf{r},\omega) + \delta \mathbf{A}_{\mathrm{xc}}^{\mathrm{viscoel.}}(\mathbf{r},\omega) \cdot \hat{\mathbf{j}}_p \right) | \phi_i \rangle . \tag{5.16}$$

In order to evaluate Eq. (5.16) it is convenient to define the velocity field elements **v** as

$$\mathbf{v}_{ia}(\mathbf{r}) = \frac{\mathbf{j}_{ia}(\mathbf{r})}{\rho_0(\mathbf{r})}, \tag{5.17}$$

where the transition current elements are defined as

$$\mathbf{j}_{ia}(\mathbf{r}) = \frac{-i}{2}\left(\phi_a^*(\mathbf{r}) \nabla \phi_i(\mathbf{r}) - \phi_i(\mathbf{r}) \nabla \phi_a^*(\mathbf{r}) \right). \tag{5.18}$$

Arjan Berger has shown in his Master thesis [75] that using some vector identities, integration by parts and the fact that total differentials integrate to zero due to Gauss' integral theorem, the contribution to the interaction containing all terms linear in $\tilde{\eta}_{\mathrm{xc}}(\rho_0(\mathbf{r}),\omega)$ can be evaluated as

$$\begin{aligned} H_{ia}^{\eta}(\omega) = & \frac{i}{\omega}\int \left(\nabla \times \mathbf{v}_{ia}(\mathbf{r})\right) \cdot \tilde{\eta}_{\mathrm{xc}}(\rho_0(\mathbf{r}),\omega) \left(\nabla \times \mathbf{u}(\mathbf{r},\omega)\right) d\mathbf{r} \\ & + \frac{4i}{3\omega}\int \left(\nabla \cdot \mathbf{v}_{ia}(\mathbf{r})\right) \tilde{\eta}_{\mathrm{xc}}(\rho_0(\mathbf{r}),\omega) \left(\nabla \cdot \mathbf{u}(\mathbf{r},\omega)\right) d\mathbf{r} \\ & + \frac{2i}{\omega}\int \left(\nabla \cdot \mathbf{v}_{ia}(\mathbf{r})\right) \nabla \tilde{\eta}_{\mathrm{xc}}(\rho_0(\mathbf{r}),\omega) \cdot \mathbf{u}(\mathbf{r},\omega) d\mathbf{r} \\ & + \frac{2i}{\omega}\int \mathbf{v}_{ia}(\mathbf{r}) \cdot \nabla \nabla \tilde{\eta}_{\mathrm{xc}}(\rho_0(\mathbf{r}),\omega) \cdot \mathbf{u}(\mathbf{r},\omega) d\mathbf{r} \\ & + \frac{2i}{\omega}\int \mathbf{v}_{ia}(\mathbf{r}) \cdot \nabla \tilde{\eta}_{\mathrm{xc}}(\rho_0(\mathbf{r}),\omega) \left(\nabla \cdot \mathbf{u}(\mathbf{r},\omega)\right) d\mathbf{r} \end{aligned} . \tag{5.19}$$

Similarly for the terms linear in $\tilde{\zeta}_{\mathrm{xc}}(\rho_0(\mathbf{r}),\omega)$ we obtain

$$H_{ia}^{\zeta}(\omega) = \frac{i}{\omega}\int \left(\nabla \cdot \mathbf{v}_{ia}(\mathbf{r})\right) \tilde{\zeta}_{\mathrm{xc}}(\rho_0(\mathbf{r}),\omega) \left(\nabla \cdot \mathbf{u}(\mathbf{r},\omega)\right) d\mathbf{r} . \tag{5.20}$$

From these expressions we see that we only need to evaluate the velocity fields $\mathbf{v}_{ia}$ and $\mathbf{u}$ as well as their divergence and curl. Moreover we need to calculate the first and second derivatives of the functions $\tilde{\eta}_{\mathrm{xc}}\left(\rho_0(\mathbf{r}),\omega\right)$ and $\tilde{\zeta}_{\mathrm{xc}}\left(\rho_0(\mathbf{r}),\omega\right)$. Since they are simple functions of the density these derivatives can be evaluated once we know the first and second derivatives of the ground state density. For our calculations we use the VK-functional in the static limit ($\omega \to 0$), as we explained in Chapter 4 the coefficient $\omega\tilde{\zeta}_{\mathrm{xc}}(\omega)$ vanishes in this limit ($\omega \to 0$) and we only need to consider Eq. (5.19). We obtain the following equations for the divergence and curl of $\mathbf{v}_{ia}$:

$$\nabla\cdot\mathbf{v}_{ia}(\mathbf{r}) = \frac{1}{\rho_0(\mathbf{r})}\left(i\left(\varepsilon_i-\varepsilon_a\right)\phi_a^*(\mathbf{r})\phi_i(\mathbf{r}) - \frac{\nabla\rho_0(\mathbf{r})}{\rho_0(\mathbf{r})}\cdot\mathbf{j}_{ia}(\mathbf{r})\right), \tag{5.21}$$

$$\nabla\times\mathbf{v}_{ia}(\mathbf{r}) = \frac{1}{\rho_0(\mathbf{r})}\left(\left\{-i\nabla\phi_a^*(\mathbf{r})\times\nabla\phi_i(\mathbf{r})\right\} - \frac{\nabla\rho_0(\mathbf{r})}{\rho_0(\mathbf{r})}\times\mathbf{j}_{ia}(\mathbf{r})\right). \tag{5.22}$$

Here we have explicitly used that the orbitals are eigenstates of the ground state Kohn-Sham Hamiltonian. These expressions only involve first order derivatives of the orbitals. For the divergence and curl of $\mathbf{u}$ we obtain

$$\nabla\cdot\mathbf{u}(\mathbf{r},\omega) = \frac{1}{\rho_0(\mathbf{r})}\left(i\omega\delta\rho(\mathbf{r},\omega) - \frac{\nabla\rho_0(\mathbf{r})}{\rho_0(\mathbf{r})}\cdot\delta\mathbf{j}(\mathbf{r},\omega)\right),$$

$$\nabla\times\mathbf{u}(\mathbf{r},\omega) = \frac{1}{\rho_0(\mathbf{r})}\left(\delta\mathbf{m}(\mathbf{r},\omega) - \delta\mathbf{j}(\mathbf{r},\omega)\times\frac{\nabla\rho_0(\mathbf{r})}{\rho_0(\mathbf{r})}\right).$$

We used the continuity equation $\nabla\cdot\delta\mathbf{j}(\mathbf{r},\omega) - i\omega\delta\rho(\mathbf{r},\omega) = 0$ to relate the divergence of the induced current to the induced density. The curl of the current, $\delta\mathbf{m}(\mathbf{r},\omega) = \nabla\times\delta\mathbf{j}(\mathbf{r},\omega)$, is obtained by

$$\begin{aligned}\delta\mathbf{m}(\mathbf{r},\omega) = &\int\left(\chi_{\mathbf{mj}}(\mathbf{r},\mathbf{r}',\omega) - \chi_{\mathbf{mj}}(\mathbf{r},\mathbf{r}',0)\right)\cdot\delta\mathbf{A}_s(\mathbf{r}',\omega)\,d\mathbf{r}' \\ &+\int\chi_{\mathbf{m}\rho}(\mathbf{r},\mathbf{r}',\omega)\delta v_s(\mathbf{r}',\omega)\,d\mathbf{r}'\end{aligned} \tag{5.23}$$

Here the response functions $\chi_{\mathbf{mj}}(\mathbf{r},\omega)$ and $\chi_{\mathbf{m}\rho}(\mathbf{r},\omega)$ can be obtained from Eq. (3.27) by substituting the operator $\hat{\mathbf{m}} = -i\left(\nabla^\dagger\times\nabla\right)$. From the previous discussion we see that we can evaluate the matrix elements of the VK-functional once we have the induced density $\delta\rho$, the induced current $\delta\mathbf{j}$, and its curl $\delta\mathbf{m}$. The equations (3.20), (3.21), and (5.23) become a coupled

set. Note that in this way we have avoided the explicit evaluation of orbital derivatives higher than first order. By including the ALDA in the scalar potential instead of in the vector potential we also avoid evaluation of the gradient of $\delta\rho$ and conform to standard implementations of TDDFT.

As we mentioned in Section 5.1 in ADF the exact ground state density, expressed as one and two-center products of basis functions, is represented by an expansion in one-center functions only [76]. This is done to facilitate the calculation of the Coulomb potential, but also to enable the evaluation of the first and second order derivatives of the density. A drawback, however, is that this fitted density can become zero or negative due to the incompleteness of the basis, which is unphysical. This poses problems for the evaluation of terms of the form, $\nabla\rho_0/\rho_0$ and $\nabla\nabla\rho_0/\rho_0$. To prevent this problem, the absolute value of the fitted density is used and a small offset is introduced. The fitted density is replaced by $\rho_0^{\text{safe}} = \left|\rho_0^{\text{fit}}\right| + \Delta$ with $\Delta = 1.0 \cdot 10^{-3}$. We checked that the value of Δ did not have a significant influence on the results while ensuring the stability of the calculation.

Until now we have made no comments on our choice of the external electric field. Our initial choice for the external electric field was $\mathbf{E}_{\text{ext}}(\omega) = -i\omega\hat{\mathbf{e}}_j$. This choice makes sure that we do not divide by ω in our set of linear equations, but this choice means that we need to obtain the polarizability tensor via,

$$\alpha_{ij}(\omega) = \left\{ \frac{-1}{\omega^2} \int \delta j_i(\mathbf{r},\omega)\, d\mathbf{r} \right\}_{\mathbf{E}(\omega) = -i\omega\hat{\mathbf{e}}_j} . \tag{5.24}$$

From this expression the disadvantage of our choice is immediately clear. We cannot obtain the static polarizability directly in this way. Our solution was to calculate the polarizability at several frequencies close to zero and extrapolate the result to the static limit. In this way we obtained the results in Refs. [77] and [78]. An alternative, and better, solution is to use the external field $\mathbf{E}_{\text{ext}}(\omega) = -i\hat{\mathbf{e}}_j$ for $\omega > 0$ (and with a reversed sign for frequencies smaller than zero to ensure real valued electrical fields in the time domain). To avoid terms that include $1/\omega$ we need to rewrite some equations. The equation for the induced density remains unchanged, but for the induced current density and its curl we write

$$\begin{aligned} \frac{1}{\omega}\delta\mathbf{j}(\mathbf{r},\omega) = & \int \frac{i}{\omega^2}\left(\chi_{\mathbf{jj}}(\mathbf{r},\mathbf{r}',\omega) - \chi_{\mathbf{jj}}(\mathbf{r},\mathbf{r}',0)\right)\cdot\delta\mathbf{E}_s(\mathbf{r}',\omega)\, d\mathbf{r}' \\ & + \frac{1}{\omega}\int \chi_{\mathbf{j}\rho}(\mathbf{r},\mathbf{r}',\omega)\,\delta v_s(\mathbf{r}',\omega)\, d\mathbf{r}' \end{aligned} \tag{5.25}$$

$$\frac{1}{\omega}\delta\mathbf{m}(\mathbf{r},\omega) = \int \frac{i}{\omega^2}\left(\chi_{\mathbf{mj}}(\mathbf{r},\mathbf{r}',\omega) - \chi_{\mathbf{mj}}(\mathbf{r},\mathbf{r}',0)\right)\cdot\delta\mathbf{E}_s(\mathbf{r}',\omega)\,d\mathbf{r}' + \frac{1}{\omega}\int \chi_{\mathbf{m}\rho}(\mathbf{r},\mathbf{r}',\omega)\,\delta v_s(\mathbf{r}',\omega)\,d\mathbf{r}' \quad . \tag{5.26}$$

Terms like $\chi_{\mathbf{j}\rho}/\omega$ and $\left(\chi_{\mathbf{jj}}(\mathbf{r},\mathbf{r}',\omega) - \chi_{\mathbf{jj}}(\mathbf{r},\mathbf{r}',0)\right)/\omega^2$ remain finite in the limit $\omega \to 0$ and can be evaluated directly. In this way we can directly calculate the static polarizability from

$$\alpha(\omega)_{ij} = \left\{\int\left(\frac{-1}{\omega}\delta j_i(\mathbf{r},\omega)\right)d\mathbf{r}\right\}_{\mathbf{E}=-i\hat{\mathbf{e}}_j} \quad . \tag{5.27}$$

This is the approach we used in our other works [79-83]. The difference between the results obtained with these two methods is negligibly small.

5.4 The spin-dependent case

We showed in Chapter 4 that in case of spin-restricted singlet excitations we could use the same formulation for the VK-functional as for the spin-independent case. We also showed that in the case of triplet excitation energies in the static limit the only thing that essentially changes when using the VK-functional is the $\tilde{\eta}_{\mathrm{xc}}$. We discuss our choices for $\tilde{\eta}_{\mathrm{xc}}$ in the next section.

5.5 The response kernels

The only part of the VK-functional (Eqs. (4.54) and (4.63)) that needs to be specified are the coefficients $\tilde{\eta}_{\mathrm{xc}}^{\sigma\sigma'}(\omega)$ and $\tilde{\zeta}_{\mathrm{xc}}^{\sigma\sigma'}(\omega)$. We saw in Chapter 4 that these coefficients are related to the regular component of the xc-kernel of the homogeneous electron gas by the following relations [60],

$$\tilde{\eta}_{\mathrm{xc}}^{\sigma\sigma'}(\omega) = -\frac{\rho_{0,\sigma}(\mathbf{r})\rho_{0,\sigma'}(\mathbf{r})}{i\omega}B_{\mathrm{T}}^{\sigma\sigma'}(\omega)\,, \tag{5.28}$$

$$\tilde{\zeta}_{\mathrm{xc}}^{\sigma\sigma'}(\omega) = -\frac{\rho_{0,\sigma}(\mathbf{r})\rho_{0,\sigma'}(\mathbf{r})}{i\omega}\left(B_{\mathrm{L}}^{\sigma\sigma'}(\omega) - \frac{4}{3}B_{\mathrm{T}}^{\sigma\sigma'}(\omega) - \frac{\partial^2\varepsilon_{\mathrm{xc}}}{\partial\rho_{0,\sigma}\partial\rho_{0,\sigma'}}\right), \tag{5.29}$$

We work in the static limit and in Chapter 4 we showed that the coefficient $\omega\tilde{\zeta}_{\mathrm{xc}}^{\sigma\sigma'}(\omega)$ vanishes in this limit and that we need to consider the following singlet and triplet combinations of the $\tilde{\eta}_{\mathrm{xc}}^{\sigma\sigma'}(\omega)$

$$\begin{aligned}\tilde{\eta}_{\mathrm{xc}}^{S}(\omega) &= -\sum_{\sigma\sigma'}\frac{\rho_{0,\sigma}\rho_{0,\sigma'}}{i\omega}B_{\mathrm{T}}^{\sigma\sigma'}(\omega)\\ &= \frac{-\rho_0^2}{i\omega}f_{\mathrm{xc}}^{\mathrm{T}}(\omega)=\tilde{\eta}_{\mathrm{xc}}(\omega)\end{aligned} \tag{5.30}$$

$$\begin{aligned}\tilde{\eta}_{\mathrm{xc}}^{T}(\omega) &= -\sum_{\sigma\sigma'}\sigma\sigma'\frac{\rho_{0,\sigma}\rho_{0,\sigma'}}{i\omega}B_{\mathrm{T}}^{\sigma\sigma'}(\omega)\\ &= \frac{-\rho_0^2}{i\omega}B^{\mathrm{T}}(\omega)\end{aligned} \tag{5.31}$$

The $\tilde{\eta}_{\mathrm{xc}}^{S}(\omega)$ is identical to the $\tilde{\eta}_{\mathrm{xc}}(\omega)$ of the spin-independent case. Since we work in the static limit, we need to find expressions for $f_{\mathrm{xcT}}(0)$ and $B^{\mathrm{T}}(0)$.

It remains to find values for $f_{\mathrm{xcT}}(0;\rho_0)$. Nifosì, Conti and Tosi [68] did a mode-coupling calculation for the electron gas and obtained values for the shear modulus μ_{xc} for a number of r_s values. We can then use that $f_{\mathrm{xcT}}(0)=\mu_{\mathrm{xc}}/\rho_0^2$ and obtain values for $f_{\mathrm{xcT}}(0;\rho_0)$ at these r_s values. To obtain values for any r_s we do a cubic spline interpolation taking into account the exact exchange-only quadratic behavior for small r_s ($f_{\mathrm{xcT}}(\omega)=3\pi/10k_F^2$ [9]). More details on this procedure and the values for $f_{\mathrm{xcT}}(0;\rho_0)$ can be found in section 5.5. More recently Qian and Vignale [66] used the explicit values of the Landau parameters obtained in Ref. [69] to obtain values for μ_{xc}, we also use these values in some of our calculations.

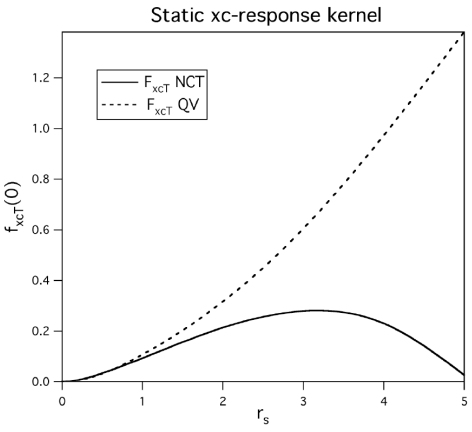

Figure 5-1. The static response kernel $f_{\mathrm{xcT}}(0)$ in [a.u.] as a function of r_s.

The transverse and longitudinal response kernels $f_{\mathrm{xcL}}(\omega)$ and $f_{\mathrm{xcT}}(\omega)$ have been investigated for the electron gas [63,65,68,84]. They are smooth functions for small frequencies [66]. In order to implement the VK-functional in the static limit we only need to obtain the values of the exchange-correlation kernel $f_{\mathrm{xcT}}(0)$ as a function of ρ_0. Nifosì, Conti and Tosi (NCT) [68] did a mode-coupling calculation for the electron gas and obtained values for the shear modulus μ_{xc} for a number of r_s values ($r_s \equiv (3/4\pi\rho)^{1/3}$). More recently Qian and Vignale (QV) [66] used explicit values of the Landau parameters obtained in Ref. [69] to

Table 5-1. $f_{\mathrm{xcT}}(0)$ and $B^{\mathrm{T}}(0)$ in a.u.

r_s	1	2	3	4	5
$f_{\mathrm{xcT}}(0)$ NCT	0.09286	0.21341	0.27897	0.02902	0.0029
$f_{\mathrm{xcT}}(0)$ QV	0.10702	0.31605	0.60404	0.97114	1.40975
$B^{\mathrm{T}}(0)$	0.11811	0.34376	0.63792	1.00457	1.43329

obtain values for μ_{xc}. We show these values in Table 5-1. We only show the NCT and QV values for $r_s \leq 5$ since only these are needed for the molecular calculations. We can then use that $f_{\mathrm{xcT}}(0) = \mu_{\mathrm{xc}} / \rho_0^2$ and obtain values for $f_{\mathrm{xcT}}(0;\rho_0)$ at these r_s values. To obtain values for any r_s we do a cubic spline interpolation in the range 0-5 for the r_s values, taking into account the exact exchange-only quadratic behavior for small r_s ($f_{\mathrm{xcT}}(\omega) = 3\pi/10k_F^2$ [9]). For values $r_s > 5$ we keep $f_{\mathrm{xcT}}(0)$ constant and equal to its value at $r_s = 5$. We checked that changing the behavior of $f_{\mathrm{xcT}}(0)$ for $r_s > 5$ did not influence our results. In Figure 5-1 the values for $f_{\mathrm{xcT}}(0)$ are plotted against r_s for $r_s \leq 5$.

The known values of $B^{\mathrm{T}}(0)$ [60,69] for $r_s \leq 5$ are also given in Table 5-1. In order to obtain the values for $B^{\mathrm{T}}(0)$ for all r_s we use the same interpolation scheme as described above for $f_{\mathrm{xcT}}(0)$.

Chapter 6

The static polarizability of oligomers

In this chapter we show our results for the static polarizability of oligomers of several polymeric systems. The systems we study in this chapter are the model hydrogen chain (H_{2n}) and the conjugated systems polyacetylene (PA), polydiacetylene (PDA), polybutatriene (PBT), polyyne (PY), polythiophene (PT), polyethylene (PE), polysilane (PSi), polysilene (PSi2), and polymethineimine (PMI). These results are presented in Refs. [77] and [78].

6.1 Introduction

So far TDDFT has been applied mainly within the adiabatic local density approximation (ALDA) in which the exchange-correlation (xc) potential v_{xc} is simply a local functional of the electron density. However, this approximation was shown to fail dramatically for the case of long molecular chains. For this case large overestimations of the polarizabilities and hyperpolarizabilities have been observed [10,11,77]. The reason for the failure of the ALDA is precisely its locality. In this approximation the potential depends only on the local density. Therefore the potential in the center of the molecular chain is insensitive to changes in the charges at the endpoints of the chain. For the exact exchange-correlation potential, however, these endpoint charges turn out to have important global effects. In particular it gives rise to a counteracting xc-field, i.e. an xc-potential that increases linearly along the molecular chain [11,85,86]. The induced density does not show an increase along the chain. Therefore such a counteracting term cannot be reproduced by a simple local approximation for v_{xc} and this causes the overestimation of the polarizability by the ALDA. To obtain such global changes in v_{xc} as a functional of the electron density, the functional must be nonlocal [87].

Nonlocal density functionals that do describe the counteracting field are, for example, the exchange-only Krieger-Li-Iafrate (KLI) [20] approximation and the common energy denominator approximation (CEDA) [21,45]. The orbital dependent KLI potential already improves the polarizability of the much discussed model hydrogen chain H_{2n} (see for example Refs. [88], [89], and references therein) compared to the local density approximation (LDA) and generalized gradient approximations (GGAs) [11,21]. The CEDA is based on the common

energy denominator approximation for the static orbital Green's function. The polarizabilities obtained for the model hydrogen chain using the CEDA improve the KLI results [21]. Basis of the success of these exchange-only potentials is their explicit dependence on the orbitals, which allows for a nonlocal dependence on the density. Currently these approaches are restricted to the exchange-only approximation.

Another way to include nonlocality, which, in addition, allows for transverse external fields, is by the use of current functionals. This is the method we explained in the previous chapters. Using the current $\mathbf{j}$ as a local indicator of global changes in the system is essential for the calculation of the macroscopic polarization of solids [90-93], which is impossible to obtain from an infinite system calculation based on pure density functional theory [87,94-96]. As we have shown in the previous chapters, the variable conjugate to the current density is the vector potential, in analogy to the scalar potential being conjugate to the electron density. In the Kohn-Sham approach to time-dependent current-density functional theory (TDCDFT) this vector potential also has an xc-component $\mathbf{A}_{xc}$. This vector xc-potential is needed to satisfy the constraint that not only the true density is obtained in the noninteracting Kohn-Sham system, but now also the true current density. The longitudinal part of the current is completely determined by the density through the continuity equation. Therefore $\mathbf{A}_{xc}$ is needed to fix the transverse part of the current. Once an approximation is given for $\mathbf{A}_{xc}$, the Kohn-Sham equations can be solved self-consistently. However, few approximations are known. Vignale and Kohn (see Chapter 4) were the first to propose such an approximation [8,9]. Their motivation was to develop an xc-functional that is nonlocal in time, but still local in space. It was found that nonlocality in time implies ultranonlocality in space, if one insists on using the density as the basic variable. However, a dynamical xc-functional that is nonlocal in time but local in space, can be constructed in terms of the current density. They did a careful analysis of the weakly inhomogeneous electron gas and arrived at an expression [8,9,23,24] for the induced xc-electric field. This expression has been applied successfully to plasmon linewidths in quantum wells [62,97] and in simplified form to calculate optical spectra of solids [7].

In this chapter we study several systems that are nonconjugated (polyethylene and the model hydrogen chain), σ-conjugated (polysilane), or π-conjugated oligomers (polyacetylene, polythiophene, polyyne, polymethineimine, polysilene, polydiacetylene, and polybutatriene).

6.2 Computational details

We studied ten systems for which the traditional TDDFT/ALDA method is known to fail. The choice of these systems was further guided by the availability of comparative accurate many-body results, as well as their chemical and physical importance [98]. We studied the model hydrogen chain (H_{2n}) and the conjugated systems polyacetylene (PA), polydiacetylene (PDA), polybutatriene (PBT), polyyne (PY), polythiophene (PT), polyethylene (PE), polysilane (PSi), polysilene (PSi2), and polymethineimine (PMI). These systems differ in their degree of bond order and chemical composition.

All calculations were performed with our modified version of ADF [25,99-103]. In these calculations we used the standard ADF basis set TZ2P (old basis V), which is a triple-zeta Slater type basis set augmented with two polarization functions. Cores were kept frozen for carbon and nitrogen up to 1*s* and for sulfur and silicon up to 2*p*. These basis sets are sufficiently large for our purpose of comparison.

In all calculations the ground state has been calculated with the LDA functional in the VWN parameterization [34]. The response calculations themselves were done with the standard adiabatic local density approximation (ALDA) and the VK-functional. For the latter we use a parameterization of the viscoelastic coefficient based on results of Conti *et al*. [65] for the transverse response of the homogeneous electron gas [77]. From now on we denote these calculations simply as ALDA and VK instead of LDA/ALDA and LDA/VK.

We compare our VK results to other (*ab initio*) calculations from the literature. Therefore we attempted in all cases to use a geometry equal or at least very close to the geometries used in the reference calculations. In each case we used a fixed monomer geometry for all oligomers of a specific type. These monomer geometries are equal to the converged geometries (with respect to chain length) from the references. Note that in some references geometries have been optimized per oligomer. The monomer geometries we used are depicted in the insets of Figure 6-1 till Figure 6-11 for PA [12], PY [104], PT [105], PMI [106], PDA [107], PBT [107], PE [108], PSi [108], PSi2 [109], and the model hydrogen chain [88]. The literature results of polyacetylene [12,13] are obtained with geometries that are optimized for each oligomer, our monomer geometry is equal to their converged geometry. In case of polydiacetylene oligomers the literature results [107] are optimized for 1-7 units, in case of 8 units and up they add converged units to the center of the oligomer. We used their converged unit as our monomer geometry. The polythiophene geometry we used is slightly different from that in Ref. [105]. The polymethineimine geometry was obtained from Ref. [106], where we used their type A trans-

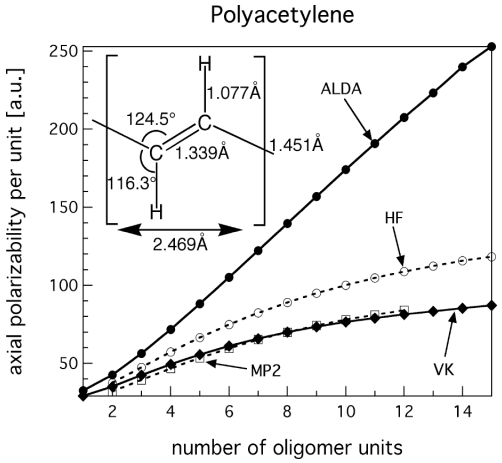

Figure 6-1. ALDA and VK static axial polarizability of polyacetylene compared with restricted Hartree-Fock [12] and MP2 [13] results.

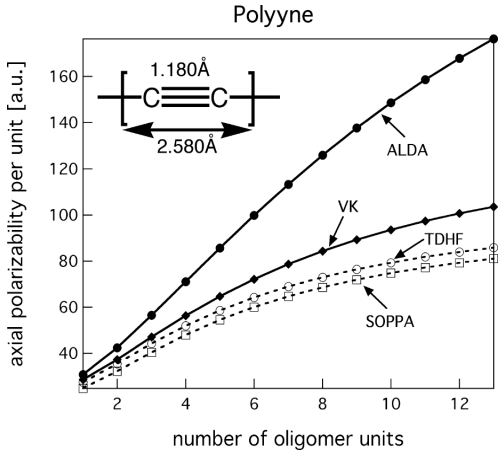

Figure6-2. ALDA and VK static axial polarizability of polyyne compared with time-dependent Hartree-Fock (TDHF) and correlated second-order polarization propagator approximation (SOPPA) results [104].

transoïd polymethineimine geometry for the monomer. The PSi2 geometry was obtained from [109] where we chose the geometry of the central units and a value of 1.500 Å for the Si-H bond length. The equilibrium bond length of the diatomic silylidyne molecule (HSi) is 1.5201Å [110], the Si-H bond length in several other silicon compounds is about 1.48Å [110]. The polarizability differs less than 0.5% by changing the Si-H distance from 1.500Å to 1.480Å.

The axial polarizability per oligomer unit can be obtained with several methods, for example by simply dividing the axial polarizability by the number of units or by subtracting the polarizability of the oligomer with N-1 units from that with N units. The results for these methods are not identical. We divided the axial polarizability by the number of units. In cases from literature where originally other methods were used, the results were recalculated to be in accordance with our method.

6.3 Results

6.3.1 Polyacetylene

The prototype of a conjugated polymeric system is polyacetylene (PA). In Figure 6-1 we compare our VK and ALDA results for the static axial polarizability for PA with restricted

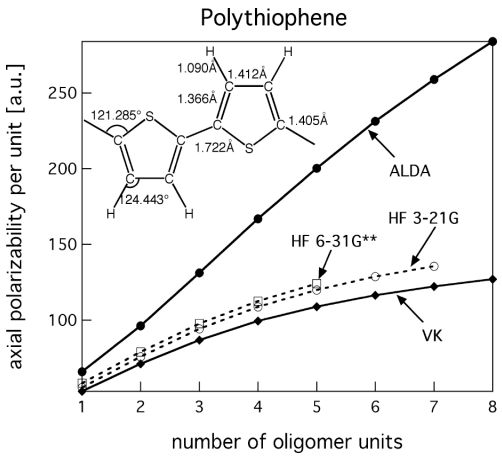

Figure 6-3. ALDA and VK static axial polarizability of polythiophene compared with coupled perturbed Hartree-Fock results [105] using the 3-21G and 6-31G** atomic basis sets.

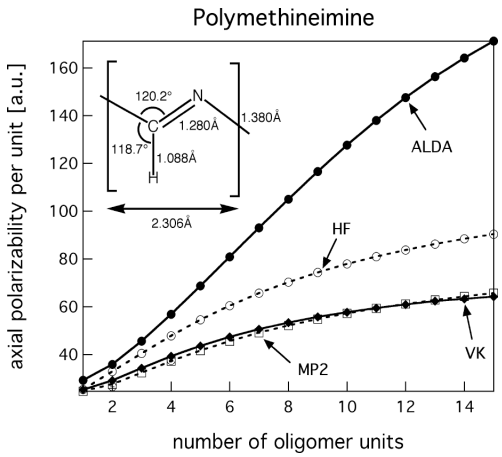

Figure 6-4. ALDA and VK static axial polarizability of polymethineimine compared with coupled Hartree-Fock (HF) [106] and MP2 [112] results.

Hartree-Fock calculations [12] and MP2 results [13]. We see that the VK-functional gives a huge correction of the ALDA results. The VK results lie close to Hartree-Fock results and are in good agreement with the MP2 values.

6.3.2 Polyyne

A system that is related to PA is polyyne (PY). Since PY has triple bonds we expect it to have a higher polarizability than PA. We show the results for PY in Figure 6-2 together with Hartree-Fock results [111]. By comparing the two systems we see that the ALDA results for PY lie lower that those for PA but the PY polarizabilities obtained with VK lie indeed at higher values than those of PA.

6.3.3 Polythiophene

A larger system we studied is polythiophene (PT). It is the first system we study that has a heteroatom (sulfur) in the backbone. Below we will also discuss polymethineimine that has a nitrogen atom in the backbone. It can be seen from Figure 6-3 that the VK results lie close to the coupled perturbed Hartree-Fock values [105], contrary to the ALDA results.

6.3.4 Polymethineimine

A system that is isoelectronic with PA is polymethineimine (PMI). Our ALDA and VK results are depicted in Figure 6-4 and compared with coupled Hartree-Fock results [106], we also compare to MP2 results with a slightly different geometry [112]. The VK results are on top of these MP2 results and give a large correction to ALDA. This is very similar to the results we observed for PA.

The MP2 results were obtained with a somewhat different geometry, namely the type B geometry from Ref. [106]. To see what the effect of a change in geometry is on our results, we did calculations on PMI oligomers of the type B geometry with 5 and 10 units and found a reduction in the axial polarizability of 3.9% and 5.7% respectively, compared to type A. In case of HF the changes are larger, with percentages of 8.1% and 12.8% respectively. This shows that, at least for this system, VK is not very sensitive to geometry changes. Therefore we believe that it is justified to compare our VK results with the MP2 results.

Recent MP2 results are very close to our values [113] for the shorter chain lengths. For the longer chains they start to deviate slightly from the VK values, but it should be noted that these MP2 results that have been obtained with an optimized geometry for each oligomer and not with a fixed monomer geometry. The MP2 values for the dimer and tetramer, with values of 26.3 a.u. and 37.2 a.u. per oligomer unit, are according to the authors of Ref. [113] within 1% of CCSD(T) values and are on top of the VK values.

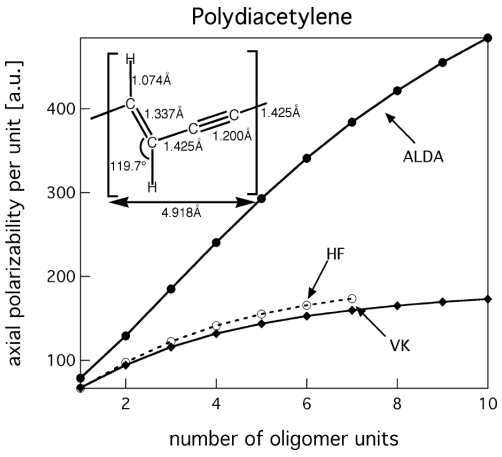

Figure 6-5. ALDA and VK static axial polarizability of polydiacetylene compared with coupled Hartree-Fock results [107].

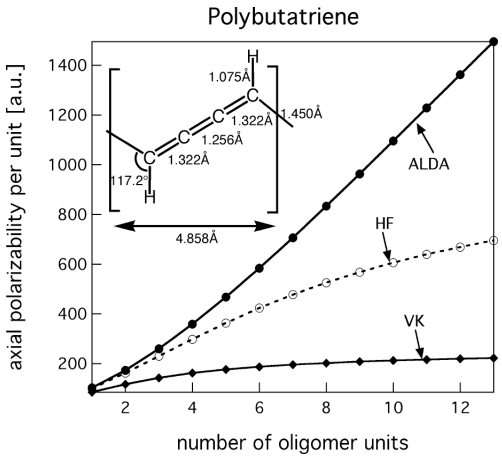

Figure 6-6. ALDA and VK static axial polarizability of polybutatriene compared with coupled Hartree-Fock (HF) [107] results.

6.3.5 The polydiacetylenes: polydiacetylene and polybutatriene

Systems, in which HF is very sensitive to the geometry whereas VK is not, are the polydiacetylenes. Depending on the nature of their side groups, polydiacetylenes can occur in a structure ranging from the acetylenic $[CR=CR'-C\equiv C]_N$ to the butatrienic $[CR=C=C=CR']_N$ form. PDA and polybutatriene (PBT) with R=R'=H are interesting systems to compare. These systems are tautomers of which PDA turns out to be the stable configuration. In Figure 6-5 we compare our ALDA and VK results for PDA with available coupled Hartree-Fock results [107]. The ALDA again strongly overestimates the polarizability and VK gives a reduction. The VK results are in good agreement with the HF values. In Figure 6-6 we compare our ALDA and VK results for PBT with available coupled Hartree-Fock results [107]. The ALDA results again severely overestimate the polarizability. Again VK gives a huge reduction of this polarizability but the values are much smaller than the HF results. Apparently the ultranonlocal effects treated by VK are very important in this system.

The difference between the axial polarizabilities for VK and HF in PBT is very different from what we observed for PDA, where the VK and HF results are in close agreement. In Figure 6-7 the results for PDA and PBT are compared for VK and HF [107]. The VK results for PBT and PDA are very similar, the values for PBT being somewhat bigger. Note that the HF results for PBT give a surprisingly large value for the axial polarizability compared with the HF results for PDA. The disagreement between HF and VK for PBT raises the question which method gives the most accurate results. Other HF results are available for infinite chains [114] and for the average polarizability small oligomers [115]. Champagne and Öhrn [114] did CPHF calculations on the infinite PDA and PBT systems. The values for the axial polarizability per oligomer unit are 134.4 a.u. for PDA and 626.4 a.u. for PBT with HF using the minimal STO-3G basis. Again the PBT value is much higher than the PDA value. These values are smaller than found by Perpète *et al.* [107] for the longer oligomers. It should be noted that the infinite chain calculations were done in a minimal STO-3G basis set. These results are in disagreement with the results for PBT of Bodart *et al.* [115] for the average polarizability $\langle\alpha\rangle = \left(\alpha_{xx} + \alpha_{yy} + \alpha_{zz}\right)/3$, obtained with finite-field HF within the minimal STO-3G basis set. Since for these polymeric systems the dominant contribution to the average polarizability is in the axial direction, we may compare these values with the value for the axial polarizability. The value of the average polarizability we obtained with VK (63.49 a.u. per unit) for the three-unit oligomer agrees with their value (61.61 a.u. per unit). Accurate benchmark results [116,117] obtained with the coupled-cluster (CCSD(T)) method in a double-zeta basis set with one polarization function, are available for the monomer and dimer of PDA and PBT in the same geometry as used by us. These results are presented in Table 5-1. From this table it is clear that the PDA results for VK, CPHF, and CCSD(T) are close to each other. Much larger differences are found for the PBT case, where the CCSD(T) values are in between the HF and VK values. Unfortunately no accurate results are available for the longer oligomers. This does not allow us to make further conclusions on the accuracy of the VK vs. HF

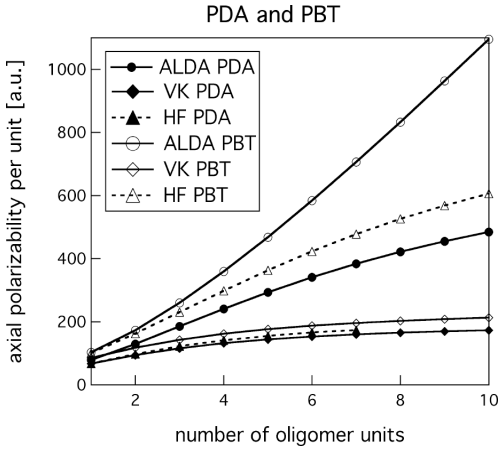

Figure 6-7. Results for the static axial polarizability of polydiacetylene and polybutatriene are compared for VK and coupled Hartree-Fock (HF) [107].

Table 6-1. The axial polarizabilities per oligomer unit in atomic units (a.u.) of the monomer and dimer of PDA and PBT at different levels of theory.

		ALDA	VK	HF[a]	CCSD(T)[b]
PDA	monomer	78.71	67.32	66.71	65.03
	dimer	129.13	94.30	97.36	92.5
PBT	monomer	102.94	85.21	100.31	92.06
	dimer	172.96	117.13	162.19	136.1

[a]Ref. [107] [b]Ref. [117]

results in case of PBT. No direct experimental results are available for this system. Perpète *et al*. [107] estimated the polarizabilities of PDA and PBT using the experimental values for the polydiacetylenes PTS (R=R'=$CH_2OSO_2C_6H_4CH_3$) and TDCU (R=R'=$(CH_2)_4OCONHC_6H_5$). They derived a value of 383 a.u. for PDA and 402 a.u. for PBT for the axial polarizability per oligomer unit for infinite chains. These values indicate that the PBT values are only slightly bigger than the PDA results. They are in the same range as our VK results and much smaller than the HF results for PBT. More insight in this issue can be obtained from accurate correlated *ab initio* methods applied to longer oligomers, which leaves an interesting future challenge.

6.3.6 Polyethylene

We studied polyethylene (PE) in its linear zigzag form. The ALDA and VK results are depicted in Figure 6-8 and compared with coupled perturbed Hartree-Fock results [108]. Contrary to the case of conjugated polymers we see that ALDA, VK, and HF curves run almost parallel. Remarkable is that ALDA does not give a large overestimation of the polarizability for the longer oligomers. VK only gives a small and reasonably constant correction to the ALDA results. The experimental average polarizability for the monomer is 29.62 a.u. [118]. This is close to the ALDA result with a very large basis set (30.74 a.u. Ref. [119]). Our VK value for the average polarizability of the monomer is 26.69 a.u.. These values for the average polarizability are already considerably larger than the HF value of 21.49 a.u.. Polarizabilities obtained with more accurate methods are therefore expected to be closer to the experimental as well as ALDA and VK values. Since VK gives a small correction on the ALDA, apparently nonlocal effects described by VK are not important in this system. This is consistent with low electron mobility in PE.

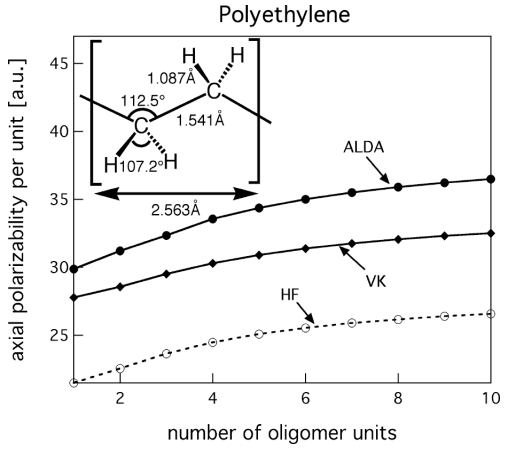

Figure 6-8. ALDA and VK static axial polarizability of polyethylene compared with coupled Hartree-Fock (HF) [108] results.

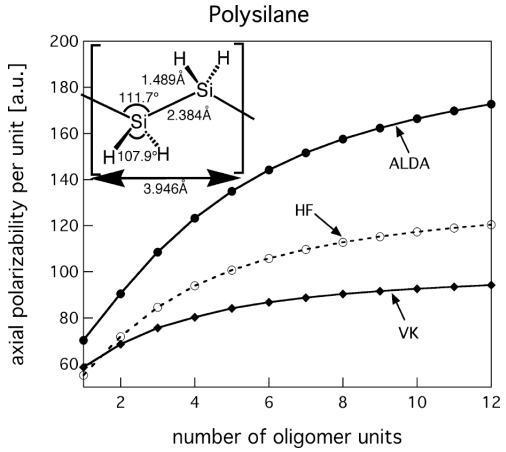

Figure 6-9. ALDA and VK static axial polarizability of polysilane compared with coupled Hartree-Fock (HF) [108] results.

6.3.7 Polysilane

The silicon analog of PE is polysilane (PSi). Unlike in PE there is experimental and theoretical evidence for σ-conjugation in PSi (see for example Ref. [108] and [109] and references therein). Our results are displayed in Figure 6-9. The polarizability per unit increases more steeply with chain length for ALDA than for HF, although the overestimation is not as severe as in the π-conjugated systems. In contrast to what we observed for PE, VK gives a large correction in PSi, which brings the results closer to the available CPHF results [108]. Apparently nonlocal effects described by VK are important for this system.

6.3.8 Polysilene

The silicon analog of PA is polysilene (PSi2). Because PSi already has a high polarizability the PSi2 molecule is expected to be even more polarizable. Coupled Hartree-Fock calculations confirm this assertion [109]. In Figure 6-10 these HF results are compared with our ALDA and VK results. As expected the ALDA strongly overestimates the polarizability per unit and increases steeply with chain length (more than linearly). In this case VK drastically modifies the results, which is indicative of very large nonlocal effects. Going from PE, via PA and PSi, to PSi2 we see an increase in the polarizability. Within this series we also observe the trend that the

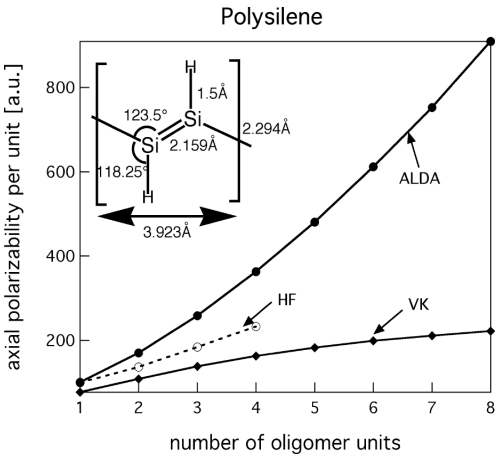

Figure 6-10. ALDA and VK static axial polarizability of polysilene compared with coupled Hartree-Fock [109] results.

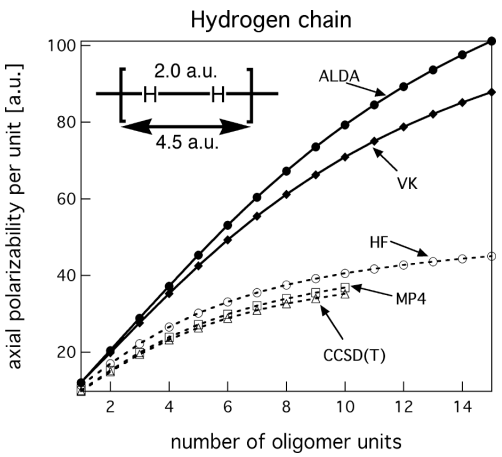

Figure 6-11. ALDA and VK static axial polarizability of the model hydrogen chain compared with coupled Hartree-Fock (HF), MP4, and coupled-cluster (CCSD(T)) results [88].

ALDA overestimation increases and the VK corrections become larger. It therefore seems that high electron mobility and nonlocal effects are connected.

6.3.9 The model hydrogen chain

An important exception to this observation seems to be the model hydrogen chain, H_{2n}. We show the ALDA and VK results in Figure 6-11, and compare our results with coupled Hartree-Fock (HF), MP4, and coupled-cluster (CCSD(T)) results [88]. In this system the ALDA overestimates the polarizability considerably and VK gives only a slight correction. This calls for an explanation. We observe that the induced current is too large since the same is true for the VK polarizability. Hence the counteracting xc-electric field that is introduced by VK is not large enough to get the correct polarizability as obtained from CCSD(T) and MP4. From Eq. (4.54) we see that the counteracting field is proportional to the induced current. If the VK-functional is able to incorporate all nonlocal effects then we can conclude that the proportionality coefficient $f_{\mathrm{xcT}}(0)$ is too small for this system. To investigate the dependence of VK on the size of the induced current we study model hydrogen chains by varying the bond length alternation (BLA). The BLA is defined as the difference in length between adjacent bonds. By increasing the bond-length alternation of the hydrogen chain, the system ranges from a metallic one-dimensional chain ($\mathrm{BLA} = 0$ a.u.) to a Peierls distorted semiconductor or insulator ($\mathrm{BLA} >> 1$ a.u.). For the

case $\mathrm{BLA} = 0$ a.u. we expect large induced currents and hence a large counteracting field. However, even in this case we only found a reduction in the order of 30% for 15 H_2 units. At this point we suggest two possible reasons for the failure of VK for model hydrogen chain. It is possible that the VK-functional has the right form but that the density behavior of the coefficients is insufficient. On the other hand, it could be that the form of the VK-functional is too restricted to treat all xc-effects that affect the polarizability. Later we will do some more analysis of this system.

6.4 Discussion

A clear picture emerges from the systems studied so far. For all systems where ALDA overestimates the polarizability, the VK correction is large, except for the model hydrogen chain. The general trend observed in hydrocarbons, is that the static polarizability decreases as one goes beyond the HF approximation [13,88,104]. We find the same trend for most VK results in relation to HF, which may indicate that the VK results are in general close to MP2.

The classical interpretation of conjugation is that there is a special distinction between delocalized systems of electrons in conjugated molecules and localized two center bonds in nonconjugated molecules [120]. However, more important for the behavior of the polarization of polymers is not the conjugation but the electron delocalization or mobility, which is measured by the polarizability. For the purpose of an overall comparison of the performance of the VK-functional, it is therefore desirable to classify the systems according to their polarizability. We found that the following power law can very well describe the polarizability as a function of the chain length:

$$\alpha(N) = AN^{\zeta}, \ (1 \le \zeta \le 3) \tag{6.1}$$

where N is the number of monomer units. The same power law has been used before in the fitting of the polarizability of oligomer chains [109]. We determined the exponent by a least squares fitting procedure to a straight line for a log-log plot, thereby weighing the N^{th} data point by N. This power law has been derived on the basis of Hückel [121,122], electron gas [123], and Hubbard models [124]. The exponent $\zeta = 3$ corresponds to the limit of free electrons on a rod, whereas the exponent $\zeta = 1$ is derived for a Hubbard model with infinite on-site repulsion, i.e. the limit of localized electrons. We can therefore consider the parameter ζ as a measure for the degree of delocalization, and order the systems accordingly. Of course our molecules differ from these idealized model systems and one may argue that for example an offset is needed to account

Table 6-2. Exponents ζ for the model hydrogen chain H_{2n} with different bond length alternations (BLAs). Exponents are calculated from the values found in the figure in this article. Here ALDA-VK denotes the difference between the ALDA and VK exponents.

BLA (a.u.)	ALDA	VK	ALDA-VK	CHF	MP4	CCSD(T)
0	2.37	2.12	0.25			
0.5	1.73	1.66	0.07	1.49	1.50	1.48
2	1.17	1.16	0.01	1.10	1.09	1.09

for the end groups. We do not expect that such modifications of the power law will substantially change the value found for the exponents, especially since end group effects become small for the long chains. Since all the systems we study are insulators, one would expect the polarizability to grow linear in the limit of large *N*. The chain lengths we studied are not long enough to see this effect, so we will in general obtain values of $\zeta > 1$.

As a first example we can look at the model hydrogen chain with different BLAs. The exponents we found are presented in Table 5-1. For $\mathrm{BLA} = 0$ a.u. we find a value of $\zeta = 2.37$ for the ALDA, which is close to the free electron limit. For the other extreme, $\mathrm{BLA} = 2$ a.u., we find $\zeta = 1.17$ for the ALDA, which is close to the limit of localized electrons. For the model hydrogen chain the VK turns out to reduce this exponent only slightly. It is clear that, at least for $\mathrm{BLA} = 0.5$ a.u. and $\mathrm{BLA} = 2$ a.u., the VK is unable to introduce a sufficient amount of localization in H_{2n}. The HF exponents, on the other hand, agree well with MP4 and CCSD(T).

In Table 6-3 we give the exponents for the other systems studied here, together with the values obtained from the cited reference data. We observe that VK in general gives a reduction of the exponent in agreement with the HF values, except for PBT and PSi2. Note, however, that for PSi2 the HF exponent is only based on 4 data points. Where comparative data are available, both the VK and HF exponents are in good agreement with correlated wave function methods. The HF values for the polarizability itself are, however, larger than those of the correlated methods due to a larger prefactor *A* in Eq. (6.1).

Earlier we observed the trend in the polarizabilities in going from PE, via PA and PSi, to PSi2, that the ALDA overestimation increases and the VK correction becomes larger. However the exponents reveal that with growing chain length the PA chains will ultimately be more polarizable than the PSi chains. In view of this, the correct order for the polarizability in the very long chain limit should be PE-PSi-PA-PSi2. The same order is observed as we look at the reduction of the ALDA exponents by VK. According to our definition of localization by means of the exponents of the power law, we can state that the electron delocalization is most prominent in PSi2 and nearly absent in PE, which is in accordance with intuitive views.

Table 6-3. Exponents ζ for various oligomers. Exponents are calculated from the values found in the figures in this article. Here ALDA-VK denotes the difference between the ALDA and VK exponents.

System	ALDA	VK	ALDA-VK	HF	MP2/SOPPA[a]
PE	1.09	1.07	0.02	1.09	
PSi	1.31	1.14	0.17	1.23	
PY	1.75	1.50	0.25	1.41	1.43
PT	1.76	1.39	0.37	1.44	
PMI	1.81	1.35	0.46	1.36	1.39
PDA	1.85	1.40	0.45	1.43	
PA	1.94	1.41	0.53	1.52	1.52
PBT	2.19	1.27	0.92	1.70	
PSi2	2.23	1.48	0.75	1.68[b]	

[a] MP2 results for PA and PMI, SOPPA results for PY
[b] This value is based on only 4 data points

In summary we can say that the ALDA exponents are more reduced by the VK if they are larger. The VK exponents are in good agreement with HF methods and beyond, except for the model hydrogen chain.

In all the graphs of the polarizability we show that convergence of the polarizability towards an infinite chain results seems to be very slow. This is partly because of the way we plot our results. We chose to plot $\Delta\alpha(N) = \alpha(N)/N$ which is a natural way of finding the polarizability per oligomers unit. Another way is to take the difference between consecutive oligomers $\Delta\alpha(N) = \alpha(N) - \alpha(N-1)$. In this way the effect of the end groups of the chains is mostly removed and it converges much faster than our method of choice.

6.5 Conclusions

We have applied TDCDFT to a range of finite oligomers. By treating the xc-effects using the current functional derived by Vignale and Kohn we were able to obtain polarizabilities in good agreement with accurate wave function methods. The VK-functional achieves large corrections to the ALDA. The latter was known to overestimate the polarizability considerably for conjugated oligomers. Moreover the large *N* behavior of VK as described by a power law was found to be in good agreement with reference data. For the model hydrogen chain we indicated that further improvements are probably needed in the VK-functional, in particular with regard to the density dependence of the static viscoelastic coefficients.

Chapter 7

Size-scaling of the polarizability of tubular fullerenes

In this chapter we present a study of the static polarizability for the tubular fullerenes $C_{60+i\times10}$, where i = 0...5, and the closely related [5,5] carbon nanotube, using time-dependent (current)-density-functional theory. Comparing the results obtained within the conventional adiabatic local-density approximation with those obtained using the VK current-dependent exchange-correlation functional it is found that the extra long-range exchange-correlation effects described by the current-density functional are important to consider, especially for the longest fullerenes. For all systems studied the current-density functional results are in good agreement with experiment, and the agreement with available ab initio self-consistent-field results and results from a point–dipole interaction model is much better than when using the adiabatic local-density functional.

7.1 Introduction

The dipole–dipole polarizability of an atomic cluster is next to being determined by its chemical composition also strongly influenced by the size and shape of the cluster. Characterizing these clusters by evaluating the dependence of the polarizability on the cluster geometry has therefore been an important research area [125-134]. The reason for the strong dependence is easily understood using an interacting point–dipole model of the cluster. As the self-consistent local fields acting upon the polarizable atoms will depend strongly on the arrangement of the atoms, so will the resulting induced dipole moments, which constitute the total response of the system. By adding more and more atoms to the cluster the effective polarizability per atom, which links the mean induced dipole moment per atom to the average local field, should converge towards a bulk value. This value is related to the experimental susceptibility of the bulk material via the famous Lorentz–Lorenz relation [134]. Typical systems studied are alkali-metal clusters [125-127] and semi-conductor clusters [128-130]. Another class is formed by the all-carbon clusters, which have attracted a lot of attention since

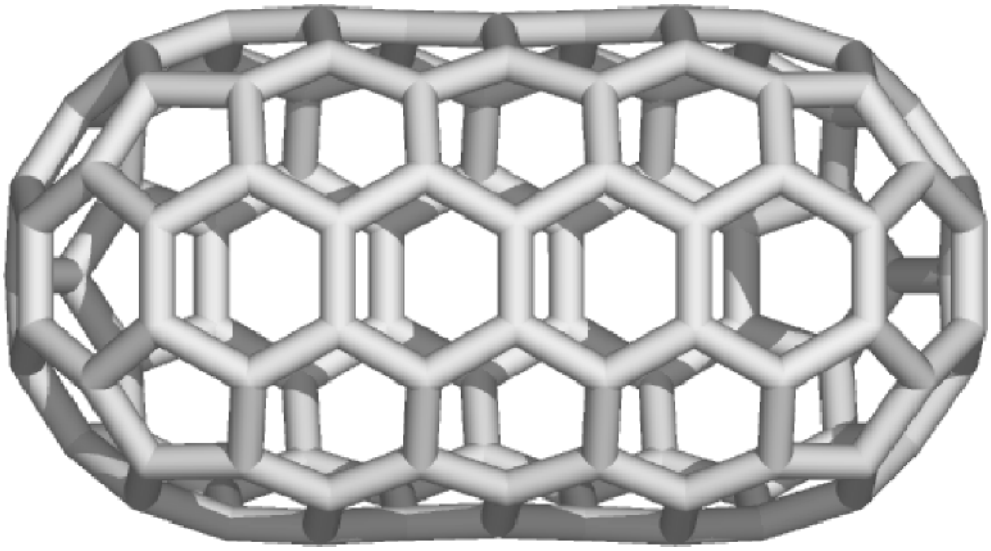

Figure 7-1. Structure of the C_{110} tubular fullerene.

their discovery, such as the fullerenes [135] and the carbon nanotubes [136]. In this chapter, we investigate the size dependence of the polarizability for the tubular fullerenes $C_{60+i\times10}$, where i = 0...5. These tubular fullerenes can be considered to be capped [5,5] carbon nanotubes as is illustrated in Figure 7-1.

We use time-dependent (current)-density-functional theory (TDCDFT) in this study. In the previous chapter we saw that the adiabatic local density approximation (ALDA) for the induced exchange-correlation effects tends to overestimate the polarizability and hyperpolarizability of conjugated polymers, especially for the longer oligomer chains [10,11]. The local approximation and also more advanced generalized gradient approximations (GGA) are unable to describe the highly nonlocal exchange and correlation effects found in these systems [10,11]. One way to overcome these shortcomings is to employ optimized effective potentials [17-19] or approximations to this potential [20,21]. We found in the previous chapter a successful alternative approach towards the solution of this problem by using TDCDFT with the VK-functional. With this method, the results obtained for the prototype conjugated polymers like polyacetylene are in excellent agreement with *ab initio* quantum chemical methods. The reason for choosing the tubular family of fullerenes in this study is that we can determine to what extent the highly nonlocal exchange-correlation effects are important for these fullerenes. If long-range effects are indeed important, it is expected from the studies of the conjugated polymers that

these contributions become more important with increasing tube length. The aim is both to investigate the size dependence of the polarizability for larger fullerenes and to assess the quality of the density- and current-density-dependent approximations for treating these all-carbon molecules within DFT.

For the smallest fullerene, C_{60}, a reasonably accurate experimental value and some theoretical calculations are available for the static polarizability. In comparing the various results it is found that the conventional DFT result of 543.8 a.u. reported in literature [137] is slightly higher than the *ab initio* self-consistent-field (SCF) result of 506.7 a.u. [138] and the result from the point dipole interaction (PDI) model of 522.9 a.u. [139]. All these results are in agreement, within the experimental uncertainty, with the experimental value of 516.2 ± 54 a.u. [131]. Other studies also indicate that conventional DFT predicts a polarizability for C_{60} that is larger than obtained with *ab initio* methods [140]. It is therefore interesting to investigate if some of the differences between the conventional DFT results and *ab initio* SCF results for the C_{60} molecule are caused by highly nonlocal exchange-correlation effects.

7.2 Computational details

We performed the TDCDFT calculations within the linear response formulation. The calculations of the polarizability were done using the ALDA and the VK approximation for exchange-correlation functionals, with the use of a modified version of the Amsterdam Density Functional (ADF) program package [25,71]. For the ALDA calculations we used a ground-state description obtained within the statistical averaging of (model) orbital potentials method (SAOP) [40], which is a shape-corrected potential constructed for the calculation of molecular response properties. The SAOP ground-state potential usually gives superior results for the (hyper)polarizability compared with LDA and GGA potentials [40]. The VK response calculations, on the other hand, were performed using the standard LDA description of the ground state, as this description is compatible with the VK-functional. The structures of the fullerenes C_{60}-C_{100} were taken from [141] and the structure of C_{110} from [142]. The structure of C_{100} was relaxed in order to obtain the correct symmetry. For the model PDI calculations, the structures used were optimized at the PM3 level and taken from [142], which is consistent with the PDI model parameterization [143].

Table 7-1. Mean static dipole-dipole polarizability (in a.u.) of tubular fullerenes calculated using TDDFT within the SAOP/ALDA approximation for a double-zeta plus polarization (DZP), valence triple-zeta plus polarization (TZP), and augmented TZP basis (TZP+).

Fullerene[a]		DZP	TZP	TZP+
C_{60}	D_{5d}	512.8	545.5	581.6
C_{70}	D_5	631.5	669.8	707.6
C_{80}	D_5	729.3	772.0	811.7
C_{90}	D_{5h}	841.1	887.6	932.5
C_{100}	D_5	976.1	1026.4	1073.2
C_{110}	D_{5h}	1126.5	1183.2	1235.0

[a] The symmetry used in the calculations.

7.3 Results and discussion

We compare our results with experimental data, with results obtained using wave function methods, and with results obtained using the PDI model [139,143]. Experimental results for the dipole–dipole polarizabilities of the C_{60} and C_{70} molecules have recently been obtained in the gas phase with the use of molecular beam experiments [131-133]. For C_{60} a value of 516.2 ± 54 a.u. was reported for the static polarizability [131], and a value of 533 ± 27 a.u. was measured for the polarizability at the frequency 0.0428 a.u. (k = 1064 nm) [132]. For both the static and the frequency-dependent polarizability, the experimental results are in good agreement with recent quantum chemical calculations [137,138] and results from a frequency-dependent PDI model [139,143]. For C_{70} an experimental value of 688 ± 94 a.u. was reported for the static value [133] whereas the *ab initio* SCF result is 605.9 a.u. [138]. Thus far there have been no DFT calculations reported for the polarizability of the fullerenes larger than C_{60}.

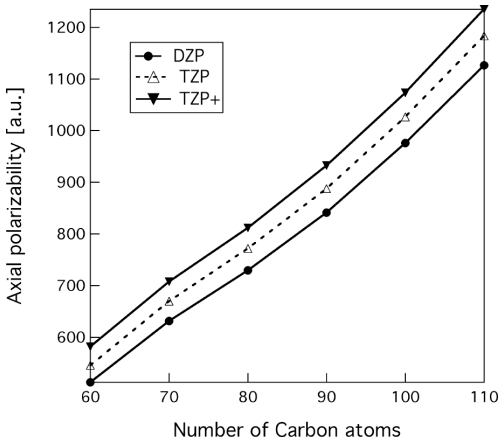

Figure 7-2. Mean polarizability in a.u. of the tubular fullerenes calculated using TDDFT with SAOP and different basis sets.

We first study the basis-set dependence of the results for the mean polarizability, $\bar{\alpha} = \frac{1}{3}\left(2\alpha_{\perp} + \alpha_{\parallel}\right)$ with $\parallel$ and $\perp$ indicating the directions along and perpendicular to the long axis of the molecule, that are obtained using the SAOP/ALDA combination of ground state and response potentials. The basis sets used are the standard ADF basis set of double-zeta plus polarization function (DZP) quality, the valence triple-zeta plus polarization function

Table 7-2. Static dipole-dipole polarizability for tubular fullerenes (in a.u.) obtained using TDCDFT within the SAOP/ALDA and LDA/VK approximations and using the PDI model. Given are the tensor components along ($\alpha_{\|}$) and perpendicular ($\alpha_{\perp}$) to the long axis, together with the mean value ($\bar{\alpha}$).

	$\alpha_{\|}$			$\alpha_{\perp}$			$\bar{\alpha}$		
	SAOP/ ALDA	LDA/ VK	PDI	SAOP/ ALDA	LDA/ VK	PDI	SAOP/ ALDA	LDA/ VK	PDI
C_{60}	581.60	533.59	522.76	581.60	533.59	522.76	581.60	533.59	522.77
C_{70}	758.90	683.44	668.82	681.89	620.00	591.82	707.56	641.14	617.49
C_{80}	947.33	836.76	814.11	743.87	677.63	665.87	811.68	730.67	715.28
C_{90}	1160.1	1005.5	977.55	818.67	752.95	735.98	932.47	837.14	816.50
C_{100}	1420.4	1193.8	-	899.57	821.75	-	1073.2	945.76	-
C_{110}	1698.2	1392.3	1328.8	1003.4	913.16	876.86	1235.0	1072.9	1027.5

(TZP) quality, and the TZP basis augmented with additional first-order field-induced polarization functions (TZP+) [144]. The TZP+ basis set is expected to give results for the polarizability, which are close to the basis-set limit [144]. Attempts to go beyond the TZP+ quality induced linear dependency of the basis set, effectively reducing the accuracy of the calculations. In Table 7-1 we present the mean polarizability for the tubular fullerenes calculated using the SAOP/ALDA potentials and different basis sets. The results are also plotted in Figure 7-2. From these results we see that the mean polarizability for each fullerene gradually increases in going from DZP to TZP+. We also see that for the larger fullerenes the difference in the polarizability obtained with TZP and TZP+ becomes smaller. From Figure 7-2 we see that the size-dependence of the polarizability for the fullerenes is similar for the different basis sets used. Therefore we do not expect that basis-set effects will affect our conclusions regarding the size dependence. Since TZP+ is expected to give results close to the basis-set limit we use this basis set in the remainder.

We can now study the results for the mean value and the two tensor components separately of the static polarizability as function of the fullerene size for the SAOP/ALDA and LDA/VK combinations. In Table 7-2 we present results for $\bar{\alpha}$, $\alpha_{\|}$, and $\alpha_{\perp}$ for the various fullerenes. The results for the tensor components $\alpha_{\|}$ and $\alpha_{\perp}$ have been plotted in Figure 7-3 as function of the system size for the SAOP/ALDA and LDA/VK approximations. In the same figure we have also plotted the results obtained with the PDI model. From the results in Table 7-2 and Figure 7-3 we see that for all fullerenes the polarizabilities obtained using LDA/VK are smaller than those obtained using SAOP/ALDA, and that the LDA/VK results are in close agreement with the PDI model calculations. Furthermore, we see that the differences are larger in the direction along the tube and that there is an increase in the difference as the size of the fullerenes becomes longer.

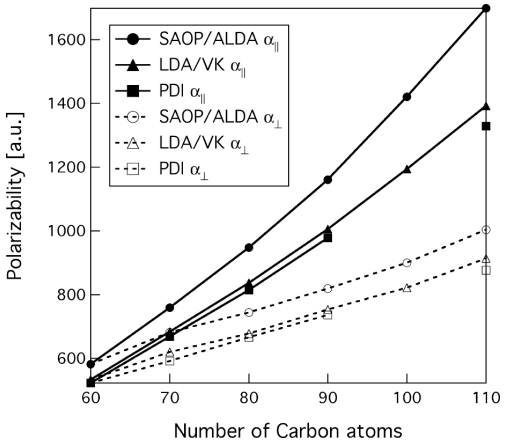

Figure 7-3. The polarizability in a.u. for the fullerenes as a function of the number of Carbon atoms.

For $\alpha_{\|}$ we see that the difference is 10% for C_{60} whereas for C_{110} this is 22%. Especially the values for $\alpha_{\|}$ obtained with SAOP/ALDA deviate more and more from the LDA/VK and the PDI results as the fullerene size increases. These results confirm that the highly nonlocal exchange-correlation effects added by the VK-functional become increasingly important in the longer fullerenes. In Figure 7-3 we see that the size-dependence of the perpendicular component, $\alpha_{\perp}$ is nearly linear, with some scattering due to the geometries used. We see that the SAOP/ALDA results are about 65 a.u. larger than the LDA/VK results, independently from the size.

The literature LDA/ALDA value of 543.8 a.u. [137] for C_{60} was obtained in a modified TZP basis, which is in excellent agreement with the corresponding SAOP/ALDA value of 545.5 a.u. for the TZP basis. The higher SAOP/ALDA value of 581.60 a.u. obtained in the TZP+ basis is therefore mainly caused by basis set effect. This is further supported by the fact that we obtain a value of 604.47 a.u. with LDA/ALDA using the same TZP+ basis. The experimental results for the static polarizability of C_{60} is 516 ± 54 a.u. [131], which is in close agreement with the SCF result of 506.7 a.u. [138], and the PDI result of 522.6 a.u. [139]. Comparing the results from the present work, the value of 581.60 a.u. obtained using SAOP/ALDA and 533.6 a.u. using LDA/VK, we see that the correction due to the VK potential (8%) brings the polarizability in close agreement with experimental, Hartree-Fock and PDI results, whereas the SAOP/ALDA and LDA/ALDA results are much larger, and lay outside the experimental uncertainty range.

For C_{70} the experimental result of 688 ± 94 a.u. [133] is in fair agreement with the SCF result of 605.9 a.u. [138] and all results from the present study: 617.5 a.u. for the PDI model, 707.6 a.u. with SAOP/ALDA and 641.14 a.u. with LDA/VK. Again we see that the VK result is in better agreement with the SCF and PDI results, and about 10% smaller than the SAOP/ALDA value. Both the SAOP/ALDA and the LDA/VK values are nonetheless well within the uncertainty range of 94 a.u. in the experimental result. The better agreement with the SCF result

is, however, an indication that the LDA/VK result is more accurate, according to the rule of thumb that was found in the case of conjugated polymers [77,78].

In order to estimate the effect of going to very large tube lengths we also calculated the polarizability per unit cell for a [5,5] carbon nanotube of infinite length. For the [5,5] carbon nanotube the unit cell consists of 20 carbon atoms. The calculations were done using the periodic structure version of the ADF program (BAND) [101,145], which uses the same methodology and basis-set types. The TDCDFT part [90,146] of this code was modified to include the VK-functional. Since the infinite [5,5] carbon nanotube has a semi-metallic band structure, we carefully checked that our results for the response calculations were converged with respect to the reciprocal space sampling. We used a valence triple-zeta basis with two polarization functions, and a k-space sampling of 19 points in the one-dimensional irreducible wedge. As the SAOP is not available in the periodic structure code, we obtained the LDA/ALDA and LDA/VK results, and compare with the finite system results discussed above. Therefore we estimate the polarizability per unit cell, $\Delta\alpha$ by calculating the difference in the polarizability multiplied by two, $\Delta\alpha(i) = 2\{\alpha(C_{60+i\times10}) - \alpha(C_{60+(i-1)\times10})\}$, with i = 1–5. The results for $\Delta\alpha_{\|}$ and the average value for $\Delta\alpha_{\perp}$ are presented in Table 7-3 together with the values for the periodic structure calculations. The values for the polarizability per unit cell estimated from the finite fullerenes should extrapolate for large i to an asymptotic value in agreement with the results obtained for the infinite nanotube. For the perpendicular component that depends linearly on the size, we get an average value for $\Delta\alpha_{\perp}$ of 152 a.u. using the LDA/VK results, which is about 10% smaller than the SAOP/ALDA result of 169 a.u. and which agrees quite well with the DPI model result of 142 a.u. The periodic structure calculation gives a similar reduction of 15%, from 150 a.u. (LDA/ALDA) to 128 a.u. (LDA/VK). For the parallel component of the polarizability per unit $\Delta\alpha_{\|}$ we see a qualitatively different behavior, with the SAOP/ALDA result growing more steeply with system size than the LDA/VK results. The latter agree very well with the PDI model calculations. The SAOP/ALDA result is about 18% larger than the LDA/VK result for C_{60}, which grows to 40% for C_{110} and even 47% for the infinite nanotube result. These features are in accordance with the trends observed in the conjugated polymers [77,78].

Table 7-3. The SAOP/ALDA, LDA/VK, and PDI results for the polarizability (in a.u.) per unit cell, $\Delta\alpha(i) = 2\{\alpha(C_{60+i\times10}) - \alpha(C_{60+(i-1)\times10})\}$. The component parallel to the long axis of the fullerenes is given as function of the number i of half unit cells, each containing 10 Carbon atoms. The average for the perpendicular component is calculated using the first five values. The values with $i = \infty$ correspond to the [5,5] Carbon nanotube results. The LDA/ALDA result for the nanotube given in brackets can be used as estimate for the extrapolated SAOP/ALDA value.

i	$\Delta\alpha_{\parallel}(i)$			$\Delta\overline{\alpha}_{\perp}$		
	SAOP/ ALDA	LDA/ VK	PDI	SAOP/ ALDA	LDA/ VK	PDI
1	345.6	299.7	282.1	-	-	-
2	376.8	306.6	290.6	-	-	-
3	425.4	337.5	326.9	-	-	-
4	520.6	376.5	-	-	-	-
5	555.8	397.0	351.3	168.7	151.8	141.6
∞	(643.7)	438.4	-	(150.2)	128.3	-

7.4 Conclusion

In conclusion, we have presented accurate density functional response calculations for the static dipole– dipole polarizability of the tubular fullerenes $C_{60+i\times10}$ where i = 0–5, and for the closely related [5,5] nanotube. This was done by using a large basis set and both the conventional adiabatic local-density exchange-correlation functional and the more advanced VK-functional describing long-range effects that cannot be included in the local-density functionals. The importance of the highly nonlocal exchange-correlation effects was exemplified by comparing the results for the fullerenes as function of the system size. For the C_{60} and C_{70} fullerenes, it was found that the current-functional results were in good agreement with experiment, and in much better agreement with available *ab initio* SCF results and model PDI results than the adiabatic local-density functional results. The excellent agreement with the model PDI results for the longer fullerenes suggests that the nonlocal xc-effects need to be included in the description of the polarizability. The neglect of these effects can be expected to give large deviations, up to 40–50% (10–15%) for the larger fullerenes and the [5,5] carbon nanotube, in the longitudinal (perpendicular) polarizability per unit cell.

Chapter 8

Excitation energies for a benchmark set of molecules

In this chapter we study a variety of singlet excitations for a benchmark set of molecules. The $\pi\rightarrow\pi^*$ transitions obtained with the VK-functional are in good agreement with experiment and other theoretical results and they are in general an improvement upon the adiabatic local density approximation. In case of the $n\rightarrow\pi^*$ transitions the VK-functional fails, giving results that strongly overestimate the excitation energies obtained in experiment and with other theoretical methods. The benchmark set also contains some other types of excitations for which no clear failures or improvements are observed.

8.1 Introduction

In Chapter 6 we saw that the static axial polarizability of conjugated oligomers is greatly overestimated within the ALDA. This local approximation and also more advanced generalized gradient approximations are unable to describe the highly nonlocal exchange and correlation effects found in these quasi-one-dimensional systems [10,11]. One route to overcome these shortcomings is to employ optimized effective potentials [17] derived from the energy functional that includes exact exchange (see Refs. [16], [18] and [19] and references therein), or approximations to this potential such as the Krieger-Li-Iafrate [20] and common-energy-denominator approximations [21,45].

In Chapter 6 we found that there is a successful alternative approach towards the solution of this longstanding problem by using time-dependent current-density-functional theory, in which we describe ultranonlocal exchange-correlation effects within a local current description. For this we used the VK current-functional. Vignale and Kohn were the first to propose such a functional [8,9] in which the current density is used as a local indicator of global changes. From a careful analysis of the weakly inhomogeneous perturbed electron gas they arrived at an expression [8,9,23,24] for the first-order induced exchange-correlation contributions in the form of a viscoelastic stress field.

For the prototype polyacetylene and many other systems the results obtained significantly improved upon the ALDA results and were in excellent agreement with high level *ab initio* quantum chemical methods. However, we also observed that a similar large correction was not obtained for a hydrogen chain having alternating bond lengths that is seen as a theoretical model for conjugated systems (see Ref. [88] and references therein). This indicates that the VK-functional is not able to describe all features necessary for a correct description of the axial polarizability.

To test the VK-functional further, we calculated excitation energies for a collection of molecules and analyze the way in which the VK-functional modifies the ALDA results for the excitation properties. This benchmark set mainly consists of the collection of molecular excitations devised by Parac and Grimme [147] to benchmark their multireference second-order Møller-Plesset (MRMP2) method. They chose a set for which accurate experimental data are available and such that a broad range of chemical structures with states of nontrivial electronic character is covered. For our purpose we added three other excitations to this set: the prototype $\pi \rightarrow \pi^*$ excitation in ethene and the prototype $n \rightarrow \pi^*$ excitation in formaldehyde, and finally as example of an excitation in a molecular chain the 1 ^1B_u $\pi \rightarrow \pi^*$ excitation in *trans*-1,3,5,7,9-decapentaene.

In this chapter we present and discuss our results for this benchmark set of molecules. In the next chapter we study the excitation energies for the long molecular chains as a function of chain length.

8.2 Computational details

We want to test the performance of the VK-functional for different types of excitations. For this purpose we use an augmented benchmark set [147]. We show the molecules in Figure 8-1.

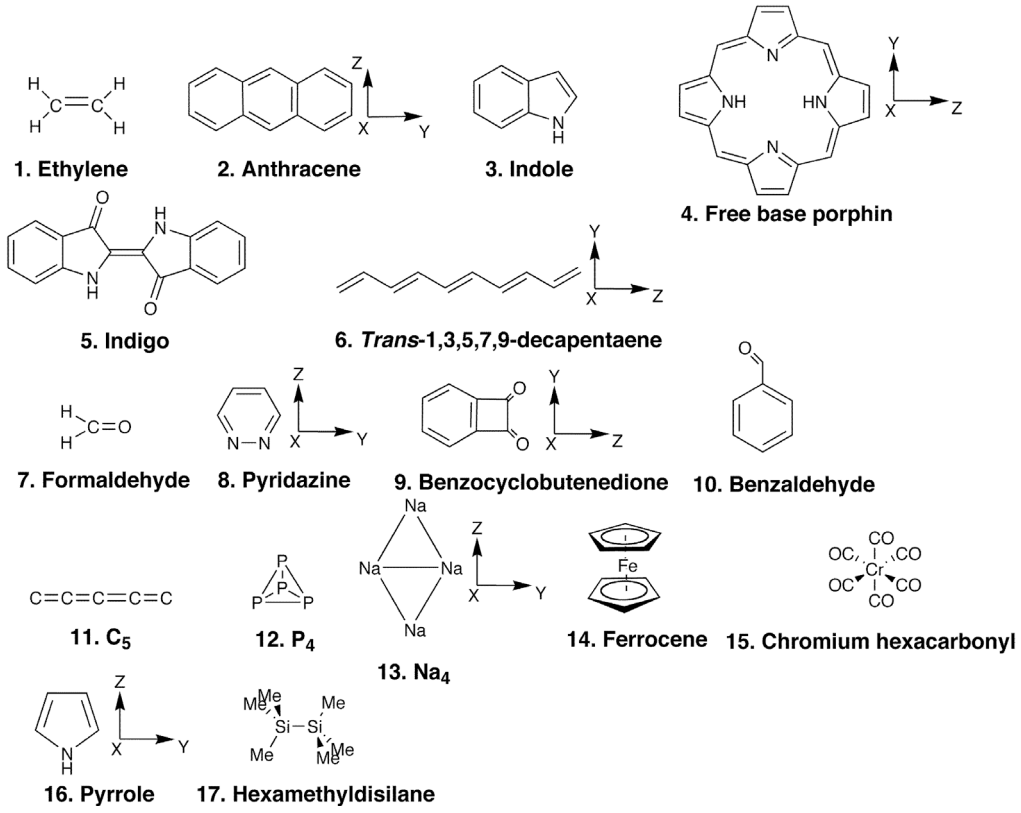

Figure 8-1. Overview of the studied molecules with their structure and orientation in case there is an ambiguity.

All calculations were performed with our modified version of ADF [25,99-103].

We optimized the geometries within the standard ADF TZ2P basis set, which is a triple-zeta Slater type basis set augmented with two polarization functions. Cores were kept frozen for carbon, oxygen, and nitrogen up to 1*s* and for phosphorus, sodium, silicon, chromium, and iron up to 2*p*. Geometry optimizations were performed with a generalized gradient approximated potential (GGA) by Becke [35] for exchange and Perdew [148] for correlation (BP functional).

For the excitation energy calculations a larger basis set was used. We used the standard ADF ET-pVQZ basis, which is an even-tempered Slater type basis set of quadruple-zeta quality. For pyrrole and hexamethyldisilane, for which we study Rydberg type excitations, we used the standard ADF ET-QZ3P-1DIFFUSE basis, which is an even-tempered Slater type basis set of quadruple-zeta quality with diffuse functions.

In all excitation energy calculations the ground state has been calculated with the LDA functional in the VWN parameterization [34]. The actual response calculations were done with the standard adiabatic local density approximation (ALDA) and with the VK-functional. For the latter we use the parameterizations of the viscoelastic coefficient based on results of Conti *et al.* [65] for the transverse response of the homogeneous electron gas [77], we denote this by NCT. As we explained in Section 5.5 we can also use different values for the transverse response kernel as obtained by Qian and Vignale [66], which we denote by QV. More information on these parameterizations can be found in Chapter 5. We denote these calculations simply as ALDA and VK (NCT or QV) instead of LDA/ALDA and LDA/VK.

In the excitation energy calculations the numerical integration accuracy was set to at least five decimals.

8.3 Results

In the following we discuss our results for the benchmark set. We have divided this part into three main sections. The first section contains the $\pi \rightarrow \pi^*$ transitions, the second section the $n \rightarrow \pi^*$ transitions, and the final section contains the remaining transitions in the benchmark set. The reason for this division is that it turns out that the $\pi \rightarrow \pi^*$ and $n \rightarrow \pi^*$ transitions form distinct classes as far as the behavior of the VK-functional is concerned.

8.3.1 The $\pi \rightarrow \pi^*$ transitions

The excitation energies for the $\pi \rightarrow \pi^*$ transitions are shown in Table 8-1.

8.3.1.1 Ethene

The prototype of a $\pi \rightarrow \pi^*$ transition is the transition to the $1\ ^1B_{1u}$ state in Ethene (known as the V-N transition). It turns out that the experimental energy of 7.66 eV [149] is difficult to reproduce even with highly accurate *ab initio* wave function methods (for a discussion and references see Ref. [150]). It is generally agreed that this experimental value does not correspond to a vertical transition [151]. Therefore a theoretical estimate of 8 eV is generally used to compare results with [152,153]. Davidson and Jarzęcki [154] derived equations to relate the vertical excitation to the average energy of the observed value. They obtain a value of 7.8 eV for the $1\ ^1B_{1u}$ state. The multireference singles-doubles configuration interaction (MRSDCI) results of 7.94 eV calculated by Lindh and Roos [150] and the more recent equation-of-motion singles doubles triples coupled-cluster results (EOM-CCSDT-3, where the 3 means that an

Table 8-1. This table shows the excitation energies of transitions with $\pi \rightarrow \pi^*$ character. All values are in eV.

Molecule	State	Exp.	MR -MP2[a]	CC2[a]	Other theory	ALDA	VK NCT	VK QV
1. C_2H_4	$1\,^1B_{1u}$	7.66[b]			7.94[c]; 7.89[d]	7.55	8.05	8.13
2. $C_{14}H_{10}$	$1\,^1B_{1u}$ (L_a)	3.43[e]; 3.60[f]	3.69	3.99	4.57[g]	2.86	3.53	3.62
	$1\,^1B_{2u}$ (L_b)	3.47[e]; 3.64[f]	3.35	3.93	5.29[g]	3.57	3.61	3.63
3. C_8H_7N	$2\,^1A'$ (L_b)	4.37[h]	4.25	4.93	4.43[i]	4.34[j]	4.66	4.67
	$3\,^1A'$ (L_a)	4.77[h]	4.95	4.33	4.73[i]	4.59[j]	4.74	5.18
4. $C_{20}H_{14}N_4$	$1\,^1B_{1u}$ (Q_x)	1.98-2.02[k]	1.67	2.32	1.63[l]	2.18	2.23	2.24
	$1\,^1B_{2u}$ (Q_y)	2.33-2.42[k]	2.33	2.71	2.11[l]	2.30	2.34	2.35
	$2\,^1B_{2u}$ (B_y)	3.13-3.33[k]	3.28	3.66	3.08[l]	2.99	3.10	3.11
	$2\,^1B_{1u}$ (B_x)	3.13-3.33[k]	3.08	3.57	3.12[l]	2.97	3.45	3.49
5. $C_{16}H_{10}N_2O_2$	$1\,^1B_u$	2.30[m]	2.10	2.36	1.96[n]	1.93	2.89	2.99
6. $C_{10}H_{12}$	$1\,^1B_u$	4.02[o]			4.33[p]; 4.05[q]	3.26	4.33	4.46

[a] Ref. [147].
[b] Ref. [149].
[c] MRSDCI results from Ref. [150].
[d] EOM-CCSDT-3 results from Ref. [152].
[e] Ref. [155], these are the (extrapolated) results for the *free* molecule.
[f] Ref. [156], these values have been corrected for solvent effects.
[g] CASSCF results from Ref. [157].
[h] Ref. [158].
[i] CASPT2 results from Ref. [159].
[j] The character of these states is L_a for the $2\,^1A'$ state and L_b for the $3\,^1A'$ state.
[k] From Ref. [160], Ref. [161], and Ref. [162].
[l] CASPT2 results from Ref. [163].
[m] Vapor spectra from Ref. [164].
[n] CASPT2 results from Ref. [165].
[o] Gas phase measurements from Ref. [166].
[p] CIS results from Ref. [167].
[q] MRMP results from Ref. [168], these values have been corrected for the basis set and active space effects

iterative method is used for the triple excitations) by Watts, Gwaltney and Bartlett [152] of 7.89 eV lie close to these values. We obtain a value of 7.55 eV with the ALDA and a value of 8.05 eV with VK/NCT and 8.13 with VK/QV. The VK value we obtain is in reasonable agreement with the estimates for the experimental value, the NCT value being the closest to experiment.

8.3.1.2 Anthracene

For anthracene we focus on two transitions of $\pi \rightarrow \pi^*$ character, the HOMO→LUMO transition and the transition resulting from the nearly degenerate HOMO-1→LUMO and HOMO→LUMO+1 states. These states are labeled in the literature [169] by L_a (short-axis polarized) and L_b (long-axis polarized). The absorption spectrum of anthracene [155,156,170]

shows that the transition to the 1^1B_{2u} state (L_b band) is hidden under the more intense 1^1B_{1u} state (L_a band). Using two-photon spectra the L_b band could be assigned with more certainty (see Ref. [155] for a discussion on this matter). Wolf and Hollneicher [155] did measurements on anthracene in several solvents, from this they found the solvent shift and extrapolated their values to the free molecule. This shows that the splitting between the L_a and L_b band in the free molecule should be very small. Grimme and Parac [156] also have corrected experimental data for solvent effects and obtained values for the excitation energies that are even closer to our VK values. They also find a small splitting of the L_a and L_b band. Our VK results show a small splitting and the values are also in good agreement with experiment and other theoretical values. The ALDA results give a splitting that is too large and the position of the L_a band is underestimated with ALDA, while the position of the L_b band is already in reasonable agreement with experiment. The order of the transitions is predicted correctly with TDDFT contrary to the CC2 [147] and MRMP2 [147] results. The CASSCF [157] results strongly overestimate the excitation energies.

8.3.1.3 Indole

For indole we again focus on the L_a ($3\ ^1A'$) and L_b ($2\ ^1A'$) bands. The VK results for the L_b and L_a bands are in good agreement with experiment [158] and CASPT2 [159] results. The ALDA results for the $2\ ^1A'$ state and the $3\ ^1A'$ state are also in good agreement, but the ALDA assigns the $2\ ^1A'$ state to the HOMO→LUMO transition (L_a) and the $3\ ^1A'$ state to a transition consisting of contributions from HOMO-1→LUMO and HOMO→LUMO+1 transitions (L_b). The ALDA thus predicts the wrong ordering of the transitions. The VK corrects for this by giving the correct character without changing the energies too much. The VK/QV value for the L_a band is considerably shifted compared to VK/NCT, leading to worse absolute values, but a better L_a-L_b splitting. The VK/NCT value is again the one that is closer to experiment.

8.3.1.4 Free base porphin

An extensive study of free base porphin (FBP) with TDDFT has already been performed using ADF by van Gisbergen *et al.* [171]. They studied the excitation energies using the LDA, the BP xc-functional and the Van Leeuwen/Baerends model xc-potential (LB94) [39] in the ground-state part of their calculations. From this study it turned out that there was not much difference between the results obtained with the different ground-state functionals. They found that the BP results support the interpretation of the spectrum by Edwards *et al.* [160] and the

CASPT2 interpretation [159]. We discuss how the VK-functional affects these results. Like the study by Parac and Grimme [147], we studied the first four excitation energies. The lowest two form the *Q* bands of experiment. After these two distinct bands, the spectrum shows a broad band with a distinct shoulder. These are called the *B* and *N* bands. There is still much debate on the assignment of these higher excitations. More information about this and references can be found in Ref. [171]. Since the purpose of this paper is to see how well VK performs, we will not discuss the assignment of the two higher excitations.

The lowest two *Q* bands are called Q_x and Q_y according to their polarization. These bands are formed by the transition to the 1^1B_{1u} and 1^1B_{2u} states. The VK-functional does not have a big effect on the excitation energies of these states compared to the ALDA. The splitting between the states is small with VK just like with the ALDA. The splitting is 0.11 eV with both VK/NCT and VK/QV. The experimental gas phase splitting is 0.44 eV.

The energy of the 2^1B_{2u} state is hardly affected by going from ALDA to VK while the energy of the 2^1B_{1u} state is raised in energy by almost 0.5 eV with VK. The VK value for these states lie close to the experimental values for the broad *B* band.

8.3.1.5 Indigo

The lowest $\pi \rightarrow \pi^*$ transition in indigo is the transition to the 1^1B_u state. The ALDA underestimates the experimental value of 2.30 eV [164] by 0.37 eV. The VK shifts this excitation energy upward, but the correction is too large leading to an overestimation compared to the experimental value (by 0.59 eV with VK/NCT and 0.69 eV with VK/QV) and the other theoretical results [147,165].

8.3.1.6 Trans-1,3,5,7,9-decapentaene

In our previous studies [77,78] we saw that the VK corrects the large overestimation of the static polarizability of oligomer chains obtained by the ALDA. It is expected that the VK-functional will also have a large effect on the excitation energies of these systems. In the next chapter we study the excitation energies of these oligomers in more detail. Here we focus on *trans*-1,3,5,7,9-decapentaene. For this molecule experimental values [166] and MRMP [168] and CIS [167] results are available, while we observed already in this short chain a correction by VK of the static polarizability. The ALDA considerably underestimates the excitation energy for this molecule (more than 1 eV). The VK corrects the underestimation and we obtain with VK/NCT a value close to the experimental, CIS, and MRMP values.

Table 8-2. Oscillator strengths, transition dipole moments and their correlation to the difference between the ALDA and VK (NCT) excitation energies for the $\pi \rightarrow \pi^*$ transitions. The direction of the transition dipole moment is denoted in italic. The oscillator strengths and transition dipole moments are in a.u. and the excitation energy differences are in eV.

Molecule	State	Oscillator strengths		Transition dipole moments		$\lvert\Delta E^{\text{ALDA-VK}}\rvert$
		ALDA	VK	ALDA	VK	
1. C_2H_4	$1\,^1B_{1u}$	0.32	0.32	1.31 *z*	1.29 *z*	0.50
2. $C_{14}H_{10}$	$1\,^1B_{1u}$	0.033	0.019	0.69 *z*	0.47 *z*	0.68
	$1\,^1B_{2u}$	<0.001	<0.001	0.039 *y*	0.078 *y*	0.05
3. C_8H_7N	$2\,^1A'$	0.050	0.006	0.46 *x*; 0.51 *y*	0.20 *x*; 0.11 *y*	0.32
	$3\,^1A'$	0.017	0.035	0.37 *x*; 0.11 *y*	0.42 *x*; 0.36 *y*	0.15
4. $C_{20}H_{14}N_4$	$1\,^1B_{1u}$	<0.001	<0.001	0.12 *z*	0.026 *z*	0.05
	$1\,^1B_{2u}$	0.001	<0.001	0.14 *y*	0.041 *y*	0.04
	$2\,^1B_{2u}$	0.034	<0.001	0.68 *y*	0.035 *y*	0.11
	$2\,^1B_{1u}$	0.11	0.004	1.26 *z*	0.22 *z*	0.48
5.$C_{16}H_{10}N_2O_2$	$1\,^1B_u$	0.22	0.13	2.07 *x*; 0.65 *y*	1.30 *x*; 0.38 *y*	0.96
6. $C_{10}H_{12}$	$1\,^1B_u$	1.78	1.50	4.71 *x*; 0.28 *y*	3.75 *x*; 0.15 *y*	1.07

8.3.2 Discussion of the $\pi \rightarrow \pi^*$ transitions

In nearly all cases studied we see an improvement by using the VK-functional, with indigo being the only exception where there is an overestimation by VK/NCT of 0.59 eV and VK/QV of 0.69 eV, which is larger then the underestimation by the ALDA of 0.37 eV. For ethene the ALDA and VK results lie equally far from the experiment and other theoretical energies. The correction is most profound for the molecular chain *trans*-1,3,5,7,9-decapentaene, where we observe an increase of more than 1 eV for the $1\,^1B_u$ in going from ALDA to VK, the VK value being close to experiment and other theory. Another nice result of the VK-functional is that is gives the correct ordering of the L_a and L_b states for indole, contrary to the ALDA.

In all cases we see that the VK slightly overestimates the excitation energies compared with experimental and other theoretical results. Since the VK/QV values are in all cases higher than the VK/NCT values, the VK/NCT are the better results for the systems studied.

Until now we have not looked explicitly at the oscillator strengths. All the $\pi \rightarrow \pi^*$ excitations studied are dipole allowed and have finite oscillator strength. In Table 8-2 we show the oscillator strengths for the various transitions together with the absolute difference in excitation energy obtained with ALDA and VK/NCT, $\lvert\Delta E^{\text{ALDA-VK}}\rvert$. We also give the transition dipole moments and their orientation. We see that in all cases except anthracene the oscillator strength is reduced with VK, where we took the correct order of the L_a and L_b transitions in account, If one looks at the four excitations of porphin, it can be seen that the larger the ALDA oscillator strength the

larger the effect of VK on this transition. This trend can also be observed for the excitations of anthracene and indole. More generally we can state that the larger the transition dipole moment obtained within the ALDA is along the long axis of the molecule the larger the VK correction will be for that excitation. In case of porphin this is true for both the *y* and *z* direction. This indicates that the larger the current in the axial molecular direction the larger the VK correction. This may indicate that the VK-functional is able to include for these excitations the counteracting field that the ALDA fails to describe.

8.3.3 The $n \rightarrow \pi^*$ Transitions

The results for the $n \rightarrow \pi^*$ transitions are shown in Table 8-3.

8.3.3.1 Formaldehyde

The prototype of a $n \rightarrow \pi^*$ transition is the transition to the $1\ ^1A_2$ state in formaldehyde. This state has a clear valence character and can be clearly identified in the absorption spectrum. The coupled-cluster CCSD value is 4.04 eV [172]. Our calculations give a value of 3.68 eV for ALDA and 8.3 eV for VK for this transition. This is a large overestimation by VK.

8.3.3.2 Pyridazine

The lowest excitation in pyridazine is the transition to the $1\ ^1B_1$ state. This excitation has been experimentally found at 3.30 eV [173]. The ALDA underestimates this value by 0.35 eV. The VK-functional overestimates strongly with a value of 7 eV.

8.3.3.3 Benzocyclobutenedione

The $n \rightarrow \pi^*$ transitions to the $1\ ^1B_1$ and $1\ ^1A_2$ states have been observed for benzocyclobutenedione in *n*-hexane solution [174]. The ALDA again underestimates the experimental and theoretical values. The VK-functional leads to an overestimation by more than 2 eV for both excitations.

Table 8-3. This table shows the excitation energies of transitions with $n \rightarrow \pi^*$ character. All values are in eV

Molecule	State	Exp.	MRMP2[a]	CC2[a]	Other theory	ALDA	VK NCT	VK QV
1. H_2CO	$1\,^1A_2$	3.79[b]; 4.07[c]			4.04[d]	3.68	8.34	8.38
2. $C_4H_4N_2$	$1\,^1B_1$	3.30[e]	3.62	3.87	3.48[f]	2.95	7.03	7.05
3. $C_8H_4O_2$	$1\,^1B_1$	2.79[g]	2.68	2.99		2.01	4.67	4.73
	$1\,^1A_2$	3.49[g]	3.62	3.83		2.76	5.27	5.30
4. C_7H_6O	$1\,^1A''$	3.8[h]	3.98	3.92	3.71[i]	3.08	4.46	4.51
5. C_5	$1\,^1\Pi_u$	2.78[j]	2.61	3.35	2.90[j]	2.50	6.74	6.76

[a] Ref. [147].
[b] Electron impact spectroscopy values from Ref. [175].
[c] Ref. [176].
[d] CCSD results from Ref. [172].
[e] Ref. [173].
[f] CASPT2 results from Ref. [177].
[g] Absorption spectra in *n*-hexane solution from Ref. [174].
[h] This value is estimated on the basis of the experimentally obtained band origin (at 3.34 eV, Ref. [178]) and the CASPT2 difference between the vertical and adiabatic transition (3.71 eV – 3.27 eV = 0.44 eV, Ref. [179]).
[i] CASPT2 results from Ref. [179].
[j] Gas phase measurements by Motylewski, Vaizert and Giezen and MRCI results from Ref. [180].

8.3.3.4 Benzaldehyde

For benzaldehyde the vertical transition to the $1\,^1A''$ state is not directly observed. A value of 3.8 eV is estimated on the basis of the experimentally obtained band origin [178] and the CASPT2 difference between the vertical and adiabatic transitions [179]. The ALDA underestimates this value by 0.72 eV and also underestimates the other theoretical results. The VK/NCT functional overestimates by 0.66 eV and VK/QV by 0.71 eV.

8.3.3.5 C_5

As the final example of a $n \rightarrow \pi^*$ transition the transition to the $1\,^1\Pi_u$ state of the highly unsaturated C_5 molecule is studied. The ALDA underestimates the experimental value [180] by 0.28 eV. The VK-functional overestimates this value by more than 3 eV.

8.3.4 Discussion of the $n \rightarrow \pi^*$ transitions

All the $n \rightarrow \pi^*$ transitions are strongly overestimated by the VK-functional except for benzaldehyde for which the overestimation is not as severe. Again the VK/QV values lie slightly higher than the VK/NCT values, leading to even greater overestimations for VK/QV.

8.3.5 Miscellaneous transitions

The remaining results are given in Table 8-4. As an example of a system having excitations involving σ orbitals the covalently bound P_4 cluster and the metallic Na_4 cluster are studied. As a severe test some low-lying excited states involving *d* orbitals of the transition metal complexes ferrocene and chromiumhexacarbonyl are considered. Finally we study Rydberg states in pyrrole and hexamethyldisilane.

8.3.5.1 P_4

The first dipole-allowed transition in P_4 is the transition to the $1\ ^1T_2$ state. It is experimentally located at 5.6 eV [181]. The ALDA underestimates this value by 0.45 eV, but the VK corrects to a value of 5.69 eV for VK/NCT and 5.71 eV for VK/QV. These values are very close to the experiment.

8.3.5.2 Na_4

The optically allowed $1\ ^1B_{1u}$ state of the Na_4 cluster is another example of a system involving σ orbitals. However, in this case the system contains only metal atoms. The experimental excitation energy is located at 1.81 eV. The ALDA value of 1.79 eV lies very close to this value. The VK overestimates by 0.8 eV.

Table 8-4. This table shows the excitation energies of transitions with various character, see the text for more detail. All values are in eV

Molecule	State	Exp.	MR -MP2[a]	CC2[a]	Other theory	ALDA	VK NCT	VK QV
1. P_4	$1\ ^1T_2$	5.6[b]	5.38	5.52		5.15	5.69	5.71
2. Na_4	$1\ ^1B_{1u}$	1.81[c]	1.85	1.83	1.74[d]	1.79	2.60	2.63
3. $C_{10}H_{10}Fe$	$1\ ^1E_{1g}$	2.81[e]	2.85	2.65		2.93	5.17	5.21
4. $Cr(CO)_6$	$1\ ^1T_{1u}$	4.43[f]	4.56	3.96	4.54-4.11[g]	4.14	4.62	4.75
	$2\ ^1T_{1u}$	5.41[f]	5.42	4.36	5.07-5.20[g]	5.68	6.31	6.44
5. C_4H_5N	$1\ ^1A_2$	5.22[h]	5.26	5.14	5.10[j]	4.81	5.04	5.05
	$1\ ^1B_1$	5.86[i]	6.00	5.80	5.85[j]	5.20	5.29	5.31
6. $Si_2(CH_3)_6$	$1\ ^1E_u$	6.35[k]	6.52	5.72		5.32	5.55	5.56

[a] Ref. [147].
[b] Absorption spectra in solid argon from Ref. [181].
[c] Photo depletion spectra from Ref. [182].
[d] CI results from Ref. [183].
[e] Absorption spectra from Ref. [184].
[f] Vapor spectra from Ref. [185].
[g] CASPT2 results from Ref. [186].
[h] Ref. [176].
[i] Vapor spectra from Ref. [187].
[j] CC3 results from Ref. [188].
[k] Electron energy loss spectra from Ref. [189].

8.3.5.3 Ferrocene

For ferrocene in the D_{5d} symmetry the transition to the $1\ ^1E_{1g}$ state is studied. The value found experimentally for this transition is 2.81 eV [184]. The ALDA results are reasonably close to the experiment and other theoretical results. The VK strongly overestimates by more than 2 eV.

8.3.5.4 Chromiumhexacarbonyl

Another example of a transition metal compound is chromiumhexacarbonyl. Two $\pi^* \leftarrow d$ charge transfer excitations are present in the test set. These excitations appear in the spectra [185] as two strong bands with maxima at 4.43 eV and 5.41 eV. The ALDA underestimates the transition to the $1\ ^1T_{1u}$ state and overestimates the transition to the $2\ ^1T_{1u}$ state. The VK again shifts these excitation energies to higher values. The excitation energy for the $1\ ^1T_{1u}$ state obtained with VK is in good agreement with the experiment and other theoretical values (except for CC2 which underestimates both excitations [147]), the VK/NCT being closest to experiment. The $2\ ^1T_{1u}$ excitation is already overestimated by the ALDA and the VK-functional makes this even worse.

8.3.5.5 Pyrrole

For pyrrole the first two low-lying Rydberg-type transitions are studied. These are experimentally observed at 5.22 eV [176] and 5.86 eV [187]. The ALDA underestimates these values and the other theoretical results. The VK increases the ALDA values but not enough; the VK values still underestimate the experiment.

8.3.5.6 Hexamethyldisilane

Another example of a Rydberg excitation is the transition to the 1^1E_u state in hexamethyldisilane. The value found experimentally is 6.35 eV [189]. With the ALDA we find 5.32 eV, which is an underestimation of more than 1 eV. With VK this value is raised to 5.5 eV, which is still a strong underestimation.

8.3.6 Discussion of the miscellaneous transitions

Except for the case of ferrocene the excitation energy shifts due to VK are moderate sometimes improving, sometimes worsening the results. The shift due to VK is upward in all cases, VK/QV giving the highest values. Except for the transition to the $2\ ^1T_{1u}$ state in chromiumhexacarbonyl and the transition to the $1\ ^1E_{1g}$ state of ferrocene the ALDA always underestimates. The too high excitation energies cannot be corrected by including a counteracting field term through the VK-functional. The VK shift in the transition metal complex chromiumhexacarbonyl is not very large, contrary to the case of ferrocene for which the transition to the $1\ ^1E_{1g}$ state is strongly overestimated by VK. The Rydberg excitation energies are still underestimated with VK, but it should be noted that for these excitations use of an asymptotically correct functional such as the LB94 [39] functional is necessary to obtain good results. A large correction is not necessary for these systems when the LB94 is used in the ground state, indicating that the fact that VK does not correct the ALDA a lot in case of the Rydberg states is not a failure of the VK.

8.4 Conclusion

In this chapter we applied TDCDFT to a benchmark set of molecules and considered excitations of various nature. For the tensor xc-kernel we used the VK approximation in the static limit. As we mentioned in section 4.8 the static limit can only be used if the frequency dependence of the longitudinal and transverse xc-kernels of the electron gas is weak. For molecules this is the case if the frequency is much smaller than the local plasma frequency. For

the valence region of molecules the plasma frequency corresponds to $\omega_p \approx 47$ eV, which is much larger than typical excitation energies we studied here.

The $\pi \rightarrow \pi^*$ excitation energies obtained with VK improve the ALDA results in all cases except indigo. This is in line with the results obtained for the polarizabilities in the π-conjugated systems [77,78], For the $n \rightarrow \pi^*$ excitation energies and the transition to the $1\ ^1E_{1g}$ state of ferrocene the VK dramatically fails. For the other type of excitations contained in the benchmark set no clear picture emerged: sometimes the VK improves and sometimes it worsens upon the ALDA, but in general no large effects were observed. Using the QV parameterization with VK instead of the NCT usually only slightly raises the excitation energy. This usually leads to slightly worse results compared with experiment.

A possible explanation that the VK-functional behaves differently for different kinds of transitions may be found in the fact that the functional is derived for a system that is very different from the ones we study. The VK-functional was derived by an expansion to second order in wave vectors *k* and *q,* which characterize the Fourier component of the current-current response function for the electron gas and the wavelength of the inhomogeneity, respectively. This expansion was shown to be valid in the regime $k, q << k_F, \omega / v_F$ where k_F is the Fermi momentum and v_F the Fermi velocity of the electron gas. This is the region above the particle-hole continuum. For the wave vector of the applied optical field the constraints $k << k_F, \omega / v_F$ are trivially met as $k = \omega / c << k_F$, and the speed of light $c >> v_F$. However, since we consider excitations in molecular systems, the self-consistent perturbing field associated with a given excitation will vary on a length scale that is determined by the inhomogeneity of the induced density and current density describing the excitation, and hence by the particular orbital structure of the transitions involved. An optimistic estimate for this perturbing field will be $k \approx 2\pi / L$, with *L* the characteristic size of the molecule, but a more realistic value would be to consider $k \approx q$, i.e. of the same order as the inhomogeneity. For the wave vector characterizing the inhomogeneity of the ground-state density, we have $q = |\nabla \rho_0| / \rho_0$. In the core and valence region *q* is of the same order as k_F and $1 / v_F$ [39,190], whereas in the asymptotic outer region $q >> k_F$ and $q << 1 / v_F$. The constraints on the wave vector *q* are violated, although not strongly, almost everywhere in the molecule, while the extent of the violation of the constraints on *k* will depend on the particular excitation considered.

One should keep in mind that meeting the constraints on *k* and *q* in itself does not justify the use of an xc-functional derived for the weakly inhomogeneous metallic electron gas to inhomogeneous systems with an excitation gap. This problem is not unique to the VK-

Table 8-5. This table shows the lowest two excitation energies of transitions for the beryllium atom. All values are in eV

Transition	Exp.[a]	ALDA results by C.A. Ullrich[b]	VK results by C.A. Ullrich[b]	ALDA	VK NCT	VK QV
$2s \rightarrow 2p$	5.27	5.07	6.23	4.83	6.03	6.14
$2s \rightarrow 3s$	6.77	5.62	5.66	6.53	6.55	6.58

[a] Ref. [191]. [b] Ref. [27].

functional, but is already present for the local density approximation and for the gradient corrections. However, the VK-functional satisfies two important constraints, which are valid for systems with arbitrary time dependence and inhomogeneity (such as molecules in external fields), stating that in linear response the xc-electric field does not exert any forces or torques on the system. Another exact property, which is satisfied for any system, is that under rigid translation of the center of mass, described by position vector $\mathbf{x}(\omega)$, the xc-potential is also translated over this vector. This immediately implies that the VK-functional satisfies the so-called harmonic potential theorem [57,58]. In view of these exact properties one may hope that the VK-functional is still applicable to the inhomogeneous systems with an excitation gap such as molecules. The particle-hole regime, for which the VK derivation is not justified, is to a large extent taken into account by the explicit evaluation of the Kohn-Sham response functions.

It is our observation that for the $\pi \rightarrow \pi^*$ transitions the results obtained are much improved when including the VK contribution to the exchange-correlation potentials. For the $\pi \rightarrow \pi^*$ transitions the region where the xc-field contributes most to the matrix elements is neither close to the nuclei nor in the remote outer region: the induced current associated with such transitions is mainly in the π-system in the direction of the long axis of the molecules, and it is more or less uniform along this axis. Even though the equilibrium density is far from homogeneous ($q \approx k_F$) in the relevant region, the density gradient is mostly in a direction perpendicular to the induced current. We may speculate that this remnant of a weak inhomogeneity might result in the xc-functional to behave in a graceful manner. A similar argument cannot be used for the $n \rightarrow \pi^*$ transitions, for which we observe that the VK-functional severely fails to describe these transitions correctly. The systems studied are however too complicated to analyze this conjecture. We propose to study simpler systems, that are chemically relevant, and that can be analyzed to a larger extent. As turns out the VK-functional also fails for some transitions in atoms. C.A. Ullrich has done an independent study

of excitation energies of atoms with the VK-functional. He obtained excitation energies using the so-called single pole approximation, in which only the diagonal elements of the coupling

matrix are included. His results [27] show that also in the case of atoms there are certain excitations that are strongly overcorrected by VK while others remain nearly unchanged. For example in case of beryllium (Table 8-5) the $2p \leftarrow 2\,s$ excitation energy is strongly overestimated by VK, while the $3s \leftarrow 2s$ excitation energy is shifted only slightly by VK, improving over the ALDA result. We see a similar effect for our implementation of the VK-functional, which takes into account all matrix elements of the coupling matrix: the large shift observed for the $2p \leftarrow 2s$ excitation energy in the single pole approximation is reduced by taking into account off-diagonal elements but it is still 0.8 eV too large. For the $3s \leftarrow 2s$ excitation both methods find a small shift, our result being closest to experiment because our ALDA value is already much closer to this value. We hope to get more insight in the range of applicability of the VK-functional in molecules, and to find the cause of its failure for particular transitions, by studying atoms in more detail. We will do this in Chapter 10.

Chapter 9

Excitation energies of oligomers

In this chapter we study the $\pi \rightarrow \pi^*$ singlet excitations of the π-conjugated oligomers of polyacetylene, polydiacetylene, polybutatriene, polythiophene, poly(para-phenylene vinylene) and the lowest singlet excitations of the hydrogen chain. By studying the dependence of the excitation spectrum on the chain length we conclude that the reduction of the static polarizability when using the VK-functional has two origins. First, the excitation energies of transitions with a large transition dipole are shifted upward. Second, the HOMO-LUMO character and oscillator strength of the lowest transition within the adiabatic local density approximation is transferred to higher transitions. The lowest transitions that have a considerable oscillator strength obtained with the VK-functional have excitation energies that are in most cases in better agreement with available reference data than the adiabatic local density approximation.

9.1 Introduction

In Chapter 6 we showed that we can use time-dependent current-density-functional theory (TDCDFT) in order to go towards the solution of this longstanding problem of the overestimation of the static polarizability of long molecular chains. With this method we describe ultranonlocal exchange-correlation effects using a functional that is dependent on the current density. Vignale and Kohn proposed such a functional [8,9] in which the current-density is used as a local indicator of global changes. From a careful analysis of the weakly inhomogeneous perturbed electron gas they arrived at an expression [8,9,23,24] for the first-order induced exchange-correlation contributions in the form of a viscoelastic stress field. Within the VK-functional we use a parameterization of the viscoelastic coefficient based on results of Conti *et al.* [65] for the transverse response of the homogeneous electron gas [77]. For the prototype polyacetylene and many other linear conjugated oligomers the results obtained using this VK-functional significantly improved upon the ALDA results, and were in excellent agreement with high level *ab initio* quantum chemical methods. However, we also observed that a similar large correction was not obtained for a hydrogen chain with alternating bond lengths,

which is seen as a theoretical model for conjugated systems (see Ref. [88] and references therein). This indicates that the VK-functional in the parameterization we use is not able to describe all features necessary for a correct treatment of the axial polarizability.

In Chapter 8 we calculated the excitation energies of a benchmark set of molecules. We studied several types of transitions. In most cases, the excitation energies of the $\pi \rightarrow \pi^*$ transitions obtained with the VK-functional were found to improve much upon the ALDA values, giving results close to other values available from literature. We also found that the $n \rightarrow \pi^*$ energies were strongly overestimated with VK and that for some other types of excitations the picture that emerges was less clear. In the π-conjugated systems studied here the low-lying $\pi \rightarrow \pi^*$ transitions determine for a large part the axial polarizability. We therefore expect that the reduction in the polarizability for these systems is linked to a modification of the $\pi \rightarrow \pi^*$ excitations.

In this chapter we study the lowest dipole-allowed singlet excitations of the oligomers of polyacetylene, polydiacetylene, polybutatriene, polythiophene, poly(*para*-phenylene vinylene), and the hydrogen chain. The singlet excitations considered here are all of the $\pi \rightarrow \pi^*$ type except for the hydrogen chain. We compare our results with available experimental and *ab initio* data. From the results for the $\pi \rightarrow \pi^*$ excitations of the small molecules and the excellent VK results for the polarizabilities of π-conjugated oligomers, we may expect a large improvement with VK upon the calculated ALDA excitation spectra.

9.2 Computational Details

All calculations were performed with our modified version of ADF [25,99-103].

For the oligomers of polyacetylene (PA), polydiacetylene (PDA), polybutatriene (PBT), polythiophene (PT) and the hydrogen chain we use the same geometry as we used in Chapter 6. This is the first chapter in which we study the poly(*para*-phenylene vinylene) (PPV) and polyacene (PAC) oligomers. We did a geometry optimization for these oligomers with a generalized gradient approximated potential (GGA) by Becke [35] for exchange and Perdew [148] for correlation (BP functional). We forced the oligomer geometries to be planar (C_s symmetry).

All calculations were done within the standard ADF TZ2P basis set, which is a triple-zeta Slater type basis set augmented with two polarization functions. Cores were kept frozen for carbon up to 1*s* and for sulfur up to 2*p*.

In all excitation energy calculations the ground state has been calculated with the LDA functional in the VWN parameterization [34]. The response calculations themselves were done with the adiabatic local density approximation (ALDA) derived from the ground-state LDA expression and the VK-functional. For the latter we use for the singlet transitions a parameterization of the viscoelastic coefficient based on results of Conti *et al*. [65] for the transverse response of the homogeneous electron gas [77]. For the triplet excitation energies we use the parameterization of Qian and Vignale [60]. From now on we denote these calculations simply as ALDA and VK instead of LDA/ALDA and LDA/VK.

9.3 Results

In Sections 9.3.1 till 9.3.7 we show our results for the excitation energies of several molecular chains. In Section 9.3.2 we discuss our results for the triplet excitation energies of polyacetylene.

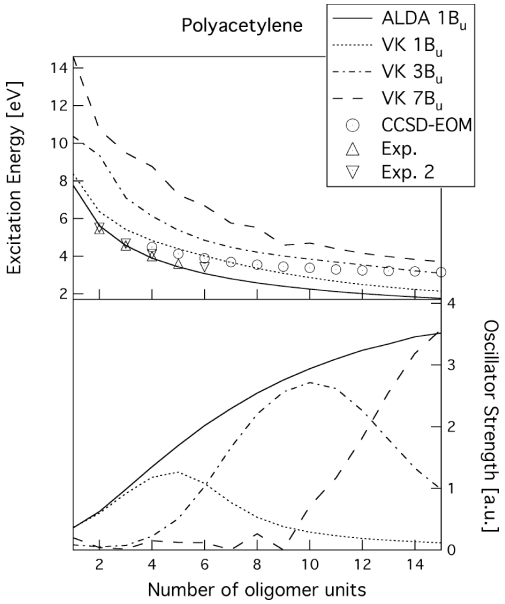

Figure 9-1. ALDA and VK singlet excitation energies and oscillator strengths of polyacetylene oligomers compared with CCSD-EOM [192] and experimental results. Exp. and Exp. 2 are both absorption spectra from Ref. [193].

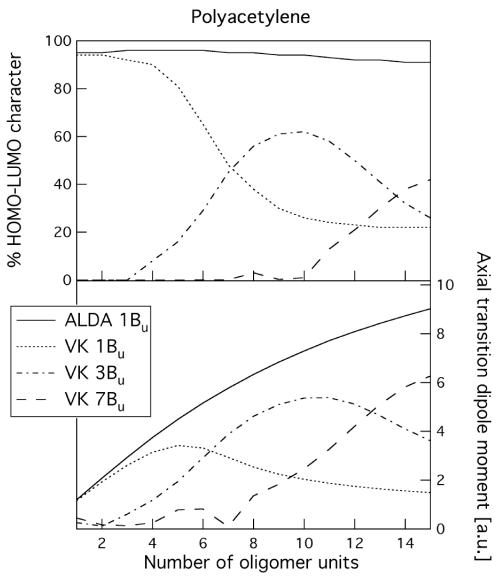

Figure 9-2. ALDA and VK HOMO-LUMO character and transition dipole moments for polyacetylene oligomers.

9.3.1 Polyacetylene

We discuss the prototype polyacetylene (PA) chain. In Ref. [77] we obtained axial polarizabilities for the PA oligomers that were very close to the available MP2 results if we use the VK-functional, but that were considerably overestimated when using the ALDA functional. In Figure 9-1 we plot the ALDA and VK results for the (dipole allowed) ^1B_u excitation energies and corresponding oscillator strengths against the number of oligomer (C_2H_2) units. We compare our data with experimental results [193] and CCSD-EOM results [192]. The 1 ^1B_u excitation energies obtained within the ALDA are close to the CCSD results for the small chain lengths (3-4 units), but for the longer chains the excitation energies are underestimated. The underestimation for the longest chain of 15 units is 1.39 eV. This result is consistent with the fact that the ALDA overestimates the polarizability as can be seen from the sum-over-states (SOS) expression for the polarizability,

$$\bar{\alpha}(\omega) = \sum_n \frac{f_n}{\omega_n^2 - \omega^2} \tag{9.1}$$

where ω_n are the excitation energies and f_n the oscillator strengths. The reduction of the static polarizability by using the VK-functional has to be a result of a decrease of the oscillator strength of the lowest transitions or an increase of their excitation energies, or both. We therefore expect that the excitation energies calculated with VK will improve upon the ALDA. Indeed the VK results for the 1 ^1B_u excitation energy are higher than the ALDA results and lie closer to the CCSD results, but from 10 units onward they also underestimate the CCSD results. If we look at the oscillator strengths we see that the ALDA oscillator strength of the 1 ^1B_u transition rises, although less steeply for larger chain lengths. This contributes to the large overestimation of the polarizability in case of the ALDA. The VK oscillator strength for the 1 ^1B_u transition also rises in the beginning but drops again after 5 units. The 2 ^1B_u transition has almost zero oscillator strength for all chain lengths, and for this excitation the effect of VK on the excitation energies is almost zero with values lying very close to the ALDA values. We have therefore not added this excitation to the graph. The oscillator strength of the 3 ^1B_u transition with VK rises at the point where the 1 ^1B_u oscillator strength drops. The 3 ^1B_u oscillator strength drops from 10 units onward, but then the 7 ^1B_u transition takes over. The 4 ^1B_u, 5 ^1B_u and 6 ^1B_u transitions have again an oscillator strength close to zero and the VK excitation energies are close to their corresponding ALDA values. In Figure 9-2 we show the HOMO-LUMO character and the transition dipole moment in the axial direction of the ^1B_u transition. The transition dipole moment, which is mainly in the axial direction, follows the same trend as the oscillator strengths. If we look at the HOMO-LUMO character we find that the 1 ^1B_u transition has almost 100% HOMO-LUMO within the ALDA. The character of the 1 ^1B_u transition with VK is also close to 100% HOMO-LUMO for the small chains, but when the chains become longer more states mix in. Just like in case of the oscillator strength it are the 3 ^1B_u and later the 7 ^1B_u transitions that gain HOMO-LUMO character. We see that the excitations with a large spectral weight are not the lowest transitions with VK and they move to higher energy as the chain becomes longer. These transitions with the largest spectral weight lie close to the CCSD results. This is consistent with the fact that we find much lower polarizabilities for PA with VK.

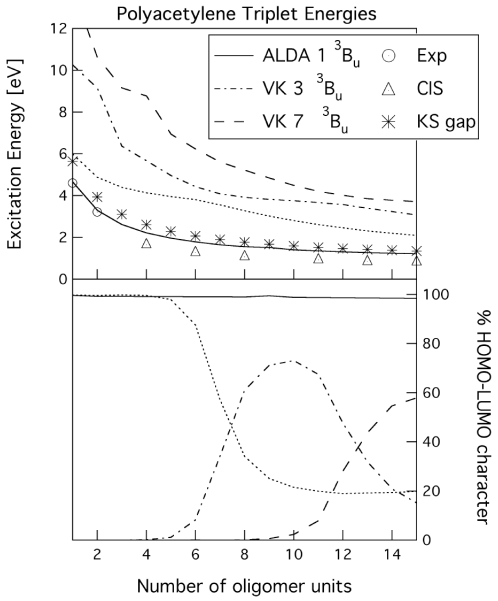

Figure 9-3. ALDA and VK triplet excitation energies and % HOMO-LUMO character of polyacetylene oligomers compared with CIS [194] and experimental results [195,196] and the Kohn-Sham HOMO-LUMO gap.

9.3.2 Triplet excitation energies of polyacetylene

For polyacetylene we also calculated the triplet ^3B_u excitation energies. We show our results in Figure 9-3. Since the triplet excitation energies have no oscillator strength we plot the % HOMO-LUMO character instead. We have also added the difference between the Kohn-Sham HOMO and LUMO orbital energies.

From the graph we see that the ALDA values lie close to the experimental [195,196] and CIS [194] results. They also lie very close the Kohn-Sham HOMO-LUMO gap. The VK-functional has a large effect, just like in the singlet case. But in this case the effect of VK is unwanted since the ALDA values are already close to experimental and CIS values. Apart from the fact that the excitation energies lie much higher than the ALDA values, the HOMO-LUMO character is transferred to the 3 ^3B_u and later the 7 ^3B_u transitions.

The reason of this large effect of VK is that the static values of B^{T}, presented in Table 5-1, are very close to the values of $f_{\mathrm{xcT}}(0)$. Therefore we can expect a similar effect of VK for both the singlet and triplet excitation energies. Since there is not much qualitative difference between the singlet and triplet energies and there is hardly any reference data available for the triplet energies, we will not give the triplet energies for the other systems.

9.3.3 Polydiacetylene and polybutatriene

In Ref. [78] we made a comparison for the polarizabilities of the oligomers of polydiacetylene (PDA) and polybutatriene (PBT). We found that the polarizabilities obtained with VK of these two systems are very similar. The value per oligomer unit, which can be estimated from the experimental values for the polydiacetylene-like PTS (R=R'=$CH_2OSO_2C_6H_4CH_3$) and polybutatriene-like TDCU (R=R'=$(CH_2)_4OCONHC_6H_5$), are also found to be close together

[107]. The Hartree-Fock polarizabilities for these systems were very different, the PDA result lying close to our VK values but the PBT value being much larger for the larger chains. Some CASSCF and CASPT2 results for the 1 ^{1}A' excitation energies of PDA and the 1 ^1B_u excitation energies of PDA were available from the literature for the shorter chains [197]. The CASPT2 values are considered the most accurate according to Ref. [197]. There are also CCSD results available for the monomers [117]. We show these results together with our VK and ALDA results in Figure 9-4 and Figure 9-5. The oligomer unit is for both molecules a C_4H_2 unit. The trends observed for the ALDA and VK excitation energies, oscillator strengths, HOMO-LUMO character and axial transition dipole moments are again similar to the previous examples. In case of PDA the CASPT2 and CASSCF results for the excitation energies lie close to the VK values with the largest oscillator strength. For PBT CASSCF results lie close to the VK results with the largest oscillator strength, but here the CASPT2 results lie closer to the ALDA. The literature data for PBT are widely spread for the longer chain lengths, and we cannot make any conclusions on whether the VK results improve upon the ALDA. As can be seen from Figure 9-5 the oscillator strength for the 3 ^1B_u transition of butatriene (1 unit of PBT) with VK is larger than the oscillator strength of the 1 ^1B_u transition, but it turns out that the stronger 3 ^1B_u excitation does not correspond to a HOMO-LUMO excitation with VK. The major contribution to this transition is from the HOMO-1→LUMO+1. Therefore the 3 ^1B_u transition of VK should be compared with the 3 ^1B_u transition of the ALDA (7.58 eV for the excitation energy and 1.21 a.u. for the oscillator strength).

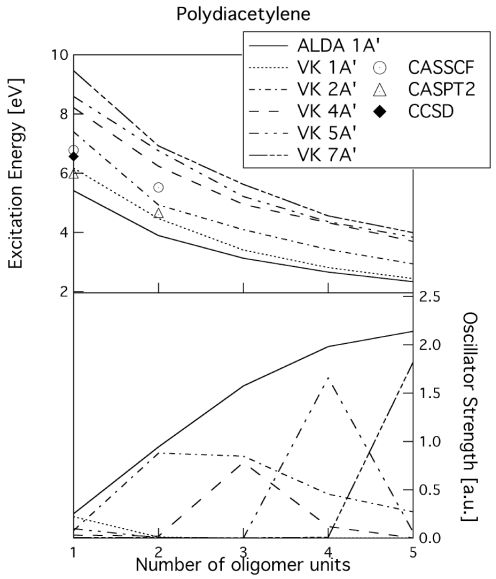

Figure 9-4. ALDA and VK singlet excitation energies and oscillator strengths of polydiacetylene oligomers compared with CASSCF [197] CASPT2 [197], and STEOM-CCSD [117] results.

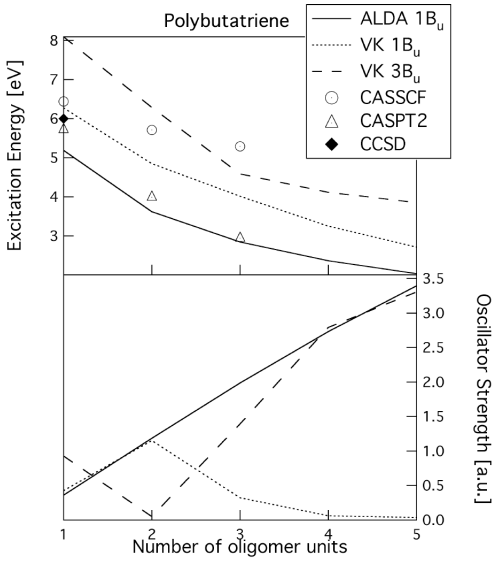

Figure 9-5. ALDA and VK singlet excitation energies and oscillator strengths of polybutatriene oligomers compared with CASSCF and CASPT2 results [197].

9.3.4 Polythiophene

In Figure 9-6 we show the excitation energies and oscillator strengths for the 1 ^1B_u (even number of thiophene rings) and 1 $^1B_2$ (odd number of thiophene rings) transitions of polythiophene (PT) against the number of SC_4H_2 units. The ALDA and VK results show the same behavior as observed for PA. The oscillator strength of the 1 $^1B_u/^1B_2$ transition of VK drops for longer chain lengths and the spectral weight is transferred to the 3 $^1B_u/^1B_2$ and 4 $^1B_u/^1B_2$ transitions. The 2 $^1B_u/^1B_2$ in between again has almost zero oscillator strength and the VK excitation energies lie close to the ALDA values. For the axial transition dipole moment and the HOMO-LUMO character we see the same trends as for polyacetylene, specifically the axial transition dipole moment shows the same trend as the oscillator strength and with VK the HOMO-LUMO character is transferred from the 1 $^1B_u/^1B_2$ to the 3 $^1B_u/^1B_2$ and later to the 4 $^1B_u/^1B_2$ transition. If we compare our results with the available CIS [198] and experimental [199-201] results it is clear that the ALDA underestimates the excitation energies for the long chain

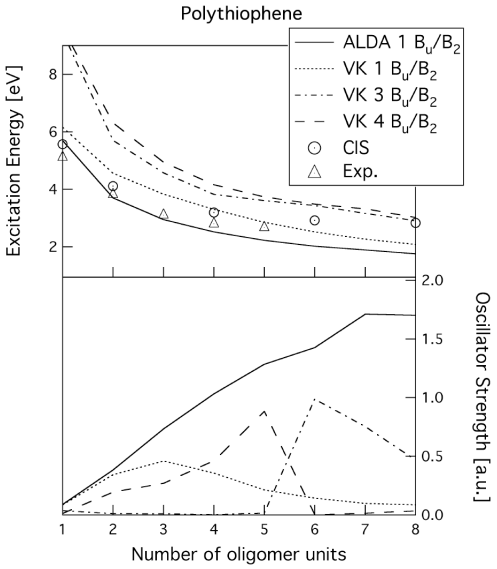

Figure 9-6. ALDA and VK singlet excitation energies and oscillator strengths of polythiophene oligomers compared with CIS [198] and experimental results (monomer and dimer from Ref. [199] tetramer and seximer from Ref. [200], and octamer from Ref. [201]).

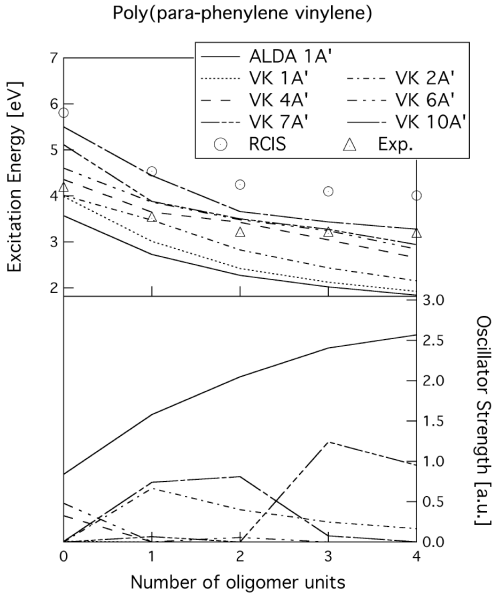

Figure 9-7. ALDA and VK singlet excitation energies and oscillator strengths of poly(para-phenylene vinylene) oligomers compared with RCIS [202] and experimental [203] results.

lengths. The VK results for the transitions with the largest oscillator strengths lie close to the CIS and experimental results, which is consistent with our earlier observations for the polarizability [77].

9.3.5 Poly(*para*-phenylene vinylene)

In Figure 9-7 we show the results for poly(*para*-phenylene vinylene) (PPV). We choose the *trans*-stilbene molecule to be zero PPV units, a new unit is obtained by adding a styrene unit between the *trans*-stilbene. It is immediately clear from the figures that with VK many states mix in. We see again the same trends as for the other systems studied. The ALDA values for the excitation energies strongly underestimate the experimental [203] and RCIS [202] results, especially for the longer chain lengths. The excitation energies with VK for the transitions with the largest oscillator strengths are all in between the experimental and RCIS results, the longer chains being closer to the experimental values.

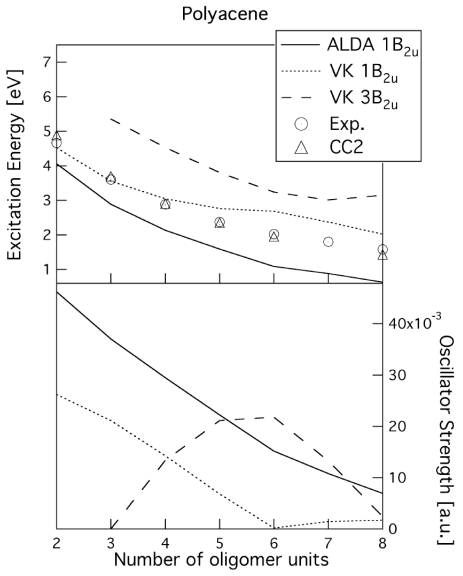

Figure 9-8. ALDA and VK singlet excitation energies and oscillator strengths of the L_a state of polyacene oligomers compared with CC2 and experimental results [156].

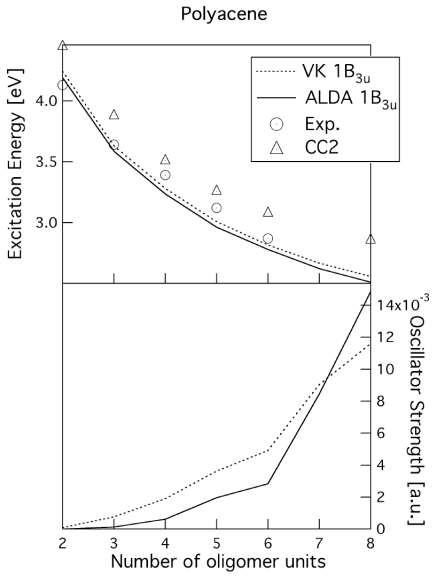

Figure 9-9. ALDA and VK singlet excitation energies and oscillator strengths of the L_b state of polyacene oligomers compared with CC2 and experimental results [156].

9.3.6 Polyacene

In Figure 9-8 we show our results for the $^1B_{2u}$ transition of polyacene (PAC) and in Figure 9-9 we show our results for the $^1B_{3u}$ transition. One phenyl ring is chosen to be one unit (so naphthalene is two units). The $^1B_{2u}$ transition is largely a HOMO→LUMO transition and is known as the L_a state. The $^1B_{3u}$ transition is known as the L_b state and is of shared HOMO-1→LUMO and HOMO→LUMO+1 character. For both transition experimental data is available up to 8 rings [156] and we also compare with available CC2 data [156]. For the 3 $^1B_{2u}$ transition we only show the values for 3 and more rings. This is because the 3 $^1B_{2u}$ transition of naphthalene has relatively high oscillator strength, but this transition is not of the L_a type. Including it would only make the graph unclear. For the L_a state we see that the ALDA again underestimates the literature values. The VK values for the 1 $^1B_{2u}$ lie close to the literature values for the smaller chains, but for the larger chains they start to overestimate and the 3 $^1B_{2u}$ state starts to mix in. For the L_b state we see that the ALDA and VK values lie very close together and are close to the experimental values.

From the graphs we see that VK has a much larger effect on the L_a state than on the L_b state. This can be explained by looking at the transition dipole moment. The HOMO→LUMO transition of the L_a state has a large transition dipole moment along the short axis of the molecule (not along the chain direction). The HOMO-1→LUMO and HOMO→LUMO+1 have large transition dipole moments along the long axis of the molecule, but these transition dipole moments counteract each other. The L_b state therefore has only a small net transition dipole moment along the chain direction. This explains the small effect of the VK-functional.

An important point that is not immediately clear from the graph is the ordering of the L_a and L_b states. For naphthalene the experiment tells us [169] that the L_b state should be below the L_a state, while for anthracene and onwards the L_a state should be below the L_b state. Within the ALDA the L_a state is always below the L_b state even for anthracene. VK corrects for this discrepancy and predicts the right ordering of the L_a and L_b states.

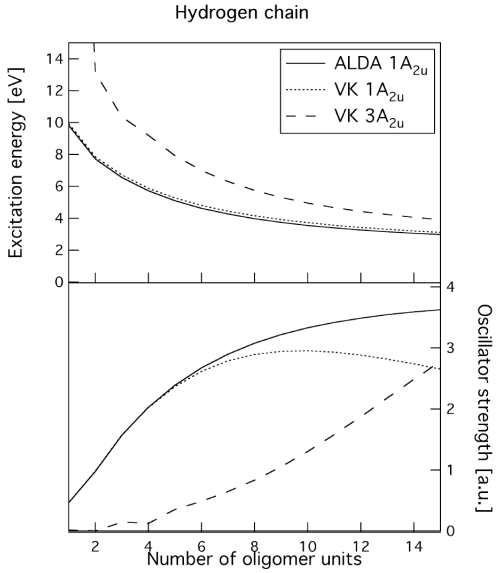

Figure 9-10. ALDA and VK singlet excitation energies and oscillator strengths of the hydrogen chain.

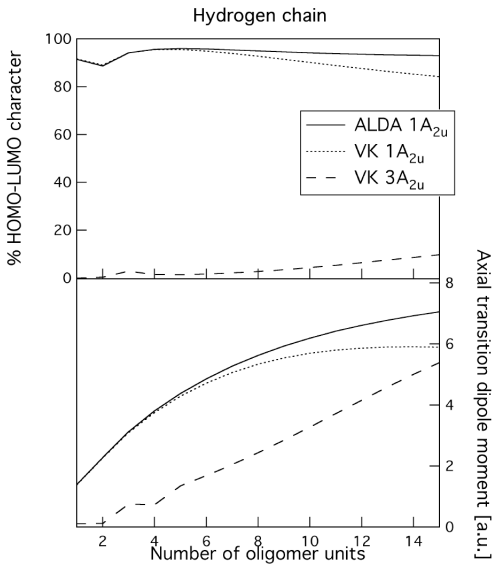

Figure 9-11. ALDA and VK HOMO-LUMO character and transition dipole moments for the hydrogen chain.

9.3.7 The model hydrogen chain

Finally we studied the hydrogen chain. In Ref. [77] we showed that VK only has a minor effect on the polarizability of the model hydrogen chain. In Figure 9-10 and Figure 9-11 we show our results for the $^1A_{2u}$ transition for ALDA and VK. To our knowledge no literature results are available for this system. We see that VK has hardly any effect on the excitation energies of the hydrogen chain. For the really long chains the 3 $^1A_{2u}$ transition takes over from the 1 $^1A_{2u}$ transition for VK but the effect is small. If we look at the HOMO-LUMO character we see that even for the long chains the HOMO-LUMO character is still >90% with VK.

9.4 Discussion

For all systems studied here we see the same trends. With VK the oscillator strength, axial transition dipole moment and HOMO-LUMO character are transferred to higher states. In all cases the excitation energies obtained with VK lie higher than the ALDA values. Except for the model hydrogen chain and PBT the excitation energies obtained with VK that have the largest

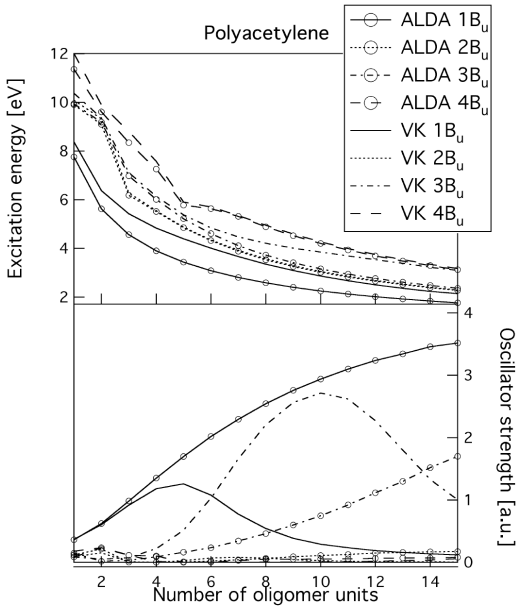

Figure 9-12. ALDA and VK excitation energies and oscillator strengths of polyacetylene.

spectral weight are closer to the available literature results. This explains why we obtain lower values for the polarizability with VK. However the individual excitation energies and oscillator strengths are not correctly described with VK.

In Figure 9-12 we again show the excitation energies and oscillator strengths of PA, but this time we added all transitions up to 4 ^1B_u for both ALDA and VK (to keep the graph readable we do not show the higher transitions). The ALDA and VK energies for the 2 ^1B_u and 4 ^1B_u transitions lie very close together. As mentioned the oscillator strengths for these transitions are very small. The 1 ^1B_u transition of VK moves away from the 1 ^1B_u transition of the ALDA until it comes close to the 2 ^1B_u transition. We see that at this point the 3 ^1B_u transition starts to move away from the ALDA, as if the 1 ^1B_u transition "pushes through" the 2 ^1B_u transition. We observe the same phenomenon when the 3 ^1B_u transition "pushes through" the 4 ^1B_u, 5 ^1B_u and 6 ^1B_u transitions and becomes the 7 ^1B_u transition. We saw in Ref. [79,80] that in case of $\pi \rightarrow \pi^*$ transitions a large oscillator strength (and a large transition dipole moment) means a large VK effect. This is exactly what we observe here. The excitation energies with little oscillator strength do not shift compared to the ALDA and the transitions with a large oscillator strength have a large shift compared to the ALDA. We see the same for the other systems studied. We also see in Figure 9-12 that the 3 ^1B_u transition within the ALDA gains oscillator strength for the long chains. With VK this excitation gets mixed in with several higher states and it is difficult to see which VK state corresponds with the 3 ^1B_u transition within the ALDA.

In all systems studied here the excitations with large oscillator strengths also have a large axial transition dipole moment. This means that there is a large global displacement of charge along the long axis of the molecule, which means a large current flow and a large VK effect. The excitations for which the oscillator strengths and transition dipole moments are small have only

a small global charge displacement (small current) and therefore the VK effect is small. The problem with VK seems to be that the transitions with small oscillator strengths do not shift upward like the transitions that do have large oscillator strengths. When transitions with large and small oscillator strength become close in energy, they can mix and the oscillator strength becomes distributed over these states. The mean weighed average of the excitation energies is however roughly at the correct position.

Finally we looked at the triplet ^3B_u transition in polyacetylene. We saw again a large effect of VK and HOMO-LUMO character being transferred to higher transitions. But in this case the effect of VK is unwanted, the ALDA values are already close to experimental and CIS values. The reason of this large effect of VK is that the static values of B^T, presented in Table 5-1, are very close to the values of $f_{xc,T}(0)$. Therefore we can expect a similar effect of VK for both the singlet and triplet excitation energies. This is indeed what we find.

9.5 Conclusion

We calculated the excitation spectra for several π-conjugated oligomers with the VK-functional. For these systems we found in our previous studies [77,78] that the axial polarizability obtained with VK lies close to the literature values, while the ALDA strongly overestimates. Previously we also studied the $\pi \rightarrow \pi^*$ transitions of some small π-conjugated systems and found an improvement of the excitation energy when using VK. In this work we find that the excitation energies, underestimated within the ALDA, are always increased by VK. For the triplet case we saw that the VK overestimates the excitation energies. For the singlet case we find that VK transfers the oscillator strength to higher excitations but that the transitions with small oscillator strengths do not shift upward like the transitions that do have large oscillator strengths. This leads to the fact that individual excitation energies and oscillator strengths are not correctly described with VK. We did observe that the VK singlet transitions that have the largest spectral weight lie close to the available literature results for all systems except PBT and the hydrogen chain.

Chapter 10

Analysis of the VK-functional: The atomic case

In this chapter we rewrite the VK-functional in spherical coordinates and do some analysis for atomic systems. On the basis of our findings we modify the exchange-correlation kernel and we see that a small modification has a large effect. At the end of this chapter we give some general conclusions on the Vignale-Kohn functional based on our findings in this thesis.

10.1 Introduction

In Chapter 8 we saw that the VK-functional does not give equally good results for different types of transitions. While the excitation energies for the $\pi \rightarrow \pi^*$ transitions obtained with the VK-functional are in good agreement with experiment and other theoretical results, the excitation energies of the $n \rightarrow \pi^*$ transitions are strongly overestimated compared with the experimental and other theoretical results.

Ullrich and Burke [27] showed that a similar problem is found in atoms. They derived a simplified procedure for calculating the excitation energies, which is an extension of the so-called small-matrix approximation (SMA) and used this in combination with the full frequency dependent VK-functional. They observed that the VK-functional gives a small improvement for the $s \rightarrow s$ transitions, but strongly overestimates the $s \rightarrow p$ excitation energies. They conclude that there are two sources to this problem. The first source is that the currents associated with the $s \rightarrow p$ excitations are highly nonuniform and, in particular, change direction between atomic shells. This can be a problem since the VK-functional is formally only justified if the system under consideration has a slowly varying ground state density and if the currents associated with a particular excitation are slowly varying on the scale of the local k_F. As a second source they suggest that the so-called exchange-correlation kernels of the homogeneous electron gas, f_{xcL} and f_{xcT}, are incompletely known, in particular in the high-density atomic core regions.

In this chapter we will also conduct a study of excitation energies in atoms. We will use the full time-dependent current-density-functional formalism (TDCDFT), but just like in the rest of

this thesis we use the VK-functional in the static limit. We will first rewrite the VK-functional for a particular transition in spherical coordinates, which will simplify the analysis. We will then analyze the VK-functional for different transitions in atoms.

10.2 Theory

Since we are only considering atoms it is convenient to work in spherical coordinates. The general form of the atomic orbitals is,

$$\psi(r,\theta,\phi) = R(r)\, c_l^m P_l^m(\cos\theta)\, e^{im\phi} \tag{10.1}$$

with

$$c_l^m = \sqrt{\frac{2l+1}{4\pi}\frac{(l-m)!}{(l+m)!}} \tag{10.2}$$

where l and m are the angular momentum quantum numbers, $R(r)$ is the radial part of the orbital and $P_l^m(\cos\theta)$ is the associated Legendre polynomial of l and m. We now want to express the VK-functional in spherical coordinates, starting from

$$\delta\mathbf{E}_{\mathrm{xc}}(\mathbf{r},\omega) = \nabla\delta v_{\mathrm{xc}}^{\mathrm{ALDA}}(\mathbf{r},\omega) - \frac{1}{\rho_0(\mathbf{r})}\sum_j \partial_j \sigma_{\mathrm{xc},ij}(\mathbf{r},\omega). \tag{10.3}$$

We first concentrate on the second part of the VK-functional. It is convenient to write the stress tensor σ_{ij} in the following way,

$$\sigma_{ij} = a e_{ij} + b\delta_{ij}\sum_k e_{kk} \tag{10.4}$$

with $a = 2\eta$ and $b = \zeta - 2\eta/3$, where we defined η and ζ in Eqs. (4.56) and (4.57). We defined

$$e_{ij} = \frac{1}{2}\left(\partial_i u_j + \partial_j u_i\right) \tag{10.5}$$

where $\mathbf{u}(\mathbf{r},\omega)$ is the velocity field. In spherical coordinates Eq. (10.4) is still valid but the tensor e_{ij} has a different form (see for example Ref. [55]),

$$e_{rr} = \frac{\partial u_r}{\partial r} \tag{10.6}$$

$$e_{\theta\theta} = \frac{1}{r}\frac{\partial u_\theta}{\partial \theta} + \frac{u_r}{r} \tag{10.7}$$

$$e_{\phi\phi} = \frac{1}{r\sin\theta}\frac{\partial u_\phi}{\partial \phi} + \frac{u_r}{r} + \frac{\cot\theta}{r}u_\theta \tag{10.8}$$

$$e_{r\theta} = \frac{1}{2}\left\{\frac{1}{r}\frac{\partial u_r}{\partial \theta} + \frac{\partial u_\theta}{\partial r} - \frac{1}{r}u_\theta\right\} \tag{10.9}$$

$$e_{\theta\phi} = \frac{1}{2}\left\{\frac{1}{r}\frac{\partial u_\phi}{\partial \theta} + \frac{1}{r\sin\theta}\frac{\partial u_\theta}{\partial \phi} - \frac{\cot\theta}{r}u_\phi\right\} \tag{10.10}$$

$$e_{r\phi} = \frac{1}{2}\left\{\frac{1}{r\sin\theta}\frac{\partial u_r}{\partial \phi} + \frac{\partial u_\phi}{\partial r} - \frac{1}{r}u_\phi\right\}. \tag{10.11}$$

We can now write the second term of Eq. (10.3) (which we from now on will call the viscoelastic part) in spherical coordinates as

$$-\rho_0 E_{\mathrm{xc},r}^{\mathrm{viscoel.}} = \frac{1}{r^2}\frac{\partial}{\partial r}\left(r^2\sigma_{rr}\right) + \frac{1}{r\sin\theta}\left[\frac{\partial}{\partial\theta}\left(\sigma_{r\theta}\sin\theta\right) + \frac{\partial\sigma_{r\phi}}{\partial\phi}\right] - \frac{1}{r}\left(\sigma_{\theta\theta} + \sigma_{\phi\phi}\right) \tag{10.12}$$

$$-\rho_0 E_{\mathrm{xc},\theta}^{\mathrm{viscoel.}} = \frac{1}{r^2}\frac{\partial}{\partial r}\left(r^2\sigma_{\theta r}\right) + \frac{1}{r\sin\theta}\left[\frac{\partial}{\partial\theta}\left(\sigma_{\theta\theta}\sin\theta\right) + \frac{\partial\sigma_{\theta\phi}}{\partial\phi}\right] + \frac{1}{r}\left(\sigma_{\theta r} - \sigma_{\phi\phi}\cot\theta\right) \tag{10.13}$$

$$-\rho_0 E_{\mathrm{xc},\phi}^{\mathrm{viscoel.}} = \frac{1}{r^2}\frac{\partial}{\partial r}\left(r^2\sigma_{\phi r}\right) + \frac{1}{r\sin\theta}\left[\frac{\partial}{\partial\theta}\left(\sigma_{\phi\theta}\sin\theta\right) + \frac{\partial\sigma_{\phi\phi}}{\partial\phi}\right] + \frac{1}{r}\left(\sigma_{\phi r} + \sigma_{\theta\phi}\cot\theta\right). \tag{10.14}$$

Let us look at a transition from orbital 1 to orbital 2. The components of the transition current density are then given by

$$j_r\left(r,\theta,\phi\right) = \frac{-i}{2}\left(\psi_2^*\frac{\partial\psi_1}{\partial r} - \psi_1\frac{\partial\psi_2^*}{\partial r}\right) \tag{10.15}$$

$$j_\theta\left(r,\theta,\phi\right) = \frac{-i}{2}\frac{1}{r}\left(\psi_2^*\frac{\partial\psi_1}{\partial\theta} - \psi_1\frac{\partial\psi_2^*}{\partial\theta}\right) \tag{10.16}$$

$$j_\phi(r,\theta,\phi) = \frac{-i}{2}\frac{1}{r\sin\theta}\left(\psi_2^*\frac{\partial\psi_1}{\partial\phi} - \psi_1\frac{\partial\psi_2^*}{\partial\phi}\right). \tag{10.17}$$

We can now easily find the components of the velocity field using $\mathbf{j} = \mathbf{u}/\rho_0$. Substituting Eq. (10.1) for the orbitals we obtain

$$u_r(r,\theta,\phi) = f_r(r)c_{l_1}^{m_1}c_{l2}^{m_2}P_{l_1}^{m_1}(\cos\theta)P_{l_2}^{m_2}(\cos\theta)e^{i(m_1-m_2)\phi} \tag{10.18}$$

$$\begin{aligned} u_\theta(r,\theta,\phi) &= f_\theta(r)c_{l_1}^{m_1}c_{l2}^{m_2} \\ &\times\left(P_{l_2}^{m_2}(\cos\theta)\frac{\partial P_{l_1}^{m_1}(\cos\theta)}{\partial\theta} - P_{l_1}^{m_1}(\cos\theta)\frac{\partial P_{l_2}^{m_2}(\cos\theta)}{\partial\theta}\right)e^{i(m_1-m_2)\phi} \end{aligned} \tag{10.19}$$

$$u_\phi(r,\theta,\phi) = f_\phi(r)c_{l_1}^{m_1}c_{l2}^{m_2}\frac{P_{l_1}^{m_1}(\cos\theta)P_{l_2}^{m_2}(\cos\theta)}{\sin\theta}e^{i(m_1-m_2)\phi} \tag{10.20}$$

where we defined the radial function

$$f_r(r) = \frac{-i}{2\rho_0(r)}\left(R_2(r)\frac{\partial R_1(r)}{\partial r} - R_1(r)\frac{\partial R_2(r)}{\partial r}\right) \tag{10.21}$$

$$f_\theta(r) = \frac{-i}{2r\rho_0(r)}R_1(r)R_2(r) \tag{10.22}$$

$$f_\phi(r) = \frac{m_1+m_2}{2r\rho_0(r)}R_1(r)R_2(r) = i(m_1+m_2)f_\theta(r). \tag{10.23}$$

Substituting everything in Eq. (10.4) we find for the elements of the stress tensor,

$$\sigma_{rr} = a_{rr}P_{l_1}^{m_1}P_{l_2}^{m_2}e^{i(m_1-m_2)\phi} \tag{10.24}$$

$$\begin{aligned} \sigma_{\theta\theta} &= a_{\theta\theta}^{(1)}\frac{\partial}{\partial\theta}\left(P_{l_2}^{m_2}\frac{\partial P_{l_1}^{m_1}}{\partial\theta} - P_{l_1}^{m_1}\frac{\partial P_{l_2}^{m_2}}{\partial\theta}\right)e^{i(m_1-m_2)\phi} \\ &+a_{\theta\theta}^{(2)}P_{l_1}^{m_1}P_{l_2}^{m_2}e^{i(m_1-m_2)\phi} \end{aligned} \tag{10.25}$$

$$\begin{aligned} \sigma_{\phi\phi} &= a_{\phi\phi}^{(1)}\left(P_{l_2}^{m_2}\frac{\partial^2 P_{l_1}^{m_1}}{\partial\theta^2} - P_{l_1}^{m_1}\frac{\partial^2 P_{l_2}^{m_2}}{\partial\theta^2}\right)e^{i(m_1-m_2)\phi} \\ &+a_{\phi\phi}^{(2)}P_{l_1}^{m_1}P_{l_2}^{m_2}e^{i(m_1-m_2)\phi} \end{aligned} \tag{10.26}$$

$$\begin{aligned}\sigma_{r\theta} &= a_{r\theta}^{(1)} \frac{\partial}{\partial\theta}\left(P_{l_1}^{m_1} P_{l_2}^{m_2}\right) e^{i(m_1-m_2)\phi} \\ &+a_{r\theta}^{(2)}\left(P_{l2}^{m_2}\frac{\partial P_{l_1}^{m_1}}{\partial\theta} - P_{l_1}^{m_1}\frac{\partial P_{l_2}^{m_2}}{\partial\theta}\right) e^{i(m_1-m_2)\phi}\end{aligned} \tag{10.27}$$

$$\sigma_{r\phi} = a_{r\phi}\frac{1}{\sin\theta} P_{l_1}^{m_1} P_{l_2}^{m_2} e^{i(m_1-m_2)\phi} \tag{10.28}$$

$$\begin{aligned}\sigma_{\theta\phi} = a_{\theta\phi}\frac{1}{\sin\theta}\Bigg(& m_1 P_{l_2}^{m_2}\frac{\partial P_{l_1}^{m_1}}{d\theta} + m_2 P_{l_1}^{m_1}\frac{\partial P_{l_2}^{m_2}}{\partial\theta} \\ & -\left(m_1+m_2\right)\cot\theta P_{l_1}^{m_1} P_{l_2}^{m_2}\Bigg) e^{i(m_1-m_2)\phi}\end{aligned} . \tag{10.29}$$

The radial parts of the stress tensor are given by,

$$a_{rr} = (a+b)\frac{\partial f_r}{\partial r} + \frac{b}{r}\left(2f_r + \left\{l_2\left(l_2+1\right) - l_1\left(l_1+1\right)\right\} f_\theta\right) \tag{10.30}$$

$$a_{\theta\theta}^{(1)} = \frac{af_\theta}{r} \tag{10.31}$$

$$a_{\theta\theta}^{(2)} = \frac{af_r}{r} + b\frac{\partial f_r}{\partial r} + \frac{b}{r}\left(2f_r + \left\{l_2\left(l_2+1\right) - l_1\left(l_1+1\right)\right\} f_\theta\right) \tag{10.32}$$

$$a_{\phi\phi}^{(1)} = -\frac{af_\theta}{r} = -a_{\theta\theta}^{(1)} \tag{10.33}$$

$$\begin{aligned}a_{\phi\phi}^{(2)} = & \frac{a}{r}\left(f_r + \left\{l_2\left(l_2+1\right) - l_1\left(l_1+1\right)\right\} f_\theta\right) + b\frac{\partial f_r}{\partial r} \\ & +\frac{b}{r}\left(2f_r + \left\{l_2\left(l_2+1\right) - l_1\left(l_1+1\right)\right\} f_\theta\right)\end{aligned} \tag{10.34}$$

$$a_{r\theta}^{(1)} = \frac{af_r}{2r} \tag{10.35}$$

$$a_{r\theta}^{(2)} = \frac{a}{2}\left(\frac{\partial f_\theta}{\partial r} - \frac{f_\theta}{r}\right) \tag{10.36}$$

$$a_{r\phi} = \frac{a}{2}\left\{ i\left(m_1 - m_2\right)\frac{f_r}{r} + \frac{\partial f_\phi}{\partial r} - \frac{f_\phi}{r} \right\} \tag{10.37}$$

$$a_{\theta\phi} = \frac{iaf_\theta}{r}\,. \tag{10.38}$$

The components of the viscoelastic part of the VK-functional are then given as

$$\begin{aligned} -\rho_0 \delta E_{\mathrm{xc},r}^{\mathrm{viscoel.}} = & \left(\frac{\partial a_{rr}}{\partial r} + \frac{1}{r}\Big[2a_{rr} - a_{\theta\theta}^{(2)} - a_{\phi\phi}^{(2)} - \left\{ l_1\left(l_1+1\right) + l_2\left(l_2+1\right) \right\} a_{r\theta}^{(1)} \right. \\ & \left. + \left\{ l_2\left(l_2+1\right) - l_1\left(l_1+1\right) \right\} a_{r\theta}^{(2)} \Big) P_{l_1}^{m_1} P_{l_2}^{m_2} e^{i(m_1-m_2)\phi} \right. \\ & \left. + \frac{2a_{r\theta}^{(1)}}{r}\left(\frac{\partial P_{l_1}^{m_1}}{d\theta}\frac{\partial P_{l_2}^{m_2}}{d\theta} + \frac{m_1 m_2}{\sin^2\theta} P_{l_1}^{m_1} P_{l2}^{m_2} \right) e^{i(m_1-m_2)\phi} \right. \end{aligned} \tag{10.39}$$

$$\begin{aligned} -\rho_0 \delta E_{\mathrm{xc},\theta}^{\mathrm{viscoel}} = & \left(\frac{\partial a_{r\theta}^{(1)}}{\partial r} + \frac{1}{r}\Big[3a_{r\theta}^{(1)} + a_{\theta\theta}^{(2)} + \left\{ l_2\left(l_2+1\right) - l_1\left(l_1+1\right) \right\} a_{\theta\theta}^{(1)} \Big] \right) \\ & \times \frac{\partial}{\partial\theta}\left(P_{l_1}^{m_1} P_{l_2}^{m_2} \right) e^{i(m_1-m_2)\phi} \\ & + \left(\frac{\partial a_{r\theta}^{(2)}}{\partial r} + \frac{1}{r}\Big[3a_{r\theta}^{(1)} + a_{\theta\theta}^{(1)} \Big] \right)\left(P_{l_2}^{m_2}\frac{\partial P_{l_1}^{m_1}}{\partial\theta} - P_{l_1}^{m_1}\frac{\partial P_{l_2}^{m_2}}{\partial\theta} \right) e^{i(m_1-m_2)\phi} \\ & + \frac{a_{\theta\theta}^{(1)}}{r}\frac{m_1 - m_2}{\sin^2\theta}\left(m_1 P_{l_1}^{m_1}\frac{\partial P_{l_2}^{m_2}}{\partial\theta} + m_2 P_{l_2}^{m_2}\frac{\partial P_{l_1}^{m_1}}{\partial\theta} \right) e^{i(m_1-m_2)\phi} \end{aligned} \tag{10.40}$$

$$\begin{aligned} -\rho_0 \delta E_{\mathrm{xc},\phi}^{\mathrm{viscoel.}} = & \left(\frac{\partial a_{r\phi}}{\partial r} + \frac{1}{r}\Big[3a_{r\phi} + i\left(m_1 - m_2\right) a_{\phi\phi}^{(2)} + \left(m_1 + m_2\right) a_{\theta\phi} \Big] \right) \\ & \times \frac{P_{l_1}^{m_1} P_{l_2}^{m_2}}{\sin\theta} e^{i(m_1-m_2)\phi} \\ & + \frac{a_{\theta\phi}}{r\sin\theta}\left\{ \left(m_1 + m_2\right)\frac{\partial P_{l_1}^{m_1}}{\partial\theta}\frac{\partial P_{l_2}^{m_2}}{\partial\theta} + m_1 P_{l_1}^{m_1}\left(\frac{\partial^2 P_{l_2}^{m_2}}{\partial\theta^2} - \cot\theta\frac{\partial P_{l_2}^{m_2}}{\partial\theta} \right) \right. \\ & \left. + m_2 P_{l_2}^{m_2}\left(\frac{\partial^2 P_{l_1}^{m_1}}{\partial\theta^2} - \cot\theta\frac{\partial P_{l_1}^{m_1}}{\partial\theta} \right) \right\} e^{i(m_1-m_2)\phi} \end{aligned} \tag{10.41}$$

We also want to compare the contribution of this viscoelastic part relative to the ALDA part. Therefore we need to write the ALDA contribution to the VK-functional in spherical coordinates too. The ground state LDA functional is given by

$$\upsilon_{\mathrm{xc}}^{\mathrm{LDA}}(\mathbf{r}) = \frac{\delta E_{\mathrm{xc}}^{\mathrm{LDA}}}{\delta\rho} = \varepsilon_{\mathrm{xc}} + \rho(\mathbf{r})\frac{\delta\varepsilon_{\mathrm{xc}}}{\delta\rho}. \tag{10.42}$$

As we mentioned in Section 1.4 the exchange-correlation energy $\varepsilon_{\mathrm{xc}}$ can be split in an exchange and a correlation part. The exchange part is given by the Dirac exchange-energy functional [33],

$$\varepsilon_{\mathrm{x}}(\rho) = -\frac{3}{4}\left(\frac{3}{\pi}\right)^{1/3}\rho(\mathbf{r})^{1/3}. \tag{10.43}$$

The correlation part is more complicated and since it is much smaller than the exchange part and we neglect this part in the following analysis. We can now write the ground state exchange only LDA functional as

$$\upsilon_{\mathrm{x}}^{\mathrm{LDA}}(\mathbf{r}) = -\left(\frac{3}{\pi}\right)^{1/3}\rho(\mathbf{r})^{1/3}. \tag{10.44}$$

The ALDA exchange potential change belonging to a transition from orbital 1 to orbital 2 is then given by

$$\begin{aligned}\delta\upsilon_{\mathrm{x}}^{\mathrm{ALDA}}(\mathbf{r},t) &= \int\int \delta(t-t')\delta(\mathbf{r}-\mathbf{r}')\left.\frac{\delta\upsilon_{\mathrm{x}}^{\mathrm{LDA}}(\mathbf{r},t)}{\delta\rho(\mathbf{r}',t')}\right|_{\rho(\mathbf{r},t)=\rho_0(\mathbf{r})}\delta\rho(\mathbf{r}',t')\,d\mathbf{r}'d\mathbf{t}' \\ &= -\frac{1}{3}\left(\frac{3}{\pi}\right)^{1/3}\rho_0(\mathbf{r})^{-2/3}\,\delta\rho(\mathbf{r},t) \\ &= -\frac{1}{3}\left(\frac{3}{\pi}\right)^{1/3}\rho_0(\mathbf{r})^{-2/3}\,\psi_2^*\psi_1\end{aligned}. \tag{10.45}$$

In spherical coordinates we obtain for the gradient of the ALDA,

$$\begin{aligned}\nabla_r\delta\upsilon_{\mathrm{x}}^{\mathrm{ALDA}}(\mathbf{r},t) = &\left[\frac{2}{9}\left(\frac{3}{\pi}\right)^{1/3}\rho_0(\mathbf{r})^{-5/3}R_1(r)R_2(r)\right. \\ &\left.-\frac{1}{3}\left(\frac{3}{\pi}\right)^{1/3}\rho_0(\mathbf{r})^{-2/3}\frac{\partial}{\partial r}\left(R_1(r)R_2(r)\right)\right] \\ &\times c_{l_1}^{m_1}c_{l_2}^{m_2}P_{l_1}^{m_1}(\cos\theta)P_{l_2}^{m_2}(\cos\theta)e^{i(m_1-m_2)\phi}\end{aligned} \tag{10.46}$$

$$\begin{aligned}\nabla_\theta\delta\upsilon_{\mathrm{x}}^{\mathrm{ALDA}}(\mathbf{r},t) = &-\frac{1}{3}\frac{1}{r}\left(\frac{3}{\pi}\right)^{1/3}\rho_0(\mathbf{r})^{-2/3}R_1(r)R_2(r) \\ &\times c_{l_1}^{m_1}c_{l_2}^{m_2}\frac{\partial}{\partial\theta}\left(P_{l_1}^{m_1}(\cos\theta)P_{l_2}^{m_2}(\cos\theta)\right)e^{i(m_1-m_2)\phi}\end{aligned} \tag{10.47}$$

$$\nabla_\phi \delta\upsilon_{\mathrm{x}}^{\mathrm{ALDA}}(\mathbf{r},t) = -\frac{1}{3}\frac{i(m_1-m_2)}{r\sin\theta}\left(\frac{3}{\pi}\right)^{1/3}\rho_0(\mathbf{r})^{-2/3}R_1(r)R_2(r) \times c_{l_1}^{m_1}c_{l_2}^{m_2}P_{l_1}^{m_1}(\cos\theta)P_{l_2}^{m_2}(\cos\theta)e^{i(m_1-m_2)\phi} \tag{10.48}$$

where $(\nabla_r,\nabla_\theta,\nabla_\phi) = (\partial/\partial r,(1/r)\partial/\partial\theta,(1/r\sin\theta)\partial/\partial\phi)$. We now have all the components of the total VK-functional for a specific transition between two orbitals.

In Chapter 3 we showed that it is not the plain functional that we are interested in but the matrix elements of its inner product with the current density, this is how the VK-functional appears in the P -matrix. So we really want to study

$$\begin{aligned}
&\int \psi_2^*(\mathbf{j}\cdot\delta\mathbf{E}_{\mathrm{xc}})\psi_1 d\mathbf{r} = \\
&\iiint\left(j_r\delta E_{\mathrm{xc},r}^{\mathrm{viscoel.}} + j_\theta\delta E_{\mathrm{xc},\theta}^{\mathrm{viscoel.}} + j_\phi\delta E_{\mathrm{xc},\phi}^{\mathrm{viscoel.}}\right)r^2\sin\theta dr d\theta d\phi \\
&+\iiint\left(j_r\nabla_r\delta\upsilon_{\mathrm{x}}^{\mathrm{ALDA}} + j_\theta\nabla_\theta\delta\upsilon_{\mathrm{x}}^{\mathrm{ALDA}} + j_\phi\nabla_\phi\delta\upsilon_{\mathrm{x}}^{\mathrm{ALDA}}\right)r^2\sin\theta dr d\theta d\phi \\
&= \int I^{\mathrm{ALDA}}(r)dr + \int I^{\mathrm{viscoel.}}(r)dr = \int I(r)dr
\end{aligned} \tag{10.49}$$

where we defined the integrand $I(r)$ and its separate VK and ALDA parts. This integrand we can easily plot in a graph and compare for different transitions. There is an arbitrariness with which we can choose this integrand. Ullrich and Burke, for example, make a different choice in Eq. 25 in Ref. [27]. But with this different choice we still draw the same conclusions from our graphs as they did.

10.3 Computational details

To generate the atomic orbitals we used a modified OPM (optimized potential model) program based on the work in Ref. [17]. The resulting OPM orbitals can then be used to calculate the components of the VK-functional (Ref. [204]) and the integrand of Eq. (10.49). The reason we use this program to calculate the integrand is that this program works with a radial grid, it is basis set independent, and since it uses a $1/r$ potential the virtual orbitals are bound.

We did calculations on the excitation energies with our modified version of ADF [25,99-103]. We used the standard ADF ET-pVQZ basis, which is an even-tempered Slater type basis set of quadruple-zeta quality. In these excitation energy calculations the ground state has been calculated with the LDA functional in the VWN parameterization [34]. The response calculations themselves were done with the standard adiabatic local density approximation (ALDA) and the VK-functional. For the latter we use the parameterizations of the viscoelastic

Table 10-1. This table shows the lowest singlet excitation energies of transitions for several closed shell atoms. All values are in eV

Transition		Exp.[a]	ALDA results by C.A. Ullrich[b]	VK results by C.A. Ullrich[b]	ALDA	VK NCT	VK QV
Be	$2s \rightarrow 2p$	5.28	5.07	6.23	4.83	6.03	6.14
Be	$2s \rightarrow 3s$	6.78	5.62	5.66	6.53	6.55	6.58
B^+	$2s \rightarrow 2p$	9.10	8.56	11.70	8.47	14.60	14.77
B^+	$2s \rightarrow 3s$	16.81	15.49	15.66	15.56	15.55	15.57
B^+	$2s \rightarrow 3p$	17.85	16.23	16.56	16.15	17.53	17.78
Mg	$3s \rightarrow 3p$	4.35	4.57	4.85	4.50	7.17	7.08
Mg	$3s \rightarrow 4s$	5.39	4.77	4.82	7.23	7.23	7.25
Mg	$2p \rightarrow 3p$				45.49	46.50	46.43
Al^+	$3s \rightarrow 3p$	7.42	7.74	8.07	7.48	11.41[c]	11.37[c]
Al^+	$3s \rightarrow 4s$	11.82	11.40	11.55	12.08	12.08	12.10
Al^+	$3s \rightarrow 4p$	13.26	12.47	12.67	12.66	16.21[c]	15.82[c]
Al^+	$2p \rightarrow 3p$				69.00	71.10	70.92

[a] Ref. [205].
[b] Ref. [27].
[c] The $3s \rightarrow 3p$ and $3s \rightarrow 4p$ transitions are strongly mixed in these cases.

coefficient based on results of Conti *et al*. [65] for the transverse response of the homogeneous electron gas [77], we denote this by NCT. As we explained in Section 5.5 we can also use different values for the transverse response kernel as obtained by Qian and Vignale [66], which we denote by QV. More information on these parameterizations can be found in Chapter 5. We denote these calculations simply as ALDA and VK (NCT or QV).

10.4 Results and discussion

In Table 10-1 we show our results for some different kinds of transitions in different atoms, we repeat the results for Beryllium that we already showed in Section 8.4. We also show the corresponding results from Ullrich and Burke [27], which they obtained using the frequency dependent VK-functional in the parameterization of Qian and Vignale [66]. From the table it is clear that the effect of the VK-functional is much larger for the $s \rightarrow p$ transitions than for the $s \rightarrow s$ transitions and $p \rightarrow p$ transitions. The ALDA results for the $s \rightarrow p$ transitions are the ones that are closest to the experimental values. We also see that the VK effect becomes smaller for the higher $s \rightarrow p$ transitions. We will see whether we can find out more about the VK-functional by looking at these particular transitions.

For an $s \rightarrow s$ transition $\delta E_{\mathrm{xc}}^{\mathrm{viscoel.}}$ is purely radial. We plot this function for the $2s \rightarrow 3s$ transition in the B^+ atom in Figure 10-1, where we used the NCT parameterization. We did not plot the

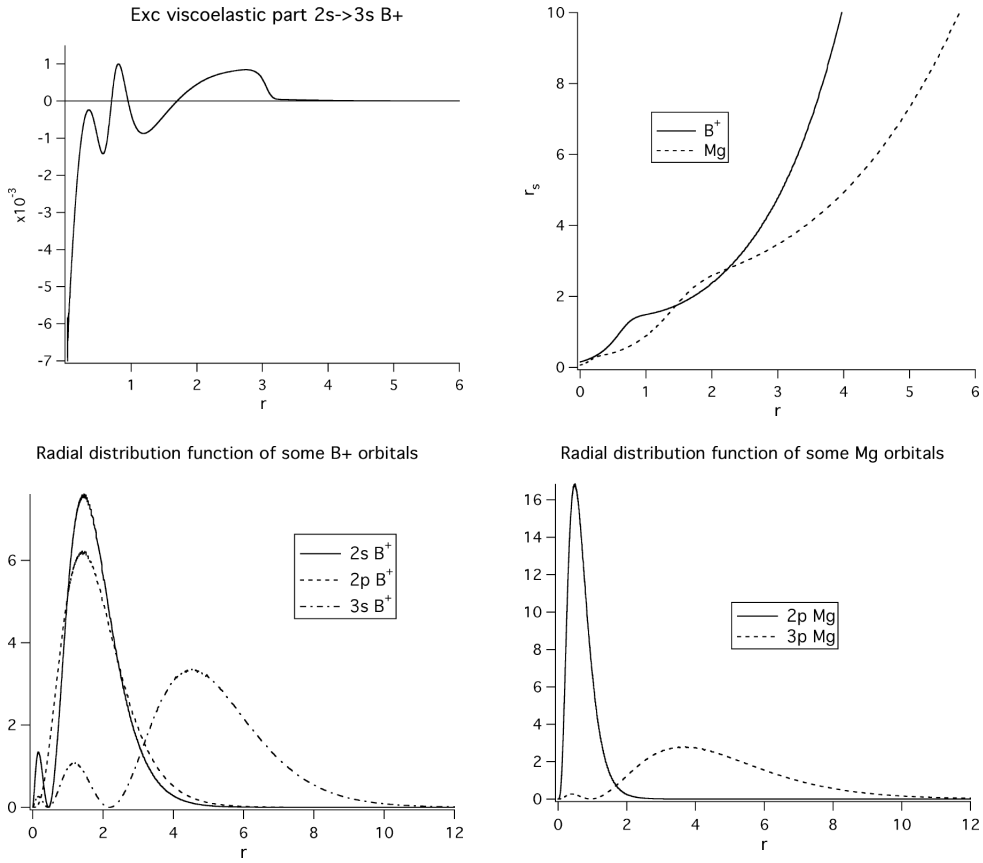

Figure 10-1. The viscoelastic part of the E_{xc} field for a $2s \rightarrow 3s$ transition in B^+ (top left). The relation between r and r_s for Mg and B^+ (top right). The radial distribution function ($4\pi r^2 \psi_i^2$) of some orbitals of Mg and B^+ (bottom).

ALDA part in this graph since it is completely dominant for this transition. We see that as a result of the fact that we take many derivatives of the orbitals, this function is rather wildly behaved, even for this rather simple transition. The sharp drop at $r \sim 3$ is a result of the fact that we choose the transverse xc-kernel f_{xcT} constant for $r_s > 5$.

In Figure 10-2 we show the integrand $I(r)$ and its ALDA and viscoelastic parts for the $2s \rightarrow 3s$, $2s \rightarrow 2p$, and $2s \rightarrow 3p$ transitions in the B^+ atom and as an example of a $p \rightarrow p$ transition we also show the $2p \rightarrow 3p$ transition in the Mg atom. As a reference we also give the radial distribution functions of the orbitals involved in Figure 10-1. We used the NCT for the xc-kernel f_{xcT}. We see for the $2s \rightarrow 3s$ transition in B^+ that the ALDA is completely dominant, as is

expected from the excitation energies we found in Table 10-1. The viscoelastic part is largest for the low-density region. For the $2s\rightarrow 2p$ and $2s\rightarrow 3p$ transitions in B^+ both the ALDA and viscoelastic parts are large in the high-density region (where r_s is small, see Figure 10-1 for the relation between r and r_s). For the $2s\rightarrow 2p$ transition the effect of the viscoelastic part on the ALDA is very large, explaining why the VK excitation energy for this transition changes so much when going from the ALDA to VK. For the $2s\rightarrow 3p$ transition the picture is similar for the high-density region, but at lower densities the ALDA starts to dominate. Therefore the ALDA contribution to the total integral is considerable and the effect of VK is smaller than for the $2s\rightarrow 3p$ transition. This is indeed what we find for the excitation energies. Finally we look at the $2p\rightarrow 3p$ ($\Delta m = 0$) transition in the Mg atom. We see that in this case the viscoelastic effect is considerable, but the ALDA is still dominating. The viscoelastic contribution is still quite large for the lower density region. These findings again correspond to our results for the excitation energies, where there effect of VK is larger for the $p\rightarrow p$ transitions than for the $s\rightarrow s$ transitions, but smaller than for the $s\rightarrow p$ transitions. We see that the largest viscoelastic contribution in the cases where the excitation energies are strongly overestimated is in the high-density (low r_s) region. The only part of the VK-functional that is not well known is the transverse xc-kernel, f_{xcT}. The f_{xcT} is in particular not well known in the high-density region up to $r_s \cong 1.0$. We see from Figure 10-2 above that this is the region were VK gives the largest contribution for the $s\rightarrow p$ transitions.

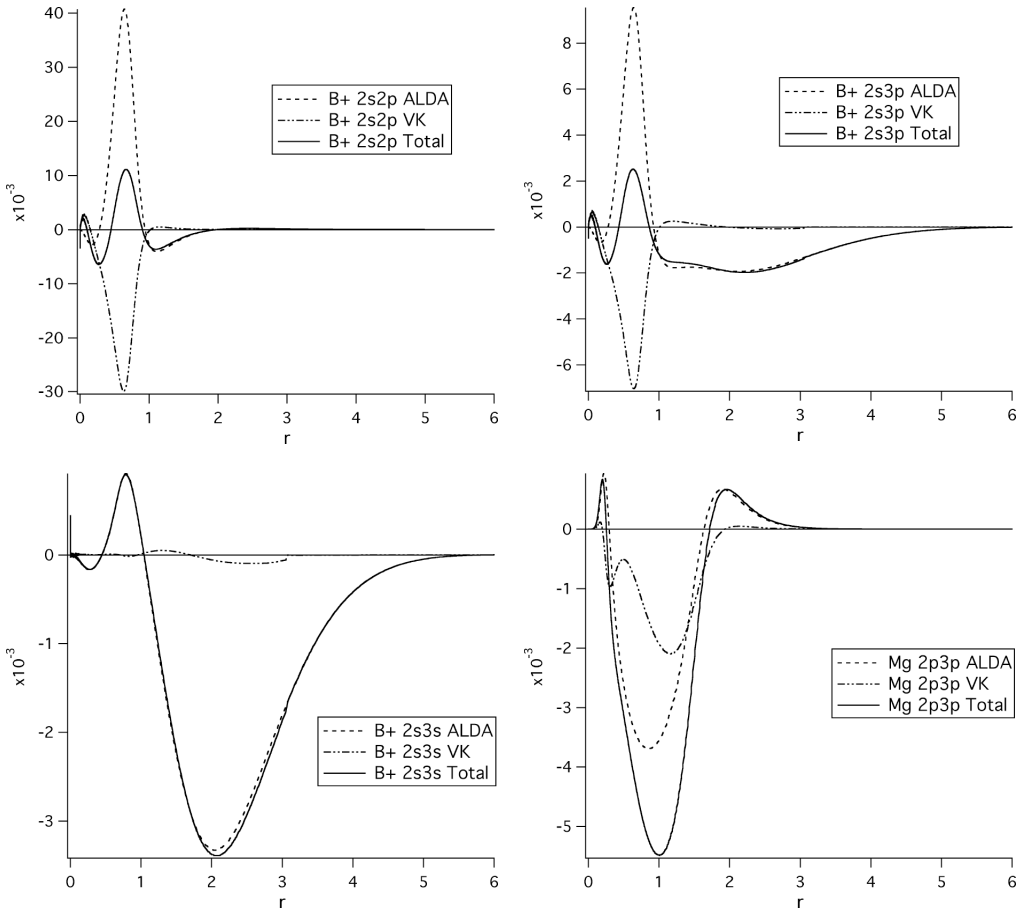

Figure 10-2. The integrand $I(r)$ ("Total") and its separate ALDA and viscoelastic ("VK") parts for the $2s \rightarrow 3s$, $2s \rightarrow 2p$, and $2s \rightarrow 3p$ transitions in the B^+ atom and the $2p \rightarrow 3p$ transition in the Mg atom.

We would like to test the influence of this region. In order to do this we will put f_{xcT} and its derivatives to zero up to a particular value of r_s after we performed the cubic spine interpolation (see section 5.5). Note that this is not the same as first putting f_{xcT} to zero and taking the derivatives afterwards. This would introduce extra surface terms that we neglect with our approach. Using this method, choosing the NCT as our basic f_{xcT}, we find that for Be and B^+ the threshold value needs to be larger than $r_s = 1.0$ in order to obtain values that are of the order of the experimental values (about $r_s = 1.8$ for Be and $r_s = 1.3$ for B^+), but for Mg and Al+ taking f_{xcT} zero up to $r_s = 1.0$ already gives a large modification of the VK values for the $s \rightarrow p$

Table 10-2. This table shows the lowest singlet excitation energies of transitions for several atoms and molecules. All values are in eV

Transition			Exp.	ALDA	VK NCT	VK NCT $r_s > 1.0$	VK NCT $r_s > 1.3$
Be		$2s \rightarrow 2p$	5.28[a]	4.83	6.03	6.32	6.08
Be		$2s \rightarrow 3s$	6.78[a]	6.53	6.55	6.55	6.55
B^+		$2s \rightarrow 2p$	9.10[a]	8.47	14.60	14.89	10.00
B^+		$2s \rightarrow 3s$	16.81[a]	15.56	15.55	15.55	15.55
B^+		$2s \rightarrow 3p$	17.85[a]	16.15	17.53	18.32	16.22
Mg		$3s \rightarrow 3p$	4.35[a]	4.50	7.17	4.72	4.70
Mg		$3s \rightarrow 4s$	5.39[a]	7.23	7.23	7.25	7.25
Mg		$2p \rightarrow 3p$		45.49	46.50	45.44	45.44
Al^+		$3s \rightarrow 3p$	7.42[a]	7.48	11.41[b]	7.84	7.77
Al^+		$3s \rightarrow 4s$	11.82[a]	12.08	12.08	12.09	12.09
Al^+		$3s \rightarrow 4p$	13.26[a]	12.66	16.21[b]	12.64	12.62
Al^+		$2p \rightarrow 3p$		69.00	71.10	68.99	68.99
C_2H_4	Ethene	$\pi \rightarrow \pi^*$ 1^1B_{1u}	7.66[c]	7.55	8.05	7.82	7.68
C_8H_7N	Indole	$\pi \rightarrow \pi^*$ $2^1A'$	4.37[d]	4.34	4.66	4.59	4.46
		$\pi \rightarrow \pi^*$ $3^1A'$	4.77[d]	4.59	4.74	4.64	4.62
$C_{10}H_{12}$	Decapentaene	$\pi \rightarrow \pi^*$ 1^1B_u	4.02[e]	3.26	4.33	3.90	3.52
CH_2O	Formaldehyde	$n \rightarrow \pi^*$ 1^1A_2	3.79[f];4.07[g]	3.68	8.34	2.24	3.53
$C_4H_4N_2$	Pyridazine	$n \rightarrow \pi^*$ 1^1B_1	3.30[h]	2.95	7.03	0.25	2.69
C_5		$n \rightarrow \pi^*$ $1^1\Pi_u$	2.78[i]	2.50	6.74	3.20	1.14

[a] Ref. [205].
[b] The $3s \rightarrow 3p$ and $3s \rightarrow 4p$ transitions are strongly mixed in this cases.
[c] Ref. [149].
[d] Ref. [158].
[e] Gas phase measurements from Ref. [166].
[f] Electron impact spectroscopy values from Ref. [175].
[g] Ref. [176].
[h] Ref. [173].
[i] Gas phase measurements from Ref. [180].

transitions. This observation can be understood since the VK-functional is very dependent on the shape of the orbitals that are involved in the transition (for example through the current matrix elements). The orbitals for the lighter atoms are more diffuse, so the outer region becomes more important. To see the effect of the high-density region we will do calculations putting f_{xcT} to zero up to $r_s = 1.0$ and $r_s = 1.3$.

In Table 10-2 we show the values we obtain if we put f_{xcT} to zero up to $r_s = 1.0$ and $r_s = 1.3$ (denoted NCT $r_s > 1.0$ and NCT $r_s > 1.3$). As mentioned above the values for the $s \rightarrow p$ transitions in Be and B^+ are still overestimated with NCT $r_s > 1.0$, but the B^+ value is improved with NCT $r_s > 1.3$. The results for Mg and Al^+ are much improved in both cases. For the $p \rightarrow p$

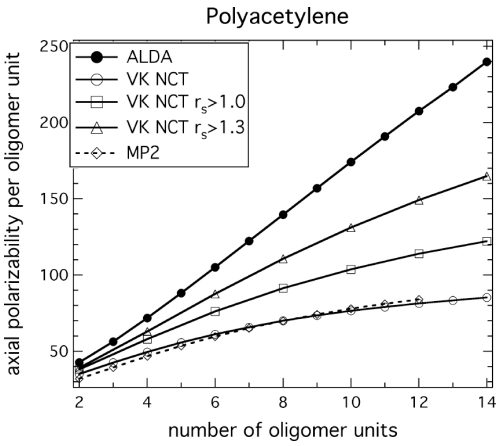

Figure 10-3. ALDA and VK (NCT, NCT $r_s > 1.0$, and NCT $r_s > 1.3$) static axial polarizability of polyacetylene compared with MP2 [13] results.

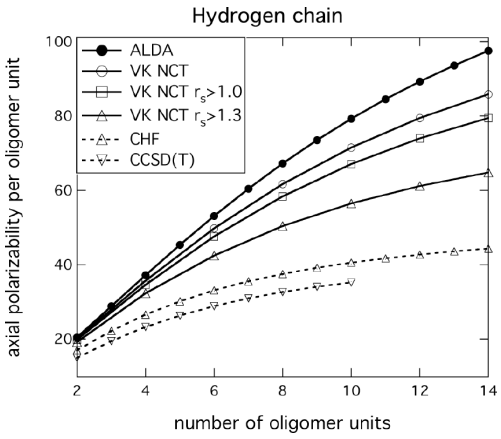

Figure 10-4. ALDA and VK (NCT, NCT $r_s > 1.0$, and NCT $r_s > 1.3$) static axial polarizability of hydrogen chains compared with coupled Hartree-Fock (HF) and coupled-cluster (CCSD(T)) results [88].

transitions the results are close to the ALDA values in both cases. Since the effect of the VK-functional is already small for the $s \rightarrow s$ transitions, they do not change a lot when putting f_{xcT} to zero in the high-density region. We see that the low-density region is especially important for the $s \rightarrow p$ transitions.

It is interesting to see what the effect of this approach is on some molecular systems. We also show these in Table 10-2. For ethane we see that the results with NCT $r_s > 1.0$ and $r_s > 1.3$ are closer to experiment than with the full f_{xcT}. For indole this is also the case, but if we look more closely the results with the modified f_{xcT} are actually worse than the full f_{xcT}. As we mentioned in Chapter 8, the ALDA predicts the wrong ordering of the transitions. It assigns the $2\ ^1\mathrm{A}'$ state to the $\mathrm{L_a}$ transition and the $3\ ^1\mathrm{A}'$ state to the $\mathrm{L_b}$ transition. The VK-functional with the full f_{xcT} corrects for this. But when we use the modified f_{xcT} we see that we obtain the same character for the transitions as with the ALDA, thus also predicting the wrong ordering of the states. So for this system the high-density region is very important to take into account. For *trans*-1,3,5,7,9-decapentaene we see that the results with the modified f_{xcT} are slightly worse than with the full f_{xcT}, but the VK effect is still rather large. For the $n \rightarrow \pi^*$ transitions we see a large reduction of the excitation energy when using the modified f_{xcT} in all cases. For formaldehyde and pyridazine the reduction is too large with NCT $r_s > 1.0$, leading to a strong underestimation

of the experimental results. With NCT $r_s > 1.3$ we obtain results for formaldehyde and pyridazine that are close to the ALDA and experimental values, but in this case the excitation energy of C_5 is strongly underestimated. It is clear that the high-density region is very important for the $n \rightarrow \pi^*$ transitions.

To see if we still retain some of the long-range properties of VK with our modified f_{xcT} we again look at the polarizability of polyacetylene. We give our results in Figure 10-3. We see that the polarizability is not by far as good as the NCT but the VK effect is still considerable, indicating that some long-range properties are retained. A chain system for which we saw that the VK-functional fails is the model hydrogen chain. To see if this problem should also be attributed to the high-density region we also used our modified f_{xcT} to calculate the axial polarizability of this system. We show our results in Figure 10-4. We see that the polarizability changes considerably when using the modified f_{xcT}. With NCT $r_s > 1.3$ the results are getting much closer to the literature values. So a large part of this problem also can be contributed to the high-density region. This result is surprising since one would expect that if we neglect a part of the VK-functional, the polarizability would come closer to the ALDA values. The fact that this is not the case indicates that there is a canceling of terms when including the full f_{xcT}.

We also looked at the excitation energies of polyacetylene and the model hydrogen chain with NCT $r_s > 1.3$. We show these in Figure 10-5 and Figure 10-6. We see that as expected from the polarizability results, the excitation energies of polyacetylene are closer to the ALDA compared with our results in Figure 9-1 and the excitation energies of the model hydrogen chain are higher compared with our results in Figure 9-10. The fact that transitions with small oscillator strength do not shift upwards when using VK does not change when using NCT $r_s > 1.3$. We see from the oscillator strengths that the states that shift upwards “push through” these non-shifting states like we found in Chapter 9. This effect is now less pronounced for polyacetylene but much more pronounced for the model hydrogen chain.

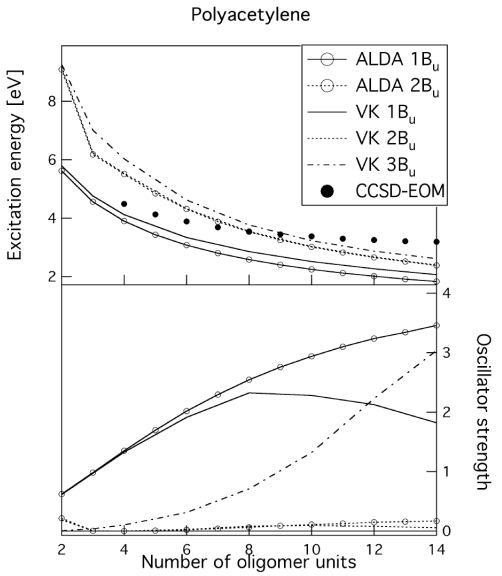

Figure 10-5. ALDA and VK NCT $r_s > 1.3$ excitation energies and oscillator strengths of polyacetylene compared with CCSD-EOM [192] results.

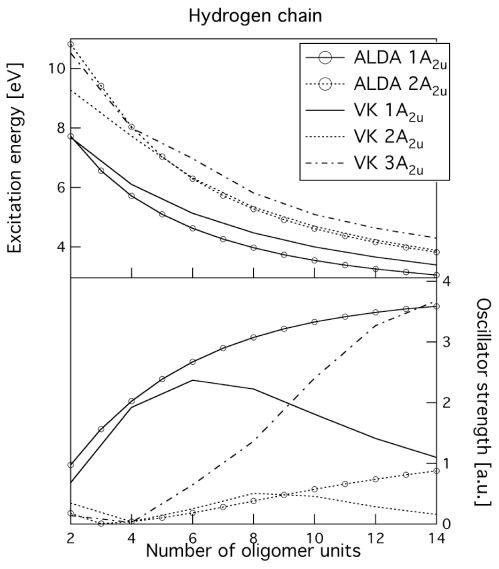

Figure 10-6. ALDA and VK NCT $r_s > 1.3$ excitation energies and oscillator strengths of the model hydrogen chain.

10.5 Conclusions

In this chapter we have rewritten the VK-functional in spherical coordinates in order to study the VK-functional in more detail for transitions in atoms. The excitation energies for the $s \rightarrow p$ transitions in atoms are strongly overestimated by the VK-functional. The excitation energies for $s \rightarrow s$ transitions are close to the ALDA and experimental values. By plotting the radial integrand of the stress tensor part of the VK-functional we saw that the largest contribution of this part to the $s \rightarrow p$ excitation energies is in the high-density (low r_s) region. This is also one of the conclusions that Ullrich and Burke made on the basis of their analysis [27].

We found that changing the xc-kernel f_{xcT} somewhat in this region by setting this kernel and its derivatives to zero, can lead to large effects for the polarizability and excitation energies. The excitation energies of the $s \rightarrow p$ transitions, for which we found that the full VK-functional strongly overestimates, are greatly reduced when changing f_{xcT} whereas the $s \rightarrow s$ transitions remain close to the ALDA and experimental results. Similarly we find that the excitation

energies of $n\rightarrow\pi^*$ transitions in some selected molecules are strongly reduced, while the effect of changing f_{xcT} on the $\pi\rightarrow\pi^*$ transitions is much smaller. These findings show that there may be a link between the problems of VK in atoms and molecules.

We also looked at the effect of modifying the VK-functional on the response properties of oligomers of polyacetylene and the model hydrogen chain. We saw that the polarizability of polyacetylene comes closer to the ALDA with our modified f_{xcT} but the effect of VK is still large, indicating we retain some long-range properties when using the modified f_{xcT}. We also see that the polarizability of the model hydrogen chain is reduced, and is closer to the available literature results. These findings are also reflected in the excitation energies of these systems. The modified f_{xcT} does not have an effect on the states with small oscillator strengths, therefore oscillator strength is still transferred to higher excitations like we found when using the full f_{xcT}.

In summary we found that the VK-functional with the currently available transverse xc-kernels works well for the polarizability of conjugated molecular chains and $\pi\rightarrow\pi^*$ transitions in smaller systems. The excitation energies of $\pi\rightarrow\pi^*$ transitions in conjugated molecular chains are also improved, apart from the fact that some higher lying states do not shift leading to a transfer of oscillator strength to higher transitions. We also saw failures, especially the large overestimation of the excitation energy of $n\rightarrow\pi^*$ transitions in molecules and $s\rightarrow p$ transitions in atoms. Another failure is that the polarizability and excitation energies of the model hydrogen chain are barely altered when using the VK-functional.

In some of the previous chapters we saw that changing f_{xcT} in the low-density region by using QV instead of NCT does not solve any of the problems described above. In this chapter we found that changing the f_{xcT} in the high-density region (where it is not well known), on the other hand, can have a large effect on the failures described above, while having a smaller effect on the $\pi\rightarrow\pi^*$ transitions. This indicates that these problems are not necessarily due to the VK-functional itself, but are for a great part due to the approximations for f_{xcT}. These observations also lead to the question whether there exists a "universal f_{xcT}" that works well for all molecular systems. Since the VK-functional is derived for the electron gas, this is not necessarily the case. In any case there is room for tweaking the f_{xcT} such that the results are improved. Assuming that the VK-functional can be universally applied to a wide range of systems (ranging from the electron gas to atoms and molecules), it would be important to know the f_{xcL} and f_{xcT} more accurately.

At the end of this thesis we must admit that we did not identify all the "magic herbs" that make the VK-functional work so well for some systems. We did learn more about the conditions

under which the functional works or fails and especially found that there is room for improvement in the exchange-correlation kernel.

Appendix A
Functional derivatives

In this appendix we give the definition of a functional derivative. More information on functional calculus and functional derivatives can be found in many mathematical textbooks. Some examples of the use of the functionals within DFT can for example be found in Refs. [29] and [28].

First we state what a functional is. A *function* is a prescription to add to each variable x a number $f(x)$; a *functional* is a prescription to add to each a function $f(x)$ a number $F[f]$. The functional derivative is a derivative of a functional: i.e., it carries information on how a functional changes, when the function changes by a small amount.

The *functional derivative* $\delta F/\delta f$ is defined by,

$$\lim_{\varepsilon\to 0}\frac{F[f+\varepsilon h]-F[f]}{\varepsilon}=\int\frac{\delta F}{\delta f(x)}h(x)\,dx\,, \tag{A.1}$$

where $h(x)$ is an arbitrary function. The functional derivative has properties similar to the ordinary derivative,

$$\frac{\delta}{\delta f(x)}\left(C_1F_1+C_2F_2\right)=C_1\frac{\delta F_1}{\delta f(x)}+C_2\frac{\delta F_2}{\delta f(x)} \tag{A.2}$$

$$\frac{\delta}{\delta f(x)}\left(F_1F_2\right)=\frac{\delta F_1}{\delta f(x)}F_2+F_1\frac{\delta F_2}{\delta f(x)}\,. \tag{A.3}$$

There exists a useful relation for functionals of the form,

$$F[\rho]=\int f\left(x,\rho,\rho^{(1)},\rho^{(2)},\ldots,\rho^{(n)}\right)dx \tag{A.4}$$

where $\rho^{(n)}(x)=d^n\rho(x)/dx^n$ and ρ vanishes at the boundary of the integration domain. For this case [28],

$$\frac{\delta F}{\delta\rho(x)}=\frac{\partial f}{\partial\rho}-\frac{d}{dx}\left(\frac{\partial f}{\partial\rho^{(1)}}\right)+\frac{d^2}{dx^2}\left(\frac{\partial f}{\partial\rho^{(2)}}\right)-\cdots+(-1)^n\frac{d^n}{dx^n}\left(\frac{\partial f}{\partial\rho^{(n)}}\right) \tag{A.5}$$

where the $\partial f/\partial\rho^{(n)}$ are partial derivatives ($\partial f/\partial\rho^{(p)}$ is taken holding $\rho^{(m)}$ constant where $m \neq p$). An important consequence of this equation is that for *local functionals*, $f = f(x,\rho)$, it reduces to $\delta F/\delta\rho(x) = \partial f/\partial\rho$.

Appendix B
Proofs

B.1 Hohenberg-Kohn

To prove the first Hohenberg-Kohn theorem [1] we need to show that there is a one-to-one mapping between the external potential $v(\mathbf{r})$ and the density $\rho(\mathbf{r})$. The map $\hat{V} \to \Psi \to \rho$ is easy to prove. An external potential $v(\mathbf{r})$ leads to a ground state wave function Ψ by solving the Schrödinger equation (Eq. (1.1)), and for each ground state wave function we can calculate the density through Eq. (1.9). To prove the Hohenberg-Kohn theorem we need to show that this map is invertible ($\hat{V} \leftarrow \Psi \leftarrow \rho$). This proof goes in two steps. The first step of the proof is to show that if two external potentials $\hat{V}_1$ and $\hat{V}_2$ differ by more than a constant they will not lead to the same wave function Ψ. For a nondegenerate ground state

$$\left(\hat{T} + \hat{V}_1 + \hat{W}\right)\left|\Psi_1\right\rangle = E_0^{(1)}\left|\Psi_1\right\rangle, \tag{B.1}$$

$$\left(\hat{T} + \hat{V}_2 + \hat{W}\right)\left|\Psi_2\right\rangle = E_0^{(2)}\left|\Psi_2\right\rangle. \tag{B.2}$$

If we assume that $\Psi_1 = \Psi_2 = \Psi$ and we subtract the two above equations, we obtain

$$\left(\hat{V}_1 - \hat{V}_2\right)\left|\Psi\right\rangle = \left(E_0^{(1)} - E_0^{(2)}\right)\left|\Psi\right\rangle \tag{B.3}$$

which leads to $\hat{V}_1 = \hat{V}_2 + C$ and contradicts our assumption. In the second part of the proof we need to show that these different wave functions cannot lead to same density $\rho(\mathbf{r})$. Assume that the two different wave functions Ψ_1 and Ψ_2 *do* lead to the same density. The variational procedure then tells us that,

$$\begin{aligned} E_0^{(1)} < \left\langle \Psi_2 \middle| \hat{H}_1 \middle| \Psi_2 \right\rangle &= \left\langle \Psi_2 \middle| \hat{H}_2 \middle| \Psi_2 \right\rangle + \left\langle \Psi_2 \middle| \hat{H}_1 - \hat{H}_2 \middle| \Psi_2 \right\rangle \\ &= E_0^{(2)} + \int \rho(\mathbf{r})\left[v_1(\mathbf{r}) - v_2(\mathbf{r})\right] d\mathbf{r} \end{aligned} \tag{B.4}$$

and similarly

$$E_0^{(2)} < \left\langle \Psi_1 \middle| \hat{H}_2 \middle| \Psi_1 \right\rangle = E_0^{(1)} - \int \rho(\mathbf{r})\left[v_1(\mathbf{r}) - v_2(\mathbf{r})\right] d\mathbf{r}. \tag{B.5}$$

Adding the two inequalities gives: $E_0^{(1)} + E_0^{(2)} < E_0^{(2)} + E_0^{(1)}$, which is a contradiction proving the one-to-one mapping $\hat{V} \leftrightarrow \Psi \leftrightarrow \rho$.

B.2 Runge-Gross

We consider densities $\rho(\mathbf{r},t)$ that evolve from a fixed initial state $|\Psi_0\rangle$. The initial time t_0 is assumed to be finite and the potentials $v(\mathbf{r},t)$ are assumed to have a Taylor expansion around t_0. This condition of Taylor expandability excludes potentials that are switched-on adiabatically from $t_0 = -\infty$. The Hamiltonian of Eq. (2.1) is of the form,

$$\hat{H}(t) = \hat{T} + \hat{V}(t) + \hat{W}\,, \tag{B.6}$$

where $\hat{T}$ and $\hat{W}$ are defined in Eqs. (1.3) and (1.5). The time-dependent external potential is of the form,

$$\hat{V}(t) = \sum_{i=1}^{N} v(\mathbf{r}_i, t)\,. \tag{B.7}$$

We now want to proof the theorem that two densities $\rho(\mathbf{r},t)$ and $\rho'(\mathbf{r},t)$ evolving from a common initial state $|\Psi_0\rangle$ under influence of two potentials $v(\mathbf{r},t)$ and $v'(\mathbf{r},t)$ always differ provided that the potentials differ by more than a purely time-dependent function,

$$v(\mathbf{r},t) \neq v'(\mathbf{r},t) + c(t)\,. \tag{B.8}$$

As mentioned above we assume the Taylor expandability of $v(\mathbf{r},t)$ leading to,

$$v(\mathbf{r},t) = \sum_{k=0}^{\infty} \frac{1}{k!} v_k(\mathbf{r}) (t - t_0)^k \tag{B.9}$$

and a similar expression for $v'(\mathbf{r},t)$. We can now restate the condition of Eq. (B.8) in the following way: There is a $k \geq 0$ such that,

$$v_k(\mathbf{r}) - v'_k(\mathbf{r}) = \frac{\partial^k}{\partial t^k} \big(v(\mathbf{r},t) - v'(\mathbf{r},t) \big) \Big|_{t=t_0} \neq \text{const.} \tag{B.10}$$

As a first step we can prove from this inequality that the current densities,

$$\mathbf{j}(\mathbf{r},t) = \langle \Psi(t) | \hat{\mathbf{j}}_p(\mathbf{r}) | \Psi(t) \rangle \tag{B.11}$$

$$\mathbf{j}'(\mathbf{r},t) = \langle \Psi'(t) | \hat{\mathbf{j}}_p(\mathbf{r}) | \Psi'(t) \rangle\,, \tag{B.12}$$

differ for different potentials $v(\mathbf{r},t)$ and $v'(\mathbf{r},t)$. The (paramagnetic) current density operator is given by,

$$\hat{\mathbf{j}}_p(\mathbf{r}) = \frac{1}{2i}\sum_{i=1}^{N}\left(\nabla_{\mathbf{r}_i}\delta(\mathbf{r}-\mathbf{r}_i) + \delta(\mathbf{r}-\mathbf{r}_i)\nabla_{\mathbf{r}_i}\right). \tag{B.13}$$

The quantum mechanical equation of motion for the expectation value of an operator $\hat{A}(t)$ is given by,

$$\frac{\partial}{\partial t}\langle\Psi(t)|\hat{A}(t)|\Psi(t)\rangle = \langle\Psi(t)|\frac{\partial\hat{A}}{\partial t} - i\left[\hat{A}(t),\hat{H}(t)\right]|\Psi(t)\rangle. \tag{B.14}$$

For the current densities we then obtain,

$$\frac{\partial}{\partial t}\mathbf{j}(\mathbf{r},t) = \frac{\partial}{\partial t}\langle\Psi(t)|\hat{\mathbf{j}}_p(\mathbf{r})|\Psi(t)\rangle = -i\langle\Psi(t)|\left[\hat{\mathbf{j}}_p(\mathbf{r}),\hat{H}(t)\right]|\Psi(t)\rangle \tag{B.15}$$

$$\frac{\partial}{\partial t}\mathbf{j}'(\mathbf{r},t) = \frac{\partial}{\partial t}\langle\Psi'(t)|\hat{\mathbf{j}}_p(\mathbf{r})|\Psi'(t)\rangle = -i\langle\Psi'(t)|\left[\hat{\mathbf{j}}_p(\mathbf{r}),\hat{H}'(t)\right]|\Psi'(t)\rangle. \tag{B.16}$$

Because the wave functions evolve from the same initial state $\Psi(t_0) = \Psi'(t_0) = \Psi_0$ we have

$$\begin{aligned}\frac{\partial}{\partial t}\left(\mathbf{j}(\mathbf{r},t) - \mathbf{j}'(\mathbf{r},t)\right)\Big|_{t=t_0} &= -i\langle\Psi_0|\left[\hat{\mathbf{j}}_p(\mathbf{r}),\hat{H}(t_0) - \hat{H}'(t_0)\right]|\Psi_0\rangle \\ &= -\rho_0(\mathbf{r})\nabla\left(v(\mathbf{r},t_0) - v'(\mathbf{r},t_0)\right)\end{aligned}, \tag{B.17}$$

with initial density $\rho_0(\mathbf{r}) = \rho(\mathbf{r},t_0)$. If the condition of Eq. (B.10) is satisfied for $k=0$ then the currents will become different infinitesimally later than t_0. If Eq. (B.10) holds for some smallest finite $k>0$ we can use the equation of motion $k+1$ times to obtain [41],

$$\frac{\partial^{k+1}}{\partial t^{k+1}}\left(\mathbf{j}(\mathbf{r},t) - \mathbf{j}'(\mathbf{r},t)\right)\Big|_{t=t_0} = -\rho_0(\mathbf{r})\nabla w_k(\mathbf{r}) \neq 0 \tag{B.18}$$

with

$$w_k(\mathbf{r}) = \frac{\partial^k}{\partial t^k}\left(v(\mathbf{r},t) - v'(\mathbf{r},t)\right)\Big|_{t=t_0}. \tag{B.19}$$

From this we can conclude that $\mathbf{j}(\mathbf{r},t) \neq \mathbf{j}'(\mathbf{r},t)$. We also want to prove that the densities are different for different potentials. For this we can use the continuity equation,

$$\frac{\partial}{\partial t}\left(\rho(\mathbf{r},t)-\rho'(\mathbf{r},t)\right)=-\nabla\cdot\left(\mathbf{j}(\mathbf{r},t)-\mathbf{j}'(\mathbf{r},t)\right). \tag{B.20}$$

If we calculate the $(k+1)^{\text{th}}$ time derivative of this equation at $t=t_0$ and insert the result of Eq. (B.18) we obtain,

$$\left.\frac{\partial^{k+2}}{\partial t^{k+2}}\left(\rho(\mathbf{r},t)-\rho'(\mathbf{r},t)\right)\right|_{t=t_0}=\nabla\cdot\left(\rho_0(\mathbf{r})\nabla w_k(\mathbf{r})\right). \tag{B.21}$$

To prove that $\rho(\mathbf{r},t)$ and $\rho'(\mathbf{r},t)$ become different infinitesimally later than t_0 we need to show that the right hand side of Eq. (B.21) cannot vanish identically. This proof is done by *reductio ad absurdum*: Assume that $\nabla\cdot\left(\rho_0(\mathbf{r})\nabla w_k(\mathbf{r})\right)\equiv 0$ and evaluate the integral

$$\begin{aligned}\int\rho_0(\mathbf{r})\left|\nabla w_k(\mathbf{r})\right|^2 d\mathbf{r}=&-\int w_k(\mathbf{r})\nabla\cdot\left(\rho_0(\mathbf{r})\nabla w_k(\mathbf{r})\right)d\mathbf{r}\\&+\oint\left(\rho_0(\mathbf{r})w_k(\mathbf{r})\nabla w_k(\mathbf{r})\right)\cdot d\mathbf{S}\end{aligned}, \tag{B.22}$$

where Gauss theorem is used. The surface integral vanishes for physically realistic potentials because for such potentials the $w_k(\mathbf{r})$ fall off at least as $1/r$ and the density decays exponentially. Together with our assumption that the first integral on the right hand side is zero this means that the integral on the left hand side must vanish, so

$$\rho_0(\mathbf{r})\left|\nabla w_k(\mathbf{r})\right|^2\equiv 0\,, \tag{B.23}$$

and $\rho_0(\mathbf{r})>0$ everywhere, which means that $\left|\nabla w_k(\mathbf{r})\right|^2=0$ in contradiction with $w_k(\mathbf{r})\neq$ const. This completes the proof.

Appendix C
The P-matrix

In this appendix we give a little more detail on how we arrive at the form of the P-matrix. The equations we start from are equations (3.20) and (3.24),

$$\begin{aligned}\delta\rho(\mathbf{r},\omega) = \sum_{\sigma}\Big\{&\int \chi^{\sigma}_{\rho\mathbf{j}}(\mathbf{r},\mathbf{r}',\omega)\cdot\delta\mathbf{A}_{s,\sigma}(\mathbf{r}',\omega)\,d\mathbf{r}' \\ &+\int \chi^{\sigma}_{\rho\rho}(\mathbf{r},\mathbf{r}',\omega)\,\delta v_{s,\sigma}(\mathbf{r}',\omega)\,d\mathbf{r}'\Big\}\end{aligned} \tag{C.1}$$

$$\begin{aligned}\delta\mathbf{j}(\mathbf{r},\omega) = \sum_{\sigma}\Big\{&\int \Big(\chi^{\sigma}_{\mathbf{jj}}(\mathbf{r},\mathbf{r}',\omega)-\chi^{\sigma}_{\mathbf{jj}}(\mathbf{r},\mathbf{r}',0)\Big)\cdot\delta\mathbf{A}_{s,\sigma}(\mathbf{r}',\omega)\,d\mathbf{r}' \\ &+\int \chi^{\sigma}_{\mathbf{j}\rho}(\mathbf{r},\mathbf{r}',\omega)\,\delta v_{s,\sigma}(\mathbf{r}',\omega)\,d\mathbf{r}'\Big\}\end{aligned} \tag{C.2}$$

The difference between the response functions in the first term of Eq. (C.2) we can rewrite, using the explicit form of the response functions Eq. (3.27), as,

$$\begin{aligned}&\chi^{\sigma}_{\mathbf{jj}}(\mathbf{r},\mathbf{r}',\omega)-\chi^{\sigma}_{\mathbf{jj}}(\mathbf{r},\mathbf{r}',0) \\ &=\sum_{i,a}\Bigg\{\frac{\phi_{i\sigma}(\mathbf{r})\hat{\mathbf{j}}\phi_{a\sigma}(\mathbf{r})\phi_{a\sigma}(\mathbf{r}')\hat{\mathbf{j}}\phi_{i\sigma}(\mathbf{r}')}{(\varepsilon_{i\sigma}-\varepsilon_{a\sigma})+\omega}-\frac{\phi_{i\sigma}(\mathbf{r})\hat{\mathbf{j}}\phi_{a\sigma}(\mathbf{r})\phi_{a\sigma}(\mathbf{r}')\hat{\mathbf{j}}\phi_{i\sigma}(\mathbf{r}')}{(\varepsilon_{i\sigma}-\varepsilon_{a\sigma})} \\ &+\frac{\phi_{i\sigma}(\mathbf{r})\hat{\mathbf{j}}^{\dagger}\phi_{a\sigma}(\mathbf{r})\phi_{a\sigma}(\mathbf{r}')\hat{\mathbf{j}}^{\dagger}\phi_{i\sigma}(\mathbf{r}')}{(\varepsilon_{i\sigma}-\varepsilon_{a\sigma})-\omega}-\frac{\phi_{i\sigma}(\mathbf{r})\hat{\mathbf{j}}^{\dagger}\phi_{a\sigma}(\mathbf{r})\phi_{a\sigma}(\mathbf{r}')\hat{\mathbf{j}}^{\dagger}\phi_{i\sigma}(\mathbf{r}')}{(\varepsilon_{i\sigma}-\varepsilon_{a\sigma})}\Bigg\} \\ &=\sum_{i,a}\Bigg\{\frac{-\omega}{(\varepsilon_{i\sigma}-\varepsilon_{a\sigma})}\frac{\phi_{i\sigma}(\mathbf{r})\hat{\mathbf{j}}\phi_{a\sigma}(\mathbf{r})\phi_{a\sigma}(\mathbf{r}')\hat{\mathbf{j}}\phi_{i\sigma}(\mathbf{r}')}{(\varepsilon_{i\sigma}-\varepsilon_{a\sigma})+\omega} \\ &+\frac{\omega}{(\varepsilon_{i\sigma}-\varepsilon_{a\sigma})}\frac{\phi_{a\sigma}(\mathbf{r})\hat{\mathbf{j}}\phi_{i\sigma}(\mathbf{r})\phi_{i\sigma}(\mathbf{r}')\hat{\mathbf{j}}\phi_{a\sigma}(\mathbf{r}')}{(\varepsilon_{i\sigma}-\varepsilon_{a\sigma})-\omega}\Bigg\}\end{aligned} \tag{C.3}$$

where we used that $\phi_i\hat{\mathbf{j}}^{\dagger}\phi_a=\phi_a\hat{\mathbf{j}}\phi_i$. Using this result and substituting the other response operators in Eqs. (C.1) and (C.2) we obtain,

$$\begin{aligned}\delta\rho(\mathbf{r},\omega) = \sum_{\sigma}\sum_{ia}\Bigg\{&\phi_{i\sigma}\phi_{a\sigma}\frac{1}{(\varepsilon_{i\sigma}-\varepsilon_{a\sigma})+\omega}\\ &\times\Big[\int\phi_{a\sigma}\hat{\mathbf{j}}\phi_{i\sigma}\delta\mathbf{A}_{\mathrm{s},\sigma}(\omega)\,d\mathbf{r}'+\int\phi_{a\sigma}\delta\upsilon_{\mathrm{s},\sigma}(\omega)\phi_{i\sigma}d\mathbf{r}'\Big]\\ &+\phi_{a\sigma}\phi_{i\sigma}\frac{1}{(\varepsilon_{i\sigma}-\varepsilon_{a\sigma})-\omega}\\ &\times\Big[\int\phi_{i\sigma}\hat{\mathbf{j}}\phi_{a\sigma}\delta\mathbf{A}_{\mathrm{s},\sigma}(\omega)\,d\mathbf{r}'+\int\phi_{i\sigma}\delta\upsilon_{\mathrm{s},\sigma}(\omega)\phi_{a\sigma}d\mathbf{r}'\Big]\Bigg\}\end{aligned} \tag{C.4}$$

and

$$\begin{aligned}\delta\mathbf{j}(\mathbf{r},\omega) = \sum_{\sigma}\sum_{i,a}\Bigg\{&\phi_{i\sigma}\hat{\mathbf{j}}\phi_{a\sigma}\frac{1}{(\varepsilon_{i\sigma}-\varepsilon_{a\sigma})+\omega}\\ &\times\left[\frac{-\omega}{(\varepsilon_{i\sigma}-\varepsilon_{a\sigma})}\int\phi_{a\sigma}\hat{\mathbf{j}}\phi_{i\sigma}\delta\mathbf{A}_{\mathrm{s},\sigma}(\omega)\,d\mathbf{r}'+\int\phi_{a\sigma}\delta\upsilon_{\mathrm{s},\sigma}(\omega)\phi_{i\sigma}d\mathbf{r}'\right]\\ &+\phi_{a\sigma}\hat{\mathbf{j}}\phi_{i\sigma}\frac{1}{(\varepsilon_{i\sigma}-\varepsilon_{a\sigma})-\omega}\\ &\times\left[\frac{\omega}{(\varepsilon_{i}-\varepsilon_{a\sigma})}\int\phi_{i\sigma}\hat{\mathbf{j}}\phi_{a\sigma}\delta\mathbf{A}_{\mathrm{s},\sigma}(\omega)\,d\mathbf{r}'+\int\phi_{i\sigma}\delta\upsilon_{\mathrm{s},\sigma}(\omega)\phi_{a\sigma}d\mathbf{r}'\right]\Bigg\}\end{aligned} \tag{C.5}$$

In our implementation we combine all terms such that,

$$\begin{aligned}\delta\rho(\mathbf{r},\omega) = \sum_{\sigma}\sum_{ia}&\phi_{i\sigma}\phi_{a\sigma}\left(\frac{1}{(\varepsilon_{i\sigma}-\varepsilon_{a\sigma})+\omega}+\frac{1}{(\varepsilon_{i\sigma}-\varepsilon_{a\sigma})-\omega}\right)\\ &\left[\frac{-\omega}{(\varepsilon_{i\sigma}-\varepsilon_{a\sigma})}\int\phi_{a\sigma}\hat{\mathbf{j}}\phi_{i\sigma}\delta\mathbf{A}_{s,\sigma}(\omega)\,d\mathbf{r}'+\int\phi_{a\sigma}\delta\upsilon_{s,\sigma}(\omega)\phi_{i\sigma}d\mathbf{r}'\right]\end{aligned} \tag{C.6}$$

$$\begin{aligned}\delta\mathbf{j}(\mathbf{r},\omega) &= \sum_{\sigma}\sum_{i,a}\phi_{i\sigma}\hat{\mathbf{j}}\phi_{a\sigma}\left(\frac{1}{(\varepsilon_{i\sigma}-\varepsilon_{a\sigma})+\omega}-\frac{1}{(\varepsilon_{i\sigma}-\varepsilon_{a\sigma})-\omega}\right)\\ &\times\left[\frac{-\omega}{(\varepsilon_{i\sigma}-\varepsilon_{a\sigma})}\int\phi_{a\sigma}\hat{\mathbf{j}}\phi_{i\sigma}\delta\mathbf{A}_{s,\sigma}(\omega)\,d\mathbf{r}'+\int\phi_{a\sigma}\delta\upsilon_{s,\sigma}(\omega)\phi_{i\sigma}d\mathbf{r}'\right]\\ &= \sum_{\sigma}\sum_{i,a}\frac{-\omega}{(\varepsilon_{i\sigma}-\varepsilon_{a\sigma})}\phi_{i\sigma}\hat{\mathbf{j}}\phi_{a\sigma}\left(\frac{1}{(\varepsilon_{i\sigma}-\varepsilon_{a\sigma})+\omega}+\frac{1}{(\varepsilon_{i\sigma}-\varepsilon_{a\sigma})-\omega}\right)\\ &\times\left[\frac{-\omega}{(\varepsilon_{i\sigma}-\varepsilon_{a\sigma})}\int\phi_{a\sigma}\hat{\mathbf{j}}\phi_{i\sigma}\delta\mathbf{A}_{s,\sigma}(\omega)\,d\mathbf{r}'+\int\phi_{a\sigma}\delta\upsilon_{s,\sigma}(\omega)\phi_{i\sigma}d\mathbf{r}'\right]\end{aligned} \tag{C.7}$$

From these equations our choice to introduce the extra factors $-\omega/(\varepsilon_{i\sigma} - \varepsilon_{a\sigma})$ in our definitions for $\delta\mathbf{j}$ and the P-matrix becomes clear. It can be easily verified that Eq. (C.6) is identical to Eqs. (C.4) and (3.48), and that Eq. (C.7) is identical to Eqs. (C.5) and (3.49).

Appendix D
Singlet/Triplet equations

We start from Eq. (3.62),

$$\begin{pmatrix} \mathbf{A} & \mathbf{B} \\ \mathbf{B} & \mathbf{A} \end{pmatrix} \begin{pmatrix} \mathbf{X} \\ \mathbf{Y} \end{pmatrix} = \omega \begin{pmatrix} -\mathbf{1} & 0 \\ 0 & \mathbf{1} \end{pmatrix} \begin{pmatrix} \mathbf{X} \\ \mathbf{Y} \end{pmatrix}. \tag{D.1}$$

If we assume a closed-shell system for which $\phi_{i\uparrow} = \phi_{i\downarrow}$ for all i, we can split this matrix equation in a singlet and triplet part by the unitary transformation,

$$\begin{pmatrix} \mathbf{X}^S \\ \mathbf{X}^T \end{pmatrix} = \frac{1}{\sqrt{2}} \begin{pmatrix} 1 & 1 \\ 1 & -1 \end{pmatrix} \begin{pmatrix} \mathbf{X}^\uparrow \\ \mathbf{X}^\downarrow \end{pmatrix} \tag{D.2}$$

$$\begin{pmatrix} \mathbf{Y}^S \\ \mathbf{Y}^T \end{pmatrix} = \frac{1}{\sqrt{2}} \begin{pmatrix} 1 & 1 \\ 1 & -1 \end{pmatrix} \begin{pmatrix} \mathbf{Y}^\uparrow \\ \mathbf{Y}^\downarrow \end{pmatrix}. \tag{D.3}$$

We can also write,

$$\begin{pmatrix} \mathbf{X}^\uparrow \\ \mathbf{X}^\downarrow \end{pmatrix} = \frac{1}{\sqrt{2}} \begin{pmatrix} 1 & 1 \\ 1 & -1 \end{pmatrix} \begin{pmatrix} \mathbf{X}^S \\ \mathbf{X}^T \end{pmatrix} \tag{D.4}$$

$$\begin{pmatrix} \mathbf{Y}^\uparrow \\ \mathbf{Y}^\downarrow \end{pmatrix} = \frac{1}{\sqrt{2}} \begin{pmatrix} 1 & 1 \\ 1 & -1 \end{pmatrix} \begin{pmatrix} \mathbf{Y}^S \\ \mathbf{Y}^T \end{pmatrix}. \tag{D.5}$$

Since we assume all orbitals are real and that the calculation is spin restricted, we can rewrite Eq. (D.1) explicitly as,

$$\begin{pmatrix} \mathbf{A}^{\uparrow\uparrow} & \mathbf{A}^{\uparrow\downarrow} & \mathbf{B}^{\uparrow\uparrow} & \mathbf{B}^{\uparrow\downarrow} \\ \mathbf{A}^{\downarrow\uparrow} & \mathbf{A}^{\downarrow\downarrow} & \mathbf{B}^{\downarrow\uparrow} & \mathbf{B}^{\downarrow\downarrow} \\ \mathbf{B}^{\uparrow\uparrow} & \mathbf{B}^{\uparrow\downarrow} & \mathbf{A}^{\uparrow\uparrow} & \mathbf{A}^{\uparrow\downarrow} \\ \mathbf{B}^{\downarrow\uparrow} & \mathbf{B}^{\downarrow\downarrow} & \mathbf{A}^{\downarrow\uparrow} & \mathbf{A}^{\downarrow\downarrow} \end{pmatrix} \begin{pmatrix} \mathbf{X}^\uparrow \\ \mathbf{X}^\downarrow \\ \mathbf{Y}^\uparrow \\ \mathbf{Y}^\downarrow \end{pmatrix} = \omega \begin{pmatrix} -1 & 0 & 0 & 0 \\ 0 & -1 & 0 & 0 \\ 0 & 0 & 1 & 0 \\ 0 & 0 & 0 & 1 \end{pmatrix} \begin{pmatrix} \mathbf{X}^\uparrow \\ \mathbf{X}^\downarrow \\ \mathbf{Y}^\uparrow \\ \mathbf{Y}^\downarrow \end{pmatrix} \tag{D.6}$$

Transforming this equation gives,

$$\begin{aligned}
&\frac{1}{2}\begin{bmatrix}1 & 1 & 0 & 0\\ 1 & -1 & 0 & 0\\ 0 & 0 & 1 & 1\\ 0 & 0 & 1 & -1\end{bmatrix}\begin{bmatrix}\mathbf{A}^{\uparrow\uparrow} & \mathbf{A}^{\uparrow\downarrow} & \mathbf{B}^{\uparrow\uparrow} & \mathbf{B}^{\uparrow\downarrow}\\ \mathbf{A}^{\downarrow\uparrow} & \mathbf{A}^{\downarrow\downarrow} & \mathbf{B}^{\downarrow\uparrow} & \mathbf{B}^{\downarrow\downarrow}\\ \mathbf{B}^{\uparrow\uparrow} & \mathbf{B}^{\uparrow\downarrow} & \mathbf{A}^{\uparrow\uparrow} & \mathbf{A}^{\uparrow\downarrow}\\ \mathbf{B}^{\downarrow\uparrow} & \mathbf{B}^{\downarrow\downarrow} & \mathbf{A}^{\downarrow\uparrow} & \mathbf{A}^{\downarrow\downarrow}\end{bmatrix}\begin{bmatrix}1 & 1 & 0 & 0\\ 1 & -1 & 0 & 0\\ 0 & 0 & 1 & 1\\ 0 & 0 & 1 & -1\end{bmatrix}\begin{pmatrix}\mathbf{X}^S\\ \mathbf{X}^T\\ \mathbf{Y}^S\\ \mathbf{Y}^T\end{pmatrix}\\
&=\frac{1}{2}\omega\begin{bmatrix}1 & 1 & 0 & 0\\ 1 & -1 & 0 & 0\\ 0 & 0 & 1 & 1\\ 0 & 0 & 1 & -1\end{bmatrix}\begin{bmatrix}-1 & 0 & 0 & 0\\ 0 & -1 & 0 & 0\\ 0 & 0 & 1 & 0\\ 0 & 0 & 0 & 1\end{bmatrix}\begin{bmatrix}1 & 1 & 0 & 0\\ 1 & -1 & 0 & 0\\ 0 & 0 & 1 & 1\\ 0 & 0 & 1 & -1\end{bmatrix}\begin{pmatrix}\mathbf{X}^S\\ \mathbf{X}^T\\ \mathbf{Y}^S\\ \mathbf{Y}^T\end{pmatrix}
\end{aligned}. \tag{D.7}$$

This equation is blocked out and can be spit in an **A** and a **B** part. For the **A** part we obtain,

$$\begin{aligned}
&\begin{bmatrix}1 & 1\\ 1 & -1\end{bmatrix}\begin{bmatrix}\mathbf{A}^{\uparrow\uparrow} & \mathbf{A}^{\uparrow\downarrow}\\ \mathbf{A}^{\downarrow\uparrow} & \mathbf{A}^{\downarrow\downarrow}\end{bmatrix}\begin{bmatrix}1 & 1\\ 1 & -1\end{bmatrix}\begin{pmatrix}\mathbf{X}^S\\ \mathbf{X}^T\end{pmatrix}\\
&=\begin{bmatrix}2\left(\delta_{ab}\delta_{ij}\left(\varepsilon_a-\varepsilon_i\right)+K^{\uparrow\uparrow}_{ia,jb}+K^{\downarrow\uparrow}_{ia,jb}\right) & 0\\ 0 & 2\left(\delta_{ab}\delta_{ij}\left(\varepsilon_a-\varepsilon_i\right)+K^{\uparrow\uparrow}_{ia,jb}-K^{\downarrow\uparrow}_{ia,jb}\right)\end{bmatrix}\begin{pmatrix}\mathbf{X}^S\\ \mathbf{X}^T\end{pmatrix}
\end{aligned} \tag{D.8}$$

and for the **B** part,

$$\begin{aligned}
&\begin{bmatrix}1 & 1\\ 1 & -1\end{bmatrix}\begin{bmatrix}\mathbf{B}^{\uparrow\uparrow} & \mathbf{B}^{\uparrow\downarrow}\\ \mathbf{B}^{\downarrow\uparrow} & \mathbf{B}^{\downarrow\downarrow}\end{bmatrix}\begin{bmatrix}1 & 1\\ 1 & -1\end{bmatrix}\begin{pmatrix}\mathbf{Y}^S\\ \mathbf{Y}^T\end{pmatrix}=\\
&=\begin{bmatrix}2\left(K^{\uparrow\uparrow}_{ia,bj}+K^{\uparrow\downarrow}_{ia,bj}\right) & 0\\ 0 & 2\left(K^{\uparrow\uparrow}_{ia,bj}-K^{\uparrow\downarrow}_{ia,bj}\right)\end{bmatrix}\begin{pmatrix}\mathbf{Y}^S\\ \mathbf{Y}^T\end{pmatrix}
\end{aligned}. \tag{D.9}$$

We used that $K^{\uparrow\uparrow}=K^{\downarrow\downarrow}$ and $K^{\uparrow\downarrow}=K^{\downarrow\uparrow}$. If we insert these results in Eq. (D.7) we obtain a matrix equation that can be split in a singlet and triplet part,

$$\begin{aligned}
&\begin{bmatrix}\delta_{ab}\delta_{ij}\left(\varepsilon_a-\varepsilon_i\right)+K^{\uparrow\uparrow}_{ia,jb}+K^{\downarrow\uparrow}_{ia,jb} & K^{\uparrow\uparrow}_{ia,bj}+K^{\downarrow\uparrow}_{ia,bj}\\ K^{\uparrow\uparrow}_{ia,bj}+K^{\downarrow\uparrow}_{ia,bj} & \delta_{ab}\delta_{ij}\left(\varepsilon_a-\varepsilon_i\right)+K^{\uparrow\uparrow}_{ia,jb}+K^{\downarrow\uparrow}_{ia,jb}\end{bmatrix}\begin{pmatrix}\mathbf{X}^S\\ \mathbf{Y}^S\end{pmatrix}\\
&=\omega\begin{bmatrix}-1 & 0\\ 0 & 1\end{bmatrix}\begin{pmatrix}\mathbf{X}^S\\ \mathbf{Y}^S\end{pmatrix}
\end{aligned} \tag{D.10}$$

$$\begin{bmatrix} \delta_{ab}\delta_{ij}\left(\varepsilon_a-\varepsilon_i\right)+K^{\uparrow\uparrow}_{ia,jb}-K^{\downarrow\uparrow}_{ia,jb} & K^{\uparrow\uparrow}_{ia,bj}-K^{\downarrow\uparrow}_{ia,bj} \\ K^{\uparrow\uparrow}_{ia,bj}-K^{\downarrow\uparrow}_{ia,bj} & \delta_{ab}\delta_{ij}\left(\varepsilon_a-\varepsilon_i\right)+K^{\uparrow\uparrow}_{ia,jb}-K^{\downarrow\uparrow}_{ia,jb} \end{bmatrix}\begin{pmatrix}\mathbf{X}^T\\ \mathbf{Y}^T\end{pmatrix} = \omega\begin{bmatrix}-1 & 0\\ 0 & 1\end{bmatrix}\begin{pmatrix}\mathbf{X}^T\\ \mathbf{Y}^T\end{pmatrix} \tag{D.11}$$

We rewrite this in a more compact notation as,

$$\begin{bmatrix}\mathbf{C}^S & \mathbf{D}^S\\ \mathbf{D}^S & \mathbf{C}^S\end{bmatrix}\begin{pmatrix}\mathbf{X}^S\\ \mathbf{Y}^S\end{pmatrix} = \omega\begin{bmatrix}-1 & 0\\ 0 & 1\end{bmatrix}\begin{pmatrix}\mathbf{X}^S\\ \mathbf{Y}^S\end{pmatrix} \tag{D.12}$$

$$\begin{bmatrix}\mathbf{C}^T & \mathbf{D}^T\\ \mathbf{D}^T & \mathbf{C}^T\end{bmatrix}\begin{pmatrix}\mathbf{X}^T\\ \mathbf{Y}^T\end{pmatrix} = \omega\begin{bmatrix}-1 & 0\\ 0 & 1\end{bmatrix}\begin{pmatrix}\mathbf{X}^T\\ \mathbf{Y}^T\end{pmatrix}. \tag{D.13}$$

Since these equations are of the same form, we concentrate on the singlet equation. The set of equations we need to solve is,

$$\begin{aligned}\mathbf{C}^S\mathbf{X}^S+\mathbf{D}^S\mathbf{Y}^S &= -\omega\mathbf{X}^S\\ \mathbf{D}^S\mathbf{X}^S+\mathbf{C}^S\mathbf{Y}^S &= \omega\mathbf{Y}^S\end{aligned}. \tag{D.14}$$

If we add and subtract the above equations we obtain

$$\begin{aligned}\left(\mathbf{C}^S+\mathbf{D}^S\right)\left(\mathbf{X}^S+\mathbf{Y}^S\right) &= -\omega\left(\mathbf{X}^S-\mathbf{Y}^S\right)\\ \left(\mathbf{C}^S-\mathbf{D}^S\right)\left(\mathbf{X}^S-\mathbf{Y}^S\right) &= -\omega\left(\mathbf{X}^S+\mathbf{Y}^S\right)\end{aligned}. \tag{D.15}$$

We can now combine this set op equations into one new equation,

$$\left(\mathbf{C}^S+\mathbf{D}^S\right)\left(\mathbf{X}^S+\mathbf{Y}^S\right) = \omega^2\left(\mathbf{C}^S-\mathbf{D}^S\right)^{-1}\left(\mathbf{X}^S+\mathbf{Y}^S\right) \tag{D.16}$$

Since $\left(C^{S/T}_{ia,jb}-D^{S/T}_{ia,jb}\right)=\delta_{ab}\delta_{ij}\left(\varepsilon_a-\varepsilon_i\right)$ is diagonal we can rewrite this as,

$$\left(\mathbf{C}^S-\mathbf{D}^S\right)^{1/2}\left(\mathbf{C}^S+\mathbf{D}^S\right)\left(\mathbf{C}^S-\mathbf{D}^S\right)^{1/2}\left(\mathbf{X}^S+\mathbf{Y}^S\right)' = \omega^2\left(\mathbf{X}^S+\mathbf{Y}^S\right)' \tag{D.17}$$

where $\left(\mathbf{X}^S+\mathbf{Y}^S\right)' = \left(\mathbf{C}^S-\mathbf{D}^S\right)^{-1/2}\left(\mathbf{X}^S+\mathbf{Y}^S\right)$. This is a Hermitian eigenvalue equation of the form

$$\boldsymbol{\Omega}\mathbf{F}_n = \omega_n{}^2\mathbf{F}_n \tag{D.18}$$

Appendix E

Structure of the response function

We want to prove that if $S^2|\Psi_0\rangle = S_z|\Psi_0\rangle = 0$ then $\chi^{\uparrow\uparrow} = \chi^{\downarrow\downarrow}$ and $\chi^{\uparrow\downarrow} = \chi^{\downarrow\uparrow}$. We only show that this is true for the case of the density-density response functions. A similar proof exists for the other response functions. The density-density response function is given by

$$\chi_{\rho\rho}^{\sigma\sigma'}(\mathbf{r},t,\mathbf{r}',t') = -i\Theta(t-t')\langle\Psi_0|\left[\hat{\rho}_\sigma(\mathbf{r},t),\hat{\rho}_{\sigma'}(\mathbf{r}',t')\right]|\Psi_0\rangle \tag{E.1}$$

Consider the following spin operators,

$$\hat{s}_z(\mathbf{r}) = \sum_{i=1}^{N}\delta(\mathbf{r}-\mathbf{r}_i)s_{z,i} \tag{E.2}$$

$$\hat{s}_+(\mathbf{r}) = \sum_{i=1}^{N}\delta(\mathbf{r}-\mathbf{r}_i)s_{+,i} \tag{E.3}$$

$$\hat{s}_-(\mathbf{r}) = \sum_{i=1}^{N}\delta(\mathbf{r}-\mathbf{r}_i)s_{-,i} \tag{E.4}$$

where $s_{z,i}$ is the operator for the z-component of electron i and the operators $s_{\pm,i} = s_{x,i} \pm s_{y,i}$ are the spin raising and lowering operators of electron i. The spin density and total density operators are given by

$$\hat{\rho}_\sigma(\mathbf{r}) = \sum_{i=1}^{N}\delta(\mathbf{r}-\mathbf{r}_i)\delta_{\sigma\sigma_i} \tag{E.5}$$

$$\hat{\rho}(\mathbf{r}) = \hat{\rho}_\uparrow(\mathbf{r}) + \hat{\rho}_\downarrow(\mathbf{r}) = \sum_{i=1}^{N}\delta(\mathbf{r}-\mathbf{r}_i). \tag{E.6}$$

From this it follows that

$$\hat{s}_z(\mathbf{r}) = \frac{1}{2}\left(\hat{\rho}_\uparrow(\mathbf{r}) - \hat{\rho}_\downarrow(\mathbf{r})\right). \tag{E.7}$$

Now we can express $\hat{\rho}_{\uparrow}(\mathbf{r})$ and $\hat{\rho}_{\downarrow}(\mathbf{r})$ as linear combinations of the density operator $\hat{\rho}(\mathbf{r})$ and the spin density operator $\hat{s}_z(\mathbf{r})$:

$$\hat{\rho}_{\uparrow}(\mathbf{r}) = \frac{1}{2}\hat{\rho}(\mathbf{r}) + \hat{s}_z(\mathbf{r}) \tag{E.8}$$

$$\hat{\rho}_{\downarrow}(\mathbf{r}) = \frac{1}{2}\hat{\rho}(\mathbf{r}) - \hat{s}_z(\mathbf{r}). \tag{E.9}$$

An irreducible tensor operator of rank k is a collection of operators $\hat{T}_q^k$ with $q = k, k-1, \ldots, -k$ for which,

$$\left[S_z, \hat{T}_q^k\right] = q\hat{T}_q^k \tag{E.10}$$

$$\left[S_{\pm}, \hat{T}_q^k\right] = \sqrt{k(k+1) - q(q\pm 1)}\,\hat{T}_{q\pm 1}^k. \tag{E.11}$$

In these equations we used that the total spin operators are given by

$$S_z = \sum_{i=1}^{N} s_{z,i} \tag{E.12}$$

$$S_{\pm} = \sum_{i=1}^{N} s_{\pm,i}. \tag{E.13}$$

Using the above definitions and the commutation relations of the spin operators we can see that $\hat{\rho}(\mathbf{r})$ is an irreducible tensor operator of rank zero and that $\hat{s}_z(\mathbf{r})$ is an irreducible tensor operator of rank one. We can then use the Wigner-Eckart theorem that states that for an irreducible tensor operator $\hat{T}_q^k$,

$$\left\langle S'M_S' \middle| \hat{T}_q^k \middle| SM_S \right\rangle = c(S')\left(S'M_S' \middle| kq, SM_S\right) \tag{E.14}$$

where c depends on S' and the form of the tensor operator and the last term on the right is a Clebsch-Gordan coefficient. From the properties of the Clebsch-Gordan coefficient it immediately follows that the matrix elements of an irreducible tensor operator are zero unless $M_S' = M_S + q$ and $|S - S'| \le k \le S + S'$. We can now see that

$$\left\langle SM_S \middle| \hat{\rho}(\mathbf{r}) \middle| 00 \right\rangle = c(S)\left(SM_S \middle| 00, 00\right) \tag{E.15}$$

is zero unless $S = M_S = 0$ and

$$\langle SM_S|\hat{s}_z(\mathbf{r})|00\rangle = c'(S)\big(SM_S|10,00\big) \tag{E.16}$$

is zero unless $S=1$ and $M_S=0$. We can rewrite Eqs. (E.8) and (E.9) as

$$\langle SM_S|\hat{\rho}_\uparrow(\mathbf{r})|00\rangle = \frac{1}{2}\langle SM_S|\hat{\rho}(\mathbf{r})|00\rangle + \langle SM_S|\hat{s}_z(\mathbf{r})|00\rangle \tag{E.17}$$

$$\langle SM_S|\hat{\rho}_\downarrow(\mathbf{r})|00\rangle = \frac{1}{2}\langle SM_S|\hat{\rho}(\mathbf{r})|00\rangle - \langle SM_S|\hat{s}_z(\mathbf{r})|00\rangle \tag{E.18}$$

and therefore

$$\langle SM_S|\hat{\rho}_\uparrow(\mathbf{r})|00\rangle = \langle SM_S|\hat{\rho}_\downarrow(\mathbf{r})|00\rangle \quad \text{if } S=0 \tag{E.19}$$

$$\langle SM_S|\hat{\rho}_\uparrow(\mathbf{r})|00\rangle = -\langle SM_S|\hat{\rho}_\downarrow(\mathbf{r})|00\rangle \text{ if } S=1. \tag{E.20}$$

Let us now look at the Lehmann representation of the spin-density response function

$$\chi_{\rho\rho}^{\sigma\sigma'}(1,2) = -i\Theta(t_1-t_2)\left(\sum_j e^{i(E_j-E_0)(t_1-t_2)}\langle 00|\hat{\rho}_\sigma(\mathbf{r}_1)|j\rangle\langle j|\hat{\rho}_{\sigma'}(\mathbf{r}_2)|00\rangle - (1\leftrightarrow 2)\right) \tag{E.21}$$

where $|j\rangle$ are the eigenstates of the unperturbed Hamiltonian with energy E_i. If we consider states $|j\rangle$ with $S=0$ or $S=1$ we find immediately from relations (E.19) and (E.20) that

$$\chi_{\rho\rho}^{\uparrow\uparrow}(1,2) = \chi_{\rho\rho}^{\downarrow\downarrow}(1,2) \tag{E.22}$$

$$\chi_{\rho\rho}^{\uparrow\downarrow}(1,2) = \chi_{\rho\rho}^{\downarrow\uparrow}(1,2) \tag{E.23}$$

This completes the proof.

List of acronyms

ADF	Amsterdam Density Functional theory program package
ALDA	adiabatic local density approximation [functional]
AO	atomic orbital
BLA	bond length alternation
BP	Becke-Perdew [functional]
CASPT*n*	*n*th-order complete active space perturbation theory
CASSCF	complete active space self-consistent field [model]
CC*n*	coupled-cluster [rank] *n* [hybrid model]
CCSD	coupled-cluster singles-doubles-and-triples [model]
CCSD(T)	CCSD with approximate triples correction
CEDA	common energy denominator approximation
CI	configuration-interaction [model]
CIS	CI singles [method]
CPHF	coupled-perturbed Hartree-Fock [model]
DFT	density-functional theory
DIIS	direct inversion in the iterative subspace [method]
DZP	double-zeta with one polarization function [basis]
EOM-CCSDT-3	equation-of-motion coupled-cluster singles-doubles-and-triples [model] where an iterative method is used for the triple excitations
ET	even-tempered [basis]
ET-pVQZ	ET of quadruple-zeta quality
ET-QZ3P-1Diffuse	ET quadruple-zeta with three polarization functions and one set of diffuse STOs
GGA	generalized gradient approximation
HF	Hartree-Fock [model]
HOMO	highest occupied molecular orbital
HPT	harmonic potential theorem
KLI	Krieger-Li-Iafrate [functional]
KS	Kohn-Sham

LB94	Van Leeuwen-Baerends [functional]
LCAO	linear combination of atomic orbitals
LDA	local density approximation
LUMO	lowest unoccupied molecular orbital
MP*n*	*n*th-order Møller-Plesset [perturbation theory]
MRMP	multireference Møller-Plesset [perturbation theory]
MRMP2	*n*th-order MRMP
MRSDCI	multireference singles-and-doubles CI [model]
NCT	Nifosì-Conti-Tosi [parameterization]
OEP	optimized effective potential [model]
PA	polyacetylene
PAC	polyacene
PBT	polybutatriene
PDA	polydiacetylene
PDI	point dipole interaction [model]
PE	polyethylene
PM3	parametric model number three
PMI	polymethineimine
PPV	poly(*para*-phenylene vinylene)
PSi	polysilane
PSi2	polysilene
PT	polythiophene
PY	polyyne
QV	Qian-Vignale [parameterization]
RCIS	restricted CIS
SAOP	statistical averaging of (model) orbital potentials
SCF	self-consistent field [model]
SMA	Small-matrix approximation
SOPPA	Second-order polarization propagator approximation
SOS	sum-over-states
STO	Slater-type orbital
TDCDFT	time-dependent current-density-functional theory
TDDFT	time-dependent density-functional theory

TDHF	time-dependent Hartree-Fock
TZ2P	triple-zeta plus two polarization functions [basis]
TZP	triple-zeta plus polarization function [basis]
TZP+	TZP with additional first-order field-induced polarization functions
VK	Vignale-Kohn [functional]
VWN	Vosko-Wilk- Nusair [parameterization]
xc	exchange-correlation

Samenvatting

In de kwantumchemie bestuderen we eigenschappen van atomen, moleculen en vaste stoffen door het oplossen van de zogenaamde Schrödinger-vergelijking. De oplossing van deze vergelijking, de golffunctie, geeft toegang tot alle eigenschappen van een systeem. In de praktijk kan deze vergelijking echter alleen exact worden opgelost voor zeer eenvoudige systemen. In de meeste gevallen zal de oplossing van deze vergelijking dus moeten worden benaderd. Veel kwantumchemische methodes proberen een benadering voor de golffunctie te vinden door te kijken naar de beweging en interactie van alle verschillende deeltjes gelijktijdig. Voor grotere moleculen (met veel deeltjes) betekent dit echter dat het aantal benodigde berekeningen zo groot wordt dat een goede benadering onbereikbaar is.

Hohenberg en Kohn ontdekten in de jaren zestig dat voor de beschrijving van veel van de eigenschappen van moleculaire systemen, kennis van de elektronendichtheid van de grondtoestand voldoende is. Het voordeel van deze methode is dat de dichtheid slechts afhangt van drie ruimtecoördinaten en niet van de ruimtecoördinaten van elk deeltje afzonderlijk. Kohn en Sham lieten kort na deze ontdekking zien dat de dichtheid van een systeem van deeltjes die interactie hebben verkregen kan worden door te kijken naar een denkbeeldig systeem van deeltjes die onderling geen interactie hebben, maar bewegen in een effectieve potentiaal: de Kohn-Sham potentiaal. Deze effectieve potentiaal bevat naast de bijdrage van de externe potentiaal en de klassieke Coulomb potentiaal ook een deel dat de veeldeeltjeseffecten van het echte systeem beschrijft. Deze bijdrage, de zogenaamde exchange-correlatie potentiaal, wordt eenduidig vastgelegd door een universele functionaal van de dichtheid. Voor deze dichtheidsfunctionaal zijn tot op heden alleen benaderingen bekend. Binnen deze dichtheidsfunctionaaltheorie (DFT) is het van belang om een zo goed mogelijke functionaal te vinden.

In dit proefschrift kijken we naar hoe moleculen worden beïnvloed door de aanwezigheid van een elektrisch veld. Om deze responseigenschappen te beschrijven moeten we de tijdsafhankelijke Schrödinger-vergelijking oplossen. Runge en Gross hebben bewezen dat de grondtoestand-DFT kan worden uitgebreid naar het tijdsdomein. Ook binnen de tijdsafhankelijke dichtheidsfunctionaaltheorie (TDDFT) is het nodig om een exchange-correlatie functionaal te vinden. De huidige functionalen (de adiabatische lokale dichtheid benadering

(ALDA) en meer geavanceerde gradiënt methoden (GGA)) blijken niet goed in staat om de polariseerbaarheid van lange moleculaire ketens te beschrijven. Deze functionalen overschatten de polariseerbaarheid van deze systemen zeer sterk. Het probleem in deze systemen is dat door de aanwezigheid van het veld lading zal verschuiven naar de eindpunten van de ketens. Dit is een globaal effect dat niet kan worden beschreven met een lokale functionaal van de dichtheid. Naast ruimtelijk lokaal, zijn de ALDA en GGA's ook lokaal in de tijd. Dit betekend dat de exchange-correlatie potentiaal op een bepaald tijdstip alleen afhangt van de dichtheid op dat tijdstip, en niet van de dichtheid op andere tijdstippen. Deze potentialen hebben dus geen geheugen.

Vignale en Kohn (VK) hebben een functionaal ontwikkeld op basis van de stroomdichtheid. Zij ontwikkelden deze functionaal oorspronkelijk nadat zij hadden aangetoond dat als geheugeneffecten worden meegenomen, er geen lokale dichtheid benadering voor de exchange-correlatie potentiaal bestaat. Zij toonden aan dat een benaderde functionaal die ruimtelijk niet-lokaal is ook niet-lokaal moet zijn in de tijd om aan belangrijke behoudswetten te voldoen. Echter zij bewezen dat er wel een ruimtelijk lokale functionaal met geheugen op basis van de stroomdichtheid bestaat. De lokale stroomdichtheid geeft namelijk informatie over globale dichtheidsveranderingen doordat dichtheidsveranderingen op de randen van het systeem gerelateerd zijn aan stromen binnen het systeem. Om deze functionaal toe te kunnen passen zal gebruik gemaakt worden van de tijdsafhankelijke stroomdichtheidsfunctionaal theorie (TDCDFT). In dit proefschrift beschrijven wij de statische lineaire respons (frequentie is nul) in systemen die relatief klein zijn. Men kan zich afvragen of de VK-functionaal in dat geval wel een effect heeft. Het blijkt uit ons onderzoek dat voor het geval van lange moleculaire ketens de VK-functionaal juist een groot effect heeft. De VK resultaten voor de statische polariseerbaarheid liggen voor het geval van oligomeren van polyacetyleen en andere polymeren erg dicht bij waarden verkregen met andere theoretische methodes.

In de inleidende hoofdstukken van dit proefschrift worden eerst de grondtoestand en tijdsafhankelijke DFT beschreven. Vervolgens wordt beschreven hoe de lineaire responseigenschappen kunnen worden uitgerekend met TDCDFT. Het blijkt dat het stelsel van vergelijkingen dat we verkrijgen voor het uitrekenen van de polariseerbaarheid en het excitatie spectrum sterk overeenkomt met de vergelijkingen die verkregen worden in het geval van de gewone TDDFT. Dit maakt de implementatie van deze vergelijkingen in het "Amsterdam Density Functional" (ADF) programma een stuk eenvoudiger. De lineaire respons met TDDFT is namelijk al geïmplementeerd door Stan van Gisbergen (proefschrift 1998, VU Amsterdam). In

dit proefschrift wordt daarom alleen beschreven hoe wij deze implementatie hebben aangepast voor TDCDFT en hoe de VK-functionaal is geïmplementeerd.

Het hoofdonderwerp van ons onderzoek is het bestuderen van het effect van de VK-functionaal op de lineaire responseigenschappen van moleculen. Er is daarom ook een hoofdstuk gewijd aan de achtergrond van deze functionaal. We geven in dat hoofdstuk ook een kort overzicht van de hydrodynamica en elasticiteitstheorie. Vignale, Ullrich en Conti hebben namelijk aangetoond dat het mogelijk is om de VK functionaal te schrijven in de vorm van een hydrodynamische vergelijking. Dit is ook de vorm die wij als uitgangspunt nemen. Na een beschrijving van de historische motivatie van Vignale en Kohn voor de afleiding van de functionaal geven we een kort overzicht van deze afleiding. We geven ook de functionaal in de spinafhankelijke vorm. Zoals hierboven opgemerkt kijken we naar de statische lineaire respons, we laten daarom zien wat de gevolgen van het nemen van de statische limiet zijn voor de functionaal.. Ook zeggen we iets over de geldigheid van de functionaal in het geval van eindige inhomogene systemen zoals atomen en moleculen.

De eerste responseigenschap die we hebben onderzocht is de axiale statische polariseerbaarheid van, voornamelijk π-geconjugeerde, moleculaire ketens. Zoals eerder opgemerkt wordt de polariseerbaarheid voor deze systemen sterk overschat met de ALDA. De VK-functionaal blijkt niet alleen een grote correctie te geven voor polyacetyleen, maar ook voor veel andere π-geconjugeerde ketens waaronder de buisvormige fullerenen. Een ander systeem dat veel aandacht krijgt in de literatuur is het waterstofketen-model. Dit is een keten van naast elkaar liggende waterstofmoleculen. Ook voor deze keten overschat de ALDA de polariseerbaarheid sterk. Op basis van wat we gevonden hebben voor de π-geconjugeerde ketens zouden we verwachten dat ook in dit geval de VK-functionaal een grote correctie zou geven. Dit blijkt echter niet het geval te zijn, er is slechts sprake van een klein verschil tussen de ALDA en VK resultaten.

Behalve polariseerbaarheden kunnen we ook elektronische excitatiespectra uitrekenen. We hebben de singlet excitatieënergieën uitgerekend voor een referentie set van moleculen. De $\pi \rightarrow \pi^*$ excitatieënergieën verkregen met de VK-functionaal zijn in goede overeenstemming met experimentele en andere theoretische resultaten en in het algemeen geeft de VK-functionaal een verbetering ten opzichte van de ALDA. De $n \rightarrow \pi^*$ overgangen daarentegen worden sterk overschat door de VK-functionaal. In de set van moleculen zitten ook systemen waarvan we andere typen overgangen hebben bestudeerd. Voor deze systemen krijgen we geen duidelijk beeld van het gedrag van de VK-functionaal.

We hebben ook de $\pi \rightarrow \pi^*$ overgangen onderzocht in een aantal π-geconjugeerde oligomeren en de laagste singlet excitatie in de waterstofketen. Op basis van onze resultaten voor de polariseerbaarheid verwachten we een groot effect van de VK-functionaal voor de π-geconjugeerde ketens. We hebben bestudeerd hoe het excitatie spectrum zich gedraagt als de ketenlengte toeneemt. We zien dat de excitatieënergie van overgangen die oscillatorsterkte hebben opschuiven naar hogere energie. We zien ook dat het HOMO-LUMO karakter en de oscillatorsterkte van deze overgangen overgebracht worden naar andere excitaties die hoger in energie liggen. De excitaties berekend met de VK-functionaal die de grootste bijdrage hebben aan de oscillatorsterkte, hebben in de meeste gevallen een excitatieënergie die dichter bij de referentiewaarde ligt dan het ALDA resultaat. Voor de waterstofketen vinden we slechts een kleine correctie net als voor de polariseerbaarheid. Ook hebben we de laagste triplet excitatie in polyacetyleen onderzocht. Ook in dit geval zien we een groot effect van de VK-functionaal. In dit geval is het effect echter niet gewenst, aangezien de literatuurwaarden dicht bij de ALDA waarden liggen.

In het laatste deel van dit proefschrift hebben we geprobeerd om meer inzicht te krijgen in de VK functionaal en hebben daarvoor onderzoek gedaan naar de VK-functionaal voor het geval van atomen. Voor dit geval kan de VK-functionaal omgeschreven worden naar een stelsel van bolcoördinaten, wat de analyse van de functionaal versimpelt. Dit geeft ons onder andere de mogelijkheid om de bijdrage van de VK-functionaal grafisch weer te geven. Als we dit doen voor de $2s \rightarrow 3s$ overgang in het B^+ atoom zien we dat het exchange-correlatie veld sterk oscilleert in de ruimte. Voor de excitatieënergieën van verschillende atomen vinden we dat in het geval van $s \rightarrow p$ overgangen de energie sterk overschat wordt door de VK-functionaal. Deze observatie is ook gedaan in een onafhankelijke studie door Ullrich en Burke. Een kleine verandering van de transversale exchange-correlatie kernel (die een belangrijk onderdeel vormt van de VK-functionaal) in het hoge dichtheid gebied geeft een grote vermindering van deze overschatting. Zowel met de oorspronkelijke VK-functionaal als met deze gemodificeerde kernel blijven de $s \rightarrow s$ overgangen in overeenstemming met het experiment. Als we de gemodificeerde kernel gebruiken voor moleculen zien we dat de excitatieënergieën van de $n \rightarrow \pi^*$ overgangen sterk gereduceerd worden, maar de energieën van de $\pi \rightarrow \pi^*$ overgangen blijven in overeenstemming met literatuurwaarden. Voor de polyacetyleen keten vinden we met de gemodificeerde kernel nog steeds een redelijk grote correctie van de axiale statische polariseerbaarheid ten opzichte van de ALDA. Een verrassend resultaat is dat de gemodificeerde kernel ook leidt tot een grote correctie van de axiale statische polariseerbaarheid van de

waterstofketens, waardoor de resultaten dichter bij de literatuurwaarden komen te liggen. De hoop dat een verbeterde parametrisatie van de transversale kernel of andere aanpassingen van de VK-functionaal een oplossing zou kunnen bieden voor de huidige, in dit proefschrift beschreven, tekortkomingen lijkt derhalve gerechtvaardigd.

Dankwoord

Het proefschrift dat voor u ligt is het resultaat van vier jaar onderzoek in de theoretische chemie groep van de Rijksuniversiteit Groningen. Op deze plaats wil ik graag een aantal mensen bedanken die op directe of indirecte wijze hebben bijgedragen aan het tot stand komen van dit proefschrift.

Allereerst wil ik dit dankwoord richten aan prof. dr. J. G. Snijders, die mijn eerste promotor had moeten zijn, maar deze promotie door zijn vroege en onverwachte overlijden niet kan meemaken. Ik wil Jaap graag bedanken voor het feit dat ik bij hem zowel mijn doctoraal als mijn promotie onderzoek heb mogen doen. Vooral tijdens mijn doctoraal onderzoek werd het mij duidelijk dat ik verder wilde gaan in de theoretische chemie en dit was mogelijk dankzij het promotie onderzoek dat Jaap mij aanbood. Ik zal hem herinneren als een professor bij wie de deur altijd open stond en iemand die altijd tijd had voor zijn studenten. Het feit dat zijn kamer tevens gebruikt werd als koffiekamer toont aan dat voor Jaap ook het sociale aspect erg belangrijk was, wat leidde tot een goede en gezellige sfeer in de groep. Jaap, ik hoop dat je trots bent op dit werk dat zo succesvol begon en met goed gevolg is afgerond.

Ik wil graag prof. dr. H. B. Broer bedanken voor het overnemen van de taak van eerste promotor. Ria, bedankt dat je mijn proefschrift zo aandachtig hebt bestudeerd. Je commentaar was erg nuttig. Verder hebben we tijdens mijn jaren in Groningen misschien wel meer gediscussieerd over universitaire politiek en de rol van de vrouw in de wetenschappelijke wereld dan de wetenschap zelf. Hopelijk blijf je je in de toekomst sterk maken voor vrouwen die in de wetenschap werkzaam zijn.

Verder wil ik mijn copromotores dr. ir. P. L. de Boeij en dr. R. van Leeuwen bedanken. Paul en Robert, vooral na het wegvallen van Jaap, maar ook al tijdens het vroege stadium van dit onderzoek hebben jullie mij begeleid, mijn dank hiervoor. Paul, jij was de grote drijfveer achter het project. Je hebt mij altijd rustig mijn gang laten gaan, maar met vragen (of het nou een theoretisch probleem of iets met de implementatie was) kon ik altijd bij je terecht. Robert, ik wil jou speciaal bedanken voor al die keren dat je mij de fundamentele aspecten van de theorie zo helder en duidelijk hebt uitgelegd.

Ik wil prof. dr. J. Knoester, prof. dr. E. J. Baerends en prof. dr. G. Vignale bedanken voor het zitting nemen in de leescommissie en het bestuderen van het manuscript.

Ook wil ik verschillende mensen in de theoretische chemie groep bedanken. Lasse, jij stelde voor om de berekeningen te doen aan de fullerenen en hier is een mooie publicatie uit voortgekomen (Hoofdstuk 7 van dit proefschrift). Marcel, toen ik als student in de vakgroep kwam had ik bijna geen programmeer ervaring. Jij hebt mij toen en ook na die tijd erg geholpen met alles wat met programmeren te maken heeft. Arjan, bedankt voor het voorwerk dat je gedaan hebt voor de implementatie van de VK functionaal. Rob, bedankt voor het implementeren van de VK functionaal in bolcoördinaten in een numeriek atoomprogramma. Ook wil ik de overige (oud-)leden van de vakgroep bedanken voor de gezellige sfeer in de groep. Adrian, Alex, Alexandrina, Aymeric, Freddie, Henriette, Javier, Johan. Khompat, Lasse, Liviu, Nienke, Nils, Olena, Piet, Pina, Rosanna, Thomas en alle overige studenten en gasten binnen onze groep bedankt.

I would like to thank Denis Jacquemin and Benoît Champagne for providing me with unpublished MP2 data on the polarizabilities of PMI (Chapter 6). I also want to thank Tobita Motoi, So Hirata, and Rodney J. Bartlett for many useful discussions and providing us with benchmark CCSD(T) data on the polarizability of PBT (Chapter 6). Also I want to acknowledge Carsten Ullrich and Kieron Burke for providing me with data on the use of the VK functional for beryllium and other atoms when these results were still unpublished (Chapter 10).

De jaarlijkse uitstapjes naar Han-sur-Lesse en Lunteren waren een stuk gezelliger dankzij jullie Jeroen en Chrétien. En natuurlijk vergeet ik jullie ook niet Mark, Joost en Manuel. Het was altijd fijn om lange boswandelingen met jullie te maken en ‘s avonds in Han diepe en minder diepe gesprekken te voeren onder het genot van een Belgisch biertje.

Als bestuurslid van het GAIOO heb ik mij begeven in de wereld van de universitaire politiek. Ik wil iedereen bedanken die met mij in het bestuur heeft gezeten: Radboud, Laura, Paul, Freddie, Joanneke, Peter, Bart, Kim, Ellen, Tanja, Charlotte, Annemarie, Tsjerk, Arjan en Leonoor. De vergaderingen waren altijd gezellig en ik denk dat we in die periode echt iets hebben kunnen betekenen voor de promovendi in Groningen.

Gelukkig was er tijdens deze vier jaar ook nog tijd voor ontspanning. Ik wil graag het ‘kolonisten groepje’ (Joanneke, Gerard, Bart, Jaqueline, Margot, Arjan, Annemarie, Thomas en natuurlijk ook Martijn) bedanken voor alle spelletjes avonden en competitie afsluitingen. Het testen van de algemene kennis tijdens de “Jameson Quiz Night”, met (in wisselende samenstelling) Arjan, Martijn, Gerard, Tim, Nils en Paul onder het genot van de pitcher bier die we (bijna) altijd winnen, is elke keer weer gezellig.

In het bijzonder wil ik mijn ouders bedanken die mij altijd hebben gesteund. En mijn zusjes Wendy en Lisette die mij als paranimf zullen bijstaan tijdens de verdediging van dit proefschrift.

Tenslotte wil ik Martijn bedanken voor de steun en liefde die ik elke dag krijg. Ik wil je ook graag bedanken voor het helpen met de organisatie rond de promotie.

List of publications

M. van Faassen, R. van Leeuwen, and P. L. de Boeij
Linear response with time-dependent current-density-functional theory
International Journal of Modern Physics B, in preparation

S. Hamel, M. van Faassen, P. L. de Boeij, and M. Côté
Spectra of acenes using time-dependent current-density-functional theory
In preparation

M. van Faassen and P. L. de Boeij
Excitation energies of π-conjugated oligomers within time-dependent current-density-functional theory
J. Chem. Phys. **121**, 10707-10714 (2004)

M. van Faassen, L. Jensen, J. A. Berger, and P. L. de Boeij
Size-scaling of the polarizability of tubular fullerenes investigated
Chem. Phys. Lett. **395**, 274-278 (2004)

M. van Faassen and P. L. de Boeij
Excitation energies for a benchmark set of molecules obtained within time-dependent current-density-functional theory using the Vignale-Kohn functional
J. Chem. Phys. **120**, 8353-8363 (2004); **PN**: **120**, 11967 (2004); **E**: **121**, 7035 (2004)

M. van Faassen, P. L. de Boeij, R. van Leeuwen, J. A. Berger, and J. G. Snijders
Application of time-dependent current-density-functional-theory to nonlocal exchange-correlation effects in polymers
J. Chem. Phys. **118**, 1044-1053 (2003)

M. van Faassen, P. L. de Boeij, R. van Leeuwen, J. A. Berger, and J. G. Snijders
Ultra nonlocality in time-dependent current-density-functional theory: application to conjugated polymers
Phys. Rev. Lett. **88**, 186401-1-4 (2002)

Bibliography

[1] P. Hohenberg and W. Kohn, Phys. Rev. **136**, B864 (1964).

[2] W. Kohn and L. J. Sham, Phys. Rev. **140**, A1133 (1965).

[3] E. Runge and E. K. Gross, Phys. Rev. Lett. **52**, 997 (1984).

[4] A. K. Dhara and S. K. Ghosh, Phys. Rev. A **35**, 442 (1987).

[5] S. K. Ghosh and A. K. Dhara, Phys. Rev. A **38**, 1149 (1988).

[6] G. Vignale, Phys. Rev. B **70**, 201102 (2004).

[7] P. L. de Boeij, F. Kootstra, J. A. Berger, R. van Leeuwen, and J. G. Snijders, J. Chem. Phys. **115**, 1995 (2001).

[8] G. Vignale and W. Kohn, Phys. Rev. Lett. **77**, 2037 (1996).

[9] G. Vignale and W. Kohn, in *Electronic Density Functional Theory: Recent Progress and New Directions*, edited by J. F. Dobson, G. Vignale, and M. P. Das (Plenum Press, New York, 1998).

[10] B. Champagne, E. A. Perpète, S. J. A. van Gisbergen, E. J. Baerends, J. G. Snijders, C. Soubra-Ghaoui, K. A. Robins, and B. Kirtman, J. Chem. Phys. **109**, 10489 (1998).

[11] S. J. A. van Gisbergen, P. R. T. Schipper, O. V. Gritsenko, E. J. Baerends, J. G. Snijders, B. Champagne, and B. Kirtman, Phys. Rev. Lett. **83**, 694 (1999).

[12] B. Kirtman, J. L. Toto, K. A. Robins, and M. Hasan, J. Chem. Phys. **102**, 5350 (1995).

[13] T. T. Toto, J. L. Toto, C. P. de Melo, M. Hasan, and B. Kirtman, Chem. Phys. Lett. **244**, 59 (1995).

[14] D. Jacquemin, B. Champagne, and J. M. André, Chem. Phys. Lett. **284**, 24 (1998).

[15] J. L. Toto, T. T. Toto, and C. P. de Melo, Chem. Phys. Lett. **245**, 660 (1995).

[16] S. Kümmel, L. Kronik, and J. P. Perdew, Phys. Rev. Lett. **93**, 213002 (2004).

[17] J. D. Talman and W. G. Shadwick, Phys. Rev. A **14**, 36 (1976).

[18] P. Mori-Sanchez, Q. Wu, and W. T. Yang, J. Chem. Phys. **119**, 11001 (2003).

[19] Y. H. Kim and A. Görling, Phys. Rev. B **66**, 035114 (2002).

[20] J. B. Krieger, Y. Li, and G. J. Iafrate, Phys. Rev. A **45**, 101 (1992).

[21] M. Grüning, O. V. Gritsenko, and E. J. Baerends, J. Chem. Phys. **116**, 6435 (2002).

[22] M. E. Casida, in *Recent Advances in Density-Funtional Methods*, edited by D. P. Chong (World Scientific, Singapore, 1995), pp. 155.

[23] G. Vignale, C. A. Ullrich, and S. Conti, Phys. Rev. Lett. **79**, 4878 (1997).

[24] G. Vignale, Int. J. Mod. Phys. B **15**, 1714 (2001).

[25] ADF2003.01, SCM, Theoretical Chemistry, Vrije Universiteit, Amsterdam, The Netherlands, http://www.scm.com, E. J. Baerends, J.A. Autschbach, A. Bérces, C. Bo, P. M. Boerrigter, L. Cavallo, D.P. Chong, L. Deng, R. M. Dickson, D. E. Ellis, L. Fan, T. H. Fischer, C. Fonseca Guerra, S. J. A. van Gisbergen, J. A. Groeneveld, O. V. Gritsenko, M. Grüning, F. E. Harris, P. van den Hoek, H. Jacobsen, G. van Kessel, F. Kootstra, E. van Lenthe, V. P. Osinga, S. Patchkovskii, P. H. T. Philipsen, D. Post, C. C. Pye, W. Ravenek, P. Ros, P. R. T. Schipper, G. Schreckenbach, J. G. Snijders, M. Sola, M. Swart, D. Swerhone, G. te Velde, P. Vernooijs, L. Versluis, O. Visser, E. van Wezenbeek, G. Wiesenekker, S. K. Wolff, T. K. Woo, and T. Ziegler; the version we used in this thesis was modified by M. van Faassen.

[26] S. J. A. van Gisbergen, phD Thesis, Vrije Universiteit, 1998.

[27] C. A. Ullrich and K. Burke, J. Chem. Phys. **121**, 28 (2004).

[28] R. van Leeuwen, Adv. Quantum Chem. **43**, 26 (2003).

[29] R. G. Parr and W. Yang, *Density-Functional Theory of Atoms and Molecules*. (Oxford University Press, New York, 1989).

[30] R. M. Dreizler and E. K. U. Gross, *Density Functional Theory: An Approach to the Quantum Many Body Problem*. (Springer-Verlag, Berlin, 1990).

[31] A. Szabo and N. S. Ostlund, *Modern quantum chemistry : introduction to advanced electronic structure theory*, 1st. Rev. ed. (McGraw-Hill, New York, 1989).

[32] W. Kohn, Phys. Rev. Lett. **51**, 1596 (1983).

[33] P. A. M. Dirac, Proc. Cambridge Phil. Soc. **26**, 376 (1930).

[34] S. H. Vosko, L. Wilk, and M. Nusair, Can. J. Phys. **58**, 1200 (1980).

[35] A. D. Becke, Phys. Rev. A **38**, 3098 (1988).

[36] C. Lee, W. Yang, and R. G. Parr, Phys. Rev. B **37**, 785 (1988).

[37] J. P. Perdew, K. Burke, and M. Ernzerhof, Phys. Rev. Lett. **77**, 3865–3868 (1996).

[38] J. P. Perdew, S. Kurth, A. Zupan, and P. Blaha, Phys. Rev. Lett. **82**, 2544–2547 (1999).

[39] R. van Leeuwen and E. J. Baerends, Phys. Rev. A **49**, 2421 (1994).

[40] P. R. T. Schipper, O. V. Gritsenko, S. J. A. van Gisbergen, and E. J. Baerends, J. Chem. Phys. **112**, 1344 (2000).

[41] E. K. U. Gross, J. F. Dobson, and M. Petersilka, Top. Curr. Chem. **181**, 81 (1996).

[42] R. van Leeuwen, Int. J. Mod. Phys. B **15**, 1969 (2001).

[43] M. E. Casida, in *Recent Developments and Applications of Modern Density Functional Theory*, edited by J. M. Seminario (Elsivier, Amsterdam, 1996).

[44] L. V. Keldysh, Sov. Phys. JETP **20**, 1018 (1965).

[45] F. Della Sala and A. Görling, J. Chem. Phys. **115**, 5718 (2001).

[46] G. Vignale, M. Rasolt, and D. J. W. Geldart, Adv. Quantum Chem. **21**, 235 (1990).

[47] H. Lehmann, Nuovo Cimento **11**, 342 (1954).

[48] K. L. Liu and S. H. Vosko, Can. J. Phys. **67**, 1015 (1989).

[49] P. Nozières and D. Pines, *The theory of quantum liquids*. (Perseus, Cambridge, 1999).

[50] O. L. Brill and B. Goodman, Am J Phys **35**, 832 (1967).

[51] G. Breit, Phys. Rev. **39**, 616 (1932).

[52] G. Breit, Phys. Rev. **34**, 553 (1929).

[53] D. P. Craig and T. Thirunamachandran, *Molecular Quantum Electrodynamics*. (Dober Publications Inc., New York, 1998).

[54] L. D. Landau and E. M. Lifshitz, *Fluid mechanics*, 2 ed. (Pergamon Press, Oxford, 1987).

[55] L. D. Landau and E. M. Lifshitz, *Theory of elasticity*, 3 ed. (Pergamon Press, Oxford, 1998).

[56] E. K. U. Gross and W. Kohn, Phys. Rev. Lett. **55**, 2850 (1985).

[57] J. F. Dobson, Phys. Rev. Lett. **73**, 2244 (1994).

[58] G. Vignale, Phys. Rev. Lett. **74**, 3233 (1995).

[59] G. Vignale, Phys. Lett. A **209**, 206 (1995).

[60] Z. X. Qian and G. Vignale, Phys. Rev. B **68**, 195113 (2003).

[61] Z. Qian, A. Constantinescu, and G. Vignale, Phys. Rev. Lett. **90**, 066402 (2003).

[62] C. A. Ullrich and G. Vignale, Phys. Rev. B **65**, 245102 (2002).

[63] S. Conti and G. Vignale, Phys. Rev. B **60**, 7966 (1999).

[64] I. D'Amico and G. Vignale, Phys. Rev. B **62**, 4853 (2000).

[65] S. Conti, R. Nifosì, and M. P. Tosi, J. Phys. Condens. Matt. **9**, L475 (1997).

[66] Z. Qian and G. Vignale, Phys. Rev. B **65**, 235121 (2002).

[67] J. A. Berger, P. L. de Boeij, and R. van Leeuwen, Phys. Rev. B, accepted (2005).

[68] R. Nifosì, S. Conti, and M. P. Tosi, Phys. Rev. B **58**, 12758 (1998).

[69] H. Yasuhara and Y. Ousaka, Int. J. Mod. Phys. B **6**, 3089 (1992).

[70] S. J. A. van Gisbergen, J. G. Snijders, and E. J. Baerends, Comput. Phys. Commun. **118**, 119 (1999).

[71] G. te Velde, F. M. Bickelhaupt, E. J. Baerends, C. F. Guerra, S. J. A. van Gisbergen, J. G. Snijders, and T. Ziegler, J. Comput. Chem. **22**, 931 (2001).

[72] P. Pulay, J. Comput. Chem. **3**, 556 (1982).

[73] P. Pulay, Chem. Phys. Lett. **73**, 393 (1980).

[74] E. R. Davidson, J. Comput. Phys. **17**, 87 (1975).

[75] J. A. Berger, Master Thesis, Rijksuniversiteit Groningen, http://theochem.chem.rug.nl/publications/Master.html, 2001.

[76] E. J. Baerends, D. E. Ellis, and P. Ros, Chem. Phys. **2**, 41 (1973).

[77] M. van Faassen, P. L. de Boeij, R. van Leeuwen, J. A. Berger, and J. G. Snijders, Phys. Rev. Lett. **88**, 186401 (2002).

[78] M. van Faassen, P. L. de Boeij, R. van Leeuwen, J. A. Berger, and J. G. Snijders, J. Chem. Phys. **118**, 1044 (2003).

[79] M. van Faassen and P. L. de Boeij, J. Chem. Phys. **120**, 8353 (2004).

[80] M. van Faassen and P. L. de Boeij, J. Chem. Phys. **120**, 11967 (2004).

[81] M. van Faassen and P. L. de Boeij, J. Chem. Phys. **121**, 7035 (2004).

[82] M. van Faassen and P. L. de Boeij, J. Chem. Phys. **121**, 10707 (2004).

[83] M. van Faassen, L. Jensen, J. A. Berger, and P. L. de Boeij, Chem. Phys. Lett. **395**, 274 (2004).

[84] H. M. Böhm, S. Conti, and M. P. Tosi, J. Phys. Condens. Matt. **8**, 781 (1996).

[85] O. V. Gritsenko, S. J. A. van Gisbergen, P. R. T. Schipper, and E. J. Baerends, Phys. Rev. A **62**, 012507 (2000).

[86] O. V. Gritsenko and E. J. Baerends, Phys. Rev. A **64**, 042506 (2001).

[87] X. Gonze, P. Ghosez, and R. W. Godby, Phys. Rev. Lett. **74**, 4035 (1995).

[88] B. Champagne, D. H. Mosley, M. Vračko, and J. M. André, Phys. Rev. A **52**, 1039 (1995).

[89] B. Champagne, D. H. Mosley, M. Vračko, and J. M. André, Phys. Rev. A **52**, 178 (1995).

[90] F. Kootstra, P. L. de Boeij, and J. G. Snijders, J. Chem. Phys. **112**, 6517 (2000).

[91] G. F. Bertsch, J. I. Iwata, A. Rubio, and K. Yabana, Phys. Rev. B **62**, 7998 (2000).

[92] R. Resta, Rev. Mod. Phys. **66**, 899 (1994).

[93] R. D. King-Smith and D. Vanderbilt, Phys. Rev. B **47**, 1651 (1993).

[94] R. Resta, Phys. Rev. Lett. **77**, 2265 (1996).

[95] D. Vanderbilt, Phys. Rev. Lett. **79**, 3966 (1997).

[96] R. M. Martin and G. Ortiz, Phys. Rev. B **56**, 1124 (1997).

[97] C. A. Ullrich and G. Vignale, Phys. Rev. Lett. **87**, 037402 (2001).

[98] B. Kirtman and B. Champagne, Int. Rev. Phys. Chem. **16**, 389 (1997).

[99] E. J. Baerends, D. E. Ellis, and P. Ros, Chem. Phys. **2**, 41 (1973).

[100] L. Versluis and T. Ziegler, J. Chem. Phys. **88**, 322 (1988).

[101] G. te Velde and E. J. Baerends, J. Comput. Phys. **99**, 84 (1992).

[102] S. J. A. van Gisbergen, J. G. Snijders, and E. J. Baerends, J. Chem. Phys. **103**, 9347 (1995).

[103] C. F. Guerra, J. G. Snijders, G. te Velde, and E. J. Baerends, Theor. Chim. Acta **99**, 391 (1998).

[104] E. K. Dalskov, J. Oddershede, and D. M. Bishop, J. Chem. Phys. **108**, 2152 (1998).

[105] B. Champagne, D. H. Mosley, and J. M. André, J. Chem. Phys. **100**, 2034 (1994).

[106] D. Jacquemin, B. Champagne, and B. Kirtman, J. Chem. Phys. **107**, 5076 (1997).

[107] E. A. Perpète, B. Champagne, and B. Kirtman, J. Chem. Phys. **107**, 2463 (1997).

[108] B. Champagne and J. M. André, Nonlinear Optics **9**, 22 (1995).

[109] J. Delhalle, B. Champagne, M. Dory, J. G. Fripiat, and J. M. André, Bull. Soc. Chim. Belg. **98**, 811 (1989).

[110] Anonymous, *CRC Handbook of Chemistry and Physics*, 80 ed. (CRC Press, Boca Raton, 1999-2000).

[111] J. L. Toto, T. T. Toto, C. P. de Melo, B. Kirtman, and K. Robins, J. Chem. Phys. **104**, 8586 (1996).

[112] D. Jacquemin and B. Champagne (private communication).

[113] D. Jacquemin, J. M. André, and E. A. Perpète, J. Chem. Phys. **121**, 4389 (2004).

[114] B. Champagne and Y. Öhrn, Chem. Phys. Lett. **217**, 551 (1994).

[115] V. P. Bodart, J. Delhalle, M. Dory, J. G. Fripiat, and J. M. André, J. Opt. Soc. Am. B **4**, 1047 (1987).

[116] M. Tobita, S. Hirata, and R. J. Bartlett, J. Chem. Phys. **114**, 9130 (2001).

[117] M. Tobita, S. Hirata, and R. J. Bartlett (private communication).

[118] M. Gussoni, M. Rui, and G. Zerbi, J. Mol. Struct. **447**, 163 (1998).

[119] S. J. A. van Gisbergen, V. P. Osinga, O. V. Gritsenko, R. v. Leeuwen, J. G. Snijders, and E. J. Baerends, J. Chem. Phys. **105**, 3142 (1996).

[120] M. J. S. Dewar, J. Am. Chem. Soc. **106**, 669 (1984).

[121] P. L. Davies, Trans. Faraday Soc. **47**, 789 (1952).

[122] S. Tretiak, V. Chernyak, and S. Mukamel, Phys. Rev. Lett. **77**, 4656 (1996).

[123] K. C. Rustagi and J. Ducuing, Optics. Comm. **10**, 258 (1974).

[124] A. G. Rojo and G. D. Mahan, Phys. Rev. B **47**, 1794 (1993).

[125] W. A. Heer, Rev. Mod. Phys. **65**, 661 (1993).

[126] E. Benichou, R. Antoine, D. Rayane, B. Vezin, F. W. Dalby, P. Dugourd, M. Broyer, C. Ristori, F. Chandezon, B. A. Nuber, J. C. Rocco, S. A. Blundell, and C. Guet, Phys. Rev. A **59**, R1 (1999).

[127] L. Kronik, I. Vasiliev, and J. R. Chelikowsky, Phys. Rev. B **62**, 9992 (2000).

[128] K. Jackson, M. Pederson, C.-Z. Wang, and K.-M. Ho, Phys. Rev. A **59**, 3685 (1999).

[129] R. Schäfer, S. Schlecht, J. Woenckhaus, and J. A. Becker, Phys. Rev. Lett. **76**, 471 (1996).

[130] I. Vasiliev, S. Ögüt, and J. R. Chelikowsky, Phys. Rev. Lett. **78** (1997).

[131] R. Antoine, P. Dugourd, D. Rayane, E. Benichou, F. Chandezon, M. Broyer, and C. Guet, J. Chem. Phys. **110**, 9771 (1999).

[132] A. Ballard, K. Bonin, and J. Louderback, J. Chem. Phys. **113**, 5732 (2000).

[133] I. Compagnon, R. Antoine, M. Broyer, P. Dugourd, J. Lermé, and D. Rayane, Phys. Rev. A **64**, 025201 (2001).

[134] L. Jensen, P.-O. Åstrand, and K. V. Mikkelsen, Journal of Physical Chemistry B **108**, 8226 (2004).

[135] H. W. Kroto, J. R. Heath, S. C. O'Brian, R. E. Curl, and R. E. Smalley, Nature **318**, 162 (1985).

[136] S. Iijima, Nature **354**, 56 (1991).

[137] S. J. A. van Gisbergen, J. G. Snijders, and E. J. Baerends, Phys. Rev. Lett. **78**, 3097 (1997).

[138] K. Ruud, D. Jonsson, and P. R. Taylor, J. Chem. Phys. **114**, 4331 (2001).

[139] J. Kongsted, A. Osted, L. Jensen, and P.-O. Åstrand, Journal of Physical Chemistry B **105**, 10243 (2001).

[140] R.-H. Xie, G. W. Bryant, L. Jensen, J. Zhao, and V. H. Smith Jr., J. Chem. Phys. **118**, 9441 (2003).

[141] M. Yoshida (The fullerene gallery. Available from: http://www.cochem2.tutkie.tut.ac.jp/Fuller/higher/higherE.html).

[142] L. Jensen, O. H. Schmidt, K. V. Mikkelsen, and P.-O. Åstrand, Journal of Physical Chemistry B **104**, 10462 (2000).

[143] L. Jensen, P.-O. Åstrand, A. Osted, J. Kongsted, and K. V. Mikkelsen, J. Chem. Phys. **116**, 4001 (2002).

[144] D. P. Chong, M. Grüning, and E. J. Baerends, J. Comput. Chem. **24**, 1582 (2003).

[145] G. te Velde and E. J. Baerends, Phys. Rev. B **44**, 7888 (1991).

[146] F. Kootstra, P. L. de Boeij, and J. G. Snijders, Phys. Rev. B **62**, 7071 (2000).

[147] M. Parac and S. Grimme, J. Phys. Chem. A **106**, 6844 (2002).

[148] J. P. Perdew, Phys. Rev. B **33**, 8822 (1986).

[149] K. E. Johnson, D. B. Johnston, and S. Lipsky, J. Chem. Phys. **70**, 3844 (1979).

[150] R. Lindh and B. O. Roos, Int. J. Quantum Chem. **35**, 813 (1989).

[151] C. Petrongolo, R. J. Buenker, and S. D. Peyerimhoff, J. Chem. Phys. **76**, 3655 (1982).

[152] J. D. Watts, S. R. Gwaltney, and R. J. Bartlett, J. Chem. Phys. **105**, 6979 (1996).

[153] M. P. Pérez-Casany, I. Nebot-Gil, J. Sánchez-Marín, and O. Castell, Chem. Phys. Lett. **295**, 181 (1998).

[154] E. R. Davidson and A. A. Jarzęcki, Chem. Phys. Lett. **285**, 155 (1998).

[155] J. Wolf and G. Hohlneicher, Chem. Phys. **181**, 185 (1994).

[156] S. Grimme and M. Parac, ChemPhysChem **4**, 292 (2003).

[157] Y. Kawashima, T. Hashimoto, H. Nakano, and K. Hirao, Theor. Chim. Acta **102**, 49 (1999).

[158] P. Ilich, Can. J. Spectrosc. **32**, 19 (1987).

[159] L. Serrano-Andrés and B. O. Roos, J. Am. Chem. Soc. **118**, 185 (1996).

[160] L. Edwards and D. H. Dolphin, J. Mol. Spectrosc. **38**, 16 (1971).

[161] U. Nagashima, T. Takada, and K. Ohno, J. Chem. Phys. **85**, 4524 (1986).

[162] B. F. Kim and J. Bohandy, J. Mol. Spectrosc. **73**, 332 (1978).

[163] L. Serrano-Andrés, M. Merchán, M. Rubio, and B. O. Roos, Chem. Phys. Lett. **295**, 195 (1998).

[164] M. Klessinger and W. Lüttke, Chem. Ber. **99**, 2136 (1966).

[165] L. Serrano-Andrés and B. O. Roos, Chem. Eur. J. **3**, 717 (1997).

[166] K. D. D'Amico, C. Manos, and R. L. Christensen, J. Am. Chem. Soc. **102**, 1777 (1980).

[167] C. P. Hsu, S. Hirata, and M. Head-Gordon, J. Phys. Chem. A **105**, 451 (2001).

[168] K. Nakayama, H. Nakano, and K. Hirao, Int. J. Quantum Chem. **66**, 157 (1998).

[169] J. B. Platt, J. Chem. Phys. **17**, 484 (1949).

[170] H. B. Klevens and J. B. Platt, J. Chem. Phys. **17**, 470 (1949).

[171] S. J. A. van Gisbergen, A. Rosa, G. Ricciardi, and E. J. Baerends, J. Chem. Phys. **111**, 2499 (1999).

[172] J. Pitarch-Ruiz, J. Sanchez-Marin, A. Sanchez De Meras, and D. Maynau, Mol. Phys. **101**, 483 (2003).

[173] K. K. Innes, I. G. Ross, and W. R. Moomaw, J. Mol. Spectrosc. **132**, 492 (1988).

[174] J. G. G. Simon and A. Schweig, Chem. Phys. Lett. **200**, 631 (1992).

[175] K. N. Walzl, C. F. Koerting, and A. Kuppermann, J. Chem. Phys. **87**, 3796 (1987).

[176] M. B. Robin, *Higher Excited States of Polyatomic Molecules*. (Academic Press, New York, 1985).

[177] M. P. Fülscher, K. Andersson, and B. O. Roos, J. Phys. Chem. **96**, 9204 (1992).

[178] N. Ohmori, T. Suzuki, and M. Ito, J. Phys. Chem. **92**, 1086 (1988).

[179] V. Molina and M. Merchán, J. Phys. Chem. A **105**, 3745 (2001).

[180] M. Hanrath and S. D. Peyerimhoff, Chem. Phys. Lett. **337**, 368 (2001).

[181] M. E. Boyle, B. E. Williamson, and P. N. Schatz, Chem. Phys. Lett. **125**, 349 (1986).

[182] C. R. C. Wang, S. Pollack, and M. M. Kappes, Chem. Phys. Lett. **166**, 26 (1990).

[183] V. Bonačić-Koutecký, P. Fantucci, and J. Koutecký, Chem. Phys. Lett. **166**, 32 (1990).

[184] Y. S. Sohn, N. Hendrickson, and H. B. Gray, J. Am. Chem. Soc. **93**, 3603 (1971).

[185] N. A. Beach and H. B. Gray, J. Am. Chem. Soc. **90**, 5713 (1968).

[186] K. Pierloot, E. Tsokos, and L. G. Vanquickenborne, J. Phys. Chem. **100**, 16545 (1996).

[187] M. Bavia, F. Bertinelli, C. Taliani, and C. Zauli, Mol. Phys. **31**, 479 (1976).

[188] O. Christiansen, J. Gauss, J. F. Stanton, and P. Jørgensen, J. Chem. Phys. **111**, 525 (1999).

[189] V. Huber, K. R. Asmis, A. C. Sergenton, and M. Allan, J. Phys. Chem. A **102**, 3524 (1998).

[190] M. Grüning, O. V. Gritsenko, S. J. A. v. Gisbergen, and E. J. Baerends, J. Chem. Phys. **112**, 652 (2001).

[191] S. Bashkin and J. A. Stoner Jr., *Atomic Energy Levels and Grotrian Diagrams I*. (North-Holland, Amsterdam, 1975).

[192] Z. Shuai and J. L. Brédas, Phys. Rev. B **62**, 15452 (2000).

[193] M. F. Granville, B. E. Kohler, and J. Bannon Snow, J. Chem. Phys. **75**, 3765 (1981).

[194] Z.-L. Cai, K. Sendt, and J. R. Reimers, J. Chem. Phys. **117**, 5543 (2002).

[195] G. Harbecke, E. Meier, W. Kobel, M. Egli, H. Kiess, and E. Tossatti, Solid State Commun. **55**, 419 (1985).

[196] D. D. C. Bradley and R. H. Friend, J. Mol. Electron. **5**, 19 (1989).

[197] M. Turki, T. Barisien, J.-Y. Bigot, and C. Daniel, J. Chem. Phys. **112**, 10526 (2000).

[198] D. Chakraborty and J. B. Lagowski, J. Chem. Phys. **115**, 184 (2001).

[199] J. E. Chadwick and B. E. Kohler, J. Phys. Chem. **98**, 3631 (1994).

[200] R. Colditz, D. Grebner, M. Helbig, and S. Rentsch, Chem. Phys. **201**, 309 (1995).

[201] J. Guay, P. Kasai, A. Diaz, R. Wu, J. M. Tour, and L. H. Dao, Chem. Mater. **4**, 1097 (1992).

[202] J. B. Lagowski, J. Mol. Struct. **589-590**, 125 (2002).

[203] R. A. J. Janssen, in *Primary Photoexcitations in Conjugated Polymers: Molecular Exciton versus Semiconductor Band Model*, edited by N. S. Sariciftci (World Scientific, New York, 1997).

[204] R. Klooster, Student project, Rijksuniversiteit Groningen, http://theochem.chem.rug.nl/publications/, 2004.

[205] NIST Atomic Spectra Database (available from http://physics.nist.gov/cgi-bin/AtData/main_asd).